Technische Universität München
TUM Campus Straubing für Biotechnologie und Nachhaltigkeit

Production of fatty acids and fatty alcohols with *Corynebacterium glutamicum* from first- and second-generation feedstock

Felix Bastian Werner

Vollständiger Abdruck des TUM Campus Straubing für Biotechnologie und Nachhaltigkeit der Technischen Universität München zur Erlangung eines

Doktors der Naturwissenschaften (Dr. rer. nat.)

genehmigten Dissertation.

Vorsitz: Prof. Dr. Henrike Niederholtmeyer

Prüfer*innen der Dissertation:

1. Prof. Dr. Bastian Blombach
2. Prof. Dr.-Ing. Michael Zavrel

Die Dissertation wurde am am 25.09.2023 bei der Technischen Universität München eingereicht und durch den TUM Campus Straubing für Biotechnologie und Nachhaltigkeit am 22.12.2023 angenommen.

„Da steh‘ ich nun, ich armer Tor,
Und bin so klug als wie zuvor!
Heiße Magister, heiße Doktor gar,
Und ziehe schon an die zehen Jahr‘
Herauf, herab und quer und krumm
Meine Schüler an der Nase herum –
Und sehe, daß wir nichts wissen können!“

Dr. Heinrich Faust
Protagonist in
Faust. Der Tragödie erster Teil
by Johann Wolfgang von Goethe

Funding and scientific contributions

The experimental work framing this manuscript was conducted under leadership and supervision of Prof. Dr. Bastian Blombach at the Professorship Microbial Biotechnology (Technical University of Munich, Campus Straubing for Biotechnology and Sustainability, Germany) within the time span of 2020-2023.

This work was funded by a grant from the German Federal Ministry of Education and Research (grant 031B0825C) as part of the project “ForceYield”. Parts of this work have been published in peer-reviewed journals or were presented as talks or poster presentations at international conferences.

Peer-reviewed scientific articles:

Werner, F., Schwardmann, L. S., Siebert, D., Rückert-Reed, C., Kalinowski, J., Wirth, M. T., Hofer, K., Takors, R., Wendisch, V. F., & Blombach, B. (2023). Metabolic engineering of *Corynebacterium glutamicum* for fatty alcohol production from glucose and wheat straw hydrolysate. *Biotechnology for Biofuels and Bioproducts*, *6*(1), 116. https://doi: 10.1186/s13068-023-02367-3.

Thoma, F., Appel, C., Russ, D., Huber, J., **Werner, F.**, & Blombach, B. (2023). Improving growth properties of *Corynebacterium glutamicum* by implementing an iron-responsive protocatechuate biosynthesis. *Microbial Biotechnology*, *16*(5), 1041-1053. https://doi.org/10.1111/1751-7915.14244.

Schmollack, M., **Werner, F.**, Huber, J., Kiefer, D., Merkel, M., Hausmann, R., Siebert, D., & Blombach, B. (2022). Metabolic engineering of *Corynebacterium glutamicum* for acetate-based itaconic acid production. *Biotechnology for Biofuels and Bioproducts*, *15*(1), 139. https://doi.org/10.1186/s13068-022-02238-3.

Talks and presentations:

Werner, F., Siebert, D., & Blombach, B. (2022). Fatty alcohol production in a fatty acid-producing *Corynebacterium glutamicum* strain. Public university seminar talk at TUM Campus Straubing, 5 May 2022. Straubing, Germany.

Posters at conferences:

Schwardmann, L. S., **Werner, F.**, Rückert, C., & Wendisch, V. F. (2023). ForceYield 1 & 2: Tailored central metabolism for stoichometrically-enforced high-yield bioproduction of chemicals from agricultural sidestreams. DECHEMA Himmelfahrtstagung, 15 – 17 May 2023. Weimar, Germany.

Werner, F., Schwardmann, L. S., Siebert, D., Wendisch, V. F., & Blombach, B. (2022). Utilizing wheat straw hydrolysate for the production of fatty alcohols with *Corynebacterium glutamicum*. 6th Applied Synthetic Biology in Europe, 4 – 6 November 2022. Edinburgh, United Kingdom.

Werner, F., Schwardmann, L. S., Siebert, D., Wendisch, V. F., & Blombach, B. (2022). Utilizing wheat straw hydrolysate for the production of fatty alcohols with *Corynebacterium glutamicum*. Key Technologies in the Bioeconomy 2022, 27 – 29 September 2022. Straubing, Germany.

Werner, F., Siebert, D., & Blombach, B. (2022). Fatty alcohol production in *Corynebacterium glutamicum*. VAAM annual conference, 21 – 23 February 2022. Online.

Author’s contribution and involved co-workers

The majority of work presented in this thesis was designed, performed, and analyzed by me. Exceptions are outlined below to clarify further contributions:

Prof. Dr. Bastian Blombach and Dr. Daniel Siebert supported conceptualizing and interpreting some experiments and data, respectively.

Marie-Theres Wirth assisted me experimentally as part of her Master’s research internship with the title “Optimization of fatty alcohol production in *Corynebacterium glutamicum* from wheat straw hydrolysate”. She was particularly involved in engineering the *gltA* promoter mutants (4.2.3.4), developing a hydrolysate-based fed-batch process, and analyzing respective data sets (Werner et al., 2023).

Lynn S. Schwardmann of Bielefeld University developed and integrated the xylose-utilization module gX (4.2.3.3) (Werner et al., 2023), which was here used in fatty alcohol-producing strains.

Katharina Hofer of the University of Stuttgart established a hydrolysate processing procedure (Werner et al., 2023) and assisted during the glucose-based fed batch cultivation of section (4.2.2.3).

Janine Huber prepared the master mixes required for the Gibson Assembly method (Table S. 9, Table S. 10, 3.5.8).

Acknowledgements

Three years of laboratory work went into this dissertation, and even more was invested in writing down the results discussed here. Many people were involved in this work, both actively and passively. It is to these people that I owe my thanks.

First, I would like to thank Prof. Dr. Bastian Blombach, who made it possible for me to work on this collaborative scientific project and acted as my doctoral supervisor throughout the process. Many of the ideas underlying this work would not have been developed without the regular formal and informal discussions with him. His scientific enthusiasm and support kept me motivated even when encountering apparent experimental dead ends. I greatly appreciated the scientific freedom he gave me.

I would also like to thank Dr. Daniel Siebert. His investment of time in my familiarisation with the laboratory and his knowledge of *C. glutamicum* and various relevant laboratory methods enabled me to experience a quick and pleasant start into the new working environment. Occasional informal brainstorming sessions were helpful to develop new approaches to tricky problems.

In addition, I would like to thank my namesake, Dr. Felix Thoma. His knowledge of the iron metabolism of *C. glutamicum* and his help with initial bioreactor cultivations were invaluable for this work.

Many thanks also to Katharina Hofer (IBVT, University of Stuttgart) and Lynn S. Schwardmann (Faculty of Biology, Genetics of Prokaryotes and CeBiTec, University of Bielefeld), with whose help parts of this work were developed and who were always available for an exchange of knowledge.

At the Professorship Microbial Biotechnology, I was able to work with talented colleagues who became my friends over time. The scientific and non-scientific conversations not only enriched me academically but also cleared my mind after long days in the lab. In particular, I would like to thank Janine Huber, who always kept order in the lab, provided support when needed, and always kept an eye on harmony within the group. I would also like to thank my long-time office colleague Clarissa Schulze, who put up with me even after long fermentation days and always had an open ear for professional and private issues. Her enthusiasm for German rap music made shared fermentation days more enjoyable.

Last but not least, I would like to thank my family, who have supported me not only during my doctorate but always. Without their support, this work would not have been possible. Furthermore, my girlfriend Lydia has always been at my side and encouraged me to keep going even after long, busy days (or nights).

Thank you!

Table of contents

List of figures

List of tables

List of supplementary figures

List of supplementary tables

Nomenclature

Abbreviation	Description
6PGDH	6-phosphogluconate dehydrogenase
ACC	Acetyl-CoA carboxylase
AcCC	Acyl-CoA carboxylase
AccBC	Acetyl-CoA carboxylase α-subunit
AccD1	Acetyl-CoA carboxylase β-subunit
AccD2	Acyl-CoA carboxylase β-subunit
AccD3	Acyl-CoA carboxylase β-subunit
AccE	Acetyl-CoA carboxylase ε-peptide
ACP	Acyl-carrier protein
AcpM	*Apo*-[acyl-carrier protein]
AcpP	*Apo*-[acyl-carrier protein]
AcpS	*Holo*-[acyl-carrier protein] synthase
ACR	Acyl-CoA reductase
Act	Acetate
ADH	Alcohol dehydrogenase
ADP	Adenosine diphosphate
AH-FAR	Aldehyde-forming fatty acyl-ACP/CoA reductase
AHR	Aldehyde reductase
AL-FAR	Alcohol-forming fatty acyl-ACP/CoA reductase
ALE	Adaptive laboratory evolution
AraE	Arabinose transporter
AT	Acyltransferase
ATCC	American type culture collection
ATP	Adenosine triphosphate
B. subtilis	*Bacillus subtilis*
bp	Base pair / nucleotide
BHI	Brain heart infusion
BHIS	Brain heart infusion sorbitol
BLAST	Basic local alignment search tool
bln	Billion
c	Concentration, mol L^{-1} (M), g L^{-1}
C. glutamicum	*Corynebacterium glutamicum*
C:N ratio	Carbon to nitrogen ratio
CAR	Carboxylic acid reductase
CDW	Cell dry weight
CgLP	*Corynebacterium glutamicum* landing pad
CmrA	Ketoacyl reductase
CO_2	Carbon Dioxide
CoA	Coenzyme A
CS	Citrate synthase
$c_{s,\ Feed}$	Concentration of feed
d	Day
DH	Dehydratase

DI-H_2O	Deionized water
dNTP	Deoxynucleotide triphosphate
DNA	Deoxyribonucleic acid
DO	Dissolved oxygen
E. coli	*Escherichia coli*
ER	Enoyl reductase
et al.	And others
EU	European Union
F_0	Initial feed rate
FA	Fatty acid(s)
FabA	β-hydroxyacyl-ACP dehydratase
FabB	β-ketoacyl-ACP synthase I
FabD	Malonyl-CoA ACP transacylase
FabF	β-ketoacyl-ACP synthase II
FabG	β-ketoacyl-ACP reductase
FabH	β-ketoacyl-ACP synthase III
FabI	Enoyl-ACP reductase
FabZ	β-hydroxyacyl-ACP dehydratase
FadD	Acyl-CoA synthetase
FadD2	Acyl-AMP ligase
FadD5	Acyl-CoA synthetase
FadD15	Acyl-CoA synthetase
FAEE	Fatty acid ethyl ester(s)
FAL	Fatty alcohol(s)
FAME	Fatty acid methyl ester(s)
FAR	Alcohol-forming fatty acyl-ACP/CoA reductase
Fas-IA	Fatty acid synthase A
Fas-IB	Fatty acid synthase B
FAS-I	Type I fatty acid synthase
FAS-II	Type II fatty acid synthase
fasO	Binding sequence for FasR
FasR	TetR-type transcriptional regulator of the fatty acid synthesis
FID	Flame ionization detector
G6PDH	Glucose-6-phosphate dehydrogenase
g	Gram
GC	Gas chromatography
GDH	Glutamate dehydrogenase
GHG	Greenhouse gas
Glc	Glucose
Glk	Glucokinase
GMOs	Genetically modified organisms
GRAS	Generally recognized as safe
GS/GOGAT	Glutamine synthetase/ glutamate synthase
GTP	Guanosine triphosphate
gX	Evolved and xylose-utilizing strain background (Δ*actA*::*xylAB*$_{evol}$)

h	Hours
H_2O	Water
H^+	Proton
HCO_3^-	Bicarbonate
HPLC	High-performance liquid chromatography
ICD	Isocitrate dehydrogenase
IolR	Transcriptional regulator of the *myo*-inositol metabolism
IolT1	Glucose/*myo*-inositol permease
IolT2	Glucose/*myo*-inositol permease
ISTD	Internal standard
k	Kilo (10^3)
Kan^R	Kanamycin resistance
Kan^{50}	Kanamycin concentration: 50 µg mL^{-1}
kb	1000 bases/ nucleotides
kbp	1000 base pairs
k_La	Volumetric oxygen transfer coefficient
K_m	Michaelis-Menten constant
KPI	Key performance indicator(s)
KR	3-Ketoacyl reductase
KS	3-Ketoacyl synthase
L	Liter
$LacI^q$	*lac* repressor variant
m	Meter; milli (10^{-3})
MA	Mycolic acid
MalE	Malic enzyme
Maqu_2220	Alcohol-forming fatty acyl-ACP/CoA reductase of *M. hydrocarbonoclasticus*
Maqu_2507	Alcohol-forming fatty acyl-ACP/CoA reductase of *M. hydrocarbonoclasticus*
MCS	Multiple cloning site
M. hydrocarbonoclasticus	*Marinobacter hydrocarbonoclasticus*
M. tuberculosis	*Mycobacterium tuberculosis*
min	Minutes
mln	Million
MPT	Malonyl/palmitoyl transferase
m_S	Maintenance coefficient
n.a.	Not applicable
n.d.	Not determined
NAD^+	Nicotinamide adenine dinucleotide (oxidized)
NADH	Nicotinamide adenine dinucleotide (reduced)
$NADP^+$	Nicotinamide adenine dinucleotide phosphate (oxidized)
NADPH	Nicotinamide adenine dinucleotide phosphate (reduced)
OD_{600}	Optical density at 600 nm
ODx	Oxaloacetate decarboxylase
OTR	Oxygen transfer rate
PCA	Protocatechuic acid

PCR	Polymerase chain reaction
PCx	Pyruvate carboxylase
PDHC	Pyruvate dehydrogenase complex
PEP	Phosphoenol pyruvate
PEPCk	PEP carboxykinase
PEPCx	PEP carboxylase
pH	Negative decimal logarithm of the proton concentration
P_i	Phosphate
Pks	Polyketidsynthase
PL	Phospholipid
PlsB	Glycerol-3-phosphate acyltransferase
PntAB	Transhydrogenase of *E. coli*
PpgK	Glucokinase
PP_i	Pyrophosphate
PPP	Pentose phosphate pathway
PPTase	4'-phosphopantetheinyl transferase
PptT	4'-phosphopantetheinyl transferase
PrpC1	Methylcitrate synthase
PrpC2	Methylcitrate synthase
P_{tac}	*tac* promoter
PTFE	Polytetrafluoroethylene
PTS	Phosphotransferase system
P_{tuf}	*tuf* promoter
Q_P	Volumetric productivity
q_S	Biomass-specific substrate uptake rate
$q_{S,m}$	Substrate uptake rate during fed-batch phase for respective μ_{set}
RBS	Ribosome binding site
RID	Refraction index detector
R. toruloides	*Rhodotorula toruloides*
rpm	Revolutions per minute
RT	Room temperature, approx. 22 °C, default temperature
s	Seconds
S. cerevisiae	*Saccharomyces cerevisiae*
SacB	Levansucrase
SD	Standard deviation
SF	Shaking flask
SigD	Sigma factor D
t	Time; metric tons
TC	Total carbon
TCA	Tricarboxylic acid
TDCM	Trehalose dicorynomycolate
Tes	Thioesterase
TesA	Type I thioesterase A
'TesA	Truncated version of *E. coli* TesA
TesB	Type II thioesterase B
Tet^R	Tetracycline resistance
Tet^5	Tetracycline concentration: 5 µg mL^{-1}
TIC	Total inorganic carbon
TMCM	Trehalose monocorynomycolate

TOC	Total organic carbon
TPP	Thiamine pyrophosphate
T_{rrnB}	*rrnB* terminator
UTR	Untranslated region
UV/VIS	Ultraviolet and visible light spectrum
V	Volume; Volt
V_0	Volume at end of batch phase
vvm	Volume per volume per minute
WT	Wild type
x_0	Biomass concentration at end of batch phase
x g	Relative centrifugal force
X. campestris	*Xanthomonas campestris*
Xyl	Xylose
XylA	Xylose isomerase
XylB	Xylulokinase
Y. lipolytica	*Yarrowia lipolytica*
$Y_{P/S}$	Product/substrate yield
$Y_{X/S}$	(apparent) biomass/substrate yield
$Y_{X/S}^{true}$	True biomass/substrate yield
µ	Specific growth rate; micro (10^{-6})
μ_{max}	Maximum growth rate
μ_{set}	Set growth rate
°C	Degree Celsius
% (v/v)	Percent volume per volume
% (w/v)	Percent weight per volume

Abstract

Oleochemicals in general and fatty acid-derived products such as fatty alcohols in particular find growing applications in cosmetic products, lubricants, or biofuels, to name a few. The continuously growing demand for those primarily biomass-based products drives the transition from petrol-based towards more sustainable processes. Nevertheless, current fatty acid and fatty alcohol production depends on expensive metal catalysts and extreme reaction conditions regarding temperature and pressure. Moreover, unsustainable and excessive farming practices to grow the required first-generation feedstock result in environmental and social problems (Fargione et al., 2008).

Microbial oleochemical production could be a feasible alternative to satisfy demand while reducing the production's environmental footprint. Particularly, using second-generation feedstock like lignocellulosic hydrolysates would contribute to a more sustainable production through a more responsible utilization of existing land and biomass. Consequently, this study examined the feasibility of producing fatty acids and alcohols with the industrially well-established organism *Corynebacterium glutamicum*. Studying the organism's fatty acid biosynthetic pathway highlighted the importance of decoupling it from the transcriptional regulator FasR to efficiently produce fatty acids (Nickel et al., 2010; Takeno et al., 2013). Additionally, the delicate role of the acetyl-CoA carboxylase was studied, which positioned itself as a rate-limiting enzyme at the entry point of the respective pathway. In that context, its non-catalytic subunit AccE was found to be important for the catalytic activity of the enzyme complex. By modifying the cultivation conditions, the significance of nitrogen limitation for fatty acid production was emphasized. Data gathered in that context suggested the importance of iron availability on fatty acid biosynthesis, which could be increased by using urea as a nitrogen source or by supplementing either HCO_3^- or the iron-chelating compound PCA. Both substances are known to facilitate iron availability via an abiotic reduction of Fe^{+3} to Fe^{+2} (Müller et al., 2020). The best-performing strain with a transcriptionally deregulated fatty acid biosynthesis and overexpressed acetyl-CoA carboxylase produced per liter 663 ± 48 mg fatty acids from 20 g glucose L^{-1} in nitrogen-limiting shaking flask cultivations.

As the biosynthetic pathways of fatty acid and fatty alcohol synthesis are similar until they diverge at the acyl-CoA node, a mutant of *C. glutamicum*, featuring improved fatty acid precursor supply, was used to establish fatty alcohol production from glucose. This repre-

sents the first published engineering strategy to produce long-chain alcohols with the respective organism. Fatty alcohol production was achieved by overexpression of a fatty acyl-CoA reductase (FAR). Out of two screened FAR of *Marinobacter hydrocarbonoclasticus* VT8, the best-performing reductase Maqu_2220 was used for further strain engineering. A *C. glutamicum* Δ*fasR* mutant with plasmid-based FAR expression and balanced thioesterase expression for increased precursor supply was further modified to enable xylose utilization. Plasmid-free xylose utilization was obtained by the genomic integration of an evolved *xylAB* sequence into the *actA* locus (gX). Finally, NADPH-expensive fatty alcohol production was optimized by overexpression of the *Escherichia coli* transhydrogenase PntAB. The best-performing strain *C. glutamicum* Δ*fasR* $cg2692_{TTG}$ CgLP12::(P_{tac}-*pntAB*-T_{rrnB}) gX pEKEx2_*maqu2220* was used to develop a wheat straw hydrolysate-based pulsed fed-batch process. The respective process resulted in 2.45 ± 0.09 g fatty alcohols L^{-1} with a product yield of 0.054 ± 0.005 Cmol $Cmol^{-1}$ and a volumetric productivity of 0.109 ± 0.005 g L^{-1} h^{-1} from the non-food substrate. Obtained parameters are competitive with published data from other organisms and represent a rare example of a fatty alcohol process utilizing genuine lignocellulosic hydrolysate.

Zusammenfassung

Oleochemikalien im Allgemeinen und von Fettsäuren abgeleitete Produkte wie Fettalkohole im Besonderen finden zunehmend Anwendung in beispielsweise kosmetischen Produkten, Schmiermitteln oder Biokraftstoffen. Die ständig wachsende Nachfrage nach diesen hauptsächlich auf Biomasse basierenden Produkten treibt den Übergang von erdölbasierten zu nachhaltigeren Produktionsverfahren voran. Die derzeitige Produktion von Fettsäuren und Fettalkoholen ist jedoch von teuren Metallkatalysatoren und extremen Reaktionsbedingungen hinsichtlich Temperatur und Druck abhängig. Darüber hinaus führen nicht nachhaltige und exzessive landwirtschaftliche Praktiken zum Anbau der benötigten *first-generation feedstock* zu ökologischen und sozialen Problemen (Fargione et al., 2008).

Die mikrobielle Produktion von Oleochemikalien könnte eine praktikable Alternative sein, um deren steigende Nachfrage zu decken und gleichzeitig den ökologischen Fußabdruck der zugrundeliegenden Prozesse zu verringern. Insbesondere die Verwendung von *second-generation feedstocks* wie lignozellulosischen Hydrolysaten würde zu einer nachhaltigeren Produktion durch eine verantwortungsvollere Nutzung der vorhandenen Flächen und Biomasse beitragen. In dieser Arbeit wurde daher die Möglichkeit der Herstellung von Fettsäuren und Fettalkoholen mit dem industriell etablierten Organismus *Corynebacterium glutamicum* untersucht. Die initiale Stammentwicklung verdeutlichte, dass der native Fettsäurebiosyntheseweg vom Transkriptionsregulator FasR entkoppelt werden musste, um Fettsäuren effizient zu produzieren (Nickel et al., 2010; Takeno et al., 2013). Darüber hinaus wurde die Acetyl-CoA Carboxylase untersucht, die sich als Raten-limitierendes Enzym des entsprechenden Stoffwecheslweges darstellte. In diesem Zusammenhang wurde gezeigt, dass ihre nicht katalytische Untereinheit AccE für die katalytische Aktivität des Enzymkomplexes benötigt wird. Durch Anpassung der Mediumzusammensetzung wurde zudem die Bedeutung von stickstofflimitierenden Kultivierungsbedingungen für die Fettsäureproduktion gezeigt. Die in diesem Zusammenhang gesammelten Daten wiesen darüber hinaus auf die wichtige Rolle der Eisenverfügbarkeit auf die Fettsäurebiosynthese hin, die durch die Verwendung von Harnstoff als Stickstoffquelle oder durch die Zugabe von HCO_3^- oder der chelatbildenen Verbindung PCA erhöht werden konnte. Von beiden Substanzen ist bekannt, dass sie die Eisenverfügbarkeit über eine abiotische Reduktion von Fe^{+3} zu Fe^{+2} erleichtern (Müller et al., 2020). Der leistungsstärkste Stamm mit einer transkriptionell deregulierten Fettsäurebiosynthese und überexprimierter Acetyl-CoA-Carboxylase produzierte unter stickstofflimitierten Kultivierungsbedingungen in Schüttelkolben pro Liter 663 ± 48 mg Fettsäuren aus 20 g Glucose L^{-1}.

Da die mikrobielle Fettalkoholsynthese auf dem Fettsäuresyntheseweg basiert, bis beide Stoffwechselwege am Acyl-CoA-Knotenpunkt divergieren, wurde eine Fettsäuren produzierende Mutante von *C. glutamicum* als Chassis zur Fettalkoholproduktion aus Glucose benutzt. Dies stellt die erste veröffentlichte Strategie zur Herstellung langkettiger Alkohole mit dem entsprechenden Organismus dar. Die Fettalkoholproduktion wurde durch Überexpression einer *fatty acyl-CoA reductase* (FAR) erreicht. Von zwei untersuchten FAR des marinen Bakteriums *Marinobacter hydrocarbonoclasticus* VT8 wurde die am besten funktionierende Reduktase Maqu_2220 für die weitere Stammentwicklung verwendet. Eine Δ*fasR*-Mutante von *C. glutamicum* mit plasmidbasierter FAR- und reduzierter Thioesterase-Expression wurde weiter modifiziert, um eine effiziente Xylose-Verwertung zu ermöglichen. Die plasmidfreie Xylose-Verstoffwechselung wurde durch die genomische Integration einer evolvierten *xylAB*-Sequenz in den *actA* Locus (gX) erreicht. Schließlich wurde die NADPH-aufwendige Fettalkoholproduktion durch Überexpression der *Escherichia coli* Transhydrogenase PntAB optimiert. Der beste Produktionsstamm *C. glutamicum* Δ*fasR* cg2692$_{TTG}$ CgLP12::(P_{tac}-*pntAB*-T_{rrnB}) gX pEKEx2_*maqu2220* wurde für die Entwicklung eines gepulsten Fed-Batch-Prozesses mit Weizenstrohydrolysat als primäre Kohlenstoffquelle verwendet. Der entsprechende Prozess erzielte einen Titer der Fettalkohole von 2.45 ± 0.09 g L^{-1} mit einer Produktausbeute von 0.054 ± 0.005 Cmol $Cmol^{-1}$ und einer volumetrischen Produktivität von 0.109 ± 0,005 g L^{-1} h^{-1}. Die erreichten Parameter sind konkurrenzfähig mit veröffentlichten Daten anderer Organismen und stellen ein seltenes Beispiel für einen auf Lignocellulosehydrolysat-basierten Fettalkoholprozess dar.

1. Motivation and objective

A continuously growing population and resulting societal challenges, environmental pollution, and fast-progressing climate change underline the importance of managing our finite global resources fairly and sustainably. This can be achieved by developing more efficient processes and shifting from fossil to renewable feedstock. Competition between the production of food/feed and chemicals – a result of this transition already in progress – has to be prevented. Valorization of biological, hitherto discarded products provides a solution to alleviate the respective competition, releasing land to be used for food production and avoiding the necessity to convert untouched biotopes into farmland (Lange et al., 2021). Such an approach would also be in line with the UN Sustainable Development Goals 2 (Zero Hunger), 12 (Responsible Consumption and Production), 13 (Climate Action), and 15 (Life on Land) (UN General Assembly, 2015).

Industrial biotechnology embodies the paradigm shift from fossil-based towards more sustainable processes with its scope of manufacturing products sustainably by microbial or enzymatic means (Soetaert & Vandamme, 2006). The conversion of bio-based feedstock into valuable products offers an alternative to conventional chemical processes, which often depend on fossil resources. In addition to the apparent positive environmental impact of a fossil fuel-independent process, microbial production of chemicals yields advantages over conventional processes, such as increased independence of climate, the seasons, and being less labor intensive (Liang & Jiang, 2013). However, the sustainability of biotechnological processes can further be optimized when using biomass waste, so-called second-generation feedstock (2.1.2), instead of the commonly used first-generation (2.1.1) feedstock.

In this study, the oleochemicals fatty acids (FA) and fatty alcohols (FAL) were chosen as exemplary products that can be synthesized microbially but which are so far still produced either petrochemically or through chemical conversion of primarily first-generation feedstock. Additionally, their versatile application and continuously growing demand make both products attractive to be produced microbially, preferably by utilizing second-generation feedstock.

Despite various successful attempts to engineer microbes to produce FA or FAL (Cordova et al., 2020; d'Espaux et al., 2017; Fernandez-Moya et al., 2015; Huang et al., 2016; Liu et al., 2013; Liu et al., 2012), literature about the production of the former with the industrial workhorse *Corynebacterium glutamicum* is scarce (Ikeda et al., 2020; Plassmeier et al.,

2016; Takeno et al., 2023; Takeno et al., 2018; Takeno et al., 2013), and even non-existent for the production of the latter product. Consequently, this study aims at engineering *C. glutamicum* to produce both industrially important products, thereby exemplifying oleochemical production in this well-established microorganism.

The results section **4.1** covers the development of FA-producing *C. glutamicum* strains and evolves around further understanding the organism's native FA biosynthetic pathway. The focus lies on identifying bottleneck reactions within the pathway and on general cultivation conditions benefiting the overproduction of FA.

In section **4.2**, insights from the previous section were applied to engineer FAL-producing *C. glutamicum* mutants. Respective strains were initially characterized and further optimized with the first-generation feedstock glucose before transitioning to second-generation feedstock-based cultivations. Ultimately, FAL production with lignocellulosic wheat straw hydrolysate as substrate was scaled up into a benchtop bioreactor process, proving the scalability of a hydrolysate-based bioprocess with *C. glutamicum*, thus paving the way for first-generation feedstock-independent cultivations.

2. Introduction

2.1 Biomass-based substrates

Both chemical and biological processes alike utilize substrates of varying origins to produce the desired products. While substrates used in chemical reactions are either fossil- or bio-based, biological production is often limited to biomass-derived feedstock. Depending on its origin, the respective bio-based feedstocks can be categorized into three different generations. Edible biomass belongs to the first generation, non-edible lignocellulosic biomass or waste defines the second generation, while algal biomass is referred to as third-generation feedstock (Cavelius et al., 2023). The same loose but widely accepted definitions apply to first- to third-generation biofuels, with an additional generation existing in that product-focused nomenclature. Applying synthetic biology, both targeted and non-targeted approaches, to (algal) biomass for biofuel production results in a fourth-generation biofuel (Cavelius et al., 2023; Shokravi et al., 2021).

The definitions, differences, and environmental implications of particularly first- and second-generation feedstocks will be discussed in more detail in the following two sections.

2.1.1 First-generation feedstocks

Both on laboratory and industrial scale, refined sugars like glucose or sucrose, vegetable oils or generally edible, unrefined biomass like sugar cane or sugar beets are used as substrates for biological and chemical processes (Blombach et al., 2007; Dodić et al., 2009; Hoekman et al., 2012; Luo et al., 2009; Wittmann et al., 2004). They are defined as “first-generation feedstock” based on the substrates’ inherent characteristic of being edible and thus also being used for human and animal nutrition (Lee & Lavoie, 2013). While utilizing first-generation feedstocks helps to reduce the dependency on fossil resources as substrates and products alike, their impact on the environment and society is controversial (Silver & Miya, 2001). In particular, the competition of biochemical processes with food/feed production, thus diverting edible resources towards the production of chemicals (fuels), and the competition’s negative impact on food prices are often criticized (Martin, 2010; Rulli et al., 2016). The context of poverty and hunger in many global societies gave rise to the so-called “food vs. fuel” debate (Srinivasan, 2009). This framework highlighting the competition between feed, food, and fuel production appeals both on a moral and a scientific level, even though some scholars criticized the postulated conflict for being depicted as too simplistic and one-sided (Muscat et al., 2020; Thompson, 2012). Besides

ethical aspects, repurposing arable land and yet unexploited ecosystems to grow first-generation feedstock for the production of, e.g., biofuels is associated with an extensive long-term release of greenhouse gas emissions (Fargione et al., 2008; Silver & Miya, 2001). This topic will be further explored in section 2.2.4.

2.1.2 Second-generation feedstocks: lignocellulosic biomass

Contrary to first-generation feedstocks, second-generation feedstocks are derived from biomass, which is not used in food production. That includes municipal waste or non-edible lignocellulosic biomass found, for example, in agricultural residues or waste streams of wood and paper industries (Lee & Lavoie, 2013). Besides not competing with conventional food, utilizing this type of feedstock offers a solution to otherwise required disposal and recycling approaches of the respective biomass (Leal et al., 2013). A lot of attention has been given to especially lignocellulosic biomass as it is renewable, abundantly available, and often said to be cheaper than first-generation feedstock (Chandel et al., 2018; Chandel et al., 2010; De Bhowmick et al., 2018; Lynd et al., 1999). However, while prices for unprocessed second-generation biomass are, in fact, generally lower than for their first-generation counterparts, processing costs heavily depend on the method used to convert the recalcitrant biomass into fermentable components (Lee & Lavoie, 2013). Lignocellulose, consisting of cellulose, hemicellulose, and lignin, represents a major structural component of all woody biomass (Valentine et al., 2012). Its exact composition strongly varies depending on the used plant biomass (Menon & Rao, 2012), with an average cellulose, hemicellulose, and lignin content of 40-50 % (w/w), 20-40 % (w/w) and 10-30 % (w/w), respectively (Rabemanolontsoa & Saka, 2013; Sharma et al., 2019).

Cellulose consists of D-glucose linked via β-(1,4)-glycosidic bonds, whereas the branched heteropolymer hemicellulose consists of different hexoses (D-glucose, D-galactose, D-mannose), pentoses (D-xylose, L-arabinose) and acids (galacturonic acid, glucuronic acid) (Sharma et al., 2019). The phenolic macromolecule lignin consists of phenylpropane units originating from *p*-coumaryl alcohol, coniferyl alcohol, and sinapyl alcohol and binds hemicellulose to cellulose (de Wild et al., 2012; Zoghlami & Paës, 2019). Furthermore, it contributes to the recalcitrance of lignocellulose to microbial and enzymatic hydrolysis (Zoghlami & Paës, 2019). Since most microorganisms are not equipped to adequately utilize lignocellulosic material, the respective biomass needs to be pretreated to either break down or remove lignin and to saccharify cellulose and hemicellulose to obtain second-generation sugars. The treatment usually relies on physical or (physico-)chemical processes to make cellulose and hemicellulose more accessible to subsequent enzymatic

hydrolysis into monomeric sugars (Jönsson & Martín, 2016; Zavrel et al., 2015). For example, the organosolv pretreatment uses an organic solvent (e.g., ethanol) to treat lignocellulosic material and fractionate it into solid cellulose, an aqueous hemicellulose-rich solution, and dry lignin (Zhao et al., 2017). Although this effective approach is useful for obtaining and selectively valorizing the discrete fractions, its solvent usage and recovery contribute to disadvantages like general flammability and energy intensiveness (Baruah et al., 2018; Mankar et al., 2021). A physico-chemical, organic solvent-free pretreatment is used by Clariant (Muttenz, Switzerland) in their patented sunliquid® process, resulting in the lignocellulosic hydrolysate used in this work. While the precise treatment procedure is kept secret, it is openly communicated that wheat straw is under pressure thermally treated with steam to increase the accessibility of cellulose and hemicellulose for subsequent enzymatic hydrolysis (Rarbach & Söltl, 2013). The respective steam explosion method is well-reviewed and often employed as a pretreatment. Acetic acid is released during that process as a hydrolysis product of hemicellulose and acts as a catalyst for the respective hydrolysis (Baruah et al., 2018; Singh et al., 2015). As a result of the used biomass (wheat straw) and the pretreatment method, the hydrolysate used in this study is rich in glucose, xylose, and acetic acid. The exact composition is listed in Table 6 of section 3.3.6.8.

Depending on the pretreatment method, different growth inhibitory substances like furans, phenolic compounds, and the aforementioned acetic acid are formed as byproducts (Jönsson & Martín, 2016).

2.2 Products of growing interest: oleochemicals

“Oleochemicals are defined as a class of aliphatic compounds industrially-derived from animal or vegetable lipids” (Yan & Pfleger, 2020). They differ in chain length, the terminal functional group, and additional modifications to the alkyl chain. That group of chemicals includes saturated FA, unsaturated FA, and FA derivatives such as FA esters or FAL which are used in the food, cosmetic and pharmaceutical industries as potential biofuels or lubricants (Egan et al., 1984; Hill et al., 1954; Kalscheuer et al., 2006; Marella et al., 2018; Peralta-Yahya et al., 2012; Pfleger et al., 2015). While some oleochemicals like FAL can be industrially produced via a petrochemical route (Hill et al., 1954; Munkajohnpong et al., 2020) – despite the above-cited definition of oleochemicals – the main production of this class of chemicals nowadays is linked to oil seed products like palm oil, soybean oil and rapeseed oil (Thakur & Kundu, 2016; Yan & Pfleger, 2020). Oleochemicals find application in many products. However, the following sections will focus primarily on FA and FAL to

exemplify the product portfolio, global market trends, and production of the respective compounds.

2.2.1 Surfactants

Besides the use of fats or even FA as a direct precursor for biofuels, they are also used in other products together with FAL. Those include lubricants, additives of personal care products, soaps, and detergents (Egan et al., 1984; Hill et al., 1954; Kalscheuer et al., 2006; Marella et al., 2018; Pfleger et al., 2015). In addition to the well-known, soap-forming saponification of triacylglycerides, FA themselves are an important precursor for several industrially relevant surfactants like fatty amines (Visek, 2003), methyl ester sulfonates (Sherry et al., 1995) or FAL and their derivates (Kreutzer, 1984). Especially the latter are important additives of industrial lubricants and many personal care products due to their ability to act as detergents, emulsifiers, and emollients (Egan et al., 1984; Krishnan et al., 2020; Munkajohnpong et al., 2020).

While a change in local and global policies with a strong focus on reducing CO_2 emissions fueled the demand for biodiesel and thus for bio-based fats and FA during the past two decades, the COVID-19 pandemic and its aftermath are believed to be strong current drivers of the oleochemical market. Responsible for this positive effect is the increased demand for surfactants like disinfecting and cleansing agents, paired with altered hygiene routines (Chirani et al., 2021; Daverey & Dutta, 2021; Munkajohnpong et al., 2020).

2.2.2 Biodiesel – a major driver of the oleochemical market

A major processing step of the oleochemicals FA is the conversion into fatty acid methyl esters (FAME) or fatty acid ethyl esters (FAEE), which find application as biodiesel. Those mono-alkyl esters of long-chain FA usually have a chain length of 12 to 22 carbon atoms (Hoekman et al., 2012), with 16 to 18 carbon atoms being the most prevalent chain length (Sajjadi et al., 2016). Global biodiesel production is based on vegetable oil (73 %), used cooking oil (21 %), and, to a minor extent, on cellulosic biomass (OECD & FAO, 2022, p. 241). It is commonly obtained by the transesterification of triacylglycerides with short-chain alcohols into glycerol and FAME/ FAEE. The inevitable formation of glycerol as a byproduct of biodiesel production gave rise to intensive research into utilizing the respective side stream as a platform chemical (Pagliaro et al., 2007; Zhou et al., 2008).

The continuously rising demand for a variety of oleochemicals during the last decade can partly be attributed to a rising demand for biodiesel, resulting in an increase in global vegetable oil production by 20 % between 2013 and 2018 (Yan & Pfleger, 2020). Additionally, the use of vegetable oil for biodiesel production is projected to increase in emerging markets, but also in the USA. Currently, about 15 % of the global vegetable oil production is used for conversion into biodiesel (OECD & FAO, 2022, p. 164). Despite a projected plateau of around 55 bln L between 2023 and 2031 in global annual biodiesel demand, the European Union (EU) is expected to remain the largest biodiesel-producing region, with production shares falling from currently 30.7 % to 28 % in 2031 (OECD & FAO, 2022, p. 236). The major feedstocks for biodiesel in the EU are rapeseed oil, palm oil, and used cooking oil (OECD & FAO, 2022, p. 236).

Due to the oleochemicals' inherent market position as generally cheap bulk products, they are highly dependent on vegetable oil prices. Thus, as a result of high oil and production costs, Argentine decreased the country's biodiesel blend rate in 2021 temporarily from 10 to 5 % (OECD & FAO, 2022, p. 239; USDA-FAS, 2021, p. 3). Additionally, their competitiveness is directly linked to the oil price, which severely fluctuated during the COVID-19 pandemic but also during Russia's war against Ukraine. While blending mandates require the continuous expansion of biofuel production capacities in some emerging economies, their direct competition with feedstock and land used for food production may slow down the overall process (OECD & FAO, 2022, p. 242).

2.2.3 Commercial FAL production

In contrast to FA, which can be directly obtained by the hydrolysis of bio-based oils and fats (mono-, di-, and triacylglycerides), FAL are commercially produced via three routes: the petrochemical Ziegler process and hydroformylation or via chemical conversion of bio-based feedstock (Munkajohnpong et al., 2020). The Ziegler process is based on the oligomerization and subsequent oxidation of ethylene (Hill et al., 1954), while hydroformylation reacts alkenes with H_2/CO_2 gas mixtures (syngas) to form FAL (Munkajohnpong et al., 2020; Zhang et al., 2007). The third and currently most important process is the catalytic hydrogenation of bio-based oils, FA, and FAME (Munkajohnpong et al., 2020; Yeong et al., 2012). In 2015, about 28 % of the global 2.2 mln t FAL production was fossil-based, while the remaining 72 % was produced via the hydrogenation of bio-based feedstock (Munkajohnpong et al., 2020). However, all commercial methods require the usage of expensive metal catalysts, high pressure, and high reaction temperatures (Munkajohnpong et al., 2020; Rieke et al., 1997). Additionally, the use of fossil resources and extensive

farming of oil plants in monocultures propagate global warming, deforestation, and subsequent loss of biodiversity (Fitzherbert et al., 2008; Vijay et al., 2016). A more sustainable production could be achieved by microbial FAL (and FA) synthesis, which will be briefly introduced in the following sections 2.3 and 2.4.

2.2.4 Is bio-based always sustainable? The carbon debt of first-generation biofuels

A growing oleochemical market, and in particular the skyrocketing demand for biofuels, has led to increased cultivation of oil crops over the past decades (OECD & FAO, 2022, pp. 167, 170). As arable land is a valuable and limited resource, unexploited ecosystems, especially in southern America and southeast Asia, have been sacrificed for the sake of biofuel production. The subsequent conversion of native habitat results in major greenhouse gas (GHG) emissions, both during the conversion process and for decades thereafter. Clearing land by burning causes an immediate release of CO_2, while exposed soil and microbial degradation of biomass contribute to long-term emissions (Silver & Miya, 2001). The sum of released emissions is called the “carbon debt”. Until this debt is “repaid”, biofuels derived from those converted lands have a greater impact on GHG emissions than the fossil-based counterpart they are supposed to replace. Fargione et al. (2008) calculated the time required to repay the carbon debt of biodiesel produced on different converted lands. According to the respective study, it takes between 37 years of soybean-based biodiesel production on converted Cerrado grassland (Brazil) and up to 423 years of palm-based biodiesel production on former peatland rainforest (Indonesia & Malaysia) to repay the biofuel carbon debt (Fargione et al., 2008). The authors of the same study noted that the carbon debt, together with habitat destruction, could be minimized if biofuels were produced from waste biomass (second-generation feedstock) or if degraded cropland was used to grow the respective plants (Fargione et al., 2008).

2.3 Microbial FA biosynthesis

Microbial FA biosynthesis utilizes either type I or type II fatty acid synthases, FAS-I or FAS-II, respectively (Schweizer & Hofmann, 2004b). While the dissociative FAS-II system consists of discrete enzymes catalyzing the respective reactions (Cronan & Thomas, 2009), FAS-I systems are multidomain enzymes (Sul & Smith, 2008). Both systems also differ in their substrates and products: FAS-II systems use and produce acyl-carrier protein (ACP)-bound thioesters (Cronan & Thomas, 2009), while FAS-I systems are coenzyme A (CoA)-

dependent (Schweizer & Hofmann, 2004b; Sul & Smith, 2008). Type II systems are commonly found in prokaryotes, plants, and mitochondria (Hiltunen et al., 2009; Rock & Jackowski, 2002). Even though FAS-I systems are usually located in the eukaryotic cytoplasm (Sul & Smith, 2008), they are also found in the mycolic acid (MA)-producing subgroup of the *Actinomycetales* (Bloch & Vance, 1977), including *C. glutamicum* (Radmacher et al., 2005). Interestingly, some mycobacteria like *Mycobacterium tuberculosis* possess both FAS systems to produce unusually long-chained FA, which are subsequently used to synthesize long-chained MA.

2.3.1 Type I fatty acid synthases

While animal and microbial FAS-I systems are both large multifunctional enzymes responsible for *de novo* FA synthesis in the respective organisms, they differ from each other in their enzyme domain arrangement (Schweizer & Hofmann, 2004b). Therefore, this section will give a brief overview regarding the general structure and function of the bacterial FAS-I system, while section 2.5.2 is dedicated to a more detailed description of the FA biosynthetic pathway via the FAS-I system of *C. glutamicum*.

The polypeptides of the bacterial FAS-I system contain all enzymatic domains required for the successive elongation cycles of the growing acyl chain, similar to the dissociative enzymes found in the FAS-II system (2.3.2). Those are: acyltransferase (AT), enoyl reductase (ER), dehydratase (DH), malonyl/palmitoyl transferase (MPT), ACP, 3-ketoacyl reductase (KR) and 3-ketoacyl synthase (KS) (Schweizer & Hofmann, 2004b). The polypeptides assemble as hexamers of identical subunits to form a functional FAS-I complex. Similar to a free ACP, the ACP domain of a FAS-I polypeptide needs to be phosphopantetheinylated by a 4'-phosphopantetheinyl transferase (PPTase) to become a functional *holo*-[ACP] domain. The FA biosynthesis-initiating reaction is catalyzed by the AT domain, transferring the acetyl moiety of acetyl-CoA to the prosthetic group of the *holo*-[ACP]. Then, a malonyl residue is transferred to the enzyme by MPT from malonyl-CoA. The enzyme-bound malonyl is subsequently condensed with the ACP-bound acetyl/acyl-moiety by KS, releasing CO_2. The formed β-ketoacyl residue is reduced to 3-hydroxyacyl by KR, dehydrated to enoyl by DH, and finally reduced to an acyl moiety by ER. The reduced acyl chain can then enter another elongation cycle. Once a designated chain length has been reached, the enzyme-bound acyl residue is released by an MPT-catalyzed transfer to CoA (Lynen et al., 1980; Schweizer & Hofmann, 2004b). Bloch and Vance (1977) reported that this final, acyl-CoA-forming transacylation was the rate-limiting step of the FAS-I-catalyzed FA biosynthesis in *Mycobacterium smegmatis*. It was shown that bacterial FAS-I systems

require both NADPH and NADH as cofactors for the catalytic activities of the KR and ER domains, respectively (Ariga et al., 1984; Kawaguchi & Okuda, 1977; Schweizer & Hofmann, 2004b; Seyama & Kawaguchi, 1987).

2.3.2 Type II fatty acid synthase

While the microbial FAS-II system can be based on different isoenzymes (Lu & Tonge, 2010; Massengo-Tiassé & Cronan, 2008), the general FA biosynthesis mechanism remains similar throughout all organisms utilizing the respective system for *de novo* FA synthesis. As the *Escherichia coli* FAS-II system has been extensively studied and reviewed, it is often used as an archetype for the prokaryotic FA biosynthesis system (Cronan & Thomas, 2009; White et al., 2005). Therefore, this section will focus on the *E. coli* FAS-II system as an example of prokaryotic FA biosynthesis. A schematic depiction of the *E. coli* FAS-II system is shown in Figure 1.

As both substrates required for the elongation process and growing acyl-moiety alike are bound to an ACP in the dissociative FAS-II system, a functional version of the protein is required. The respective *apo*-[ACP] is activated by 4'-phosphopantetheinylation catalyzed by the *holo*-[ACP] synthase AcpS, resulting in the protein's functional form *holo*-[ACP] (hereafter just referred to as "ACP") (Prescott et al., 1969). The activated ACP can then receive a malonyl group of malonyl-CoA, catalyzed by the malonyl-CoA:ACP transacylase FabD (Magnuson et al., 1992; Verwoert et al., 1992). Thereafter, malonyl-ACP participates in a Claisen condensation with either acetyl-CoA or acyl-ACP. The first acetoacetyl-ACP-forming reaction is catalyzed by the *β*-ketoacyl-ACP synthase III FabH and represents the initial acyl chain-forming reaction of FA biosynthesis (Jackowski & Rock, 1987; Lai & Cronan, 2003). An already existing acyl-ACP is condensed with malonyl-ACP by the *β*-ketoacyl-ACP synthase I FabB or by the *β*-ketoacyl-ACP synthase II FabF to form *β*-ketoacyl-ACP (Edwards et al., 1997; Garwin et al., 1980). Both synthases were shown to accept similar substrates, except for *cis*-9-hexadecenoyl-ACP. The respective unsaturated moiety solely serves as the substrate for FabF and not FabB, to be subsequently converted to *cis*-11-octadecenoyl-ACP (Edwards et al., 1997). FabF has a reduced K_m value at lower temperatures, allowing *E. coli* to alter its lipid composition and thus adjust its membrane fluidity depending on the temperature (de Mendoza & Cronan, 1983; Garwin et al., 1980).

After the FabB or FabF-catalyzed Claisen condensation, the growing acyl moiety is subsequently reduced by the NADPH-dependent *β*-ketoacyl-ACP reductase FabG to 3-hy-

droxyacyl-ACP (Lai & Cronan John, 2004), followed by *trans*-2-enoyl-ACP-forming dehydration by the *β*-hydroxydecanoyl-ACP dehydratase or the *β*-hydroxyacyl-ACP dehydratase FabA or FabZ, respectively (Bloch, 1971; Heath & Rock, 1996). Besides catalyzing the dehydration, FabA can also isomerize *trans*-2- to *cis*-3-decenoyl-ACP and is thus involved in the formation of unsaturated FA in *E. coli* due to the preservation of the respective double bond (Bloch, 1971; Heath & Rock, 1996). The last step of the elongation cycle is catalyzed by the enoyl-ACP reductase FabI, which forms acyl-ACP (Bergler et al., 1996; Heath & Rock, 1995). The enzyme accepts both NADH and NADPH as cofactors (Bergler et al., 1996). Acyl-ACP thioesters are either further elongated by FabB or FabZ or are used as precursors for membrane lipid synthesis. In *E. coli*, two routes are reported for the latter. Acyl-ACP is either directly phosphorylated by PlsX, followed by a PlsY-catalyzed condensation with glycerol-3-phosphate (Yoshimura et al., 2007). Alternatively, acyl-ACP can directly be condensed with glycerol-3-phosphate by PlsB (Cronan & Rock Charles, 2008).

Noteworthy, even though acyl-CoA thioesterases like the truncated version (‘TesA) of the *E. coli* TesA have been extensively used to engineer microbial FA production or to alter the FA chain length (Jawed et al., 2016; Plassmeier et al., 2016; Xu et al., 2013; Zheng et al., 2012), the biological function of those enzymes in *E. coli* remain unclear. As the type I thioesterase TesA is found in the organism’s periplasm, it was suggested that it is involved in hydrolyzing substrates, maybe even extracellularly (Cho & Cronan, 1993). The cytosolic type II thioesterase TesB could also not be linked to FA synthesis or the organism’s lipid composition (Naggert et al., 1991; Zheng et al., 2004).

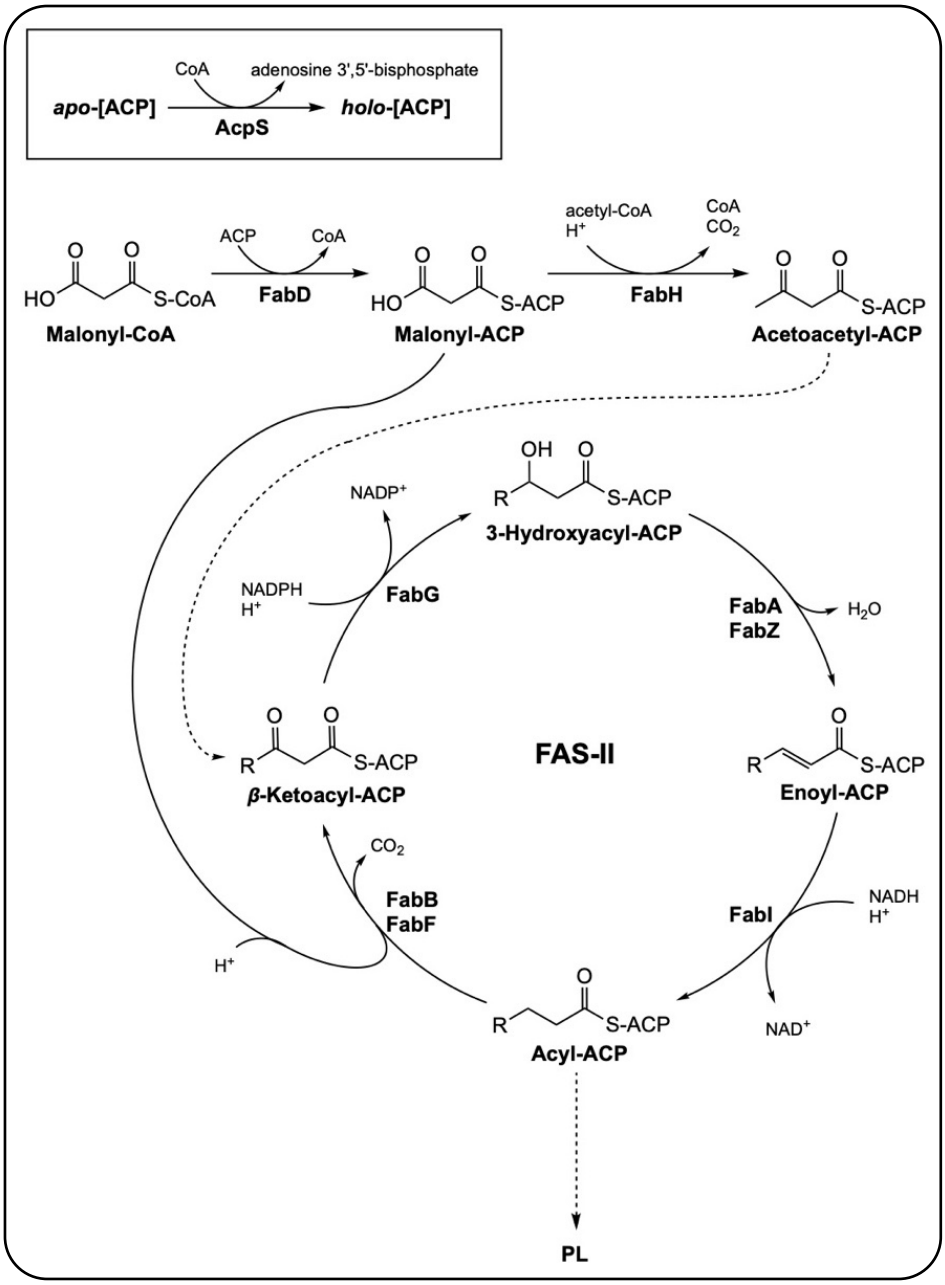

Figure 1: FAS-II system of *E. coli* as an example of bacterial FA biosynthesis. The dashed arrows represent multiple reactions and metabolites. AcpS (*acpS; holo*-[ACP] synthase); *apo*-[ACP] (*acpP*; *apo*-[acyl carrier protein]); FabA (*fabA*; *β*-hydroxydecanoyl-ACP dehydratase); FabB (*fabB*; *β*-ketoacyl-ACP synthase I); FabD (*fabD*; malonyl-CoA:ACP transacylase); FabF (*fabF*; *β*-ketoacyl-ACP synthase II); FabG (*fabG*; *β*-ketoacyl-ACP reductase); FabH (*fabH*; *β*-ketoacyl-ACP synthase III); FabI (*fabI*; enoyl-ACP reductase I); FabZ (*fabZ*; *β*-hydroxyacyl-ACP dehydratase). Abbreviated metabolites: PL (phospholipids). Enoyl-ACP is exemplified in its *trans*-2-enoyl-ACP isomer. FabI accepts both NADH and NADPH for the catalyzed

reduction (Bergler et al., 1996). Here, it is just depicted with NADH for simplification.

2.3.3 Microbial FA production strategies

Lipids and thus FA are formed by all living organisms primarily as precursors for membrane lipid biosynthesis. Additionally, neutral lipids often serve as energy storage. While all organisms produce FA and lipids, a few are known to produce and accumulate large amounts thereof. Those oleaginous organisms include species belonging to the genera *Yarrowia*, *Rhodosporidium*, *Arthrobacter,* and *Rhodococcus* (Patel et al., 2020). The latter, in particular, is known to reach a lipid content of around 80 % (w/w) of its cell dry weight (Alvarez et al., 1996). Generally, both oleaginous and non-oleaginous organisms alike have been successfully engineered to produce free FA and other lipids. Commonly used microbes are *Yarrowia lipolytica* (Gao et al., 2020; Park et al., 2018), *E. coli* (Jawed et al., 2016; Xu et al., 2013), *Saccharomyces cerevisiae* (Fernandez-Moya et al., 2015; Runguphan & Keasling, 2014), and *Rhodococcus opacus* (Alvarez et al., 2000; Huang et al., 2016). The industrially relevant bacterium *C. glutamicum* has also been used in some studies to produce triacylglycerides (Plassmeier et al., 2016) and FA (Ikeda et al., 2020; Takeno et al., 2023; Takeno et al., 2018; Takeno et al., 2013).

Strain engineering strategies often aim to (A) increase the pools of the intracellular metabolite malonyl-CoA, (B) facilitate acyl-CoA/ACP hydrolysis, (C) control the acyl chain length, (D) reduce FA degrading reactions, and (E) engineer cofactor supply. An increased flux towards the required precursor malonyl-CoA is commonly achieved by either transcriptionally deregulating the expression of acetyl-CoA carboxylase (ACC)-encoding genes (Takeno et al., 2013) or by directly overexpressing the relevant ACC subunits, often in combination with overexpression of a thioesterase to alleviate feedback inhibition by acyl-CoA/ACP (Davis et al., 2000; Lennen et al., 2010). Besides catalyzing the FA-forming hydrolysis of those respective thioesters, thioesterases can additionally be used to influence the chain length of the final released product in FAS-II-utilizing microbes. For this purpose, thioesterases with varying affinities for different acyl chain lengths' can be expressed to alter the organisms' FA portfolio (Jawed et al., 2016; Voelker & Davies, 1994). Production of short and medium-chain FA can also be achieved by an engineered reversal of the β-oxidation pathway (Dellomonaco et al., 2011). The underlying native pathway also plays a key role when trying to prevent FA degradation. In engineered *E. coli* mutants this is often achieved by deleting the acyl-CoA synthetase-encoding gene *fadD*. The encoded

enzyme catalyzes the first reaction in the FA-degrading β-oxidation pathway (Lennen et al., 2010). FA biosynthesis requires two molecules of either NADPH or NADH per elongation cycle. Therefore, cofactor engineering can be used to balance the demand and supply of the respective reduction equivalents (Wu et al., 2014; Zhang et al., 2020).

2.4 Microbial FAL biosynthesis

Microbial FAL production relies on intermediates and products of the FA biosynthesis as precursors. For the biosynthesis of FAL, two well-described pathways are commonly applied in the heterologous FAL production: (A) reduction of a free FA or of acyl-ACP/CoA to fatty aldehydes by a carboxylic acid reductase (CAR) or an aldehyde-forming fatty acyl-ACP/CoA reductase (AH-FAR) with a subsequent second reduction to a long-chain alcohol by an alcohol dehydrogenase (ADH) or aldehyde reductase (AHR) (Akhtar et al., 2013; Schirmer et al., 2010; Zhou et al., 2016). Alternatively, (B) a two-step reduction of an activated FA by an alcohol-forming fatty acyl-ACP/CoA reductase (AL-FAR; herby just referred to as FAR) (Cordova et al., 2020; Liu et al., 2013) with an aldehyde intermediate that is formed during the four-electron transfer but which is not released from the enzyme (Hofvander et al., 2011b; Willis et al., 2011). The latter pathway has been extensively exploited to heterologously produce FAL in various organisms such as *E. coli* (Liu et al., 2013), *S. cerevisiae* (Dabirian et al., 2019), and *Y. lipolytica* (Cordova et al., 2020) as it solely requires the expression of one gene and does not form free cytotoxic aldehyde intermediates. The commonly used NADPH-dependent FAR enzymes Maqu_2220 and Maqu_2507 of the marine bacterium *Marinobacter hydrocarbonoclasticus* VT8 were shown to accept both acyl-ACP and acyl-CoA as substrate, with a higher affinity for C16-C18 acyl-CoAs (Hofvander et al., 2011b; Willis et al., 2011). This renders both reductases promising candidates to be expressed in the industrially relevant bacterium *C. glutamicum*, as its native FA biosynthesis primarily produces palmityl-, stearyl- and oleoyl-CoA as intermediates (2.5.2) (Kawaguchi & Okuda, 1977; Schweizer & Hofmann, 2004b).

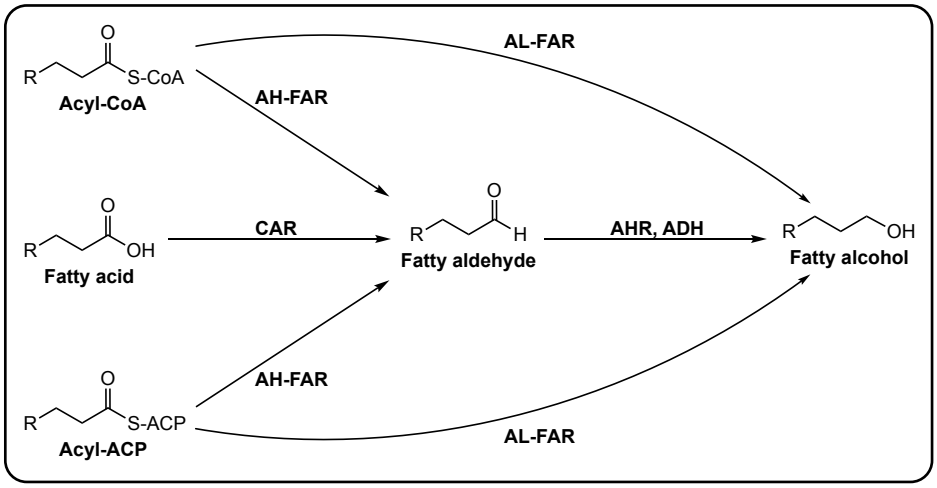

Figure 2: Possible routes for microbial FAL production. Displayed are five possible biological pathways to obtain FAL, starting from either FA, acyl-CoA, or acyl-ACP. Cofactors and other participating substrates or products are not shown. ADH: alcohol dehydrogenase; AH-FAR: aldehyde-forming fatty acyl-ACP/CoA reductase; AHR: aldehyde reductase; AL-FAR: alcohol-forming fatty acyl-ACP/CoA reductase (in this work solely referred to as FAR); CAR: carboxylic acid reductase. The graphic represents an altered version of the literature (Krishnan et al., 2020).

2.5 *Corynebacterium glutamicum* – a robust industrial organism

Ever since its discovery and subsequent characterization, the facultative anaerobic, gram-positive, and rod-shaped bacterium *Corynebacterium glutamicum* has been extensively studied and used industrially (Abe et al., 1967; Kinoshita et al., 1958). It was discovered as part of a comprehensive research program screening for organisms capable of accumulating L-glutamate extracellularly (Kinoshita et al., 1957). The originally named *Micrococcus glutamicus* was found to be capable of secreting large amounts of the respective amino acid, especially under biotin-limiting cultivation conditions (Eggeling & Bott, 2005; Kinoshita et al., 1957). Later studies revealed that the renamed bacterium *C. glutamicum* was able to accumulate not just glutamate but a variety of amino acids (Eggeling & Bott, 2005).

The biotin-auxotroph organism (Abe et al., 1967) belongs to the genus *Corynebacterium,* which is part of the family *Corynebacteriaceae*, which in turn is part of the suborder *Corynebacterineae*, as part of the order *Actinomycetales* (Stackebrandt et al., 1997). As a member of the suborder *Corynebacterineae*, *C. glutamicum* is closely related to mycobacteria

like *M. tuberculosis* (Liebl, 2005). Due to its fully sequenced genome (Ikeda & Nakagawa, 2003; Kalinowski et al., 2003), a large portfolio of well-established and accessible metabolic engineering methods and tools (Eggeling & Bott, 2005, pp. 537-568), advances in synthetic biology platforms (Woo & Park, 2014), its extensively researched metabolism and comprehensive literature (Eggeling & Bott, 2005), *C. glutamicum* ATCC 13032 has been an attractive organism for extensive strain engineering. Noteworthy, there are two known *C. glutamicum* ATCC 13032 variants whose genomes differ by about 27 kbp, mainly due to the presence of an additional prophage region in one of them (Ikeda & Nakagawa, 2003; Kalinowski et al., 2003).

C. glutamicum is *generally recognized as safe* (GRAS) and valued for its robustness. Remarkably, *C. glutamicum* is known to tolerate and metabolize inhibitors like aromatic compounds typically found in lignocellulosic hydrolysates (Becker & Wittmann, 2019; Ding et al., 2015; Shen et al., 2012; Siebert et al., 2021). Besides those phenolic compounds, *C. glutamicum* can natively utilize a variety of sugars, alcohols, and organic acids as single or combined carbon and energy sources (Becker & Wittmann, 2019; Eggeling & Bott, 2005; Merkens et al., 2005; Nishimura et al., 2007; Siebert et al., 2021; Takeno et al., 2007). Despite not being able to metabolize some substrates such as xylose and arabinose, its substrate spectrum has been expanded through metabolic engineering, enabling growth with those pentoses and also other substrates like lactose or galactose (Barrett et al., 2004; Lange et al., 2018; Sasaki et al., 2008).

Nowadays, the organism is an established workhorse for the large-scale production of several amino acids, such as L-lysine and L-glutamate, in millions of tons per year (Wendisch, 2020). Additionally, a variety of products such as FA, triacylglycerides, lactic, succinic, itaconic, 5-aminovaleric acid or 1,2-propanediol, 1-propanol, and isobutanol have been produced with *C. glutamicum* both from first- and second-generation feedstocks (Becker & Wittmann, 2012; Burgardt et al., 2021; Lange et al., 2017; Lange et al., 2018; Mao et al., 2018; Mhatre et al., 2022; Plassmeier et al., 2016; Sasikumar et al., 2021; Schmollack et al., 2022; Siebert & Wendisch, 2015; Takeno et al., 2013; Wolf et al., 2021). Ongoing scientific curiosity and industrial interest additionally fueled research into diversifying the substrate spectrum of *C. glutamicum*. Despite already being able to natively metabolize a variety of substrates (glucose, fructose, maltose, ethanol, acetate, lactate, etc.), the introduction of heterologous pathways enabled the utilization of novel carbon sources (xylose, arabinose, glycerol, cellobiose, etc.) (Becker & Wittmann, 2012; Blombach & Seibold, 2010; Buschke et al., 2013b; Zhao et al., 2018).

2.5.1 Central carbon metabolism

The central carbon metabolism of *C. glutamicum*, including sugar uptake, glycolysis, pentose phosphate pathway (PPP), and the tricarboxylic acid (TCA) cycle, have been extensively researched, engineered, and reviewed (Blombach & Seibold, 2010; Eikmanns, 2005; Yokota & Lindley, 2005). However, to fully understand the metabolic engineering strategies discussed in this work, this section provides a brief overview of the respective pathways and highlights some metabolic engineering targets.

The hexoses glucose and fructose, but also the disaccharide sucrose are primarily taken up in a phosphorylation-dependent manner, orchestrated by three different phosphoenolpyruvate (PEP)-dependent phosphotransferase systems (PTS), namely PTS^{Glc}, PTS^{Fru}, and PTS^{Suc}, respectively (Yokota & Lindley, 2005). Those three systems are constitutively expressed, allowing co-metabolization of the mentioned substrates (Dominguez et al., 1997; Yokota & Lindley, 2005). Once taken up, the respective phosphorylated sugars enter glycolysis at the level of glucose-6-phosphate or fructose-1,6-bisphosphate. The latter metabolite is formed by the phosphorylation of fructose-1-phosphate by 1-phosphofructokinase (Dominguez et al., 1998; Yokota & Lindley, 2005). Both glucose and fructose can also enter the cell in a PTS-independent manner via the glucose/*myo*-inositol permeases IolT1 and IolT2, followed by subsequent phosphorylation by the kinases Glk and PpgK (Bäumchen et al., 2009; Lindner et al., 2011). Expression of the IolT1-encoding gene *iolT1* is repressed by the GntR-type transcriptional regulator IolR in the absence of *myo*-inositol (Klaffl et al., 2013).

The PPP branches off glycolysis at the level of glucose-6-phosphate and can be divided into two distinct branches: the oxidative and the reductive branch. The oxidative branch of the PPP generates the cofactor NADPH in two separate, NADPH-forming reactions catalyzed by the glucose-6-phosphate dehydrogenase (G6PDH) and 6-phosphogluconate dehydrogenase (6PGDH) (Yokota & Lindley, 2005). The adjacent reductive branch provides anabolic precursors like ribose-5-phosphate and erythrose-4-phosphate but also refuels glycolysis at the levels of fructose-6-phosphate and glyceraldehyde-3-phosphate (Yokota & Lindley, 2005). Depending on the utilized substrates fluxes through the PPP, and thus NADPH regeneration vary strongly. For example, in *C. glutamicum* grown on glucose, 69 % of the provided carbon is channeled through the PPP (Bartek et al., 2011), while in fructose-grown cells, the carbon flux through the PPP is reduced to 20 % (Dominguez et al., 1998). Similarly, acetate (Wendisch et al., 2000) used as a primary carbon source was shown to drastically reduce carbon flux through the oxidative, NADPH-generating branch

of the PPP. In both cases, strongly increased TCA cycle activities were observed (Dominguez et al., 1998; Wendisch et al., 2000). Reducing power in the form of NADPH was thus provided by the $NADP^+$-dependent isocitrate dehydrogenase (ICD), and possibly also by the malic enzyme (MalE) (Dominguez et al., 1998; Eikmanns et al., 1995; Gourdon et al., 2000; Wendisch et al., 2000). As NADPH provision can become limiting in some processes, substantial effort has been invested to increase the cofactor's availability in some production strains. In that context, successful engineering strategies of *C. glutamicum* strains include the expression of the NADPH-regenerating *E. coli* transhydrogenase genes *pntAB* (Blombach et al., 2011; Kabus et al., 2007), replacement of the native glycolytic glyceraldehyde-3-phosphate dehydrogenase by an $NADP^+$-dependent homolog (Takeno et al., 2010), or increasing the carbon flux through the oxidative PPP branch. The latter approach was achieved by overexpression of genes involved in glyconeogenesis (*fbp*) and the oxidative PPP (*pgl*, *gnd*) (Ma et al., 2016), or by deleting the glycolytic-enzyme encoding genes *pfkA* and *gapA*, thus generating an artificially cyclized PPP (Siedler et al., 2013).

Important precursors like oxaloacetate and 2-oxoglutarate for anabolic processes, but also reducing equivalents and ATP (or GTP) are provided by the TCA cycle, in which acetyl-CoA is fully oxidized. The required substrate acetyl-CoA is usually formed by the oxidative decarboxylation of pyruvate, catalyzed by the thiamine pyrophosphate- (TPP) and Mg^{2+}-requiring pyruvate dehydrogenase complex (PDHC) (Eikmanns, 2005). However, some substrates like acetate or ethanol enter the metabolism directly at the level of acetyl-CoA (Arndt et al., 2008; Reinscheid et al., 1999). Since pyruvate is both an important precursor for microbial products and a product itself, several strain engineering approaches targeted the enzyme complex, which is comprised of several copies of the three subunits: pyruvate decarboxylase (E1p, *aceE*), dihydrolipoamide acyltransferase (E2, *aceF*), and lipoamide dehydrogenase (E3, *lpd*) (Eikmanns & Blombach, 2014). PDHC-deficient *C. glutamicum* mutants or strains with reduced PDHC activity were used to produce pyruvate, isobutanol, succinate, L-lysine, or L-valine (Eikmanns & Blombach, 2014). Besides the PDHC's substrate, its product acetyl-CoA is also of interest due to its role as a precursor for polyketides (Milke et al., 2019b), FA (Takeno et al., 2013), or polyphenols (Milke et al., 2019a). Strategies reducing the activity of the acetyl-CoA-consuming citrate synthase (CS) have been proven to be effective in increasing the metabolite's intracellular availability and, subsequently, the yields of acetyl-CoA-derived products (Chang et al., 2022; Milke et al., 2019a).

Due to its provision of anabolic precursors, metabolites of the TCA cycle need to be replenished. This is achieved by anaplerotic reactions of the PEP-pyruvate-oxaloacetate-node. Carboxylating reactions catalyzed by the PEP carboxylase (PEPCx) and the pyruvate carboxylase (PCx) regenerate oxaloacetate from PEP or pyruvate, respectively. The possession and simultaneous activity of both PEPCx and PCx is a rare feature of *C. glutamicum* in contrast to most other organisms (Eikmanns, 2005). Additionally, gluconeogenetic reactions of this metabolic node are the decarboxylation of oxaloacetate and malate. Oxaloacetate is decarboxylated to either PEP or pyruvate by the PEP carboxykinase (PEPCk) or the oxaloacetate decarboxylase (ODx), respectively. The conversion of malate into pyruvate is catalyzed by MalE in an NADPH-generating reaction (Eikmanns, 2005).

An overview of the native central carbon metabolism of *C. glutamicum* ATCC 13032, including parts of the glycolysis, the PPP, the TCA cycle, and lipid metabolism (discussed in more detail in sections 2.5.2 and 2.5.3) is depicted in Figure 3.

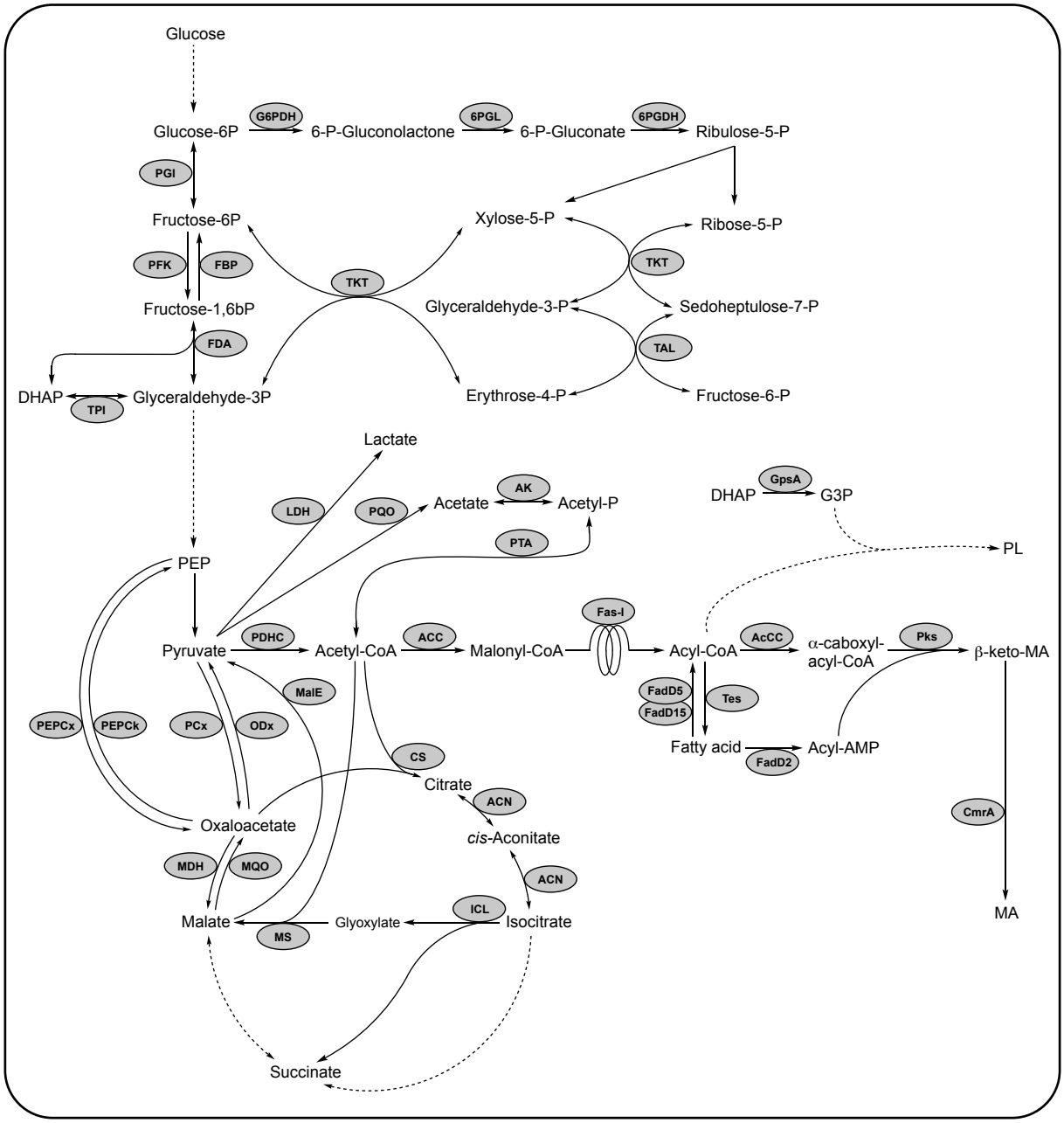

Figure 3: Schematic depiction of the central carbon metabolism of *C. glutamicum*. Parts of the glycolysis, PPP, TCA cycle, and lipid metabolism are shown. Enzymes and their corresponding reactions are visualized as grey ovals and black arrows, respectively. The dashed arrows represent multiple reactions and metabolites. 6PGDH (*gnd*; 6-phosphogluconate dehydrogenase); 6PGL (*pgl*; 6-phosphogluconolactonase); ACC (*accBC*, *accD1*, and *accE*; acetyl-CoA carboxylase complex comprising α-subunit, β-subunit and ε-peptide), AcCC (*accBC*, *accD2*, *accD3*, and *accE*; acyl-CoA carboxylase complex comprising α-subunit, β-subunit 2, β-subunit 3 and ε-peptide), ACN (*acnA*; aconitate hydratase), AK (*ackA*; acetate kinase), CmrA (*cmrA*; ketoacyl reductase), CS (*gltA*; citrate synthase), FadD2 (*fadD2*;

acyl-AMP ligase), FadD5 & FadD15 (*fadD5*, *fadD15*; acyl-CoA synthetase), Fas-I (*fasA*, *fasB*; fatty acid synthase type I), FBP (*fbp*; fructose 1,6-bisphosphatase), FDA (*fda*; fructose-bisphosphate aldolase), G6PDH (*zwf*, *opcA*; glucose-6P dehydrogenase), GPSA (*gpsA*; glycerol-3P dehydrogenase), ICD (*icd*; isocitrate dehydrogenase), ICL (*aceA*; isocitrate lyase), LDH (*ldhA*; L-lactate dehydrogenase), MalE (*malE*; malic enzyme), MDH (*mdh*; malate dehydrogenase), MQO (*mqo*; malate:quinone oxidoreductase), MS (*aceB*; malate synthase), ODx (*odx*; oxaloacetate decarboxylase), PCx (*pyc*; pyruvate carboxylase), PDHC (*aceE*, *aceF*, and *lpd*; E1p, E2, and E3 pyruvate dehydrogenase complex subunits), PEPCk (*pck*; phosphoenolpyruvate carboxykinase), PEPCx (*ppc*; phosphoenolpyruvate carboxylase), PFK (*pfk*; 6-phosphofructokinase), PGI (*pgi*; phosphoglucoisomerase), Pks (*pks*; polyketide synthase), PlsC (*plsC*; acyl-glycerol-3P acyltransferase), PQO (*pqo*; pyruvate:quinone oxidoreductase, PTA (*pta*; phosphotransacetylase), RPE (*rpe*; ribulose-5P-3-epimerase); TAL (*tal*; transaldolase); Tes (cg2692; acyl-CoA thioesterase), TKT (*tkt*; transketolase), TPI (*tpi*; triosephosphate isomerase). Abbreviated metabolites: DHAP (dihydroxyacetone phosphate), G3P (glycerol-3P), MA (mycolic acids), PEP (phosphoenolpyruvate), PL (phospholipids). The graphic represents an extended version of the literature (Eikmanns & Blombach, 2014) with emphasis on FA and MA biosynthesis.

2.5.2 FA biosynthesis using type I fatty acid synthases

The FA biosynthesis pathway in *C. glutamicum* provides precursors required for both membrane lipid and MA synthesis and is schematically visualized in Figure 4. The pathway contains the carboxylation of acetyl-CoA to malonyl-CoA by the ACC and the subsequent elongation cycles catalyzed by the two FAS-I Fas-IA and Fas-IB (Gande et al., 2007; Schweizer & Hofmann, 2004a). The pathway's precursor malonyl-CoA is supplied by the ATP-consuming carboxylation of acetyl-CoA, catalyzed by the ACC (Gande et al., 2007). The ACC consists of three subunits: the biotinylated α-subunit AccBC (biotin carboxylase), the β-subunit AccD1 (carboxyltransferase), and the non-catalytic ε-peptide AccE (Gande et al., 2007).

The successive condensation and elongation reactions of FA biosynthesis in *C. glutamicum* are catalyzed by two NADPH- and NADH-dependent FAS-I (Figure 4) (Ariga et al.,

1984; Radmacher et al., 2005). Thus, not only substrates but also products of the two multienzymes Fas-IA and Fas-IB are CoA-bound in contrast to ACP-bound thioesters found in FAS-II-utilizing microbes (Radmacher et al., 2005). Fas-IA produces oleoyl-CoA and was shown to be of essential function in *C. glutamicum*. The non-essential Fas-IB is responsible for the production of primarily palmityl-CoA and, to a lesser extent, stearyl-CoA (Radmacher et al., 2005). The mycobacterial and corynebacterial FAS-I multienzymes are structured similarly, with their domains arranged in the following order: AT-ER-DH-MPT-ACP-KR-KS (2.3.1) (Schweizer & Hofmann, 2004b). The KR requires NADPH as an electron donor, while the ER is NADH-dependent (Ariga et al., 1984). During the process, the growing acyl moiety remains bound to the ACP domain of the enzyme. Therefore, the respective domain first needs to be activated to become a functional *holo*-[ACP] domain by the transfer of a 4'-phosphopantetheine group catalyzed by a PPTase. *C. glutamicum* possesses two PPTase-encoding genes, *pptT* and *acpS*. PptT was shown to selectively 4'-phosphopantetheinylate the polyketide synthase Pks, while the *holo*-[ACP] synthase AcpS was responsible for the posttranslational modification of FAS-I (Chalut et al., 2006). Similarly, the mycobacterial homolog AcpS was suggested to also activate *apo*-[ACP] (AcpM) in *M. tuberculosis*, where the protein is an integral part of the organism's dissociative FAS-II system (Chalut et al., 2006). However, based on an *in vitro* study, Zimhony et al. (2015) reported that, in fact, the mycobacterial PptT 4'-phosphopantetheinylates AcpM in *M. tuberculosis*.

At the end of the acyl chain's elongation cycle, the acyl moiety is transferred by transacylation from the ACP domain to a free CoA by the MPT domain, forming acyl-CoA, which is used for membrane lipid biosynthesis (Knoche & Koths, 1973; Lynen et al., 1980; Schweizer & Hofmann, 2004b). This mechanism differs from animal FAS, which releases free FA due to an intrinsic thioesterase activity (Lin & Smith, 1978; Schweizer & Hofmann, 2004b). Hydrolysis of the respective acyl-CoA thioesters catalyzed by an acyl-CoA thioesterase (Tes) results in the formation of the free FA palmitic acid (hexadecenoic acid), stearic acid (octadecanoic acid), and the monounsaturated oleic acid (*cis*-9-octadecenoic acid) (Ikeda et al., 2020; Takeno et al., 2013). Those FA serve further as precursors for MA biosynthesis. The thioesterase-catalyzed hydrolysis of acyl-CoA and the opposing, acyl-CoA-forming reaction mediated by the two acyl-CoA synthetases FadD5 and FadD15 form a futile cycle to balance precursor pools required for both the membrane lipid and MA biosynthesis (Figure 3) (Ikeda et al., 2020).

FA biosynthesis is tightly regulated through feedback inhibition by FasR. The TetR-type transcriptional regulator inhibits transcription of both FAS-I-encoding genes *fasA* and *fasB* and of the ACC catalytic subunit-encoding genes *accD1* and *accBC* (Irzik et al., 2014; Nickel et al., 2010). The presence of the acyl-CoA effector molecules palmityl- and oleoyl-CoA is required for FasR to bind to the operator sequence *fasO*, located upstream of the respective genes (Irzik et al., 2014; Nickel et al., 2010). Deleting the FasR-encoding gene or mutating the *fasO* motif were shown to be effective approaches to alleviate the described feedback inhibition (Milke et al., 2019b; Takeno et al., 2013).

In contrast to many other organisms, including some other *Corynebacterium* species, *C. glutamicum* lacks several essential genes required for the *β*-oxidation of FA (Barzantny et al., 2012). This results in the organism's inability to utilize FA as a carbon source. Yet, exogenous FA can be incorporated into synthesized lipids (Ikeda et al., 2020; Radmacher et al., 2005). This metabolic feature can be exploited for the production of FA but also for FA-derived compounds.

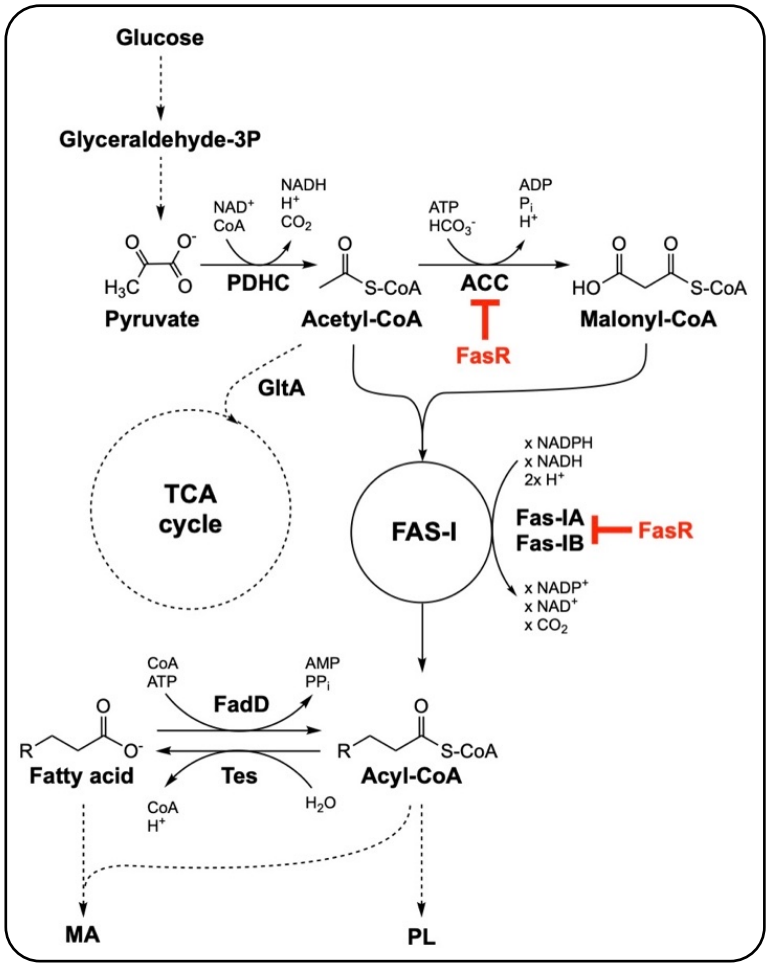

Figure 4: Lipid metabolism of *C. glutamicum*. The native FA biosynthesis is tightly regulated by the transcriptional regulator FasR in combination with the effector molecule acyl-CoA, repressing the transcription of the ACC subunit-encoding gene *accD1*, *accBC,* and of the FAS-I encoding genes *fasA* and *fasB* (Irzik et al., 2014; Nickel et al., 2010). The successive elongation of the acyl-moiety is catalyzed by two FAS-I, Fas-IA and Fas-IB. Each elongation cycle oxidizes one NADPH and one NADH until an acyl chain length of either 16 or 18 carbon atoms is reached. The dashed arrows represent multiple reactions and metabolites. ACC (*accBC*, *accD1*, and *accE*; acetyl-CoA carboxylase complex comprising α-subunit, β-subunit, and ε-peptide), FadD (*fadD5*, *fadD15*; acyl-CoA synthetase), Fas-IA & Fas-IB (*fasA*, *fasB*; fatty acid synthase type I), PDHC (*aceE*, *aceF*, and *lpd*; E1p, E2, and E3 pyruvate dehydrogenase complex subunits), Tes (cg2692; acyl-CoA thioesterase). Abbreviated metabolites: MA (mycolic acids), PL (phospholipids).

2.5.3 Mycolic acid biosynthesis

Despite being categorized as gram-positive organisms, *Mycobacterium*, *Nocardia*, *Rhodococcus,* and *Corynebacterium* species possess a membrane-like bilayer beyond their cell wall (Dover et al., 2004; Hsu et al., 2011; Marchand et al., 2012; Nishiuchi et al., 1999). This permeability barrier serves a similar function to the outer membrane of gram-negative bacteria, albeit being of different composition (Jackson, 2014). The so-called mycomembrane consists of MA, which are α-alkylated β-hydroxylated long chain FA differing in length and functional groups, depending on the organism (Barry et al., 1998; Liebl, 2005). They are synthesized by the Claisen-type condensation of an α-alkyl and a meromycolate chain (Portevin et al., 2004). Amongst other MA-producing organisms, *C. glutamicum* produces the shortest MA with a chain length ranging from 22 to 36 carbon atoms and modifies them only through desaturation (Barry et al., 1998; Collins et al., 1982b; Yang et al., 2012). Due to the generally occurring "mycolic motif", MA can be pyrolyzed into an aldehyde ("meroaldehyde") and a FA ("α-branch") at high temperatures, which allowed extensive structural studies of the respective fragments (Asselineau & Lederer, 1950; Barry et al., 1998; Collins et al., 1982b). That process is schematically depicted in Figure 5 with a $C_{32:0}$ MA, which is one of the most abundant MA species in *C. glutamicum* (Yang et al., 2012).

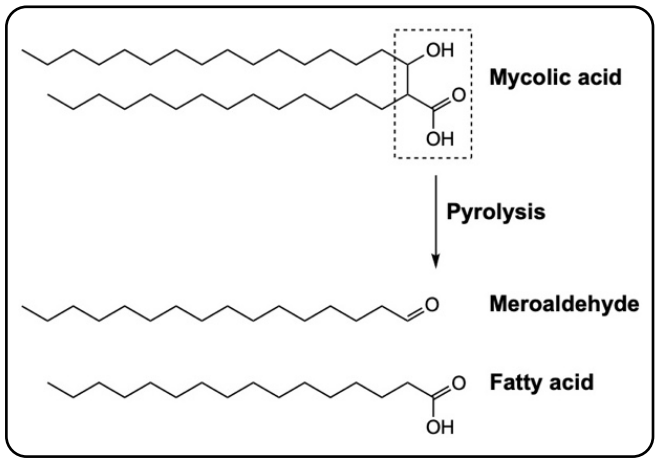

Figure 5: General structure of a *C. glutamicum* $C_{32:0}$ mycolic acid and cleavage by pyrolysis. This graphical representation was adapted from a figure published by Lanéelle et al. (2013). The mycolic motif (Lea-Smith et al., 2007) is highlighted by the dashed box.

The mycomembrane contributes to the reported resilience of MA-forming bacteria like *C. glutamicum* and *M. tuberculosis* to substances like antibiotics (Draper, 1998; Portevin et al., 2004) while also contributing to the virulence of the latter organism (Glickman et al.,

2000). Even though *C. glutamicum* devoid of an MA layer is viable, severe growth phenotypes were associated with a fully disrupted MA biosynthesis (Ikeda et al., 2020; Portevin et al., 2004; Takeno et al., 2018). In that context, it was shown that an impaired MA biosynthesis triggers the efflux of intracellular products like L-glutamate (Gebhardt et al., 2007) and FA (Takeno et al., 2018) due to an increased permeability. MA of the inner corynebacterial mycomembrane leaflet are either covalently bound to arabinogalactan attached to peptidoglycan of the cell wall or linked to trehalose as trehalose monocorynomycolate (TMCM) and trehalose dicorynomycolate (TDCM), while the outer lipid bilayer consists primarily of those free trehalose glycolipids (Daffé, 2005; Lanéelle et al., 2013).

In *C. glutamicum*, MA biosynthesis starts from the FA biosynthesis metabolites acyl-CoA and FA. For details regarding the respective pathway, refer to section 2.5.2. The α-alkyl chain is derived from acyl-CoA, which is carboxylated to α-carboxyl-acyl-CoA by the acyl-CoA carboxylase (AcCC) comprising of the subunits AccBC, AccD2, AccD3, and AccE (Gande et al., 2007; Gande et al., 2004). The α-subunit AccBC and the ε-peptide AccE are also part of the ACC (2.5.2) (Gande et al., 2007). To form the meromycolate chain, a FA is activated by the acyl-AMP ligase FadD2 to form acyl-AMP (Portevin et al., 2005). The products of FadD2 and the AcCC are condensed in a subsequent Claisen-type condensation by the polyketide synthase Pks, yielding β-keto-mycolate (Portevin et al., 2004). A reduction of the condensation product by the ketoacyl reductase CmrA results in the formation of MA (Lea-Smith et al., 2007). Mycoloyltransferases use mature MA as substrates to acylate either arabinogalactan or trehalose forming TMCM and TDCM (Brand et al., 2003; De Sousa-D'Auria et al., 2003; Tropis et al., 2005). The arabinogalactan-bound MA, together with TMCM and TDCM, form the corynebacterial mycomembrane (Daffé, 2005).

2.5.4 Heterologous D-xylose metabolization

Despite being able to utilize a broad spectrum of substrates, *C. glutamicum* is incapable of utilizing the pentose xylose as a carbon or energy source. Thus, enabling *C. glutamicum* to metabolize xylose has been an intensively studied research topic in order to more efficiently utilize xylose-rich lignocellulosic sugar mixtures (Gopinath et al., 2011; Kawaguchi et al., 2006; Lange et al., 2018; Meiswinkel et al., 2013; Radek et al., 2014; Sasaki et al., 2009). Two major heterologous pathways have emerged in that context: the xylose isomerase pathway (Kawaguchi et al., 2006) and the Weimberg pathway (Radek et al., 2014). In the isomerase pathway, xylose is first isomerized to xylulose by a heterologous xylose

isomerase (XylA), followed by xylulose-5-phosphate-forming phosphorylation by a heterologous or endogenous xylulokinase (XylB). Xylulose-5-phosphate itself is an intermediate of the reductive PPP branch, where it is quickly further metabolized. While a variety of XylA- and XylB-encoding genes of different organisms exist, the most effective gene combination for xylose utilization was found to be *xylA* of *Xanthomonas campestris* and overexpressed native *xylB* (Meiswinkel et al., 2013). However, when producing 2-oxoglutarate-derived amino acids from xylose via the isomerase pathway, about 17 % of the pentose-provided carbon is lost as CO_2, resulting in lower product yields (Radek et al., 2014). To mitigate the respective carbon loss, the Weimberg pathway of *Caulobacter crescentus* was introduced in *C. glutamicum* for more efficient xylose assimilation. Enzymes of this five-step pathway, encoded by the *xylXABCD* operon, convert xylose directly into the desired TCA cycle intermediate 2-oxoglutarate without any decarboxylation reactions by bypassing the PPP and glycolysis (Radek et al., 2014).

Even though xylose can natively be taken up by the glucose/*myo*-inositol permease IolT1 (Brüsseler et al., 2018), a variety of different heterologous xylose importers have been used to facilitate xylose utilization and co-metabolization with glucose. Amongst them are AraE of *Bacillus subtilis* (Mao et al., 2018), *C.glutamicum* ATCC 31831 (Sasaki et al., 2009) or *E. coli* (Yim et al., 2016), and XylE of *E. coli* (Yim et al., 2017). Targeting the xylose uptake has proven to be an effective approach to enable co-utilization of xylose and glucose (Brüsseler et al., 2018; Chen et al., 2017; Sasaki et al., 2009), avoiding otherwise diauxic growth behaviors under aerobic conditions (Kawaguchi et al., 2006; Radek et al., 2014; Sasaki et al., 2009; Wang et al., 2014).

Combined with the above-mentioned targeted metabolic engineering strategies, adaptive laboratory evolution (ALE) as a non-targeted approach has proven to be invaluable when further optimizing xylose utilization. An evolved, xylose-utilizing *C. glutamicum* mutant by Radek et al. (2017) displayed a mutation beneficial for xylose uptake in the transcriptional regulator IolR-encoding gene *iolR*, which subsequently led to the discovery of the native, IolT1-mediated xylose import (Brüsseler et al., 2018). Similarly, an engineered and evolved strain by Sun et al. (2022) exhibited beneficial synergistic mutations in the heterologous genes *araE* (xylose transport), *xylAB* (xylose utilization), and in the endogenous LacI-type regulator-encoding gene *ipsA*.

Similar to substrates like acetate or fructose (see 2.5.1), xylose-grown *C. glutamicum* isomerase pathway mutants exhibited a reduced carbon flux through the PPP, coupled with strongly increased TCA cycle activity (Buschke et al., 2013a).

Noteworthy, while some studies use lignocellulosic hydrolysates for their biological experiments (Gopinath et al., 2011; Mao et al., 2018; Mhatre et al., 2022), others use pure xylose or glucose/xylose mixtures as substrate instead (Chen et al., 2017; Kawaguchi et al., 2006; Meiswinkel et al., 2013; Sun et al., 2022). While the more defined experimental cultivation conditions of the latter approach enable a good understanding of how engineered strains perform with one or two carbon sources, it neglects the complex and often varying composition of second-generation substrates.

3. Material and methods

3.1 Chemicals, kits, software, and laboratory equipment

Chemicals (Table S. 1), their commonly used abbreviations (Table S. 2), commercial kits (Table S. 3), software (Table S. 4), and an overview of the most important equipment (Table S. 5) used in this study are outlined in the appendix. Kits were used according to the manufacturer's instructions.

3.2 Enzymes

All enzymes used in this study were purchased from New England Biolabs GmbH (Frankfurt am Main, Germany) and were used according to the manufacturer's instructions. A detailed enzyme list can be found in the appendix (Table S. 6).

3.3 Cultivation media

All media were prepared with deionized water (DI-H_2O) and were sterilized by autoclaving if not specified otherwise. Agar plates were prepared by adding 15 g agar-agar per liter of medium prior to autoclaving. The hot, agar-containing medium was poured into plastic petri dishes to cast the agar plates. If required, antibiotics were added aseptically to the hand-warm medium. Sterile liquid media were stored at room temperature, and agar plates were stored at 4 °C.

3.3.1 2x TY-based media

The complex medium 2x tryptone–yeast extract (2x TY) was routinely used to cultivate *E. coli* and found general application in the seed train for cultivation experiments with *C. glutamicum*. The medium was prepared according to a published procedure by Sambrook et al. (2001) and was sterilized by autoclaving. If required, antibiotics were added aseptically before inoculation. The complex medium's composition is listed in Table 1.

Table 1: Composition of 2x TY complex medium

Compound	Concentration | g L^{-1}
Tryptone	16
Yeast Extract	10
NaCl	5

3.3.2 BHI(S)

The complex media brain heart infusion (BHI) and BHI supplemented with sorbitol (BHIS) were routinely used in the preparation and transformation of electro-competent C*. glutamicum* (3.5.9.2). BHI contained BHI powder at a concentration of 37 g L^{-1} and was sterilized by autoclaving. BHIS was prepared by aseptically combining separately autoclaved sorbitol and BHI solutions to achieve the final concentrations depicted in Table 2. If required, antibiotics were added aseptically before inoculation.

Table 2: Composition of BHIS complex medium

Compound	Concentration | g L^{-1}
BHI powder	37
Sorbitol	91

3.3.3 CgXII medium

For shaking flask cultivation experiments with *C. glutamicum* (3.6.3), a modified version of the CgXII minimal medium (Buchholz et al., 2014; Eikmanns et al., 1991; Keilhauer et al., 1993) was used. It was prepared by adjusting the base medium consisting of $(NH_4)_2SO_4$, urea, 3-(N-morpholino)propanesulfonic acid (MOPS), K_2HPO_4, and KH_2PO_4 with 5 M KOH to a pH of 7.4. The medium was sterilized by autoclaving. Prior to inoculation, the base medium was complemented by the aseptic addition of $MgSO_4$ x 7 H_2O, $CaCl_2$ x 2 H_2O, biotin, and trace elements from sterile 1000x stock solutions. Glucose or wheat straw hydrolysate was added as a carbon source from sterile stock solutions. Additional supplements such as antibiotics, protocatechuic acid (PCA), $NaHCO_3$, or isopropyl β-D-1-thiogalactopyranoside (IPTG) were added aseptically when required.

The exact composition of CgXII with the compound's final concentrations (without carbon source or optional supplements) is shown in Table 3.

Table 3: Composition of the CgXII minimal medium

Compound	Concentration | g L^{-1}
$(NH_4)_2SO_4$	5
Urea	5
K_2HPO_4	1
KH_2PO_4	1
MOPS	21
Supplements	
D-biotin	$0.2 \cdot 10^{-3}$
$CaCl_2$ x 2 H_2O	$13.25 \cdot 10^{-3}$
$MgSO_4$ x 7 H_2O	0.25
Trace elements	
$CuSO_4$ x 5 H_2O	$0.313 \cdot 10^{-3}$
$FeSO_4$ x 7 H_2O	$16.4 \cdot 10^{-3}$
$MnSO_4$ x H_2O	$10 \cdot 10^{-3}$
$NiCl_2$ x 6 H_2O	$0.02 \cdot 10^{-3}$
$ZnSO_4$ x 7 H_2O	$1 \cdot 10^{-3}$

3.3.4 $CgXII_{mod}$ media variants

A derivate of the CgXII minimal medium was used as a high cell density medium in bioreactor cultivations ($CgXII_{mod}$) with *C. glutamicum* (3.6.4). The medium was prepared as described in 3.3.3. Its composition was similar to the standard CgXII medium (Table 3) but did not contain MOPS or urea, and the concentration of $(NH_4)_2SO_4$ was increased to 20 g L^{-1}. Either 20 or 40 g glucose L^{-1} was used as a carbon source.

Doubling the concentrations of $(NH_4)_2SO_4$, $MgSO_4$ x 7 H_2O, K_2HPO_4, and KH_2PO_4 to 40, 0.5, 2, and 2 g L^{-1}, respectively, in addition to doubling the added volume of trace element solution resulted in the $CgXII_{mod,2}$ medium. Further doubling of the $MgSO_4$ x 7 H_2O concentration to 1 g L^{-1} resulted in the $CgXII_{mod,3}$ medium, which is shown in Table 4. The respective medium was used for all bioreactor processes with hydrolysate and a final fed-batch process with glucose. Either 40 g glucose L^{-1} or the glucose equivalent of hydrolysate was used as a carbon source. Each experiment specifies in the respective chapters which $CgXII_{mod}$ version was used.

Table 4: Composition of the $CgXII_{mod,3}$ minimal medium

Compound	Concentration | g L^{-1}
$(NH_4)_2SO_4$	40
K_2HPO_4	2
KH_2PO_4	2
Supplements	
D-biotin	$0.2 \cdot 10^{-3}$
$CaCl_2$ x 2 H_2O	$13.25 \cdot 10^{-3}$
$MgSO_4$ x 7 H_2O	1
Trace elements	
$CuSO_4$ x 5 H_2O	$0.626 \cdot 10^{-3}$
$FeSO_4$ x 7 H_2O	$32.8 \cdot 10^{-3}$
$MnSO_4$ x H_2O	$20 \cdot 10^{-3}$
$NiCl_2$ x 6 H_2O	$0.04 \cdot 10^{-3}$
$ZnSO_4$ x 7 H_2O	$2 \cdot 10^{-3}$

3.3.5 NL-CgXII medium

The nitrogen-limiting CgXII derivate (NL-CgXII), containing 1.45 g urea L^{-1} as the sole nitrogen source, was used for shaking flask cultivation experiments with *C. glutamicum* prepared as described in section 3.3.3. The medium's final composition is shown in Table 5.

Table 5: Composition of the NL-CgXII minimal medium

Compound	Concentration | g L^{-1}
Urea	1.45
K_2HPO_4	1
KH_2PO_4	1
MOPS	21
Supplements	
D-biotin	$0.2 \cdot 10^{-3}$
$CaCl_2$ x 2 H_2O	$13.25 \cdot 10^{-3}$
$MgSO_4$ x 7 H_2O	0.25
Trace elements	
$CuSO_4$ x 5 H_2O	$0.313 \cdot 10^{-3}$
$FeSO_4$ x 7 H_2O	$16.4 \cdot 10^{-3}$
$MnSO_4$ x H_2O	$10 \cdot 10^{-3}$
$NiCl_2$ x 6 H_2O	$0.02 \cdot 10^{-3}$
$ZnSO_4$ x 7 H_2O	$1 \cdot 10^{-3}$

3.3.6 Stock solutions

All stock solutions were prepared with DI-H_2O. Sterilization was achieved by filtration through a 0.2 µm membrane, if not specified otherwise.

3.3.6.1 Antibiotics

Antibiotics were prepared as 1000x stock solutions and were stored at -20 °C. Working concentrations per milliliter were 50 µg kanamycin or 5 µg tetracycline.

3.3.6.2 Trace elements

Trace elements required to complement CgXII media were prepared as 1000x stock solutions and were stored at -20 °C. The pH was adjusted to 1 with 32 % HCl to dissolve all compounds prior to filtration. The exact composition and final concentration are stated in Table 3.

3.3.6.3 Magnesium sulfate and calcium chloride

$MgSO_4$ x 7 H_2O and $CaCl_2$ x 2 H_2O required to complement CgXII media were each prepared as 1000x stock solutions and were stored at -20 °C. The final concentration of both supplements is stated in Table 3.

3.3.6.4 Sodium bicarbonate

A 0.5 M $NaHCO_3$ stock solution (10x) was prepared freshly before each cultivation and used immediately to prevent carbon loss through CO_2 formation.

3.3.6.5 PCA

PCA was prepared as a 30 g L^{-1} (1000x) stock solution and was stored at -20 °C. An adequate amount of 10 M NaOH was added to dissolve the chemical prior to filtration (Eggeling & Bott, 2005, p. 539)

3.3.6.6 D-biotin

D-biotin was prepared as a 1000x stock solution and was stored at -20 °C. The final concentration is stated in Table 3.

3.3.6.7 D-glucose

Glucose for shaking flask experiments was prepared from glucose monohydrate as a 200 g L^{-1} stock solution and was stored at 4 °C.

Glucose stocks required for bioreactor cultivations were prepared with a concentration of either 300 or 400 g L^{-1}. Due to the increased viscosity, those bioreactor stock solutions were autoclaved and subsequently stored at room temperature.

3.3.6.8 Wheat straw hydrolysate

The wheat straw hydrolysate was obtained from Clariant (Muttenz, Switzerland). It is an intermediate product and substrate of the sunliquid® technology developed and used by the respective company. The hydrolysate's composition, according to an analysis conducted by the manufacturer, is shown in Table 6. The compounds' concentration in g L^{-1} was used to additionally calculate a corresponding carbon concentration in g_C L^{-1}.

Table 6: Composition of the used wheat straw hydrolysate. Displayed is an excerpt of the manufacturer's certificate of analysis.

Compound	Concentration | g L^{-1}	Carbon concentration | g_C L^{-1}
Glucose	380	152
Xylose	150	60
Acetate	24	9.78

For processing the acidic hydrolysate, an adequate amount was diluted with deionized water, and the pH was adjusted to 7 using 5 M KOH. Due to the hydrolysate's high viscosity, the required amount was obtained gravimetrically rather than by pipetting. The final volume was adjusted to obtain a stock solution containing the designated glucose concentration.

The growth medium used for shaking flask experiments was complemented using a stock with a glucose concentration of 125 g L^{-1}. The stock was sterilized by autoclaving, and precipitated solids were removed thereafter by centrifugation at 4000 x g for 20 min at room temperature. The particulate-free supernatant was decanted into a new vessel and was used for all shaking flask cultivations requiring hydrolysate as a carbon source.

$CgXII_{mod}$ used in bioreactor cultivations was complemented using a stock solution with a glucose concentration of 350 g L^{-1}. The stock solutions were solely centrifuged (4000 x g for 20 min, room temperature) after adjusting pH and volume, and the supernatant was used as a substrate without further processing.

3.3.6.9 IPTG

IPTG was prepared as a 1 M (1000x) stock solution and was stored at -20 °C.

3.4 Bacterial strains and plasmids

A detailed list of all strains and plasmids used in this study, including corresponding references, is given in the appendix in Table S. 7.

3.5 Molecular biology and strain engineering

3.5.1 Oligonucleotides

Oligonucleotides were purchased from Sigma-Aldrich Chemie GmbH (Taufkirchen, Germany) and are listed with name, sequence, purpose, and corresponding template in Table S. 8. Each oligonucleotide was designed with CloneManager (Sci Ed Software LLC, Westminster, United States) to have a melting temperature of 65 °C. Oligonucleotides required for the amplification of genes for further cloning purposes were designed to contain an artificial RBS (GAAAGGAGA) with a corresponding spacer (GGATTG) (Shi et al., 2018) upstream of the gene's start codon. If a DNA sequence was amplified to be further used in a Gibson Assembly reaction (3.5.8), the respective oligonucleotides were designed to contain about 20 bp homologous overlaps at their 5' end.

3.5.2 Polymerase chain reaction

DNA fragments required for cloning procedures were amplified in a polymerase chain reaction (PCR) (Mullis & Faloona, 1987; Saiki et al., 1985). The amplifications were performed using the Phusion® High-Fidelity DNA Polymerase (New England Biolabs GmbH, Frankfurt am Main, Germany) in a 50 µL reaction volume per fragment. The composition of one single PCR reaction is shown in Table 7, with its corresponding temperature program in Table 8. A purified plasmid (100 ng) or purified genomic DNA (1 ng) were used as templates for the amplification reaction.

Table 7: PCR reaction mixture to amplify DNA fragments using Phusion® polymerase

Compound	Volume | µL
Template DNA	(1-100 ng)
5x HF buffer	10
dNTPs (2 mM)	5
forward primer (10 µM)	2
reverse primer (10 µM)	2
DMSO	1.5
Phusion® Polymerase	0.5
DI-H_2O	*Ad* 50

Table 8: Temperature program for Phusion® PCR

	Step	Temperature	Time
	Initial Denaturation	98 °C	30 s
30 cycles	Denaturation	98 °C	30 s
	Annealing	60 °C	30 s
	Elongation	72 °C	30 s kb^{-1}
	Final Extension	72 °C	5 min
	Hold	10 °C	∞

3.5.3 Colony PCR

Colony PCR was applied to screen for positive/negative *C. glutamicum* and *E. coli* transformants and to verify successful deletions or integrations in *C. glutamicum*. A small amount of biomass served as the template for all reactions. It was obtained by touching a colony with a pipette tip, to be thereafter transferred into the corresponding reaction mixture.

All colony PCR products requiring no further sequencing were obtained by using the QuickLoad® *Taq* 2x Master Mix (New England Biolabs GmbH, Frankfurt am Main, Germany). The composition of one single 10 µL colony PCR reaction is shown in Table 9, with its corresponding temperature program in Table 10.

Table 9: Colony PCR reaction mixture to amplify DNA fragments using Quick-Load® *Taq* 2x Master Mix

Compound	Volume | µL
Template DNA (biomass)	-
forward primer (10 µM)	0.2
reverse primer (10 µM)	0.2
Quick-Load® *Taq* 2x Master Mix	5
DI-H_2O	*Ad* 10

Table 10: Temperature program for colony PCR using Quick-Load® *Taq* 2x Master Mix

	Step	Temperature	Time
	Initial Denaturation	94 °C	10 min
30 cycles	Denaturation	94 °C	30 s
	Annealing	60 °C	30 s
	Elongation	68 °C	1 min kb^{-1}
	Final Extension	69 °C	5 min
	Hold	10 °C	∞

Genomically integrated expression cassettes were amplified using a Phusion®-based colony PCR to be subsequently sent for sequencing. The composition of one single 50 µL Phusion® colony PCR reaction is shown in Table 11, with its corresponding temperature program in Table 12.

Table 11: Colony PCR reaction mixture to amplify DNA fragments using Phusion® polymerase

Compound	Volume | µL
Template DNA (biomass)	-
5x HF buffer	10
dNTPs (2 mM)	5
forward primer (10 µM)	2
reverse primer (10 µM)	2
DMSO	1.5
Phusion® Polymerase	0.5
DI-H_2O	*Ad* 50

Table 12: Temperature program for Phusion® colony PCR

	Step	Temperature	Time
	Initial Denaturation	98°C	3 min
30 cycles	Denaturation	98°C	30 s
	Annealing	60°C	30 s
	Elongation	72°C	30 s kb^{-1}
	Final Extension	72°C	5 min
	Hold	10°C	∞

3.5.4 DNA isolation and purification

Genomic DNA, PCR products, linearized and circular plasmids were purified using the following commercial kits from MACHEREY-NAGEL GmbH & Co. KG (Düren, Germany) according to the manufacturer's instructions: NucleoSpin® Microbial DNA, NucleoSpin® Gel and PCR Clean-up, NucleoSpin® Plasmid (Table S. 3). Each purification was conducted according to the manufacturer's instructions. Samples were eluted with DI-H_2O.

Solely genomic DNA of *M. hydrocarbonoclasticus* VT8 (DSM No.: 11845) was directly purchased from the German Collection of Microorganisms and Cell Cultures GmbH (Braunschweig, Germany) and therefore needed no purification.

3.5.5 Agarose gel electrophoresis

The length and purity of all PRC fragments and linearized plasmids were analyzed by separating them by size on a 1 % (w/v) agarose gel in an electric field. 10 g agarose L^{-1} were dissolved in the adequate amount of 1x TAE buffer (per liter: 4.84 g tris(hydroxymethyl)aminomethane, 1.142 mL acetic acid, 0.372 g ethylenediaminetetraacetic acid; pH 8.3) and was heated in a microwave until fully dissolved. The agarose solution was stored at 70 °C. 5 µL of GelGreen® Nucleic Acid Gel Stain (Biotium Inc., Fremont, United States) were added per 50 mL of liquid agarose solution prior to casting a gel. A comp was inserted into the freshly cast gel to form pockets. The solidified gel was placed into a Biometra Compact electrophoresis chamber (Analytik Jena GmbH, Jena, Germany) and was fully submerged with 1x TAE.

Routinely, 5 µL of Phusion® PCR reactions, linearized or digested plasmids were mixed with 1 µL of Gel Loading Dye, Purple (6x) (New England Biolabs GmbH, Frankfurt am Main GmbH, Germany), before loading them onto the solidified gel. Quick-Load® *Taq* 2x Master Mix colony PCR reactions were directly loaded onto the gel without any additional preparation. The Ready-to-Use 1 kb DNA Ladder (Biotium Inc., Fremont, United States) was used as the size standard for double-stranded DNA fragments.

Fragments were separated by size for 20-60 min at 140 V (Biometra Standard Power Pack P25 T; Analytik Jena GmbH, Jena, Germany). DNA bands were visualized and documented using an E-BOX CX5 TS System (Vilber Lourmat Deutschland GmbH, Eberhardzell, Germany).

3.5.6 Quantification of DNA concentration

Concentrations of DNA were determined by measuring the absorbance of 1 µL samples at 260 nm with a NanoPhotometer® NP80 (Implen GmbH, Munich, Germany). DI-H_2O was used as a blank.

3.5.7 Plasmid linearization

The plasmids pEKEx2 and pK19*mobsacB* were primarily cut with *Eco*RI-HF and *Sma*I (New England Biolabs GmbH, Frankfurt am Main, Germany), respectively. The construction of pK19*mobsacBlacI*^{q} required the linearization of pK19*mobsacB* with *Nhe*I-HF (New England Biolabs GmbH, Frankfurt am Main, Germany).

In general, 500 ng of plasmid were linearized in 25 µL batches containing 0.5 µL restriction enzyme and 2.5 µL CutSmart buffer (New England Biolabs GmbH, Frankfurt am Main, Germany) for 30 min. The remaining volume was filled up with DI-H_2O. All enzymatic digestions were conducted at 37 °C; solely *Sma*I was used at 25 °C. After incubating the mixture for 1 h at the designated temperature, 1 µL of the calf intestinal alkaline phosphatase-based Quick CIP (New England Biolabs GmbH, Frankfurt am Main, Germany) was added for dephosphorylating the linearized plasmid. The mixture was incubated for 10 min at 37 °C. The successful linearization was verified by agarose gel electrophoresis before purifying the fragment, as described in section 3.5.4.

3.5.8 Isothermal plasmid assembly (Gibson Assembly)

Plasmids were constructed by using the isothermal Gibson Assembly method (Gibson, 2011; Gibson et al., 2009). The composition of the required 5x Iso reaction buffer (Table S. 9) and the Iso enzyme-reagent mix (Table S. 10) is listed in the appendix.

Linearized, dephosphorylated plasmids were mixed with PCR fragments in a molar ratio of 1:3. 5 µl of that mixture were added to a 15 µL of the Iso enzyme-reagent mix and were incubated at 50 °C for 1 h. 10 µl of the incubated reaction mixture were subsequently used to transform chemically competent *E. coli* 3.5.9.1.

3.5.9 Preparation and transformation of competent cells

3.5.9.1 Chemically competent *E. coli*

Chemically competent *E. coli* DH5α for subsequent transformation by heat-shock were prepared following a protocol for $CaCl_2$ competent cells by (Sambrook et al., 2001). Briefly, 500 µl of a 2x TY *E. coli* overnight culture was used to inoculate 50 mL of 2x TY in a baffled shaking flask. The culture was then further incubated at 37 °C, 180 rpm, until the OD_{600} reached a value of about 0.5. The broth was transferred into a 50 mL tube, incubated on ice for 15 min, and then centrifuged at 4000 x g, 4 °C for 10 min. The supernatant was discarded, and the cell pellet was resuspended in 15 mL of an ice-cold 70 mM $CaCl_2$ 20 mM $MgSO_4$ solution. The mixture was incubated on ice for 30 min and centrifuged again at 4000 x g, 4 °C for 10 min. After discarding the supernatant, the cell pellet was suspended in 5 mL of the 70 mM $CaCl_2$ and 20 mM $MgSO_4$ solution and was incubated on ice. After 30 min, 1.25 mL of sterile 86 % (v/v) glycerol was added, and the cell suspension was aliquoted (100 µL) into pre-chilled 1.5 mL tubes and immediately frozen in liquid nitrogen. Competent cells were stored at -80 °C.

Chemically competent *E. coli* DH5α were transformed via heat-shock with Gibson Assembly reaction mixtures obtained from the procedure described in section 3.5.8. For that purpose, an aliquot of competent cells was thawed on ice, and 10 µL of the Gibson reaction mixture were added. The 30 min incubation step on ice was followed by a heat-shock at 42 °C for 1.5 min. The mixture was allowed to cool down on ice for 1 min before 1 mL of 2x TY was added to the reaction tube. After incubating the culture for 1 h at 37 °C, 180 rpm, 100 µL were plated out onto a 2x TY agar plate containing the correct antibiotic. The plates were incubated for 1 d at 37 °C.

3.5.9.2 Electrocompetent *C. glutamicum*

Competent *C. glutamicum* for electroporation were prepared based on a modified protocol by Liebl et al. (1989). Briefly, 5 mL BHI were inoculated with a single colony of the designated strain and was cultivated for 6-8 h at 30°C, 180 rpm. The entire broth was subsequently transferred into a 500 mL baffled shaking flask containing 50 mL BHIS and incubated overnight at 30 °C, 180 rpm. 5 mL of the overnight-grown culture were used to inoculate 250 mL BHIS in a 1 L baffled shaking flask, and were further cultivated at 30 °C, 120 rpm. The entire broth was harvested in 50 mL tubes at 4000 x g for 20 min at 4 °C when an OD_{600} of about 1.75 was reached. All of the following steps were conducted on ice. The supernatant was discarded after centrifugation, and pellets were resuspended in 20 mL ice-cold 10 % (v/v) glycerol solution. The resuspended cultures were pooled in two 50 mL tubes and centrifuged at 4000 x g for 15 min at 4 °C. The cell pellets were washed two more times, with increasing the centrifugation step by 2 min each round. The cell pellets obtained during the last centrifugation step were resuspended in 800 µl of the 10 % (v/v) glycerol solution. The cell suspension was aliquoted (150 µL) into pre-chilled 1.5 mL reaction tubes and frozen immediately with liquid nitrogen. Competent cells were stored at -80 °C.

Electrocompetent cells were transformed with correctly assembled plasmids via electroporation, followed by a heat-shock at 46 °C (Liebl et al., 1989; Tauch et al., 2002; van der Rest et al., 1999). Frozen cells were thawed on ice, and either 100 ng of an expression plasmid or up to 10 µg of a pK19*mobsacB*-based plasmid were added per aliquot. The solution was immediately transferred into a sterile, pre-chilled GenePulser®/MicroPulser™ electroporation cuvette (2 mm gap; Bio-Rad Laboratories, Hercules, USA) and was incubated on ice for 5 min. After electroporation at 2.5 kV for ~4 ms (Gene Pulser Xcell™, Bio-Rad Laboratories, Hercules, USA), the broth was transferred into 5 mL BHIS pre-heated to 46 °C and was subsequently incubated in a water bath at 46 °C for 6 min. The heat

shock was followed by an incubation at 30 °C, 180 rpm for 1-1.5 h before an adequate volume was plated onto a 2x TY agar plate containing the correct antibiotic. The plate was incubated at 30 °C for 2-3 days.

3.5.10 Sequencing

All relevant sequences of newly constructed plasmids and genomic integrations were verified via Sanger-Sequencing conducted by Microsynth Seqlab GmbH (Göttingen, Germany). Sequencing data was analyzed using CloneManager (Sci Ed Software LLC, Westminster, United States). Deletions were solely confirmed by analysis of colony-PCR fragments on an agarose gel.

3.5.11 Chromosomal alterations in *C. glutamicum*

Chromosomal alterations in *C. glutamicum* were introduced by using derivates of the non-replicative plasmid pK19*mobsacB* (Schäfer et al., 1994). Cells were transformed as described in section 3.5.9.2. Colonies growing 2-3 d after transformation were picked and used to inoculate 5 mL 2x TY with kanamycin. The culture was incubated for 6-8 h at 30 °C, 180 rpm, and 100 µL of a 1:20 to 1:50 dilution were plated onto 2x TY + 10 % (w/v) sucrose agar plates. The conversion of sucrose by the *sacB*-encoded levansucrase into the cytotoxic levan applies a selection pressure, forcing the transformants to either lose the *sacB*-containing plasmid backbone via a second homologous recombination event or by silencing the gene by mutation. Colonies growing after 2 d at 30 °C were picked and streaked out onto 2x TY and 2x TY + kanamycin agar plates and were incubated overnight at 30 °C. Clones solely growing on 2x TY without kanamycin were subjected to colony PCR (3.5.3). Integrations were additionally verified by sequencing the relevant chromosomal segment (3.5.10).

3.6 Cultivation experiments

3.6.1 General cultivation conditions

Shaken liquid cultures were cultivated in an orbital shaking incubator (Ø 25 mm, Multitron®2, INFORS GmbH, Einsbach, Germany) at 37 °C or 30 °C for *E. coli* or *C. glutamicum*, respectively. Shaking frequencies were 180 rpm or 120 rpm for all FAL and some FA cultivation experiments.

E. coli DH5α were always cultivated on 2x TY agar plates or in 2x TY liquid culture. *C. glutamicum* were standardly cultivated in 2x TY (complex medium pre-cultures & transformation), different CgXII derivates (minimal medium pre-culture & main culture), or in BHI and BHIS (preparation of competent cells & transformation).

3.6.2 Cryogenic cultures

All bacterial strains were maintained as a cryogenic culture in 30 % (v/v) glycerol and were stored at -80 °C. Cryogenic cultures were prepared by pipetting 1 mL of a culture grown overnight in 2x TY into a sterile cryogenic tube containing 0.5 mL 86 % (v/v) glycerol. The suspension was mixed gently before storing it in the freezer.

3.6.3 Shaking flask experiments

C. glutamicum was cultivated aerobically in 500 mL shaking flasks (4 baffles), following published seed train procedures (Siebert et al., 2021), as depicted in Figure 6.

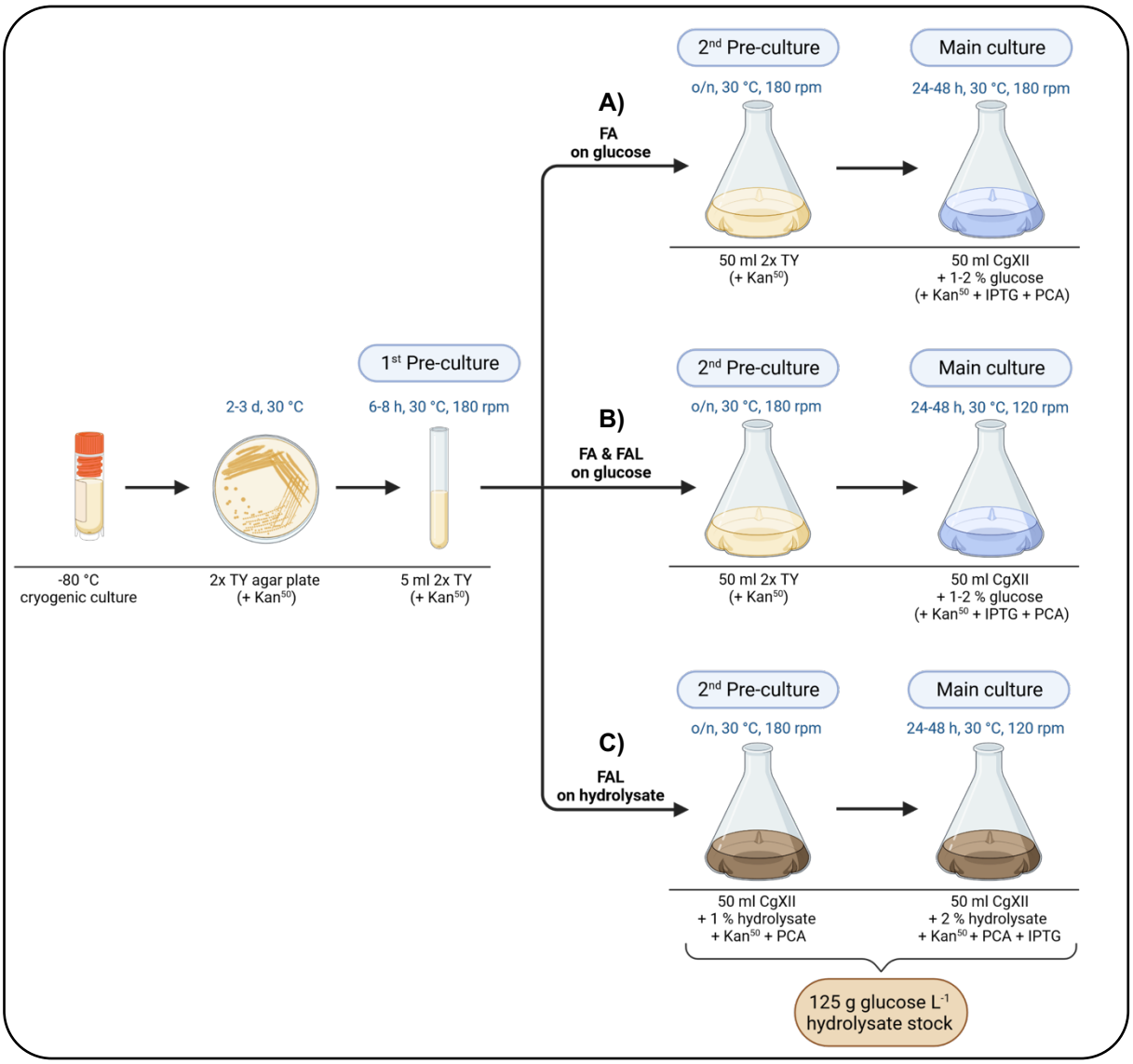

Figure 6: Seed train for shaking flask growth experiments. A) FA production on glucose at 180 rpm; B) FA and FAL production on glucose at 120 rpm; C) FAL production on wheat straw hydrolysate at 120 rpm. The first steps of the pre-culture preparation were similar for all three approaches, as indicated. Created with BioRender.com.

Briefly, designated strains were streaked from a cryogenic culture on 2x TY agar plates and were cultivated for 2-3 days. A single colony was used to inoculate 5 mL 2x TY in a reaction tube and was allowed to grow for 6-8 h (1st pre-culture), before the entire broth was transferred into 50 mL 2x TY (2nd pre-culture). If hydrolysate was the designated carbon source, 50 mL CgXII containing PCA and hydrolysate at a final glucose concentration of 10 g L^{-1} was inoculated instead. After cultivating the 2nd pre-culture overnight, the OD_{600} was measured, and an adequate culture volume was centrifuged at 4000 x g for 5 min to obtain an initial OD_{600} of 1 of the following main culture. The supernatant was discarded,

and the cell pellet was suspended in 50 mL of the required complemented minimal medium before ultimately transferring the inoculated medium into a shaking flask. Growth, substrate consumption, and product formation were monitored via OD_{600}, HPLC, or GC analysis as specified in the corresponding experiments.

All media were supplemented with antibiotics when required. Gene expression of plasmid-harboring strains was induced by adding 1 mM IPTG in the main culture.

3.6.4 Bioreactor cultivation

Bioreactor cultivations were conducted in a 1 L BioFlo120® bioreactor system (Eppendorf SE, Hamburg, Germany) with an initial cultivation volume of 0.5 L. The cultivations were performed at 30 °C using different $CgXII_{mod}$ variants, following the general seed train described in 3.6.3 and is visualized in Figure 7. The batch phase was conducted with per liter 20 to 40 g glucose or the equivalent amount of hydrolysate. The latter was provided by using a non-autoclaved hydrolysate stock solution with a glucose concentration of 350 g L^{-1} (3.3.6.8). The batch cultivation described in chapter 4.2.2.1 was conducted with 100 g glucose L^{-1}. In contrast to shaking flask cultivations, the initial OD_{600} was adjusted to be around 4. The pH was kept at 7.4 using a 5 M KOH solution. Dissolved oxygen (DO) was kept above 30 % by adjusting the agitation between 300 (400 for cultivations on hydrolysate) and 1500 rpm, with a constant air inflow rate of 0.25 L min^{-1} (0.5 vvm). If necessary, aeration was increased manually. Agitation was provided by a 6-bladed Rushton-type impeller. Default settings for both pH and DO control were used.

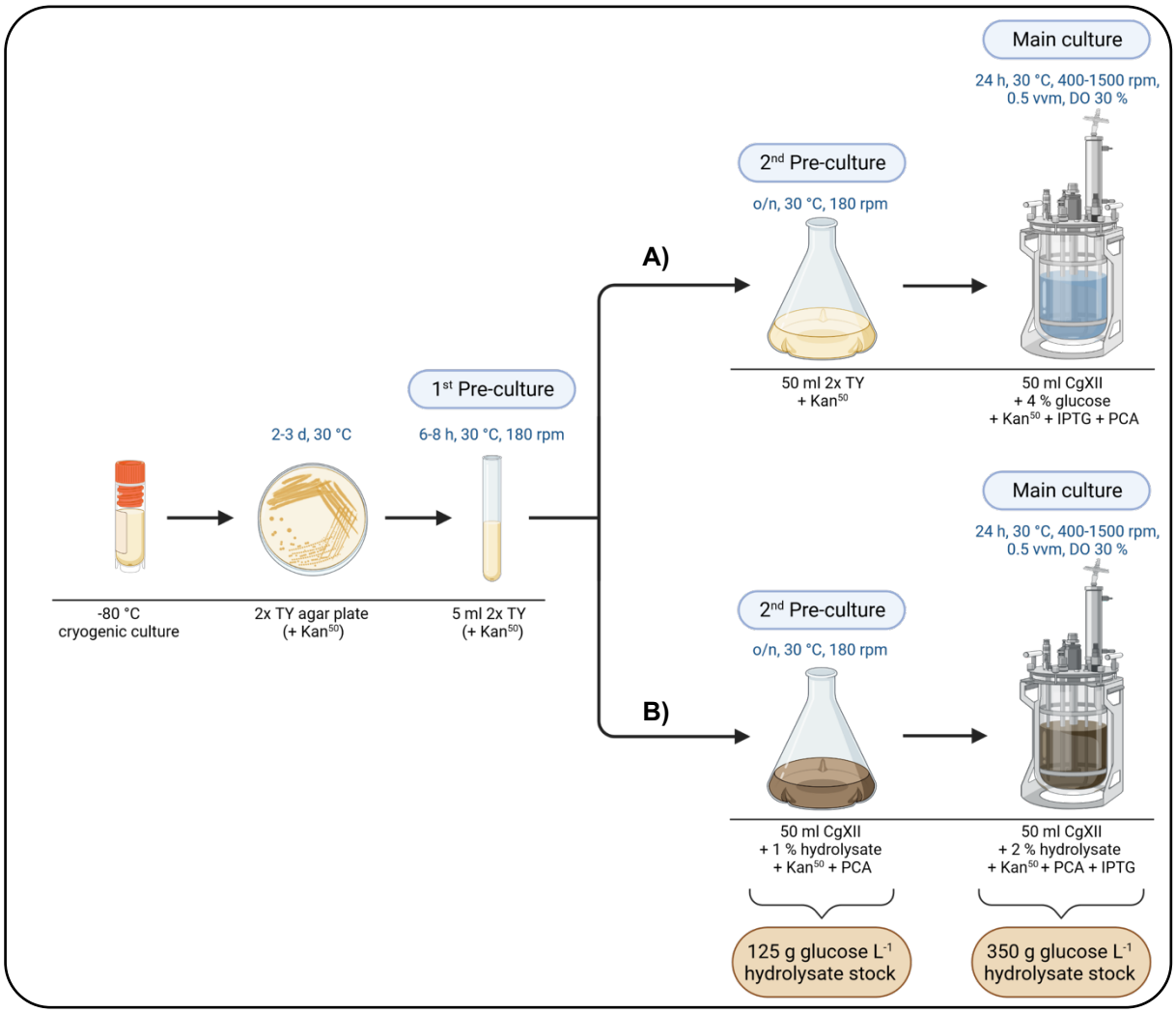

Figure 7: Seed train for bioreactor cultivations. A) FAL production on glucose; B) FAL production on hydrolysate. The first steps of the pre-culture preparation were similar for all three approaches, as indicated. Created with BioRender.com.

For glucose-based processes, an exponential feed profile adjusting the growth rate to 0.15 h^{-1} was started upon depletion of the carbon source, indicated by a spike of the DO. The required feed rate F(t) was calculated with eq. 1, where F_0 (mL h^{-1}) denotes the initial feed rate, μ_{set} (h^{-1}) is the adjusted growth rate, and t (h) is the time.

$$F(t) = F_0 * e^{\mu_{set} * t} \quad (1)$$

The initial feed rate F_0 was calculated using eq. 2-4 with the true biomass substrate yield $Y_{X/S}^{true}$ (g_{CDW} g^{-1}), the maintenance coefficient m_S (g g_{CDW}^{-1} h^{-1}), the biomass concentration

at the start of the fed-batch phase x_0 (g_{CDW} L^{-1}), the batch volume V_0 (L), the glucose concentration of the feed $c_{S,Feed}$ (g L^{-1}), the maximum specific growth rate μ_{max} (h^{-1}) and the apparent biomass substrate yield $Y_{X/S}$ (g_{CDW} g^{-1}).

$$F_0 = \left(\frac{\mu_{set}}{Y_{X/S}^{true}} + m_S\right) * \frac{x_0 * V_0}{c_{s,Feed}} = \frac{q_{s,m} * x_0 * V_0}{c_{s,Feed}} \quad (2)$$

$$q_S = \frac{\mu_{max}}{Y_{X/S}^{true}} + m_S = \frac{\mu_{max}}{Y_{X/S}} \quad (3)$$

$$Y_{X/S}^{true} = Y_{X/S} * \frac{\mu_{max}}{\mu_{max} - Y_{X/S} * m_S} \quad (4)$$

The published maintenance coefficient of 0.44 mmol g_{CDW}^{-1} h^{-1} (0.079 g g_{CDW}^{-1} h^{-1}) (Graf et al., 2020) was used for the shown calculations, while all other parameters were derived empirically for the specified strains. Generally, a $Y_{X/S}$ of 0.4 g_{CDW} g^{-1} was assumed.

Hydrolysate-based fed-batch processes were run by repeatedly pulsing 30 mL of a 350 g glucose L^{-1} hydrolysate stock solution upon depletion of the carbon source, as indicated by a spike of the DO. Samples for HPLC, GC, and TC analysis were taken before and after each pulse to accurately quantify the process.

3.7 Analytics

3.7.1 Biological replicates and general data analysis

Experimental data presented in this work was obtained from at least three independent biological replicates with individual seed trains and individually prepared batches of the minimal medium. If not stated otherwise, data represents means of ≥ 3 biological replicates with respective standard deviations. Due to the low sampling sizes, the Excel command “STABW.S” was used to calculate the respective standard deviations (Cumming et al., 2007). The underlying formula for the standard deviation SD is shown in eq. 5, where x represents a value in the data set, $\overline{x}$ is the mean of the data set, and n is the number of data points within the respective set.

$$SD = \sqrt{\frac{\sum(x-\bar{x})^2}{(n-1)}} \quad (5)$$

3.7.2 HPLC analysis

Glucose, xylose, pyruvate, lactate, and acetate were quantified via high-performance liquid chromatography (HPLC) using an Agilent 1260 Infinity II system (Agilent Technologies, Waldbronn, Germany) equipped with a Hi-Plex H column (7.7 x 300 mm, 8 µm) and a Hi-Plex H guard cartridge (3 x 5 mm, 8 µm). Samples were isocratically eluted at 50 °C for 35 min using 5 mM H_2SO_4 as a mobile phase with a flow rate of 0.4 mL min^{-1}. Analytes were detected via a refractive index detector (RID) kept at 50 °C (Siebert et al., 2021).

3.7.3 Qualitative glucose measurement

Growth experiments with glucose as the sole carbon source were qualitatively monitored by using test strips for glucose analysis (Medi-Test Glucose, MACHEREY-NAGEL GmbH & Ko. KG, Düren, Germany) to determine if glucose was fully consumed at designated sampling points. About 10 µL of culture broth were pipetted directly onto the test area of the strip and were allowed to soak into the paper. If no color change occurred, the test was interpreted as negative. The test's qualitative accuracy was verified by quantitative HPLC analysis prior to its regular application.

3.7.4 Quantification of FAL and FA

Gas chromatography (GC) was used to quantify FAL and FA, the latter in the derivatized form of FAME. All samples were analyzed on an Agilent 8890 GC system (Agilent Technologies, Waldbronn, Germany) equipped with an Agilent DB-FATWAX-UI GC column (30 m x 0.25 mm x 0.25 µm). The injected sample volume was 1 µL with a split ratio of 10:1 for FAL and extracellular FA samples. A split ratio of 50:1 was applied for intracellular FA samples. The initial oven temperature was 90 °C for 0.5 min, followed by a 40 °C min^{-1} ramp to 165 °C, held for 1 min, and a final 3 °C min^{-1} ramp to 230 °C, held for 10 min. The method was operated with a constant flow of 0.89 mL min^{-1} of the carrier gas nitrogen. The temperatures of the flame ionization detector (FID) and the inlet were maintained at 280 °C and 250 °C, respectively.

FAL were extracted and analyzed similar to previously described methods (Cao et al., 2015; Cordova et al., 2020; Wang et al., 2016). Briefly, 0.5 mL of either supernatant or culture broth were mixed with heptadecanol as an internal standard (ISTD) with a final concentration of 50 µg mL^{-1} and were extracted with 0.5 mL ethyl acetate for 30 min under vigorous vortexing. The organic phase was dried over sodium sulfate and subsequently

used for GC-FID analysis to determine extracellular and total FAL concentrations. Intracellular FAL concentrations were obtained by subtracting extracellular from total FAL concentrations.

Extracellular FA were extracted from 0.8 mL supernatant containing 62.5 µg heptadecanoic acid mL^{-1} as ISTD by the Bligh-Dyer method (Bligh & Dyer, 1959). 1 mL of the lipid-containing organic phase was evaporated under vacuum using a Concentrator plus (Eppendorf SE, Hamburg, Germany). The dried extracts were resuspended in 0.5 mL methanol and transferred into a glass tube with a PTFE-lined screw cap. Acid-catalyzed methylation was achieved by adding 1 mL of 5 % (v/v) methanolic H_2SO_4 to the samples and incubating them for 2 h in a water bath at 95 °C. After cooling to room temperature, 0.5 mL hexane were added, and the samples were vortexed vigorously. The acidic solution was neutralized by adding 2.5 mL aqueous 6 % (w/v) $NaHCO_3$ before transferring the hexane layer into a GC vial for analysis.

Intracellular FA were analyzed based on an acid-catalyzed whole-cell transesterification described previously (Plassmeier et al., 2016). Cell pellets obtained from 1 mL of cell culture were washed with 3 mL saline and subsequently dried at 70 °C before adding 50 µg heptadecanoic acid as an ISTD. 1 mL of 5 % (v/v) methanolic H_2SO_4 was added, and the samples were subjected to transesterification at 95 °C for 2 h. FAMEs were extracted with hexane using the same procedure applied for extracellular FA samples and were subjected to analysis. The total FA content of a sample was obtained by adding extracellular and intracellular FA concentrations.

FAL were quantified using authentic 1-hexadecanol, 1-octadecanol, and oleyl alcohol standards, while FA were quantified using palmitic acid and oleic acid standards. Relative FA content was defined as the ratio of the intracellular FA concentration to cell dry weight (CDW) when applicable.

3.7.5 Total organic carbon

The total organic carbon (TOC) content of hydrolysate-containing supernatants was determined as described previously (Buchholz et al., 2014) by using a Multi N/C 2100s analyzer (Analytik Jena, Jena, Germany). Briefly, to determine a sample's total carbon (TC) content, 100 µL culture supernatant were injected and combusted at 800 °C. For the determination of the total inorganic carbon (TIC) content, 100 µL sample were injected and subsequently

acidified with 10 % (w/v) o-phosphoric acid. CO_2 released by either procedure was measured by a nondispersive infrared sensor and used to derive the corresponding carbon content. The measured signals were converted into a carbon concentration in $g_C\ L^{-1}$ by applying calibration curves from Marc Schmollack, obtained from sodium carbonate and potassium hydrogen phthalate standard mixtures in the range of 0.1-1.5 $g_C\ L^{-1}$ (TIC) and 0.4-3 $g_C\ L^{-1}$ (TC), respectively. The TOC was calculated differentially from obtained TC and TIC data (eq. 6).

$$\mathrm{TOC} = \mathrm{TC} - \mathrm{TIC} \tag{6}$$

3.7.6 Determination of growth parameters

Growth was monitored by measuring the optical density at 600 nm (OD_{600}) using a Ultrospec® 10 Cell Density Meter (Biochrom Ltd, Cambridge, United Kingdom). A previously determined conversion factor of 0.23 was used to convert OD_{600} into a CDW biomass concentration in $g_{CDW}\ L^{-1}$ (Schmollack et al., 2022).

The growth rate μ (h^{-1}) was calculated by linear regression of $\ln(OD_{600})$ plotted vs. the cultivation time. If possible, the biomass yield $Y_{X/S}$ ($g_{CDW}\ g^{-1}$) was determined by linear regression of the biomass concentration during the exponential growth phase vs. the respective substrate concentration. The product yield $Y_{P/S}$ was always calculated differentially for the respective sampling points with the highest titers. It was calculated both in $g\ g^{-1}$ and $Cmol\ Cmol^{-1}$ for cultivations with glucose. The $Y_{P/S}$ for cultivations on hydrolysate was calculated differentially based on the total organic carbon consumed between the cultivation start and the sampling point with the highest measured FAL titer. Extracellular FAL concentrations were taken into account, and the corresponding carbon concentration was subtracted from the TOC data before forming the quotient of formed product over consumed carbon ($Cmol\ Cmol^{-1}$). The biomass-specific substrate uptake rate q_S ($g\ g_{CDW}^{-1}\ h^{-1}$) was calculated by dividing μ by $Y_{X/S}$. The volumetric productivity Q_P ($g\ L^{-1}\ h^{-1}$) was calculated by dividing the highest titer of a cultivation by the respective cultivation time.

4. Results

4.1 Physiological studies of the FA biosynthesis in *C. glutamicum*

The following section is dedicated to studying FA biosynthesis in *C. glutamicum* in order to gain novel insights into the respective biosynthetic pathway and to subsequently engineer an FA-producing mutant.

4.1.1 Decoupling the native FA biosynthesis from transcriptional regulation

4.1.1.1 Transcriptional regulator FasR

In the non-oleaginous bacterium *C. glutamicum*, the native FA biosynthesis pathway is tightly regulated by the transcriptional regulator FasR (Nickel et al., 2010). It was shown in that context that the "[…] loss of the function of *fasR* is essential for FA production by *C. glutamicum*" (Takeno et al., 2013). Therefore, *C. glutamicum* Δ*fasR* was constructed to obtain an initial chassis strain with deregulated FA biosynthesis.

Even though FA production increased from 383 ± 8 to 452 ± 7 mg_{FA} L^{-1} upon deleting *fasR*, solely a small fraction thereof was measured extracellularly when cultivated in CgXII medium (Figure 8). This observation was in contrast to previous reports of high extracellular FA concentrations in similar *C. glutamicum* mutants (Ikeda et al., 2020; Plassmeier et al., 2016; Takeno et al., 2018; Takeno et al., 2013).

Upon cultivation in the modified minimal medium NL-CgXII containing 1.45 g urea L^{-1} as the sole nitrogen source, FA efflux was observed (Figure 8). Simultaneously, the relative FA content of the Δ*fasR* mutant strongly increased from 57 ± 2 to 120 ± 16 mg_{FA} g_{CDW}^{-1} and was even 2.7 times higher compared to the wild type (WT), indicating nitrogen-starvation-induced lipid accumulation (Figure 8).

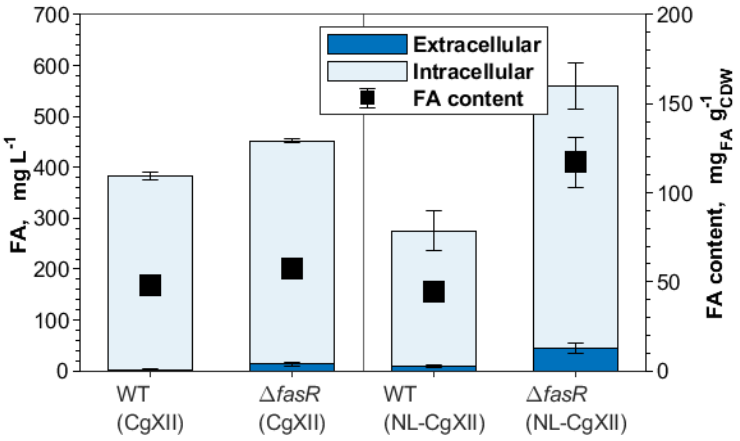

Figure 8: FA production in CgXII and NL-CgXII medium. Cultivations of *C. glutamicum* ATCC 13032 (WT) and the Δ*fasR* mutant were conducted in standard CgXII and in the nitrogen-limiting NL-CgXII medium with 20 g glucose L^{-1}. Samples for analysis were taken after 24 h. Data represents the means of ≥ 3 biological replicates with standard deviations.

FA secretion and accumulation thereof was exclusively observed in the Δ*fasR* mutant upon entering the nitrogen limitation-induced stationary phase after 12 h (Figure 9, B1 and B2), further supporting the positive impact of nitrogen starvation on FA production. The engineered strain produced 524 ± 29 mg_{FA} L^{-1} during 24 h of cultivation time, of which 56 ± 3 mg_{FA} L^{-1} were found extracellularly. This corresponded to a more than 2-fold increase in total FA production and a more than five times higher extracellular FA titer compared to the WT (Figure 9, Table 13). This observation was further supported by the calculated $Y_{P/S}$, which increased by more than two-fold in the Δ*fasR* strain from 20 ± 2 mg_{FA} g^{-1} during the growth phase to 46 ± 10 mg_{FA} g^{-1} during the nitrogen limitation-induced stationary phase (Table 13). The product yield, including both production phases, was 25 ± 1 mg_{FA} g^{-1}. In comparison, the WT achieved a $Y_{P/S}$ of 13 ± 1 mg_{FA} g^{-1} during the entire cultivation, with a yield of solely 2 ± 2 mg_{FA} g^{-1} during the stationary phase (Table 13). Generally, key performance indicators (KPI) such as the product yield and final FA titers were strongly increased in Δ*fasR* mutants.

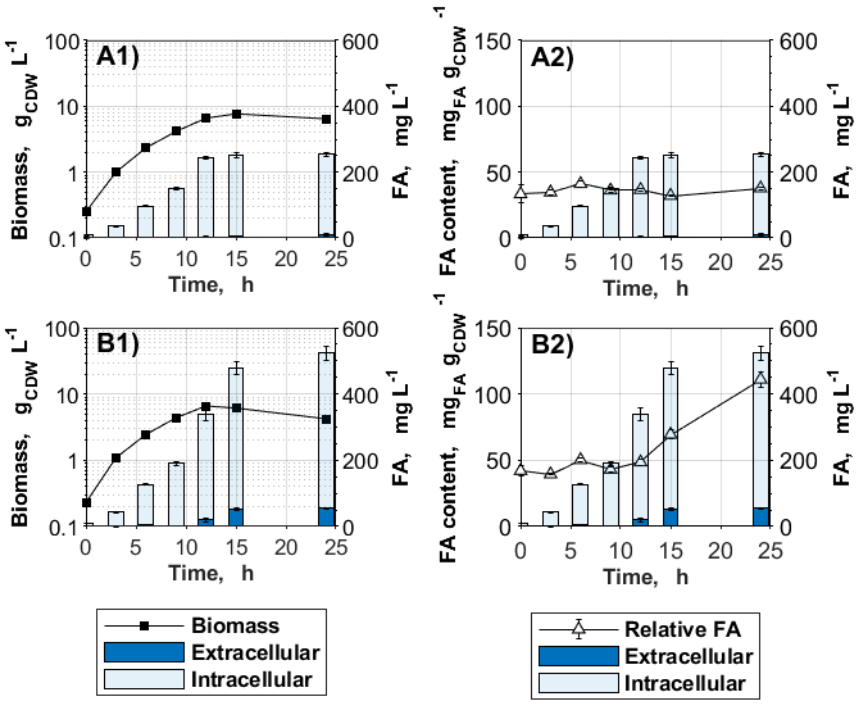

Figure 9: Influence of *fasR* deletion on FA production under nitrogen-limiting conditions. Cultivations were conducted in the nitrogen-limiting NL-CgXII minimal medium containing per liter 20 g glucose as the carbon source. A) *C. glutamicum* ATCC 13032 (WT); B) *C. glutamicum* Δ*fasR*. 1) displays growth and FA production kinetics, while 2) compares FA production and the relative FA content. Data represents the means of ≥ 3 biological replicates with standard deviations.

Table 13: KPI of *C. glutamicum* ATCC 13032 (WT) and *C. glutamicum* Δ*fasR* cultivated under nitrogen-limiting conditions. Cultivations were conducted in NL-CgXII with 20 g glucose L^{-1} as the sole carbon source. Data represents the means of 3 biological replicates ± standard deviations.

KPI	Interval | h	WT	Δ*fasR*
μ | h^{-1}	6-12	0.17 ± 0.01	0.16 ± 0.00
$Y_{X/S}$ | g g^{-1}	0-12	0.42 ± 0.00	0.38 ± 0.01
	0-12	16 ± 1	20 ± 2
$Y_{P/S}$ | mg g^{-1}	12-24	2 ± 2	46 ± 10
	0-24	13 ± 1	25 ± 1
$c_{FA, Extra}$ | mg L^{-1}	24	10 ± 5	56 ± 3
$c_{FA, Intra}$ | mg L^{-1}	24	243 ± 9	468 ± 26
$c_{FA, Total}$ | mg L^{-1}	24	253 ± 10	524 ± 29

Due to the observed positive impact of nitrogen starvation on FA production, the nitrogen-limited NL-CgXII medium was used for all subsequent cultivations.

4.1.1.2 Influence of the FAS-I system and the ACC on FA production

Decoupling FA synthesis from FasR-mediated transcriptional regulation was shown to be essential for efficient FA production in *C. glutamicum* (Takeno et al., 2013). Besides deleting *fasR*, a second strategy was pursued, simultaneously aiming at the directed decoupling of FasR-controlled transcription of *fasA*, *fasB*, *accD1*, and *accBC*. Since the FasR-binding motif *fasO* is located within or downstream of the respective promoter regions of those four genes essential for FA synthesis (Nickel et al., 2010; Pfeifer-Sancar et al., 2013), a promoter exchange strategy was chosen.

Exchanging the native promoter sequences of both FAS-encoding genes for the strong, constitutive promoter of the elongation factor TU (P_{tuf}) led to a decrease of FA production in the resulting *C. glutamicum* P_{tuf}-*fasAB*, emphasizing the reported importance of the acetyl-CoA carboxylase (ACC) in FA synthesis (Ikeda et al., 2017; Milke et al., 2019a; Schweizer & Hofmann, 2004b).

Therefore, both genes encoding for the catalytically active subunits of the ACC, AccD1, and AccBC were overexpressed using the constructed plasmid pEKEx2_*accD1BC*. The plasmid contained both genes *accD1* and *accBC*, each preceded by a strong synthetic

RBS and spacer described by Shi et al. (2018) in an operon configuration. Due to a sequence overlap of the *fasO* motif and the encoding sequence of *accD1* (Nickel et al., 2010), the nucleotides of the conserved *fasO*-engulfing region were altered as described by Milke et al. (2019b).

pEKEx2_*accD1BC*-harboring WT and *C. glutamicum* P_{tuf}-*fasAB* strains displayed an increased intra- and extracellular FA production compared to their empty plasmid control strains (Figure 10 A1-2, C1-2), emphasizing the ACC's role in FA synthesis. Total FA production was increased from 241 ± 8 and 220 ± 1 $mg_{FA}\ L^{-1}$ by about 50 % and 130 % to 369 ± 4 and 505 ± 153 $mg_{FA}\ L^{-1}$, respectively.

However, strongly varying extracellular FA concentrations of *C. glutamicum* P_{tuf}-*fasAB* (pEKEx2_*accD1BC*) and generally lower intracellular FA concentrations compared to the Δ*fasR* mutant (532 ± 54 $mg_{FA}\ L^{-1}$) were observed. Therefore, decoupling FA synthesis from transcriptional regulation by exchanging the *fasO* motif-containing native promoters did not prove to be superior to the simpler approach of deleting *fasR.* Though, ACC overexpression in a Δ*fasR* strain background further improved FA production. Intra- and extracellular FA concentrations increased from 483 ± 51 $mg_{FA}\ L^{-1}$ and 49 ± 3 $mg_{FA}\ L^{-1}$ to 585 ± 61 and 77 ± 14 $mg_{FA}\ L^{-1}$, respectively.

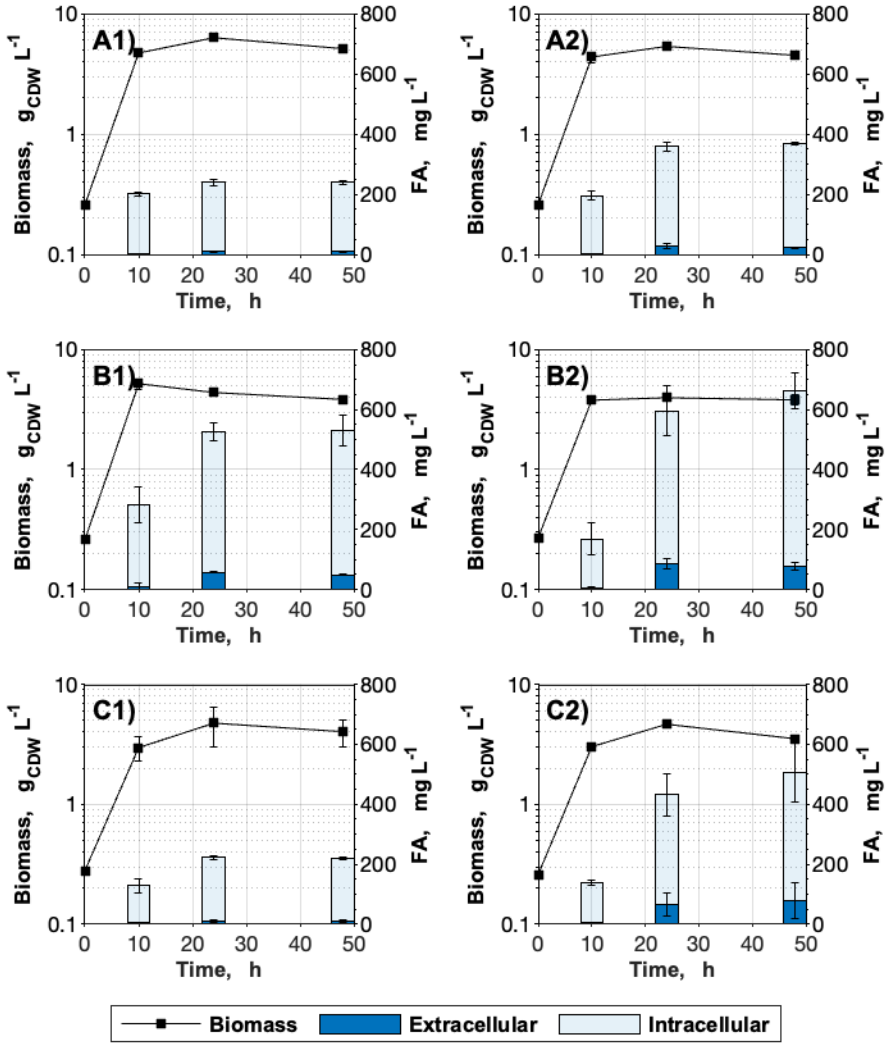

Figure 10: Impact of ACC overexpression on FA synthesis. Cultivations were conducted in the nitrogen-limiting NL-CgXII minimal medium containing per liter 20 g glucose as the carbon source. A) *C. glutamicum* ATCC 13032, B) *C. glutamicum* Δ*fasR* or C) *C glutamicum* P_{tuf}-*fasAB* harboring either 1) pEKEx2 or 2) pEKEx2_*accD1BC*. Data represents the means of ≥ 3 biological replicates with standard deviations.

4.1.2 Reduction of acyl-CoA-consuming side reactions by *sigD* deletion

Mycolic acid (MA) synthesis provides a metabolic sink for acyl-CoA, therefore competing with the production of FA and FA-derived products. Decreasing the enzymatic activity of acyl-CoA-consuming enzymes (Takeno et al., 2018) and deletion of key enzymes involved in MA production (Ikeda et al., 2020) were shown to be suitable approaches to increase extracellular FA titers in *C. glutamicum*. The SigD-encoding gene *sigD* poses a promising target in that context, as Taniguchi et al. (2017) observed decreased transcript levels of genes in the pathway such as *accE*, *accD2*, *accD3*, *fadD2*, and *pks* upon deletion of the sigma factor-encoding gene. Those published results highlighted the sigma factor's role in mycomembrane synthesis and cell wall integrity (Taniguchi et al., 2017) (Figure 11).

Complete deletion of mycolic acid-synthesizing genes such as *pks* were shown to drastically increase doubling times (Portevin et al., 2004). It was therefore hypothesized that deleting *sigD* in an FA-producing *C. glutamicum* strain instead might decrease consumption of FA, increase efflux thereof and avoid undesired negative growth phenotypes.

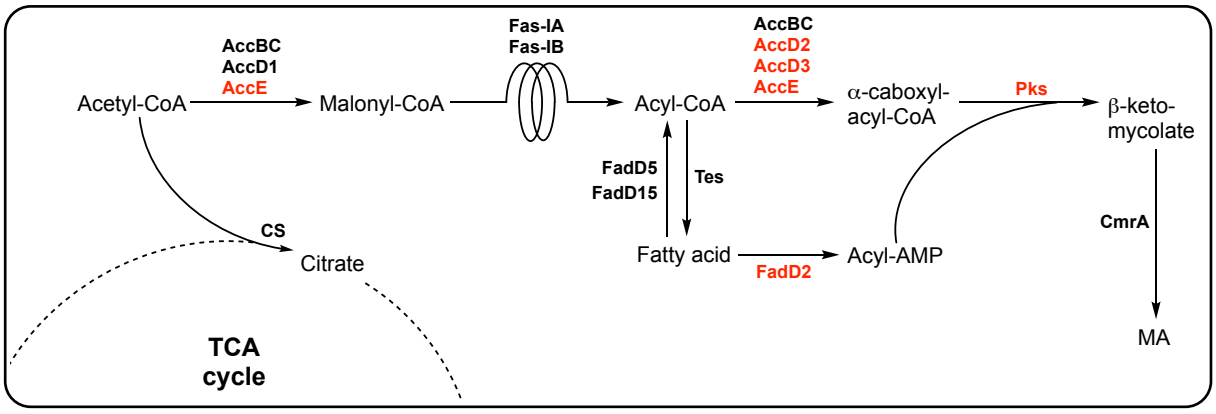

Figure 11: Simplified MA biosynthetic pathway. Expression of the genes encoding for the red-highlighted enzymes and enzymatic subunits is σ^D-dependent. AccBC: acetyl-CoA carboxylase α-subunit; AccD1: acetyl-CoA carboxylase β-subunit; AccD2: acyl-CoA carboxylase β-subunit; AccD3: acyl-CoA carboxylase β-subunit; AccE: acetyl-CoA carboxylase ε-peptide; CmrA: mycolate reductase; CS: citrate synthase; FadD2: acyl-AMP ligase 2; FadD5: acyl-CoA synthetase 5; FadD15: acyl-CoA synthetase 15; Fas-IA: type I fatty acid synthase A; Fas-IB: type I fatty acid synthase B; MA: mycolic acid; TCA cycle: tricarboxylic acid cycle; Tes: fatty acyl-CoA thioesterase; Pks: polyketide synthase.

Interestingly, deleting *sigD* in the FA-producing *C. glutamicum* Δ*fasR* resulted in a morphological change of the colonies' shape. The usually smooth colonies turned rough in the Δ*sigD* mutant. Similar morphological changes were reported for *C. glutamicum* Δ*pks* mutants, indicating alterations of the mycolic acid layer (Portevin et al., 2004).

Besides, the sigma factor's deletion led to a more than two-fold decreased FA production and additionally to extracellular pyruvate titers of up to 3.06 ± 1.38 g L^{-1}, as depicted in Figure 12 B) and Figure 12 E), respectively. It was hypothesized that the reported decrease of *accE* transcripts (Taniguchi et al., 2017) negatively affected the ACC-catalyzed flux towards malonyl-CoA, thus resulting in pyruvate accumulation and subsequent efflux thereof. To counteract the observed effect, the acetyl-CoA carboxylase ε-peptide-encoding gene *accE* was expressed in a *C. glutamicum* Δ*fasR* Δ*sigD* strain background using a pEKEx2-based plasmid.

FA synthesis could be restored upon plasmid-based expression of *accE* in a Δ*fasR* Δ*sigD* mutant (Figure 12 D). Even though intracellular FA concentrations of the pEKEx2_*accE*-harboring strains (447 ± 57 mg_{FA} L^{-1}) were still reduced on average by 15 % compared to the *C. glutamicum* Δ*fasR* control (529 ± 74 mg_{FA} L^{-1}), extracellular FA concentrations increased by 34 % from 49 ± 16 to 66 ± 28 mg_{FA} L^{-1}. Additionally, maximal pyruvate concentrations in the supernatant of *C. glutamicum* Δ*fasR* Δ*sigD* (pEKEx2_*accE*) culture broths decreased to 0.81 ± 1.17 g L^{-1}, indicating a restored flux through the ACC compared to the Δ*fasR* Δ*sigD* parental strain. HPLC analysis showed that glucose was fully consumed by all strains after 24 h (data not shown).

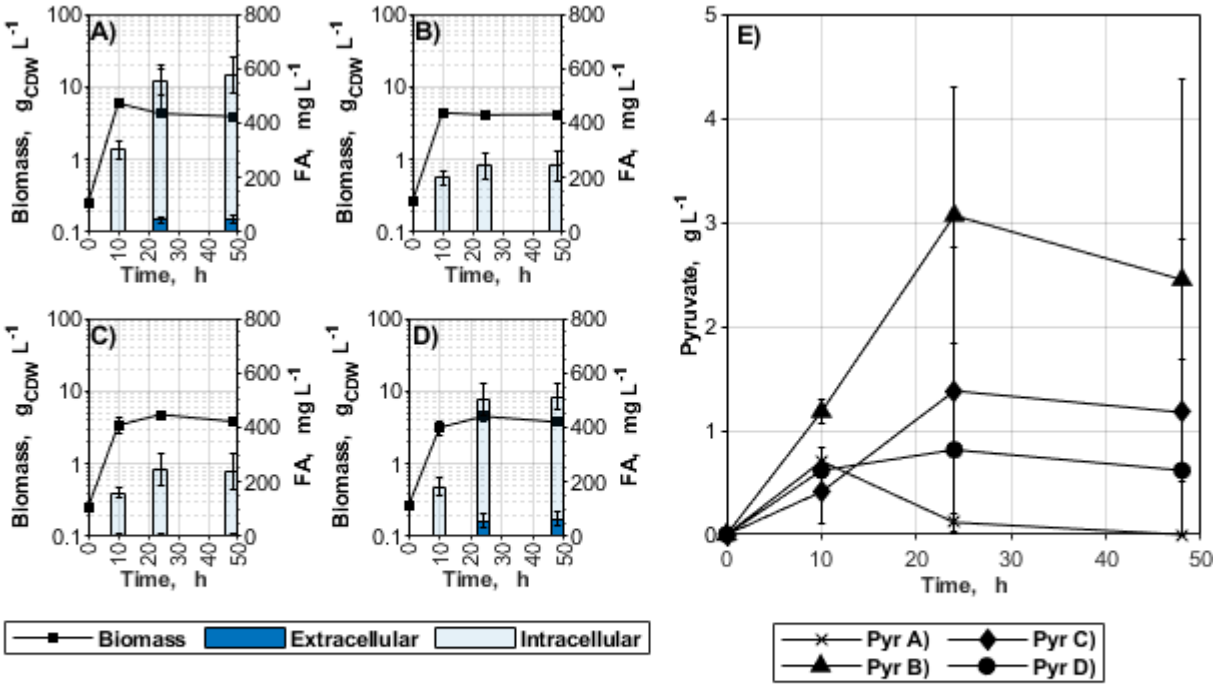

Figure 12: Impact of *sigD* deletion in a *C. glutamicum* Δ*fasR* strain background on FA production and growth. Cultivations were conducted in the nitrogen-limiting NL-CgXII minimal medium containing per liter 20 g glucose as the carbon source. A) *C. glutamicum* Δ*fasR*; B) *C. glutamicum* Δ*fasR* Δ*sigD;* C) *C. glutamicum* Δ*fasR* Δ*sigD* (pEKEx2)*;* D) *C. glutamicum* Δ*fasR* Δ*sigD* (pEKEx2_*accE*)*;* E) pyruvate production by the respective strains A-D. Data represents the means of ≥ 3 biological replicates with standard deviations.

Interestingly, macroscopic cell aggregates of *C. glutamicum* Δ*fasR* Δ*sigD* harboring pEKEx2 or pEKEx2_*accE* were observed during the shaking flask experiments. No such aggregates were observed in cultivations with the plasmid-free strain.

4.1.3 Studying nitrogen limitation and its influence on FA biosynthesis in a Δ*fasR* Δ*gdh* mutant

As shown in 4.1.1, FA synthesis with the engineered *C. glutamicum* strains was only possible under nitrogen-limiting cultivation conditions. The main FA efflux and membrane lipid-independent FA synthesis generally occurred after reaching the nitrogen starvation-induced stationary phase. As the glucose uptake rate q_s was reported to decrease strongly in the limitation-induced stationary phase (Chubukov et al., 2014), obtaining a growth-coupled FA production seemed desirable. Instead of triggering FA production through a me-

dium-induced nitrogen limitation, it was assessed whether triggering an intracellular nitrogen starvation response might also be sufficient to trigger FA production. Müller et al. (2006) reported that deleting the glutamate dehydrogenase (GDH)-encoding gene *gdh* resulted in an intracellular nitrogen starvation response in *C. glutamicum.* Therefore, a *C. glutamicum* Δ*fasR* Δ*gdh* mutant with impaired nitrogen assimilation was constructed and subsequently characterized under carbon-limiting cultivation conditions.

When cultivated in CgXII, intracellular FA concentrations after 48 h produced by *C. glutamicum* Δ*fasR* (443 ± 3 mg_{FA} L^{-1}) and the Δ*gdh* mutant (419 ± 29 mg_{FA} L^{-1}) were similar (Figure 13). However, the *gdh* deletion led to an over four-fold increase from 8 ± 4 to 34 ± 6 mg_{FA} L^{-1} of extracellular FA compared to its parental strain under the tested condition. This induced FA efflux under nitrogen surplus upon deleting *gdh* lines up with previously obtained results, underlining the importance of a nitrogen-starvation response on FA synthesis and efflux thereof in *C. glutamicum* (4.1.1). Glucose test strips indicated that glucose was fully consumed after 24 h by all strains. Yet, the generally lower intra- and extracellular FA concentrations and impaired growth compared to cultivating *C. glutamicum* Δ*fasR* under nitrogen-limiting conditions in NL-CgXII rendered the tested approach unfeasible for further strain engineering.

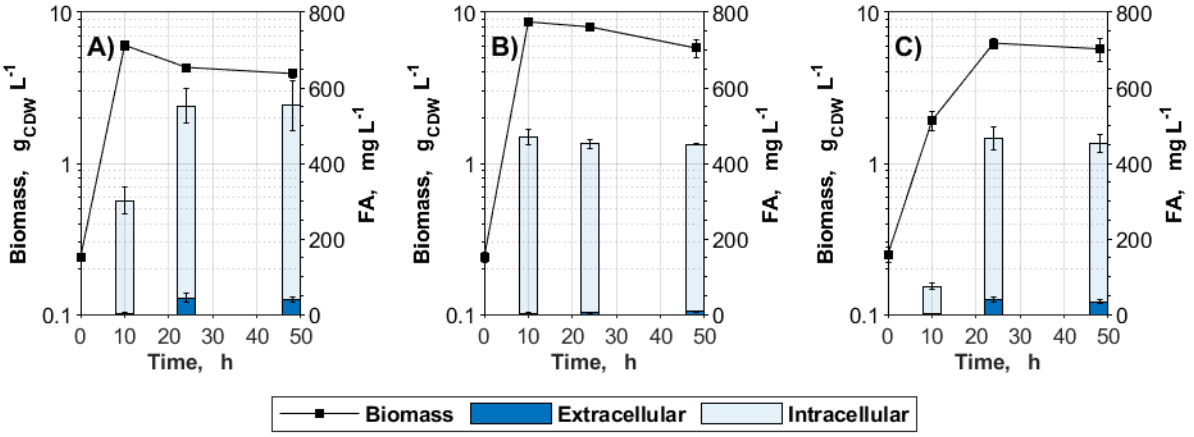

Figure 13: FA production under nitrogen-limiting and non-limiting conditions. Cultivations of *C. glutamicum* Δ*fasR* were conducted in either the A) nitrogen-limiting NL-CgXII or B) CgXII minimal medium. Cultivations of *C. glutamicum* Δ*fasR* Δ*gdh* were solely conducted in C) CgXII medium. All media contained per liter 20 g glucose as the carbon source. Data represents the means of ≥ 3 biological replicates with standard deviations.

4.1.4 Influence of the nitrogen source on FA production

Urea present in the NL-CgXII medium is converted into ammonium (NH_4^+) and bicarbonate (HCO_3^-) by the natively expressed urease (Mobley et al., 1995). As CO_2 and its hydrated form HCO_3^- serve as substrates for carboxylation reactions such as the ACC-catalyzed carboxylation and due to their beneficial impact on *C. glutamicum* biomass-formation (Blombach et al., 2013; Krüger et al., 2019; Müller et al., 2020), a CO_2/HCO_3^--dependent effect on FA formation was studied. Since it was shown that HCO_3^- also facilitates intracellular iron availability through an abiotic process (Müller et al., 2020), its impact on FA production in *C. glutamicum* was additionally investigated.

To study the general effect of HCO_3^- on FA synthesis, FA-producing *C. glutamicum* Δ*fasR* were cultivated with $NaHCO_3$ supplementation in a modified NL-CgXII medium containing $(NH_4)_2SO_4$ instead of urea as the sole nitrogen source. Per liter, 3.19 g $(NH_4)_2SO_4$ were used to provide an equimolar amount of NH_4^+ to 1.45 g urea L^{-1}. 195 µM of the iron chelator protocatechuic acid (PCA) were supplemented to the $(NH_4)_2SO_4$-based NL-CgXII medium to clarify whether HCO_3^--related effects were solely due to its role as a substrate for carboxylation reactions or were also attributed to an increased iron availability.

Theoretically, 1 mol of urea releases 1 mol of CO_2/HCO_3^- during the urease-catalyzed hydrolysis. Therefore, 1.45 g urea L^{-1} would provide a maximal amount of 24.14 mM CO_2/HCO_3^-. However, in order to counteract continuous CO_2 degassing from the shaken culture broth, experiments were conducted using 50 mM $NaHCO_3$ supplementation. Modified NL-CgXII medium supplemented with 50 mM NaCl was used as an osmolarity control in the $(NH_4)_2SO_4$-based medium.

Total FA production plummeted by 65 % from 581 ± 87 to 203 ± 29 mg_{FA} L^{-1} when $(NH_4)_2SO_4$ was used as the sole nitrogen source instead of urea. The biomass concentration decreased likewise from 3.84 ± 0.29 to 3.17 ± 1.06 g L^{-1}. However, FA biosynthesis was strongly enhanced when HCO_3^- was added to the $(NH_4)_2SO_4$-containing culture medium, resulting in a total FA concentration of 773 ± 71 mg_{FA} L^{-1}. Of those, 115 ± 9 mg_{FA} L^{-1} were measured extracellularly (Figure 14 A). The biomass concentration increased to 3.86 ± 0.08 g L^{-1}. The addition of 50 mM HCO_3^- to the urea-based NL-CgXII medium also had a positive effect on total FA production, which increased to 709 ± 52 mg_{FA} L^{-1}, of which 80 ± 8 mg_{FA} L^{-1} were measured extracellularly.

Upon the addition of PCA to the $(NH_4)_2SO_4$-based NL-CgXII medium, the biomass concentration increased by 64 % to 5.17 ± 0.13 g L^{-1}. Total FA production increased to

550 ± 67 g_{FA} L^{-1}, which corresponded to an increase of 170 % relative to the control but was still 29 % lower than the respective FA concentration obtained by 50 mM HCO_3^--supplemented cultures (Figure 14).

Glucose was fully consumed in all cultivation conditions after 48 h, as indicated by glucose test strips.

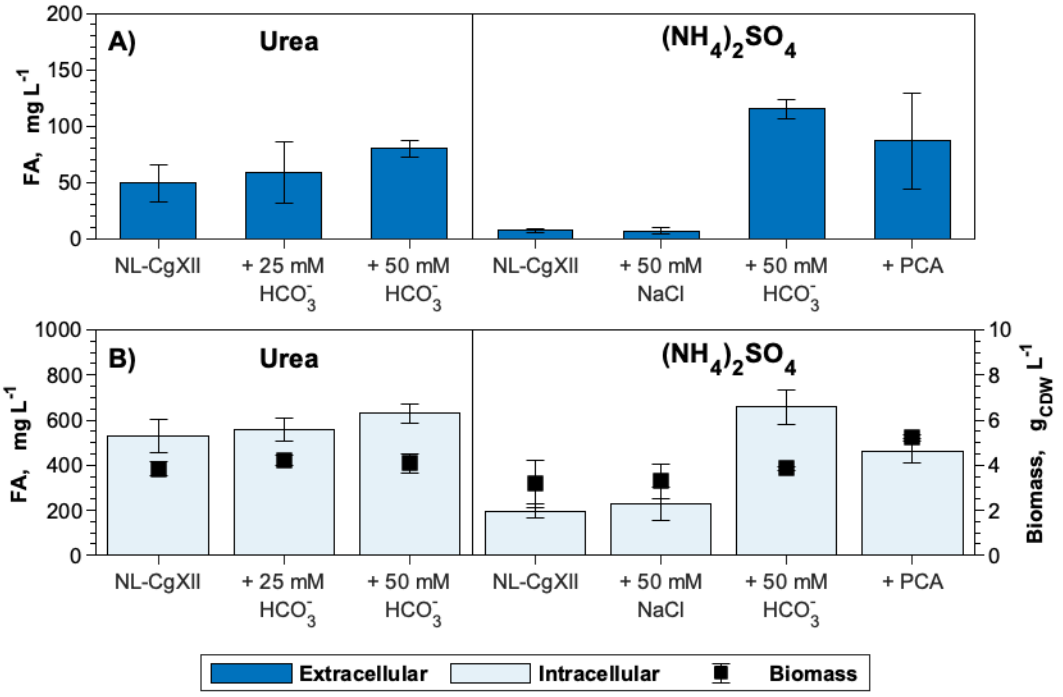

Figure 14: Effect of the nitrogen source on FA production with *C. glutamicum* Δ*fasR*. A) Extracellular FA concentrations, B) intracellular FA concentrations. Cultivations were conducted in NL-CgXII medium containing per liter either 1.45 g urea or 3.19 g ammonium sulfate (providing an equimolar amount of NH_4^+) at 30 °C, 180 rpm. The two different media were supplemented with nothing ('NL-CgXIII'), varying concentrations of $NaHCO_3$, NaCl, or 195 µM PCA as indicated. All media contained per liter 20 g glucose as the carbon source. Data represents means of ≥ 3 biological replicates with standard deviations.

4.2 FAL production in a FA-producing *C. glutamicum* strain background

Excerpts of the following sections, including figures, tables, and whole paragraphs, were published as part of the publication “Metabolic engineering of *Corynebacterium glutamicum* for fatty alcohol production from glucose and wheat straw hydrolysate” (Werner et al., 2023).

In an effort to expand the product portfolio, the production of FAL in FA-producing *C. glutamicum* Δ*fasR* was pursued. FAL represent an interesting product due to their reported lower cytotoxicity compared to FA and for being an extracellular product (Liu et al., 2016). Additionally, the biosynthetic pathways of FA and FAL synthesis are similar until they diverge at the acyl-CoA node (Figure 4). Therefore, strains constructed in chapter 4.1 and insights gained into FA biosynthesis and respective cultivation conditions could be utilized as a solid basis for the strain engineering described in this chapter.

4.2.1 Strain development for FAL production with glucose

4.2.1.1 Validation of a new cultivation condition – 120 vs. 180 rpm

Due to general changes in the laboratory regarding cultivations of *C. glutamicum*, the shaking frequency of the main culture was reduced from 180 to 120 rpm. To verify that the adjusted conditions did not affect FA production negatively in the WT and the engineered chassis strain *C. glutamicum* Δ*fasR*, the cultivation experiments described in chapter 4.1.1.1 were repeated at 120 rpm (Figure S. 1, Figure S. 2).

Both strains performed similarly at 120 rpm in CgXII and NL-CgXII medium as they did at 180 rpm (Figure S. 1, Figure 8). Interestingly, FA titers obtained by *C. glutamicum* Δ*fasR* cultivated in CgXII increased by 25 % from 452 ± 7 (Figure 8) to 587 ± 37 mg_{FA} L^{-1} (Figure S. 1). The concentration of the fermentation products pyruvate, lactate, and acetate remained similar to cultivations at 180 rpm (data not shown), indicating sufficient oxygen availability at the reduced shaking frequency.

4.2.1.2 Screening of two fatty acyl-CoA reductases (FAR)

To catalyze FAL-formation, pEKEx2-based overexpression of the well-described *M. hydrocarbonoclasticus* VT8 fatty acyl-CoA reductases (FAR) Maqu_2220 and Maqu_2507

(Hofvander et al., 2011b; Willis et al., 2011) was chosen as an initial strategy. Similar approaches using *E. coli* or *Y. lipolytica* as production strains yielded successful results (Cordova et al., 2020; Liu et al., 2013; Liu et al., 2016), but no study using *C. glutamicum* for the production of FAL exists yet. In contrast to other known FAR, both *M. hydrocarbonoclasticus* FARs display a high affinity to C16-C18 acyl-CoAs and do not release the cytotoxic aldehyde intermediate (Hofvander et al., 2011a; Willis et al., 2011), making both optimal candidates for FAL production with *C. glutamicum.*

Both reductases Maqu_2220 and Maqu_2507 were episomally expressed in the FA-producing Δ*fasR* mutant to test whether both enzymes were active in *C. glutamicum*. For either enzyme, FAL production was observed when cultivated in the NL-CgXII medium. Maqu_2220-expressing strains produced 482 ± 33 mg_{FAL} L^{-1}, of which 78 ± 3 mg_{FAL} L^{-1} were measured extracellularly. Strains expressing Maqu_2507 produced 356 ± 82 mg_{FAL} L^{-1}, of which 59 ± 15 mg_{FAL} L^{-1} were measured extracellularly (Figure 15, A). The observed product distribution was similar for both tested reductases, which both produced about 50 % oleyl alcohol and 40 % 1-hexadecanol (Figure 15 B) relative to the total amount of produced FAL.

As expected, the FA production decreased in FAL-producing strains, reaching FA concentrations comparable to the WT (Figure 15, C; level indicated by the red line). Glucose was fully consumed after 24 h by strains harboring Maqu_2220, while residual glucose was still present in the medium of Maqu_2507-expressing strains, as indicated by glucose test strips.

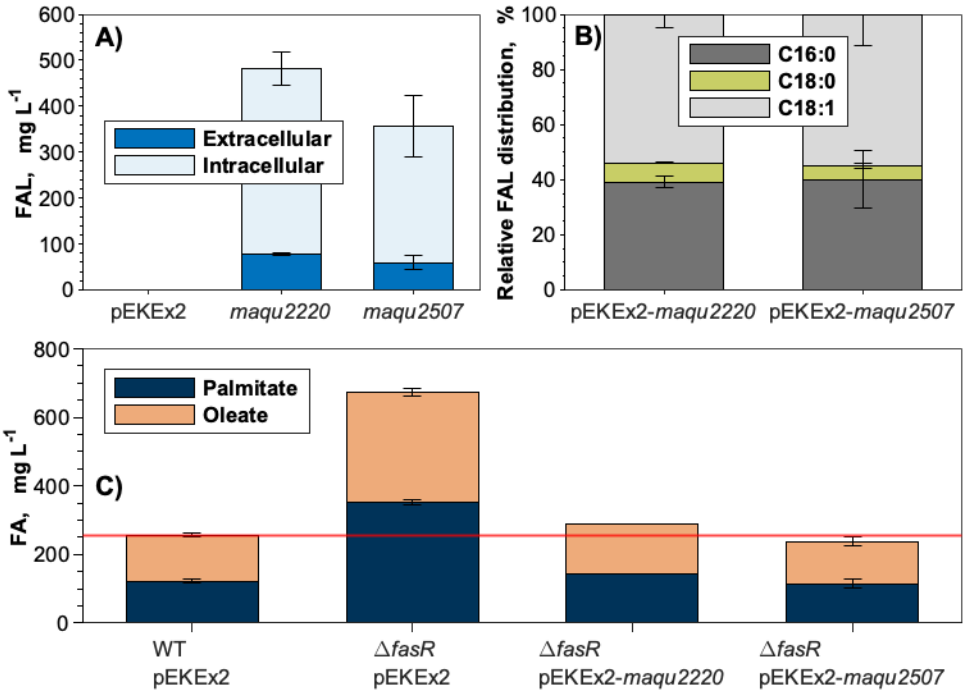

Figure 15: Screening of two FAR in *C. glutamicum* Δ*fasR*. A) Extra- and intracellular FAL concentrations obtained by Δ*fasR* mutants harboring pEKEx2-*maqu2220* or pEKEx2-*maqu2507*; B) distribution of 1-hexadecanol (C16:0), octadecanol (C18:0) and oleyl alcohol (C18:1) of the total FAL; C) total FA produced by the FAR-expressing strains in comparison to WT and Δ*fasR* empty plasmid controls. The red horizontal line indicates the FA level of the WT. Samples for FAL and FA analysis were taken after 24 h. Cultivations were conducted in NL-CgXII medium containing 20 g glucose L^{-1} as the carbon source. Data represents the means of ≥ 3 biological replicates with standard deviations. (Werner et al., 2023)

4.2.1.3 Plasmid-free FAL production

In order to construct a plasmid-free FAL producer, the best-performing reductase Maqu_2220 was integrated into the stable landing pad CgLP11 (Lange et al., 2018) under the control of P_{tac} and terminated by T_{rrnB}. However, FAL production of the newly constructed strain *C. glutamicum* Δ*fasR* CgLP11::(P_{tac}-*maqu_2220*-T_{rrnB}) was reduced by 94 % with 31 ± 2 mg_{FAL} L^{-1}, of which 8 ± 2 mg_{FAL} L^{-1} were measured extracellularly, compared to the plasmid-harboring control. Since the FAL concentration in the genomic integration mutant was reduced by a similar factor as the reported copy number of the pBL1-based pEKEx2 (Baumgart et al., 2013; Santamaría et al., 1984) a correlation between gene number and FAL production was assumed. Therefore, alternative strategies were pursued to boost FAL production.

4.2.1.4 Utilizing a stronger plasmid system for the constitutive expression of *maqu_2220*

The pECXT$_{Psyn}$-based plasmid (Henke et al., 2021b) pECXT$_{Psyn}$-*maqu2220* was constructed to examine the influence of the reportedly strong, constitutive promoter P$_{syn}$ on FAL production.

FAL production decreased in pECXT$_{Psyn}$-*maqu2220*-harboring strains from 482 ± 33 mg$_{FAL}$ L^{-1} of the control strain to 358 ± 150 mg$_{FAL}$ L^{-1} (Figure 16). Glucose test strips indicated that the carbon source was fully consumed by the pEKEx2-*maqu2220* control after 24 h, while residual glucose was still left in the medium of pECXT$_{Psyn}$-*maqu2220*-harboring strains. No glucose was detected in the broth of the empty plasmid controls after 24 h.

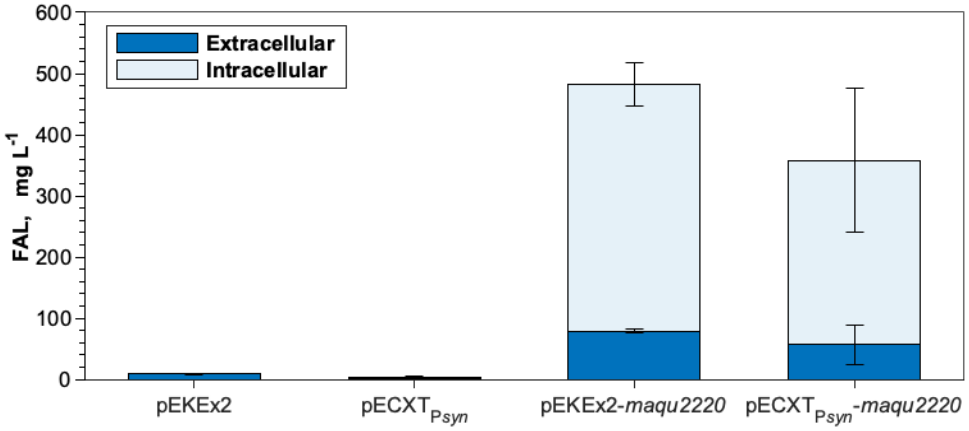

Figure 16: Comparison of pEKEx2- and pECXT$_{Psyn}$-based *maqu_2220* expression. Cultivations were conducted in NL-CgXII medium containing 20 g glucose L^{-1} as the carbon source. Samples for extra- and intracellular FAL analysis were taken after 24 h. Data represents the means of 3 biological replicates with standard deviations.

4.2.1.5 Attenuating the native thioesterase expression to increase acyl-CoA precursor supply

Thioesterase-catalyzed and FA-forming reactions provide a metabolic sink for acyl-CoA and, therefore, compete with the fatty acyl-CoA reductase (FAR)-catalyzed reduction towards the formation of FAL. Interestingly, *C. glutamicum* reportedly has a high thioesterase activity “comparable to ‘*tesA*-overexpressing *E. coli*” (Takeno et al., 2013). It thus seemed crucial to attenuate thioesterase expression in order to favor the FAL-forming reduction.

Since deleting the native thioesterase-encoding gene cg2692 was shown to severely impact growth of *C. glutamicum* (Ikeda et al., 2020), a different strategy was chosen to redirect the carbon flux. For that purpose, the native start codon ATG of cg2692 was exchanged for either GTG or TTG in *C. glutamicum* Δ*fasR* CgLP11::(P_{tac}-*maqu_2220*-T_{rrnB}).

FAL production of the resulting strains *C. glutamicum* Δ*fasR* $cg2692_{GTG}$ CgLP11::(P_{tac}-*maqu_2220*-T_{rrnB}) and *C. glutamicum* Δ*fasR* $cg2692_{TTG}$ CgLP11::(P_{tac}-*maqu_2220*-T_{rrnB}) was analyzed and compared to the parental strain.

Upon exchange of the start codon to either GTG or TTG, FAL production increased by 350 % and 750 %, respectively. The obtained FAL titers were accompanied by a strong reduction in FA production. The highest FAL titer was obtained by *C. glutamicum* Δ*fasR* $cg2692_{TTG}$ CgLP11::(P_{tac}-*maqu_2220*-T_{rrnB}) with 256 ± 67 mg_{FAL} L^{-1}, while that strain also displayed the lowest total FA concentration of 229 ± 64 mg_{FA} L^{-1} (Figure 17).

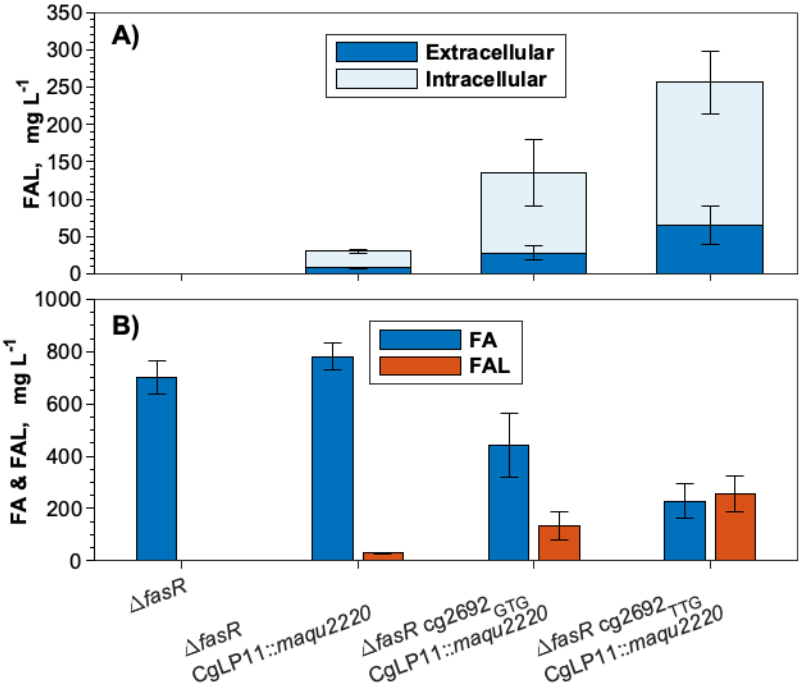

Figure 17: FAL production of plasmid-free *C. glutamicum* Δ*fasR* CgLP11::*maqu2220* mutants. The native start codon ATG of the thioesterase-encoding gene cg2692 was exchanged for either GTG or TTG in *C. glutamicum* Δ*fasR* CgLP11::*maqu2220*. Cultivations were conducted in NL-CgXII medium containing 20 g glucose L^{-1} as the carbon source. A) Extra- and intracellular FAL concentrations; B) total FA and FAL production. Samples for FA and FAL analysis were taken after 48 h. Data represents the means of 3 biological replicates with standard deviations. (Werner et al., 2023)

When mutating the native thioesterase start codon in plasmid-harboring FAL producers, total FAL production decreased. GTG start codon mutants produced 282 ± 57 mg_{FAL} L^{-1} while TTG mutants produced 353 ± 22 mg_{FAL} L^{-1}, which corresponded to a 32 % and 14 % decreased FAL production relative to the control strain (Figure 18 A). However, extracellular FAL titers increased from 76 ± 10 (control) to 92 ± 44 and 133 ± 9 mg_{FAL} L^{-1} during the cultivations with the GTG and TTG mutants, respectively. Titers obtained by all plasmid-harboring strains were higher than those obtained by the plasmid-free FAL producers.

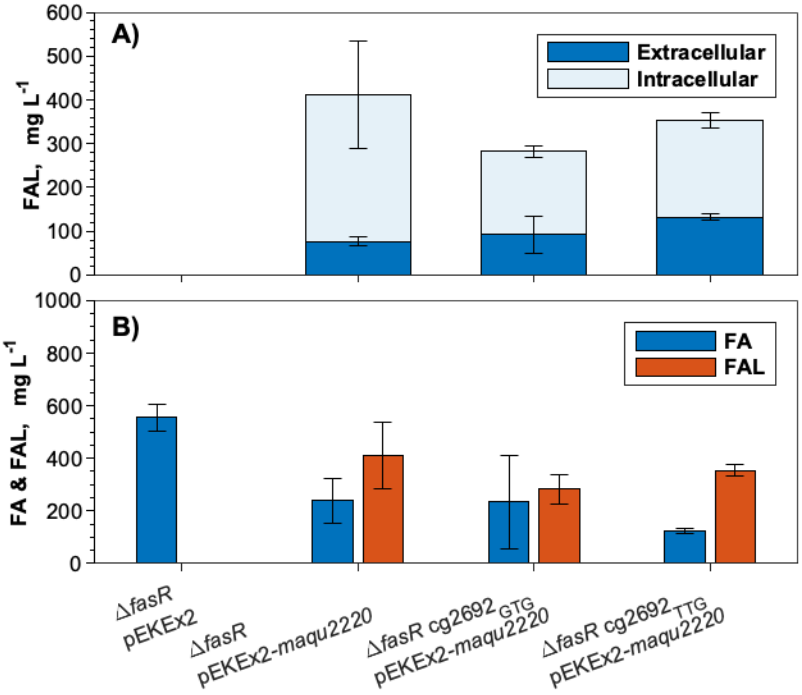

Figure 18: FAL production of pEKEx2-*maqu2220*-harboring *C. glutamicum* Δ*fasR* mutants. The native start codon ATG of the thioesterase-encoding gene cg2692 was exchanged for either GTG or TTG in *C. glutamicum* Δ*fasR*. Cultivations were conducted in NL-CgXII medium containing 20 g glucose L^{-1} as the carbon source. A) Extra- and intracellular FAL concentrations; B) total FA and FAL production. Samples for FA and FAL analysis were taken after 48 h. Data represents the means of 3 biological replicates with standard deviations.

4.2.1.6 Adjustment of the cultivation conditions for the growth-coupled production of FAL

As best-performing strains in regard to obtained FAL titers, the plasmid-harboring strains *C. glutamicum* Δ*fasR* (pEKEx2-*maqu2220*) and *C. glutamicum* Δ*fasR* cg2692$_{TTG}$ (pEKEx2-*maqu2220*) were further characterized regarding their growth and production kinetics.

In contrast to the previously described FA synthesis (Figure 9), FAL appeared to be formed primarily in a growth-coupled manner (Figure 19 A). Additionally, 42 ± 3 and 20 ± 2 mM glucose were left in the supernatant of *C. glutamicum* Δ*fasR* cg2692$_{TTG}$ (pEKEx2-*maqu2220*) after 24 and 48 h, respectively, indicating suboptimal cultivation conditions (Figure S. 3).

To test whether FAL production could be improved by solely adjusting the cultivation conditions, *C. glutamicum* Δ*fasR* (pEKEx2-*maqu2220*) and *C. glutamicum* Δ*fasR* cg2692$_{TTG}$ (pEKEx2-maqu2220) were cultivated in standard CgXII medium with and without PCA. Interestingly, while FAL production by the former strain plummeted under both conditions, growth-coupled FAL production by the latter strain was strongly improved in CgXII medium and in CgXII supplemented with PCA compared to the nitrogen-limited medium (Figure 19 B1-3). Within 15 h, *C. glutamicum* Δ*fasR* cg2692$_{TTG}$ (pEKEx2-maqu2220) produced 544 ± 20 mg_{FAL} L^{-1} in CgXII medium supplemented with PCA. That corresponded to a 33 % increase in the total FAL titer, a 35 % higher product yield (0.054 ± 0.001 Cmol $Cmol^{-1}$), and a 117 % improved volumetric productivity compared to *C. glutamicum* Δ*fasR* (pEKEx2-*maqu2220*) cultivated under nitrogen-limiting conditions (Figure 19; A2-3, B2-3; Table 14). Thus, all subsequent cultivations were conducted using the optimized cultivation conditions and the best-performing FAL producer *C. glutamicum* Δ*fasR* cg2692$_{TTG}$ (pEKEx2-*maqu2220*). Even though the yield remained similar of *C. glutamicum* Δ*fasR* cg2692$_{TTG}$ (pEKEx2-*maqu2220*) cultivated under both conditions, the final titer and volumetric productivity increased by 47 and 240 %, respectively. Additionally, glucose was fully consumed within 15 h (Figure S. 3). Besides the positive impact of the new cultivation condition on FAL production in the TTG start codon mutant, decreasing FAL titers were observed in both strains between entering the stationary phase and the end of the cultivation after 24 h. A mechanism of FAL degradation has yet to be elucidated.

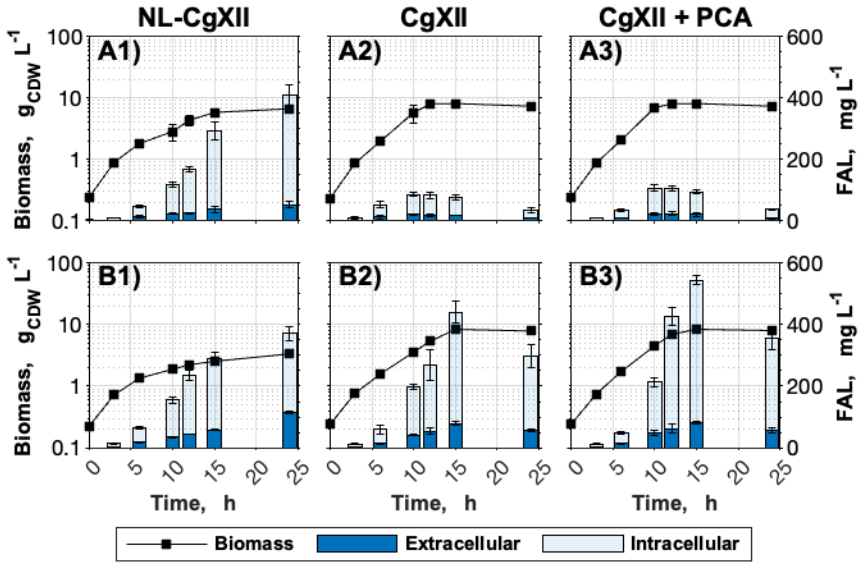

Figure 19: Optimization of the medium composition for the efficient production of FAL. The two best-performing strains (A) *C. glutamicum* Δ*fasR* (pEKEx2-*maqu2220*) and (B) *C. glutamicum* Δ*fasR* cg2692$_{TTG}$ (pEKEx2-*maqu2220*) were cultivated in media: (1) NL-CgXII, (2) CgXII or (3) CgXII with 195 µM PCA. All media contained per liter 20 g glucose as the carbon source. Data represents the means of 3 biological replicates with standard deviations. (Werner et al., 2023)

Table 14: KPI of FAL-producing strains cultivated on glucose in shaking flasks. Cultivations of *C. glutamicum* Δ*fasR* (pEKEx2-*maqu2220*) and *C. glutamicum* Δ*fasR* cg2692$_{TTG}$ (pEKEx2-*maqu2220*) were conducted in either NL-CgXII or CgXII medium supplemented with 195 µM PCA. All media contained per liter 20 g glucose as the carbon source. Data represents the means of 3 biological replicates ± standard deviations.

KPI	**Δ*fasR***		**Δ*fasR* cg2692$_{TTG}$**	
	NL-CgXII	**CgXII + PCA**	**NL-CgXII**	**CgXII + PCA**
$c_{FAL, Total}$ | mg L^{-1}	408 ± 45	105 ± 13	370 ± 27	544 ± 20
$Y_{P/S}$ | g g^{-1}	0.020 ± 0.003	0.005 ± 0.001	0.029 ± 0.002	0.027 ± 0.001
$Y_{P/S}$ | Cmol $Cmol^{-1}$	0.040 ± 0.005	0.009 ± 0.001	0.057 ± 0.005	0.054 ± 0.001
Q_P | mg L^{-1} h^{-1}	17 ± 2	9 ± 1	15 ± 1	36 ± 1

4.2.1.6.1 Native FAL-degradation in *C. glutamicum*

Despite the positive effect on FAL production of switching from the nitrogen-limited NL-CgXII medium back to standard CgXII medium, a decrease of FAL during the stationary phase could be observed under those new cultivation conditions.

To study the effect, the WT was cultivated in CgXII medium supplemented with 195 µM PCA and 125 mg oleyl alcohol L^{-1}. Oleyl alcohol (C18:1-OH) was chosen as a representative FAL as its liquid state at room temperature made it possible to easily prepare a 25 g L^{-1} stock solution in DMSO. A shaking flask containing solely minimal medium spiked with FAL was used as a control to rule out any non-biological degradation processes (Figure 20). Blank samples for OD_{600} measurements were also taken from the control shaking flask.

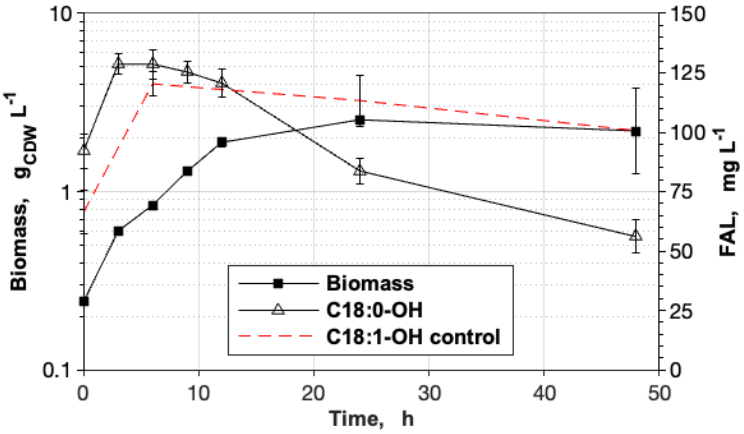

Figure 20: Degradation of oleyl alcohol (C18:1-OH) by *C. glutamicum* ATCC 13032. Cultivations were conducted in CgXII medium supplemented with 195 µM PCA and 125 $mg_{C18:1-OH}$ L^{-1}. Glucose was used as the carbon source at a concentration of 10 g L^{-1}. FAL and biomass data obtained from the medium inoculated with *C. glutamicum* ATCC 13032 are shown in black. FAL data obtained from the biomass-free control medium is indicated in red. Data represents the means of 3 (biological) replicates with standard deviations.

Samples of both shaking flasks showed lower initial oleyl alcohol concentration than what was to be expected, which increased to the target concentration within the first hours of the cultivation. Oleyl alcohol is not miscible with water and thus did not form a homogenous solution with the aqueous medium right away. However, constant shaking of the baffled

shaking flask on the orbital shaker led to the formation of an emulsion and homogenized the mixture.

While the alcohol concentration decreased linearly from 120 ± 5 $mg_{C18:1-OH}$ L^{-1} (6 h) to 101 ± 18 $mg_{C18:1-OH}$ L^{-1} (48 h) over the course of the cultivation in the control shaking flask, a strong consumption was observed in the biological flask. The alcohol concentration already started to decrease from 129 ± 4 $mg_{C18:1-OH}$ L^{-1} (3 h) to 121 ± 6 $mg_{C18:1-OH}$ L^{-1} (12 h) during the exponential growth phase but strongly dropped upon approaching and entering the stationary phase. After 48 h, just 56 ± 7 $mg_{C18:1-OH}$ L^{-1} were left in the culture broth, indicating that over 50 % of the initially present alcohol were consumed during the cultivation. Since the entire cell broth was extracted with ethyl acetate, a decrease in alcohol concentration did not indicate solely an uptake but a metabolization of oleyl alcohol into a so far unknown product.

Therefore, *C. glutamicum* seems to be natively equipped to metabolize olely alcohol and most likely other FAL as well, as observed in previous cultivations with *C. glutamicum* ATCC 13032-derived strains (Figure 19). Nevertheless, since the degradation process primarily occurred towards the stationary phase, it was assumed that most FAL is generally not degraded while glucose is still present in the medium. Therefore, the observed effect did not affect the strain engineering and process development strategies.

4.2.2 Scale-up: development of a fed-batch process on glucose

Once FAL-producing strains were characterized with glucose as substrate, scaling up the process from a 50 mL shaking flask scale to a small benchtop bioreactor was targeted. Therefore, the development of a fed-batch process with an exponential feed profile using the 1 L BioFlo120® bioreactor system (Eppendorf SE, Hamburg, Germany) was pursued. The latest strain iteration, *C. glutamicum* Δ*fasR* $cg2692_{TTG}$ (pEKEx2-*maqu2220*), was used.

However, initial cultivations in $CgXII_{mod}$ medium were unstable due to extensive and rapid foam formation. Despite the regular addition of the antifoaming agent Struktol® J 673 A (Schill+Seilacher GmbH, Hamburg, Germany), the dense foam was almost non-collapsible, which ultimately led to an overflow of the bioreactors. Besides general drawbacks regarding handling a heavily foaming bioreactor, uncontrollable overflow meant that an adequate mass balance could not be established to accurately characterize the fed-batch

process. Additionally, biomass formation generally ceased at CDW concentrations between 17 and 22 $g_{CDW}\,L^{-1}$, leading to an accumulation of glucose provided by the exponential feed. One of those respective processes is exemplarily displayed in the appendix as Figure S. 4.

4.2.2.1 Media optimization for high cell density cultivations

Ceasing growth and subsequent glucose accumulation in bioreactor cultivations indicated a limiting substrate other than the used carbon source. Based on an elemental analysis by Liebl (2005), some trace elements would be limiting in the used $CgXII_{mod}$ medium. Interestingly, the elemental analysis suggests that Fe, Cu, and Zn would become limiting already at biomass concentrations between 5 to 7 $g_{CDW}\,L^{-1}$, which was not observed in previous shaking flask experiments and has also not been observed in other studies using the same medium composition (Buchholz et al., 2014; Müller et al., 2020). The reported elemental biomass composition of *C. glutamicum* grown in CgXII minimal medium (Liebl, 2005), the respective elements' concentration in the $CgXII_{mod}$ medium, and the theoretical maximal biomass obtainable for each element are listed in Table 15.

Table 15: Elemental composition of *C. glutamicum* and the theoretical maximal biomass concentrations. The biomass composition was published by Liebl (2005). Given concentrations of the respective elements are based on the composition of $CgXII_{mod}$ minimal medium (3.3.4). Based on both parameters, the theoretical maximum of formed biomass was calculated.

Element	Biomass composition | $g\,g_{CDW}^{-1}$	Concentration in $CgXII_{mod}$ | $g\,L^{-1}$	Maximal biomass | $g_{CDW}\,L^{-1}$
N	0.0845	4.24	50.15
S	0.004	4.92	1230
P	0.0145	$4.05 * 10^{-1}$	27.96
Mg	0.00159	$5.05 * 10^{-2}$	31.75
Ca	0.000035	$3.61 * 10^{-3}$	103.18
Mn	0.000201	$3.25 * 10^{-3}$	16.17
Fe	0.00051	$3.29 * 10^{-3}$	6.46
Cu	0.000012	$8.02 * 10^{-5}$	6.68
Zn	0.000046	$2.27 * 10^{-4}$	4.94
Ni	0.00000043	$4.94 * 10^{-6}$	11.49

As all elements of the trace element solution (Mn, Fe, Cu, Zn, Ni) would, according to the elemental analysis, quickly become limiting, their concentration was doubled in following bioreactor cultivations. Similar adjustments were made by Kiefer et al. (2021) in their high cell density CgXII version. As the respective study used $MgSO_4$ x 7 H_2O at a concentration of 1.25 g L^{-1} to achieve a high cell density in a fed-batch cultivation (Kiefer et al., 2021), its concentration was also adjusted from 0.25 to 0.5 g L^{-1} in the constructed $CgXII_{mod}$ medium derivate. Also, since P might become limiting at a biomass concentration of about 28 g_{CDW} L^{-1}, its concentration was doubled by increasing the concentrations of K_2HPO_4 and KH_2PO_4 from 1 to 2 g L^{-1} each. Lastly, the $(NH_4)_2SO_4$ concentration was doubled from 20 to 40 g L^{-1} because no additional nitrogen source, such as ammonia, was used for controlling the pH of the process. The adjusted minimal medium was called $CgXII_{mod,2}$.

To test whether the adjusted $CgXII_{mod,2}$ medium allowed for higher biomass formation, a batch process with *C. glutamicum* Δ*fasR* $cg2692_{TTG}$ (pEKEx2-*maqu2220*) and a glucose concentration of 100 g L^{-1} was conducted (Figure 21). After 15.25 h, the aeration rate was increased as part of the DO cascade to ensure adequate oxygen supply for the exponentially growing cells. Due to extensive, uncontrollable foaming, the process was terminated after 16 h. By the end of the cultivation, a biomass concentration of 31.28 g_{CDW} L^{-1} was reached, and growth was still following an exponential growth kinetic (Figure 21). An almost doubled final biomass concentration compared to previous cultivations suggested that respective adjustments of the medium's composition eliminated previously observed substrate limitations. Thus, the adjusted $CgXII_{mod,2}$ medium was used for subsequent bioreactor experiments. Later cultivations additionally showed that the presented results obtained from a batch cultivation were also valid in a fed-batch mode (Figure 23).

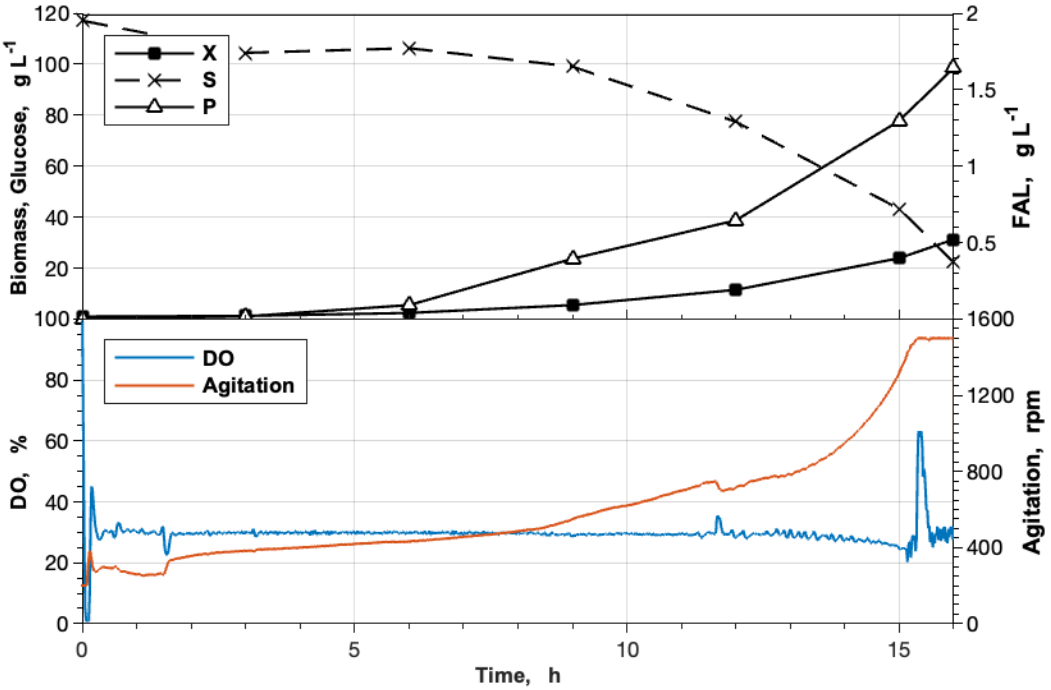

Figure 21: Adjusted $CgXII_{mod,2}$ medium in a batch cultivation. Batch cultivations were conducted in a 1 L BioFlo120® bioreactor system with an initial batch volume of 0.5 L. The cultivations of *C. glutamicum* Δ*fasR* $cg2692_{TTG}$ (pEKEx2-*maqu2220*) were performed at 30 °C in $CgXII_{mod,2}$ medium. The medium was supplemented with 195 µM PCA. Glucose with a concentration of 100 g L^{-1} was used as the carbon source. Data was obtained from a single experiment. X: biomass; S: glucose; P: FAL; DO: dissolved oxygen.

4.2.2.2 Tackling foam formation as the hurdle of a stable bioprocess

Heavy foam formation needed to be strongly reduced in order to successfully scale up FAL production and develop a stable aerobic bioprocess. Two strategies, applying an organic phase overlay for *in situ* product removal and using different commercially available antifoaming agents, were tested and will be discussed in the next two sections.

4.2.2.2.1 Testing *in situ* product removal strategies via organic phase overlay

1-hexadecanol, as one of the main FAL produced by the engineered strains, is known to have foam-stabilizing properties (Rand, 1984). It was therefore suspected that the extensive foam formation during previous bioreactor cultivations and the foam's resilience towards antifoaming agents were contributed to the amphiphilic alcohol's properties. Re-

moving the foam stabilizing product during the cultivation would thus be a reasonable approach to reduce foaming while also preventing potentially occurring product inhibition at later stages of the process and providing a first downstream processing step. Consequently, different organic solvents for an *in situ* product removal approach were investigated.

Several organic solvents suitable to extract FAL from aqueous media are available. However, they should not negatively affect growth and FAL production of *C. glutamicum*, while also being preferably harmless for the environment and safe to handle for lab personnel.

The in lab-scale commonly used solvent dodecane (Cordova et al., 2020; Frohwitter et al., 2014) was not considered due to its flash point of about 70 °C, the ability to form explosive air-solvent vapors, and due to its hazard to human health. Similar reasons excluded dodecane from a solvent screening study conducted by Tharmasothirajan et al. (2021).

In contrast, the solvent tributyrin was shown to be non-toxic for humans and the environment, while not affecting growth of *C. glutamicum* (Tharmasothirajan et al., 2021). Additionally, at least 40 g oleyl alcohol L^{-1} as a representative FAL were soluble in the organic solvent (data not shown). Despite appearing as the optimal solvent for *in situ* product removal, its miscibility with virtually any organic solvent, its low volatility, and its retention time close to the FAL of interest (data not shown) made tributyrin unsuitable for the quantification of extracted FAL via GC-FID and potentially unsuitable for subsequent downstream processing.

Two other promising solvents, methyl decanoate and ethyl decanoate, which proved to be compatible with *C. glutamicum*, were published by Tharmasothirajan et al. (2021). Both solvents exhibit limited environmental hazards, pose little to no danger to human health and safety, and can be easily distinguished from FAL via GC-FID. Additionally, methyl decanoate was successfully used as an *in situ* extractant of rhamnolipids produced by *Pseudomonas putida*, while also mitigating foam formation in the described process (Demling et al., 2020).

To assess the suitability of methyl and ethyl decanoate, a standard shaking flask cultivation with *C. glutamicum* Δ*fasR* $cg2692_{TTG}$ (pEKEx2-*maqu2220*) was conducted, to which 2.5 mL of both solvents (5 % v/v overlay) were added aseptically after 6 h. Additionally, propyl decanoate was also used in the experimental setup to simultaneously study the effect of the alkyl moiety on growth and product formation. The solvent has similar safety

characteristics to its methyl and ethyl derivate; however, no biocompatibility data in *C. glutamicum* existed.

As the formation of emulsions made OD_{600} and cell dry weight measurements impossible, solely FAL production and glucose consumption were monitored. As shown in Figure 22 A, FAL production ceased immediately upon the addition of methyl decanoate, while FAL production proceeded in the ethyl and propyl decanoate-exposed cultures. Similarly, glucose consumption came to a halt after 15 h in the methyl decanoate cultures, while it decreased linearly in the ethyl decanoate flasks. After 24 h, about 50 % and 34 % of the initially present 20 g glucose L^{-1} were still found in the cultures' supernatants, respectively. Solely cultures exposed to propyl decanoate exhibited a glucose consumption kinetic similar to the control strain, resulting in complete glucose consumption after 24 h. Product yields for the control and the strains cultivated with methyl, ethyl, and propyl decanoate overlay were 0.027 ± 0.001, 0.005 ± 0.001, 0.023 ± 0.001, and 0.016 ± 0.001 g_{FAL} g^{-1}, respectively (Table 16).

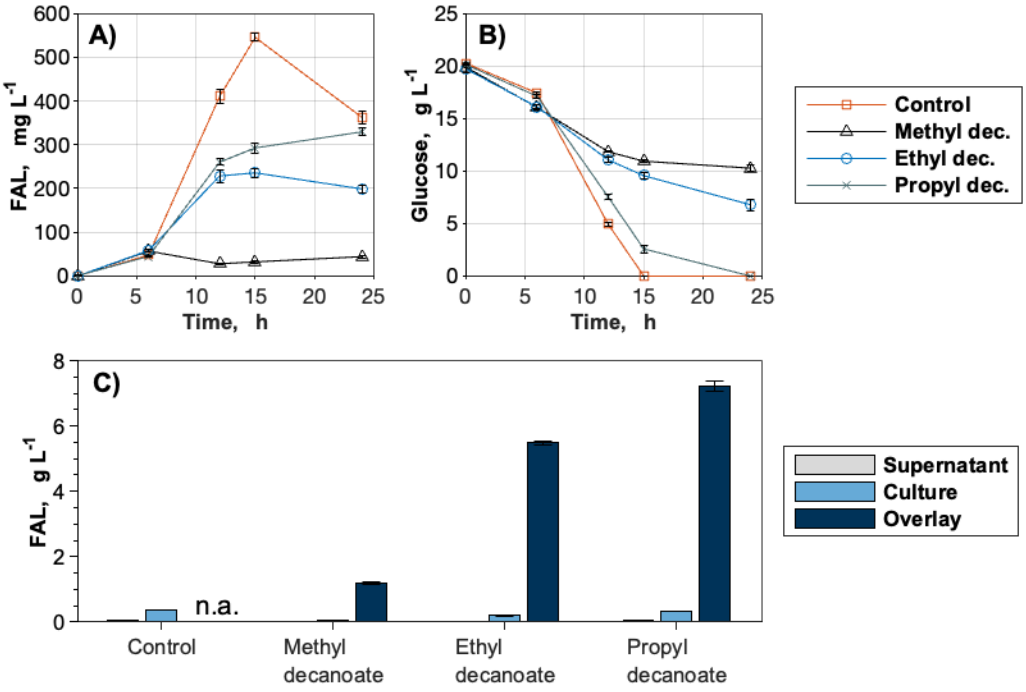

Figure 22: FAL production with an organic phase overlay for *in situ* product removal. Cultivations of *C. glutamicum* Δ*fasR* cg2692$_{TTG}$ (pEKEx2-*maqu2220*) were conducted in baffled shaking flasks containing CgXII medium supplemented with 195 µM PCA. Glucose was used as the carbon source at a concentration of 20 g L^{-1}. 2.5 mL Methyl, ethyl, or propyl decanoate (dec.) were added to the culture after 6 h. The sample "control" was cultivated without the addition of any solvent. A) kinetic FAL production data over the cultivation time; B) glucose concentration over the cultivation time; C) FAL concentration in the supernatant, culture, and organic phase (overlay) after 24 h. Data represents the means of 3 biological replicates with standard deviations. n.a.: not applicable.

Nevertheless, final FAL titers were still reduced by over 40 % compared to titers obtained by the control cultivations with no organic phase overlay. All three solvents worked well as an antifoaming agent and extractant, extracting almost all produced FAL from the aqueous phase (Figure 22 B). The final FAL concentration in the propyl decanoate layer was >7 g L^{-1}, which corresponded to a concentrating step by a factor of 22. Besides their usefulness in effectively extracting and thus concentrating FAL from a culture broth, methyl and ethyl decanoate's apparent cytotoxicity for the used strain made both solvents unsuitable for further use. Propyl decanoate showed better results in terms of biocompatibility

and product formation but was still inferior to cultivations without any organic phase overlay. Cells exposed to any of the three solvents formed big, macroscopic aggregates during the cultivation time. Additionally, a so far unidentified peak with a growing peak area over the course of the cultivation was detected for all three solvents (data not shown). Its retention time was greater than the solvent's retention time but smaller than the FAL's retention times. The appearance of that unidentified substance and its increase during the cultivation indicated a bioconversion of methyl, ethyl, and propyl decanoate into an unknown product. The metabolization of ethyl decanoate was already hypothesized but not further verified by Tharmasothirajan et al. (2021). As all three solvents were deemed to be unsuitable for cultivations with the engineered FAL-producing strains, no further investigations regarding the unknown product's identity were conducted.

Table 16: KPI of FAL production with organic phase overlay. Cultivations of *C. glutamicum* Δ*fasR* cg2692$_{TTG}$ (pEKEx2-*maqu2220*) were conducted in CgXII medium supplemented with 195 µM PCA. Glucose was used as the carbon source at a concentration of 20 g L^{-1}. Methyl decanoate (Methyl), ethyl decanoate (Ethyl), or propyl decanoate (Propyl) were added after 6 h. Cultivations without organic solvent were used as a control (Control). Data represents the means of 3 biological replicates ± standard deviations. n.a.: not applicable.

KPI		Control	Methyl	Ethyl	Propyl
$Y_{P/S}$ | g g^{-1}		0.027 ± 0.001	0.005 ± 0.001	0.023 ± 0.001	0.016 ± 0.001
$Y_{P/S}$ | Cmol $Cmol^{-1}$		0.053 ± 0.001	0.008 ± 0.002	0.046 ± 0.002	0.033 ± 0.001
$c_{FAL, max,}$ | mg L^{-1}	Supernatant	58 ± 5	1 ± 2	8 ± 1	43 ± 12
	Culture	545 ± 11	44 ± 4	236 ± 13	329 ± 11
	Overlay	n.a.	1192 ± 47	5490 ± 69	7220 ± 194

4.2.2.2.2 Screening of commercially available antifoaming agents

The use of chemical antifoaming agents is a common practice in lab-scale microbial cultivations to prevent foam formation or to collapse already existing foam (Buchholz et al., 2013; Kiefer et al., 2021).

Therefore, three commercially available antifoaming agents of Schill+Seilacher GmbH (Hamburg, Germany) Struktol® SB 2121, Struktol® J 673 A, Struktol® J 647 and CONTRASPUM® A 4050 of Zschimmer & Schwarz GmbH & Co KG (Lahnstein, Germany) were screened for their suitability in a fed-batch FAL process. According to the manufacturers, the products are based on non-ionic alkylene oxide (Struktol® SB 2121), alkoxylated fatty acid esters (Struktol® J 673 A), polyglycol ethers of aliphatic alcohols (Struktol® J 647) and on C6-11 branched alkenes (CONTRASPUM® A 4050). Nevertheless, the precise compositions of the complex mixtures remain unknown.

Before using any of the respective compounds in a bioprocess, their compatibility with the FAL extraction and subsequent GC analysis was tested. Thus, an aqueous solution containing 0.2 % (v/v) antifoaming agent was extracted with ethyl acetate and analyzed via the standard FAL GC method (3.7.4). While the extracted CONTRASPUM® led to an elevated baseline, no discrete peaks interfering with the analytes of interest were detected in the antifoaming agents-containing matrixes (Figure S. 5). Therefore, all four products were used in subsequent bioprocesses.

As described by Kiefer et al. (2021), 0.5 mL of each compound were added to 500 mL growth medium prior to inoculation. When required, more antifoaming agent was injected manually with a syringe during the running process. The cultivations were performed using $CgXII_{mod,2}$ medium. The glucose feed for the fed-batch phase was adjusted to obtain a growth rate of 0.15 h^{-1}.

Visualized data of all processes using Struktol® products as antifoaming agents can be found in the appendix (Figure S. 6, Figure S. 7, Figure S. 8). The use of CONTRASPUM® A 4050 enabled the most stable process, resulting in a final FAL concentration of almost 2 g_{FAL} L^{-1} (Figure 23). Product yields of 0.020 to 0.022 g g^{-1} were similar for all tested process conditions during the batch phase but decreased during the fed-batch phase for all Struktol®-utilizing processes. Just in the CONTRASPUM® setup, the $Y_{P/S}$ increased by 35 % to 0.027 g g^{-1} (Table 17), which was comparable to the yields obtained in shaking flask experiments with glucose (Table 14). That data indicated that the product yield as one of the important KPI could be kept constant during scale-up for a fed-batch process.

Additionally, a volumetric productivity of 0.118 g_{FAL} L^{-1} h^{-1} was obtained in the CONTRASPUM®-utilizing process, which represented a 327 % increase compared to cultivations in shaking flasks (Table 14).

Yet, frequent manual addition of the antifoaming agent was still required in all setups, in particular towards the end of the cultivations. Several milliliters of each antifoaming agent had to be added to the corresponding processes. Nevertheless, collapsing foam or even preventing its formation was not possible using any of the tested four products. All processes were stopped when foam formation was not manageable anymore.

Differences in increasing agitation as an automated measure to keep the DO constant in relation to the formed biomass could be observed. While the best-performing process with CONTRAPUM® reached a maximum agitation rate of about 1200 rpm at a biomass concentration of 31.28 g L^{-1}, the upper agitation threshold of 1500 rpm was reached in processes using Struktol® SB 2121 and Struktol® J 647. The biomass concentrations in both processes were lower than 30 g L^{-1} when the upper agitation limit was reached. The steeper rise of the agitation rate as a response to counteract the DO drop after administering both Struktol® products indicated a stronger impact on the volumetric mass transfer coefficient k_La compared to CONTRASPUM® A 4050. Both negative and positive effects of chemical antifoaming agents on the k_La and, thus, on the oxygen transfer rate (OTR) were thoroughly reviewed elsewhere (Morão et al., 1999; Vardar-Sukan, 1998).

Besides, a cease in growth, also indicated by a drop of the agitation and slight accumulation of glucose, was observed towards the end of the CONTRAPUM® process (Figure 23). Similar phenomena were observed previously at lower final biomass concentrations prior to increasing some media components (4.2.2). It therefore seems plausible that the observed cease in growth was again caused by a limiting co-substrate. However, a final reached biomass concentration of 31.28 g_{CDW} L^{-1} compared to 17 to 22 g_{CDW} L^{-1} obtained with the $CgXII_{mod}$ medium (4.2.2) showed that the performed media optimization (4.2.2.1) was successful.

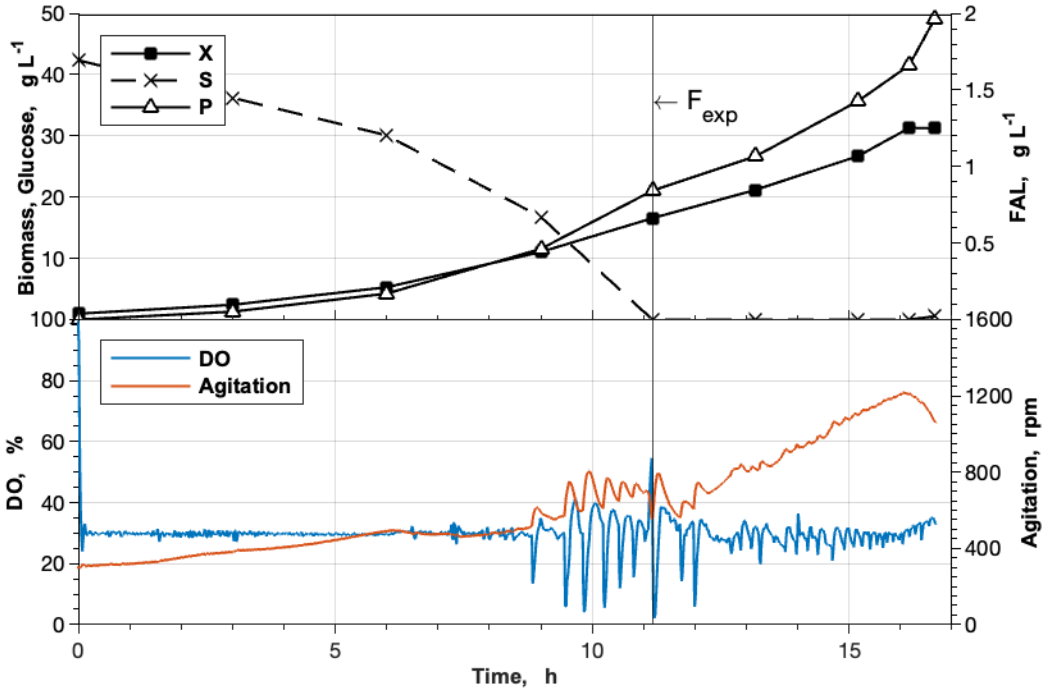

Figure 23: Usage of CONTRASPUM® A 4050 as an antifoaming agent in a fed-batch cultivation. Fed-batch cultivations were conducted in a 1 L Bio-Flo120® bioreactor system with an initial batch volume of 0.5 L. The cultivations of *C. glutamicum* Δ*fasR* cg2692$_{TTG}$ (pEKEx2-*maqu2220*) were performed at 30 °C in CgXII$_{mod,2}$ medium. The medium was supplemented with 195 µM PCA, 0.5 mL CONTRASPUM® A 4050, and had an initial glucose concentration of 40 g L^{-1}. The exponential feed rate was set to obtain a growth rate of 0.15 h^{-1}. F_{exp} indicates the start of the feed upon depletion of the carbon source. Data was obtained from a single experiment. X: biomass; S: glucose; P: FAL; DO: dissolved oxygen.

Table 17: KPI of fed-batch processes with different antifoaming agents. A 1 L BioFlo120® bioreactor system with an initial batch volume of 0.5 L was used. The cultivations of *C. glutamicum* Δ*fasR* cg2692$_{TTG}$ (pEKEx2-*maqu2220*) were performed at 30 °C in CgXII$_{mod,2}$ medium. The medium was supplemented with 195 µM PCA and had an initial glucose concentration of 40 g L^{-1}. CONTRASPUM® A 4050, Struktol® SB 2121, Struktol® J 673 A, or Struktol® J 647 were used as antifoaming agents.

Phase	KPI	CONTRASPUM®	SB 2121	J 673 A	J 647
Batch phase	µ | h^{-1}	0.26	0.23	0.24	0.23
	$Y_{X/S}$ | g_{CDW} g^{-1}	0.38	0.37	0.38	0.38
	q_S | g g_{CDW}^{-1} h^{-1}	0.68	0.62	0.61	0.61
	$Y_{P/S}$ | g g^{-1}	0.020	0.021	0.020	0.022
	$Y_{P/S}$ | Cmol Cmol^{-1}	0.040	0.042	0.038	0.043
Fed-batch phase	µ | h^{-1}	0.16	0.14	0.18	0.14
	Q_P | g L^{-1} h^{-1}	0.205	0.140	0.119	0.125
	$Y_{P/S}$ | g g^{-1}	0.027	0.019	0.018	0.018
	$Y_{P/S}$ | Cmol Cmol^{-1}	0.053	0.038	0.036	0.036
Total	Q_P | g L^{-1} h^{-1}	0.118	0.090	0.073	0.090
	$Y_{P/S}$ | g g^{-1}	0.024	0.020	0.019	0.020
	$Y_{P/S}$ | Cmol Cmol^{-1}	0.048	0.040	0.037	0.040
	CDW_{max} | g_{CDW} L^{-1}	31.28	22.08	21.16	28.52
	$c_{FAL,max}$ | g L^{-1}	1.97	1.48	1	1.51

4.2.2.3 Glucose-based fed-batch process

A final fed-batch cultivation with glucose as the carbon source was conducted as a duplicate. The promising antifoaming agent CONTRASPUM® (4.2.2.2.2) was added continuously with a feed rate of 100 µL h^{-1} 8 h after the start of the cultivations to control foam formation. Previous experiments and unpublished data of Katharina Hofer (University of Stuttgart, Stuttgart, Germany) suggested that $MgSO_4$ might be a limiting substrate during conducted cultivations. Thus, its concentration in the used CgXII$_{mod,2}$ was doubled to 1 g L^{-1} and is hereby referred to as CgXII$_{mod,3}$ medium.

In contrast to previous cultivations, a lag phase of 3-5 h was observed in both processes, prolonging the respective cultivation times and influencing volumetric productivities negatively. As observed before, extensive foaming occurred, rendering both processes extremely unstable. Despite using a constant feed of antifoaming agent, manual addition of CONTRASPUM® was required regularly. Nevertheless, both processes ultimately had to be stopped because of uncontrollable foaming. Final titers of 1.91 and 1.65 g_{FAL} L^{-1} and volumetric productivities of 0.090 and 0.074 g_{FAL} L^{-1} h^{-1} were reached in both processes (Figure 24, Table 18).

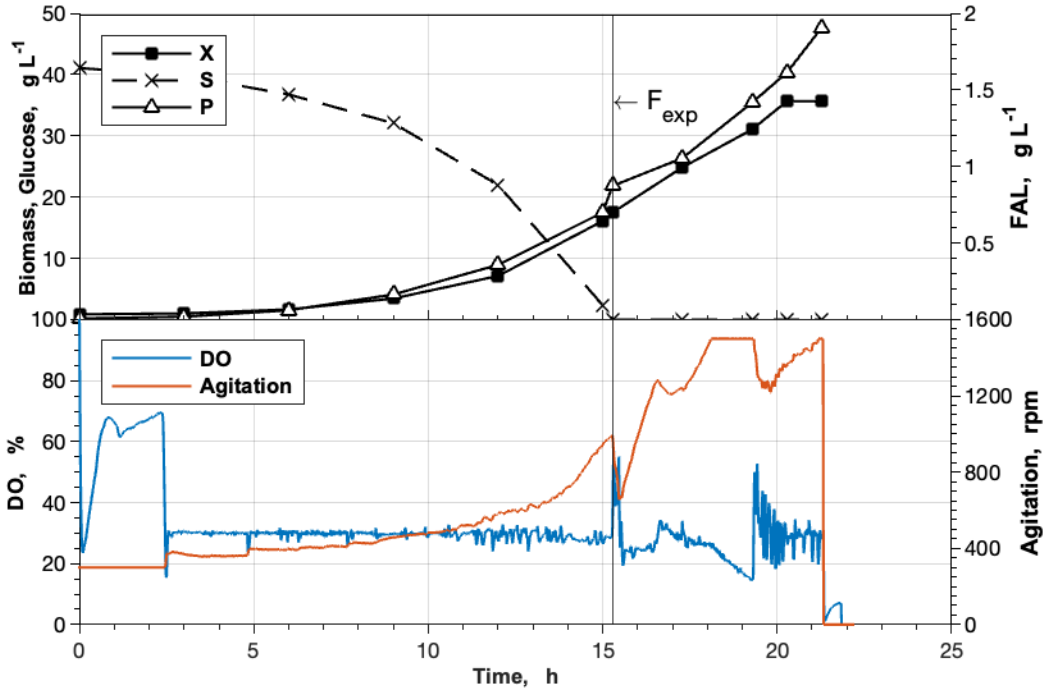

Figure 24: Fed-batch process with glucose as carbon source. Fed-batch cultivations were conducted in a 1 L BioFlo120® bioreactor system with an initial batch volume of 0.5 L. The cultivations of *C. glutamicum* Δ*fasR* cg2692$_{TTG}$ (pEKEx2-*maqu2220*) were performed at 30 °C in CgXII$_{mod,3}$ medium. The medium was supplemented with 195 µM PCA and had an initial glucose concentration of 40 g L^{-1}. The exponential feed rate was set to obtain a growth rate of 0.15 h^{-1}. F_{exp} indicates the start of the feed upon depletion of the carbon source. The shown process data is representative of two conducted bioreactor cultivations using the same process conditions. X: biomass; S: glucose; P: FAL; DO: dissolved oxygen.

The aeration rate in both processes was increased from 0.25 to 0.5 L min^{-1} 4 h after the glucose feeds were started because the agitation was already operating at its maximum

and could thus not further control the DO. As observed in previous processes, biomass formation plateaued towards the end of the cultivation, indicating a limiting substrate other than glucose. As doubling the $MgSO_4$ concentration did not prevent stagnating biomass formation between 30 and 40 g_{CDW} L^{-1}, it seems plausible that another substrate was limiting. Nevertheless, the increased $MgSO_4$ concentration still influenced the final biomass concentration positively, as the obtained biomass concentrations of about 35.65 and 36.8 g_{CDW} L^{-1} were 14 and 17 % higher than previously obtained ones (Table 17, Table 18).

Table 18: KPI of fed-batch processes with glucose as carbon source. A 1 L BioFlo120® bioreactor system with an initial batch volume of 0.5 L was used. The cultivations of *C. glutamicum* Δ*fasR* cg2692$_{TTG}$ (pEKEx2-*maqu2220*) were performed at 30 °C in CgXII$_{mod,3}$ medium. The medium was supplemented with 195 µM PCA and had an initial glucose concentration of 40 g L^{-1}. CONTRASPUM® A 4050 was used as an antifoaming agent. Shown data are from two identical processes.

Phase	KPI	Cultivation 1	Cultivation 2
Batch phase	μ^* | h^{-1}	0.25	0.27
	$Y_{X/S}^*$ | g_{CDW} g^{-1}	0.42	0.42
	q_S^* | g g_{CDW}^{-1} h^{-1}	0.60	0.64
	$Y_{P/S}$ | g g^{-1}	0.021	0.019
	$Y_{P/S}$ | Cmol $Cmol^{-1}$	0.042	0.037
Fed-batch phase	µ | h^{-1}	0.16	0.17
	Q_P | g L^{-1} h^{-1}	0.173	0.148
	$Y_{P/S}$ | g g^{-1}	0.024	0.020
	$Y_{P/S}$ | Cmol $Cmol^{-1}$	0.047	0.041
Total	Q_P | g L^{-1} h^{-1}	0.090	0.074
	$Y_{P/S}$ | g g^{-1}	0.023	0.020
	$Y_{P/S}$ | Cmol $Cmol^{-1}$	0.045	0.039
	CDW_{max} | g_{CDW} L^{-1}	35.65	36.80
	$c_{FAL,max}$ | g L^{-1}	1.91	1.65

*determined between 6 h and the end of the batch phase

4.2.3 FAL production with wheat straw hydrolysate

While initial strain engineering and respective characterization were conducted with the first-generation feedstock glucose, further strain engineering and process development were focused on utilizing the second-generation feedstock wheat straw hydrolysate.

4.2.3.1 Analysis of the hydrolysate matrix

Before conducting growth experiments, CgXII medium containing 20 g glucose L^{-1} provided by hydrolysate was analyzed via HPLC and GC to determine the compatibility of the established analytical methods with the novel matrix (Figure 25). The standard carbohydrate HPLC method was suitable to detect and separate glucose and xylose, which are the two most abundant carbohydrates of the hydrolysate (Figure 25, A & B). However, xylose and a so far unknown analyte with similar retention time were not separable (Figure 25, B). In that context, it was shown that the unidentified analyte was not arabinose, another pentose present in the hydrolysate (data not shown). Another possible candidate for the unknown analyte was fructose, as glucose partially isomerizes into fructose upon heat-sterilization (Takors et al., 2007). The noticeably increased peak area of the unknown analyte after autoclaving supported the assumption. However, xylose and fructose were not satisfactorily separable by the used HPLC method. Nevertheless, due to similar retention times of the unknown analyte and fructose, it seemed plausible that at least some fructose was formed and contributed to the xylose peak's shoulder (Figure 25 C).

Unidentified peaks were also detected using the GC method used for FAL quantification. Since those peaks had different retention times and showed good resolution to their neighboring signals, no method adjustment was necessary (Figure 25, C). Analytes with similar retention times to 1-hexadecanol and heptadecanol were present in the hydrolysate matrix (Figure 25, C). Due to their small peak area, they were considered negligible.

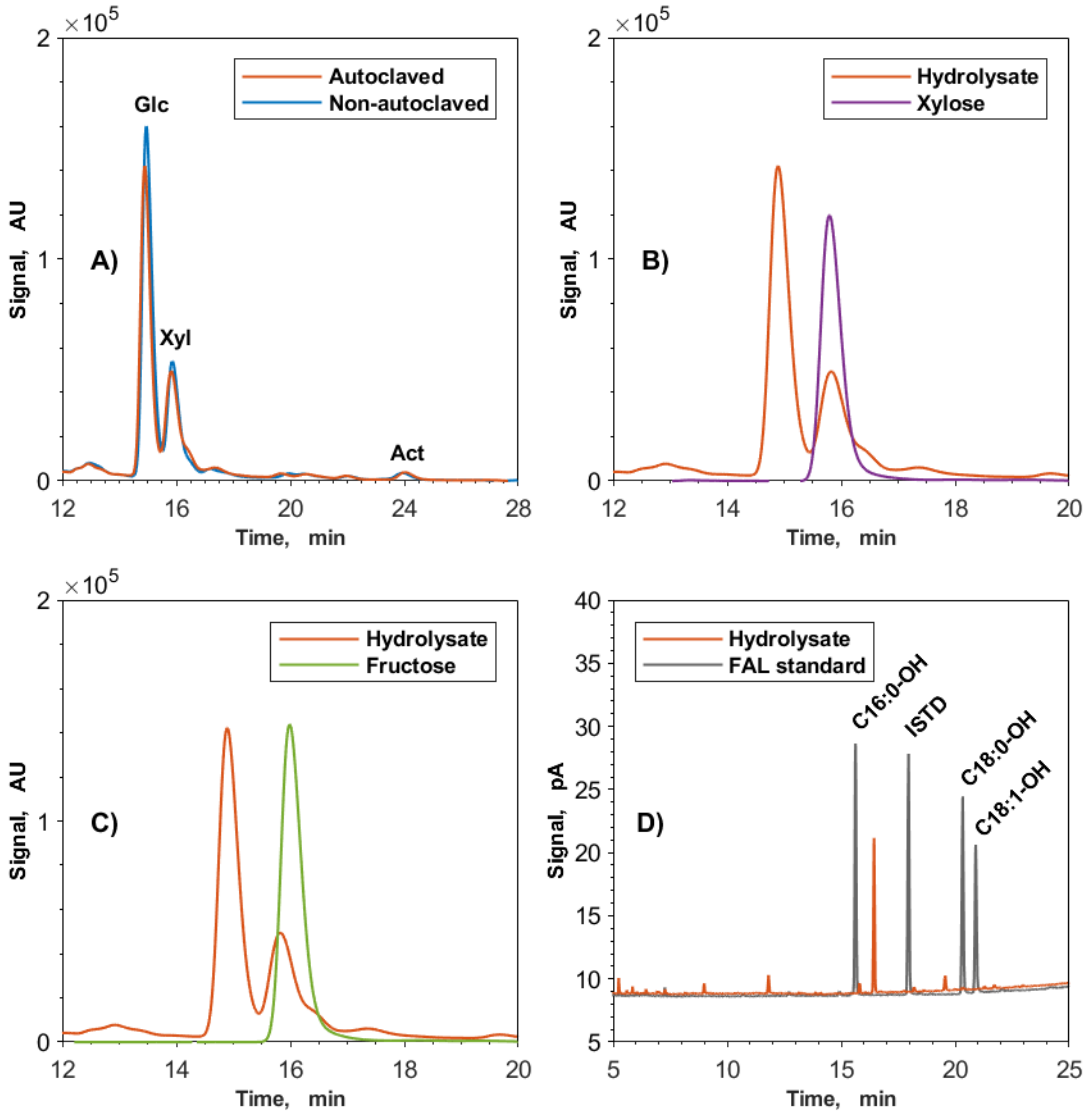

Figure 25: Testing established HPLC and GC methods on the hydrolysate matrix. A) HPLC: CgXII + 2 % hydrolysate before and after autoclaving with labeled peaks of glucose (Glc), xylose (Xyl), and acetate (Act); B) HPLC: CgXII + 2 % hydrolysate (autoclaved) and 100 µM xylose; C) HPLC: CgXII + 2 % hydrolysate (autoclaved) and 100 µM fructose; D) GC: CgXII + 2 % hydrolysate (autoclaved) and 1-hexadecanol (C16:0-OH), heptadecanol (ISTD), octadecanol (C18:0-OH), and oleyl alcohol (C18:1-OH) (50 mg L^{-1} each).

4.2.3.2 Impact of autoclaving on the hydrolysates' composition

The observed partial degradation of the hydrolysate during autoclaving (4.2.3.1) was further studied. Four different hydrolysate stock solutions (125, 200, 300 and 350 g glucose L^{-1}) were prepared and analyzed before and after autoclaving to test

whether the degradation effect was dependent on the hydrolysate's concentration. Glucose, xylose, and acetate as the main quantifiable carbon sources were monitored.

While the 125 g glucose L^{-1} hydrolysate stock lost 15 % glucose and 4 % xylose during autoclaving, a 40 % and 28 % decrease in the glucose and xylose concentration were observed in the 350 g glucose L^{-1} hydrolysate stock, respectively. The acetate concentration remained almost unaffected by the heat exposure independently of the stock's concentration. The relative loss of the three carbon sources in the different hydrolysate stock solutions is visualized in Figure 26.

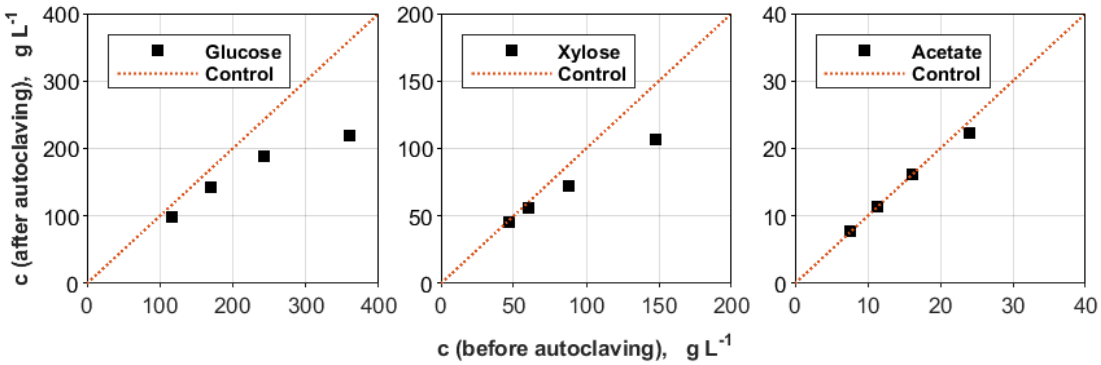

Figure 26: Effect of autoclaving on the main carbon sources in different hydrolysate stock solutions. Four hydrolysate stock solutions with glucose concentrations of 125, 200, 300, and 350 g L^{-1} were analyzed via HPLC before and after autoclaving. The respective concentrations of glucose (A), xylose (B), and acetate (C) were quantified. The orange line visualizes a hypothetical sample with no degradation during the autoclaving process. Data was obtained from one technical replicate.

For shaking flask experiments, a loss of up to 15 % glucose was assumed to be acceptable. Thus, an autoclaved 125 g glucose L^{-1} hydrolysate stock was used for respective cultivations. However, for fed-batch cultivations, it was desirable to use a highly concentrated substrate solution to prevent excessive dilution of the fermentation broth. As autoclaving highly concentrated hydrolysate stocks was shown to be unsuitable, a non-autoclaved 350 g glucose L^{-1} hydrolysate stock was used for bioreactor cultivations. Due to the use of antibiotics, the acidic pH of the hydrolysate, the presence of growth-inhibiting lignocellulosic degradation products, and the hydrolysate's generally high sugar content contaminations were assumed to not be a problem.

4.2.3.3 Implementation of a xylose-utilization module and cofactor engineering for the efficient valorization of wheat straw hydrolysate

Xylose, the second-most abundant carbohydrate after glucose in the hydrolysate, cannot be natively metabolized by *C. glutamicum*. Consequently, a xylose-metabolizing strain was engineered by Lynn S. Schwardmann (Bielefeld University) to fully harness the hydrolysate's potential as an alternative carbon source (Werner et al., 2023). The constructed strain *C. glutamicum* Δ*actA*::*xylAB* harbored the xylose isomerase-encoding gene *xylA* (*X. campestris*) and the xylulokinase-encoding gene *xylB* (*C. glutamicum*) integrated into the *actA* locus. ALE yielded strain Δ*actA*::*xylAB*$_{evol}$ (*C. glutamicum* gX), which featured improved growth with xylose due to a beneficial mutation in the 5` coding sequence and the immediate 5' UTR of *xylA*.

In order to obtain FAL production from xylose, the gX module, comprising the genes *xylA* and *xylB* with the evolved sequence, was transferred to *C. glutamicum* Δ*fasR* cg2692$_{TTG}$, which subsequently was transformed with pEKEx2-*maqu2220* to yield strain *C. glutamicum* Δ*fasR* cg2692$_{TTG}$ gX (pEKEx2-*maqu2220*).

However, the first cultivations of that newly constructed strain in CgXII medium containing hydrolysate at a concentration of 20 g glucose L^{-1} resulted in no observed growth when the standard seed train for a shaking flask experiment on glucose was followed. Thus, a CgXII + 10 g glucose L^{-1} obtained from hydrolysate pre-culture was implemented instead of a 2x TY pre-culture (suggestion of Katharina Hofer, University of Stuttgart), restoring growth in a subsequent 20 g glucose L^{-1} hydrolysate-containing main culture (Figure 27). The seedtrain was adjusted accordingly (3.6.3).

Generally, using hydrolysate as a carbon source seemed to be beneficial for FAL production as *C. glutamicum* Δ*fasR* cg2692$_{TTG}$ (pEKEx2-*maqu2220*) reached a titer of 681 ± 27 mg_{FAL} L^{-1} with a product yield and volumetric productivity of 0.071 ± 0.004 Cmol $Cmol^{-1}$ and 57 ± 2 mg_{FAL} L^{-1} h^{-1}, respectively (Table 19). However, neither product yield nor volumetric productivity were improved by enabling xylose utilization in strain *C. glutamicum* Δ*fasR* cg2692$_{TTG}$ gX (pEKEx2-*maqu2220*). While the titer of 705 ± 77 mg_{FAL} L^{-1} remained comparable to the control strain, the product yield decreased by 18 % to 0.058 ± 0.009 Cmol $Cmol^{-1}$. The volumetric productivity decreased comparably (Table 19).

From the initially provided carbon of about 27 g_C L^{-1}, 18.3 ± 0.2 and 17.5 ± 0.5 g_C L^{-1} remained after 15 h in the supernatant of both the control strain and the gX mutant, respectively. A carbon content of 8.44 g_C L^{-1} can be attributed to the non-metabolizable buffering agent MOPS. Even taking into account the non-utilized xylose at the respective sampling points, about 40 % of the organic carbon provided by the hydrolysate was not utilized by any of the FAL-producing strains.

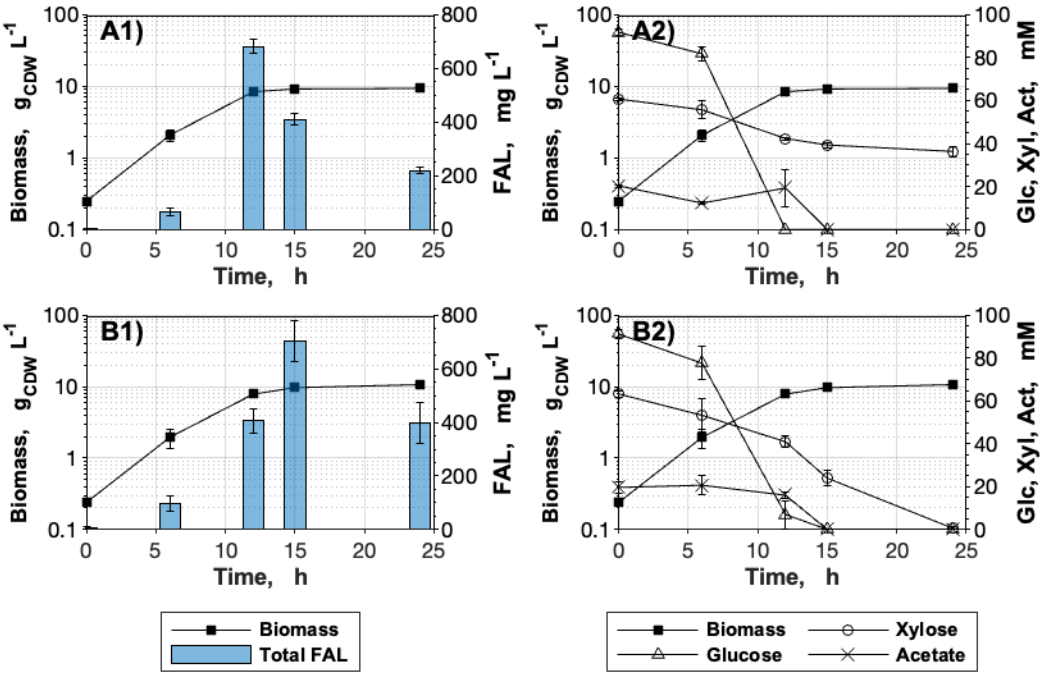

Figure 27: FAL production with hydrolysate. Cultivations were conducted in CgXII medium supplemented with 195 µM PCA. The carbon source was provided by hydrolysate, normalized to a concentration of 20 g glucose L^{-1}. A) *C. glutamicum* Δ*fasR* cg2692$_{TTG}$ (pEKEx2-*maqu2220*); B) *C. glutamicum* Δ*fasR* cg2692$_{TTG}$ gX (pEKEx2-*maqu2220*). Data represents the means of 3 biological replicates with standard deviations. (Werner et al., 2023)

Evidently, the majority of carbon supplied by xylose did not end up in the product of interest. Buschke et al. (2013a) reported an insufficient NADPH supply through the oxidative PPP of a modified *C. glutamicum* strain cultivated on xylose. In order to ensure an adequate supply of the cofactor for the NADPH-expensive FAL biosynthesis, the well-studied *E. coli* transhydrogenase-encoding genes *pntAB* (Blombach et al., 2011; Zhan et al., 2019) were genomically integrated into the landing pad CgLP12 (Lange et al., 2018), resulting in the strain *C. glutamicum* Δ*fasR* cg2692$_{TTG}$ CgLP12::(P_{tac}-*pntAB*-T_{rrnB}) gX (pEKEx2-

maqu2220). The genomic integration of the transhydrogenase increased the volumetric productivity by 32 % to 62 ± 1 mg_{FAL} L^{-1} h^{-1} with the gX strain background while also increasing the product yield by 29 % to 0.075 ± 0.003 Cmol $Cmol^{-1}$. No positive effects on FAL production upon expressing the transhydrogenase were observed in the control strain lacking the xylose utilization module (Table 19). Similar to previous cultivations, a major fraction of the carbon provided by the hydrolysate remained in the culture's supernatant.

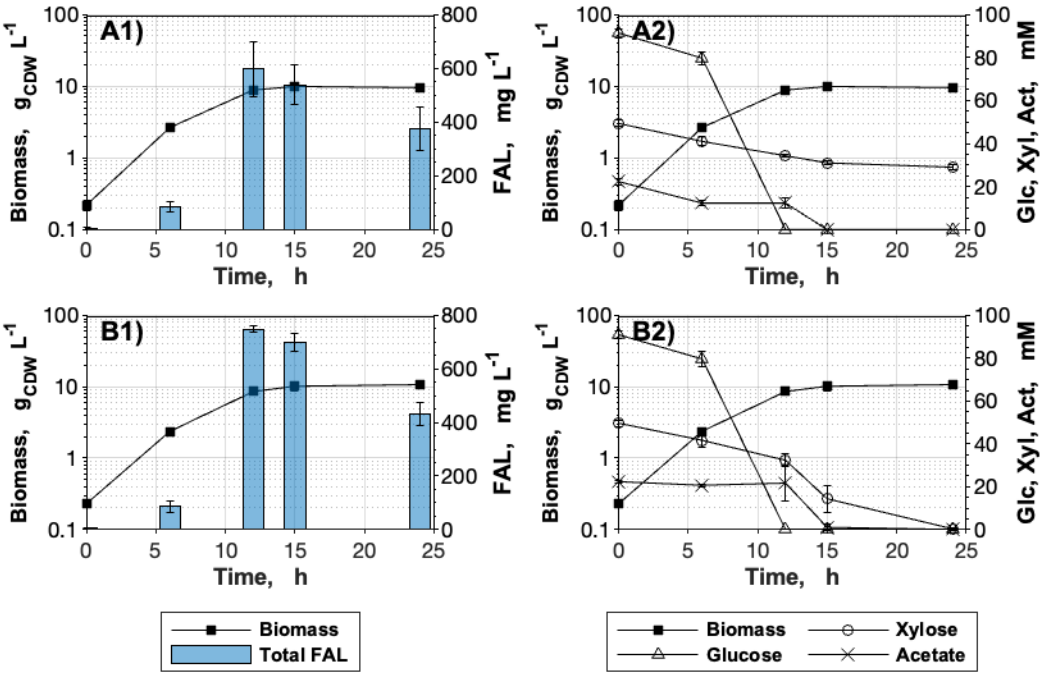

Figure 28: Influence of transhydrogenase expression on FAL production for cultivations with hydrolysate. Cultivations were conducted in CgXII medium supplemented with 195 µM PCA. The carbon source was provided by hydrolysate, normalized to a concentration of 20 g glucose L^{-1}. A) *C. glutamicum* Δ*fasR* $cg2692_{TTG}$ CgLP12::(P_{tac}-*pntAB*-T_{rrnB}) (pEKEx2-*maqu2220*); B) *C. glutamicum* Δ*fasR* $cg2692_{TTG}$ CgLP12::(P_{tac}-*pntAB*-T_{rrnB}) gX (pEKEx2-*maqu2220*). Data represents the means of 3 biological replicates with standard deviations. (Werner et al., 2023)

Table 19: KPI of FAL-producing strains cultivated on hydrolysate. Cultivations of *C. glutamicum* Δ*fasR* cg2692$_{TTG}$ (pEKEx2-*maqu2220*) (control), *C. glutamicum* Δ*fasR* cg2692$_{TTG}$ gX (pEKEx2-*maqu2220*) (gX), *C. glutamicum* Δ*fasR* cg2692$_{TTG}$ CgLP12::(P$_{tac}$-*pntAB*-T$_{rrnB}$) (pEKEx2-*maqu2220*) (*pntAB*) and *C. glutamicum* Δ*fasR* cg2692$_{TTG}$ CgLP12::(P$_{tac}$-*pntAB*-T$_{rrnB}$) gX (pEKEx2-*maqu2220*) (*pntAB* gX) were conducted in CgXII medium supplemented with 195 µM PCA. The carbon source was provided by hydrolysate, normalized to a concentration of 20 g glucose L^{-1}. Data represents the means of 3 biological replicates ± standard deviations. (Werner et al., 2023)

KPI	Control	gX	*pntAB*	*pntAB* gX
$c_{FAL, Total}$ | mg L^{-1}	681 ± 27	705 ± 77	597 ± 103	748 ± 12
$Y_{P/S}$ | Cmol Cmol^{-1}	0.071 ± 0.004	0.058 ± 0.009	0.065 ± 0.01	0.075 ± 0.003
Q_P | mg L^{-1} h^{-1}	57 ± 2	47 ± 5	50 ± 9	62 ± 1

4.2.3.4 Reduction of the citrate synthase expression for a reduced carbon flux into the TCA cycle

Despite the positive effect of *pntAB* expression on the yield and volumetric productivity in a gX background, HPLC data suggested that xylose-derived carbon was still not sufficiently channeled into FAL formation (Figure 28 B2). To provide more acetyl-CoA for the conversion into malonyl-CoA, the competing flux into the TCA cycle, catalyzed by the *gltA*-encoded citrate synthase (CS), had to be decreased (Milke et al., 2019b). A reduction of *gltA* expression was achieved by exchanging its native promoter in *C. glutamicum* Δ*fasR* cg2692$_{TTG}$ CgLP12::(P$_{tac}$-*pntAB*-T$_{rrnB}$) gX (pEKEx2-*maqu2220*) for the P$_{dapA}$ variants A25, L1, and C7 which reportedly result in a remaining CS activity of 26, 16, and 10 %, respectively (van Ooyen et al., 2012). FAL titers decreased in a promoter strength-dependent manner to 448 ± 11, 277 ± 31, and 254 ± 33 mg$_{FAL}$ L^{-1} for A25, L1, and C7, respectively (Table 20). As the maximal titers were obtained for all strains after cultivating them for 12 h, the volumetric productivities decreased similarly.

Table 20: KPI of FAL-producing *gltA* promoter mutants. Cultivations of *C. glutamicum* Δ*fasR* cg2692$_{TTG}$ CgLP12::(P$_{tac}$-*pntAB*-T$_{rrnB}$) gX (pEKEx2-*maqu2220*) (control), *C. glutamicum* Δ*fasR* cg2692$_{TTG}$ CgLP12::(P$_{tac}$-*pntAB*-T$_{rrnB}$) ΔP$_{gltA}$::P$_{dapA}$_A25 gX (pEKEx2-*maqu2220*) (A25), *C. glutamicum* Δ*fasR* cg2692$_{TTG}$ CgLP12::(P$_{tac}$-*pntAB*-T$_{rrnB}$) ΔP$_{gltA}$::P$_{dapA}$_L1 gX (pEKEx2-*maqu2220*) (L1) and *C. glutamicum* Δ*fasR* cg2692$_{TTG}$ CgLP12::(P$_{tac}$-*pntAB*-T$_{rrnB}$) ΔP$_{gltA}$::P$_{dapA}$_C7 gX (pEKEx2-*maqu2220*) (C7) were conducted in CgXII medium supplemented with 195 µM PCA. The carbon source was provided by hydrolysate, normalized to a concentration of 20 g glucose L^{-1}. Data represents the means of 3 biological replicates ± standard deviations.

KPI	Control	A25	L1	C7
$c_{FAL, Total}$ | mg L^{-1}	748 ± 12	448 ± 11	277 ± 31	254 ± 33
$Y_{P/S}$ | Cmol Cmol^{-1}	0.075 ± 0.003	0.049 ± 0.002	0.033 ± 0.005	0.028 ± 0.008
Q_P | mg L^{-1} h^{-1}	62 ± 1	37 ± 1	23 ± 3	21 ± 3

4.2.3.5 Scale-up: development of a fed-batch process with hydrolysate

A scaled-up bioprocess on hydrolysate was conducted using *C. glutamicum* Δ*fasR* cg2692$_{TTG}$ CgLP12::(P$_{tac}$-*pntAB*-T$_{rrnB}$) gX (pEKEx2-*maqu2220*) as the best-performing iteration of the FAL producing strains. Based on data obtained in chapter 4.2.3.2, a non-autoclaved 350 g glucose L^{-1} hydrolysate stock was used to provide the carbon source. Due to the observed sequential xylose utilization, a pulsed feed profile was chosen. The process was conducted three times and the corresponding KPI characterizing the batch phase, fed-batch phase, and the entire process (total) are listed in Table 21, while process data of one process is shown exemplarily in Figure 29. Process data of the other two fed-batch cultivations are shown in the appendix in Figure S. 9 and Figure S. 10.

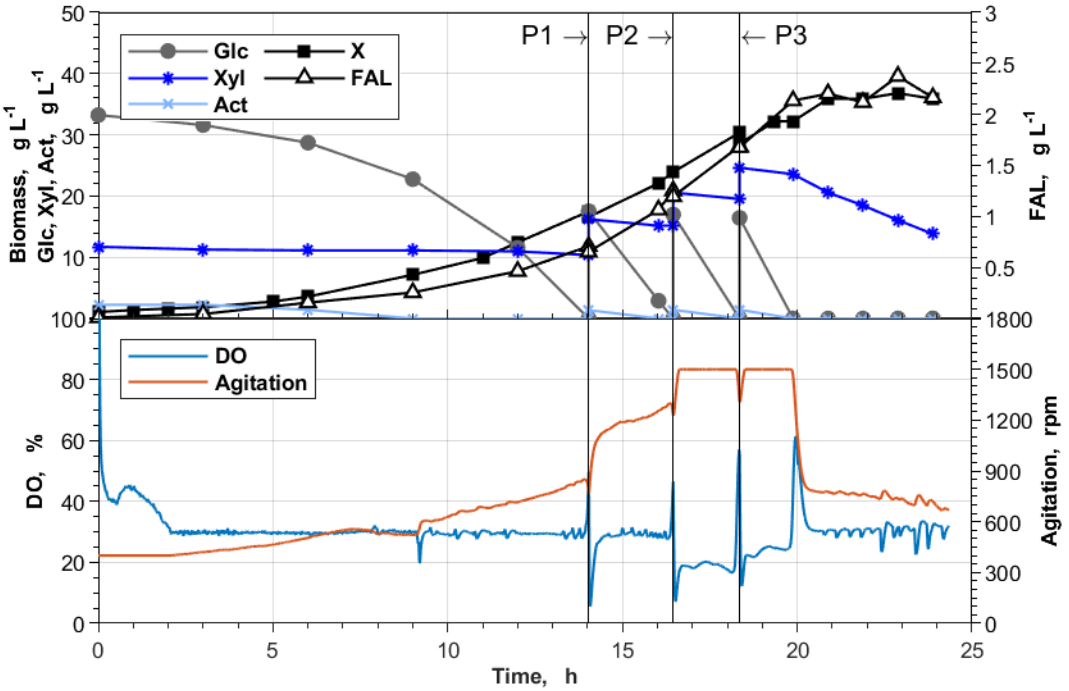

Figure 29: Pulsed fed-batch cultivation with wheat straw hydrolysate. Fed-batch cultivations of *C. glutamicum* Δ*fasR* cg2692$_{TTG}$ CgLP12::(P_{tac}-*pntAB*-T_{rrnB}) gX (pEKEx2-*maqu2220*) were conducted in a 1 L BioFlo120® bioreactor system with an initial batch volume of 0.5 L in $CgXII_{mod,3}$ medium supplemented with 195 µM PCA. The carbon source during the batch phase was provided by hydrolysate, normalized to a concentration of 40 g glucose L^{-1}. 30 mL Pulses (P) of a 350 g glucose L^{-1} hydrolysate stock solution were added three times upon a sharp increase of the DO signal. The shown process data is representative of three conducted bioreactor cultivations using the same process conditions. Act: acetate; DO: dissolved oxygen; Glc: glucose; X: biomass; Xyl: xylose. (Werner et al., 2023)

During the batch phase, the product yield of 0.038 ± 0.002 Cmol $Cmol^{-1}$ was, on average, 42 % lower than the yield obtained during the fed-batch phase (0.065 ± 0.008 Cmol $Cmol^{-1}$). Glucose and acetate were always fully consumed during the pulses, while xylose accumulated and was just consumed when glucose was depleted. Once xylose consumption started, no notable biomass- or product formation was observed. While extensive foam formation was encountered in a glucose-based fed-batch process, the hydrolysate-based process ran stably. Solely when the glucose provided by the third pulse (Figure 29, P3) was depleted, foaming occurred. The conducted processes resulted in a final FAL titer of 2.45 ± 0.09 g_{FAL} L^{-1} and a volumetric productivity of 0.109 ± 0.005 g_{FAL} L^{-1} h^{-1} (Table 21), which represented a more than 3-fold and 1.8-fold

increase compared to the shaking flask experiments, respectively (Table 19). Generally, maximal titers were increased by 28 % relative to comparable fed-batch processes using glucose as the sole carbon source (Table 18). This was also contributed to the more stable process conditions, allowing for longer cultivations.

Table 21: KPI of a pulsed fed-batch process with wheat straw hydrolysate. Cultivations of *C. glutamicum* Δ*fasR* cg2692$_{TTG}$ CgLP12::(P_{tac}-*pntAB*-T_{rrnB}) gX (pEKEx2-*maqu2220*) were conducted in $CgXII_{mod,3}$ medium supplemented with 195 µM PCA. The carbon source during the batch phase was provided by hydrolysate, normalized to a concentration of 40 g glucose L^{-1}. 30 mL pulses of a 350 g glucose L^{-1} hydrolysate stock solution were added three times upon a sharp increase of the DO signal. Data represents the means of 3 biological replicates ± standard deviations. (Werner et al., 2023)

Phase	KPI	
Batch phase	Q_P | g L^{-1} h^{-1}	0.049 ± 0.001
	$Y_{P/S}$ | Cmol $Cmol^{-1}$	0.038 ± 0.002
Fed-batch phase	Q_P | g L^{-1} h^{-1}	0.227 ± 0.028
	$Y_{P/S}$ | Cmol $Cmol^{-1}$	0.065 ± 0.008
Total	Q_P | g L^{-1} h^{-1}	0.109 ± 0.005
	$Y_{P/S}$ | Cmol $Cmol^{-1}$	0.054 ± 0.005
	CDW_{max} | g_X L^{-1}	37.4 ± 1.1
	$c_{FAL,max}$ | g L^{-1}	2.45 ± 0.09

5. Discussion

This work studied the FA biosynthesis of the non-oleaginous organism *C. glutamicum*. Insights into the respective metabolic pathways were used to engineer FA-producing mutants and to optimize corresponding cultivation conditions. On this basis, strains and process conditions were further modified to achieve efficient heterologous FAL production from the first- and second-generation feedstocks glucose and lignocellulosic wheat straw hydrolysate, respectively.

5.1 Physiological studies of the FA biosynthesis in *C. glutamicum*

5.1.1 Complex interplay: Nitrogen limitation-induced FA production

Despite reports of efficient FA-production with *C. glutamicum* mutants under solely carbon-limited cultivation conditions (Ikeda et al., 2020; Takeno et al., 2023; Takeno et al., 2018; Takeno et al., 2013), in this work accumulation and efflux thereof could just be observed when nitrogen was the limiting substrate. Plassmeier et al. (2016) reported using a nitrogen-limiting CgXII medium derivate for the lipid production with *C. glutamicum* but neither published any comparative experiments with standard CgXII medium nor offered an explanation for the chosen medium. However, it is known that cultivating oleaginous microorganisms (prokaryotes and eukaryotes alike) under nitrogen-limited conditions seems to be beneficial, if not essential, for the production of microbial lipids (Alvarez et al., 2019; Alvarez et al., 2000; Lopes et al., 2020; Olukoshi & Packter, 1994). In some actinobacteria, including *Rhodococcus* and *Mycobacterium*, the positive influence of nitrogen starvation on lipid accumulation was traced back to the transcriptional regulator NlpR. Despite being closely related to both genera (Liebl, 2005), the respective regulator is absent in members of the *Corynebacterium* genus (Hernández et al., 2017). However, other microbial regulatory mechanisms are also known to affect lipid production under nitrogen starvation. Exemplary, Gerhardt et al. (2015) showed *in vitro* that the P_{II}-type protein GlnB reduced the ACC activity of *E. coli*, while another P_{II} protein GlnK was also able to bind to the biotinylated ACC subunit AccB (Rodrigues et al., 2014), without affecting ACC activity (Gerhardt et al., 2015). Under low nitrogen or high 2-oxoglutarate conditions, GlnB is uridynylated by GlnD, thus relieving the inhibitory effect on the ACC. A conserved regulatory effect was proposed since the effect has also been reported for *Arabidopsis thaliana* (Feria Bourrellier et al., 2010) and *Azospirillum basiliense* (Gerhardt et al., 2015). However, studies *in vivo*

suggested that the binding of both P_{II} proteins GlnB and GlnK needed to be prevented to stimulate FA biosynthesis (Rodrigues et al., 2019). *C. glutamicum* only possesses GlnK as a member of the P_{II} protein family. There, it is involved in nitrogen control and transduction of respective signals through its adenylation rather than its uridylylation status, controlled by the adenylyltransferase GlnD (Nolden et al., 2001; Strösser et al., 2004). Additionally, it was suggested that the intracellular metabolites 2-oxoglutarate and ammonium serve as effector molecules to communicate nitrogen availability (Müller et al., 2006; Nolden et al., 2001). Due to the protein's central role in nitrogen response, similar to the well-characterized P_{II}-type proteins of *E. coli*, it may be speculated whether the corynebacterial ACC is not just regulated transcriptionally by the FasR/acyl-CoA complex (Irzik et al., 2014; Nickel et al., 2010), but also on a protein level by GlnK, depending the protein's adenylation status. While experimental evidence is lacking to support that hypothesis, results presented in this study showing that both *fasR* deletion and nitrogen-limiting cultivation conditions were required to produce, accumulate, and secrete FA with *C. glutamicum* suggest some yet uncharacterized regulation of the organism's native FA biosynthetic pathway. It would, however, also be possible that nitrogen limitation-induced changes in gene expression redistribute intracellular fluxes favoring FA biosynthesis. While no changes in ACC or FAS-I-encoding genes are reported, a reduced expression level of genes involved in the amino acid biosynthesis might favor precursor supply (Silberbach et al., 2005).

As the glucose uptake rate q_s was reported to decrease strongly in the nitrogen limitation-induced stationary phase (Chubukov et al., 2014), obtaining a growth-coupled FA production seemed desirable. Ammonium is assimilated in *C. glutamicum* through the NADPH-dependent GDH when abundantly available. In contrast, under nitrogen deficit, the more energy-intensive glutamine synthetase/ glutamate synthase (GS/GOGAT) pathway takes over (Tesch et al., 1999). When triggering a nitrogen starvation response by deleting the GDH-encoding gene *gdh* (Müller et al., 2006), FA production was generally not increased. However, efflux thereof was observed when the respective strain *C. glutamicum* Δ*fasR* Δ*gdh* was cultivated in standard CgXII medium, which was previously solely associated with medium-induced nitrogen limitation. Similarly, Müller et al. (2006) reported an increased GlnK concentration, which was just partially adenylated in a *gdh* deletion mutant cultivated under nitrogen surplus conditions. The reported effect of a not fully activated nitrogen starvation response of a *gdh* mutant, manifested in the considerable amount of unmodified GlnK (Müller et al., 2006), might also explain the limited effect of deleting *gdh* on total FA production.

Besides showing the generally positive impact of nitrogen-limiting cultivation conditions on FA production, this work further investigated the impact of different nitrogen sources, namely urea and $(NH_4)_2SO_4$, on the observed lipid-accumulating effect. It was shown that urea was the preferred nitrogen source when producing FA with *C. glutamicum*, likely due to the urease-catalyzed release of CO_2/HCO_3^-. Additional HCO_3^- supplementation did not just enhance intracellular FA synthesis but also induced a substantial efflux thereof under all tested conditions. Therefore, this observation might prove helpful in bioreactor cultivations, where the HCO_3^- concentration can be kept high by aerating with CO_2-enriched air. However, the actual mode of action of HCO_3^- on FA synthesis has yet to be elucidated. A higher HCO_3^- availability might benefit the ACC-catalyzed, malonyl-CoA-forming carboxylation reaction due to increased co-substrate availability, thus increasing the carbon flux through the FA biosynthesis pathway. A similar argumentation was proposed by Michel et al. (2015), who observed an enhanced growth with glucose and tryptone under anaerobic conditions with elevated CO_2 concentrations. Another possible explanation was provided by Blombach et al. (2013), who reported the activation of the iron homeostasis-controlling DtxR/RipA regulon in *C. glutamicum* under high CO_2/HCO_3^- conditions (Blombach et al., 2013). This observation was further studied by Müller et al. (2020), who linked the CO_2/HCO_3^--stimulated growth to an increased intracellular Fe^{2+} availability due to an abiotic, HCO_3^--dependent effect (Müller et al., 2020). There, HCO_3^- participated in the reduction of Fe^{3+} to the biologically available Fe^{2+} by phenolic compounds (Müller et al., 2020). The positive impact of the iron chelator PCA on FA production in the chosen experimental setup supports the hypothesis that FA production at least partially benefits from improved iron availability. Even though iron is not directly involved in any enzymatic reactions of the FA biosynthesis pathway, it was suggested that iron deficiency in *C. glutamicum* leads to an impaired TPP synthesis (Küberl et al., 2020). TPP itself plays a vital role in the oxidation of pyruvate by the PDHC. The reduced flux through the PDHC as a direct result of the iron starvation response may, therefore, subsequently impair FA synthesis.

5.1.2 The bottleneck in FA biosynthesis: ACC and the role of its ε-peptide AccE

Besides decoupling the FA biosynthetic pathway from the transcriptional regulator FasR, it was tested to determine whether it would be sufficient to obtain an FA-producing stain by constitutively overexpressing *fasA* and *fasB*. The reduced FA production as a result of the conducted promoter exchange supported the suggested rate-limiting role of the ACC in FA synthesis (Ikeda et al., 2017; Milke et al., 2019a; Schweizer & Hofmann, 2004b). This assumption was further validated by the positive impact of overexpressing the ACC's

catalytic subunit-encoding genes *accD1* and *accBC* on FA production. All tested strains, including the WT, showed an increased FA production upon overexpression of the respective genes.

Interestingly, while the ACC catalytic subunits AccD1 and AccBC of *C. glutamicum* have been characterized (Gande et al., 2007) and corresponding genes were often expressed heterologously (Cheng et al., 2016; Milke et al., 2019a; Wang et al., 2022), little is known about the ε-peptide AccE (Gande et al., 2007). Despite being part of the ACC and the acyl-CoA carboxylase as a non-catalytic peptide (Gande et al., 2007), no studies have focused on the physiological impact of deleting or overexpressing the AccE-encoding gene *accE* in *C. glutamicum* yet. However, Gago et al. (2006) showed that all actinomycetes examined in their study, including *C. glutamicum*, possessed putative ε-peptide-encoding genes in close proximity to genes encoding for the β-subunits of the ACC or acyl-CoA carboxylase. The cited study also showed that the homologous ε-peptide AccE5 of *M. tuberculosis* was essential for the enzymatic activity of the catalytically active α- and β-subunits of the mycobacterial acyl-CoA carboxylase (Gago et al., 2006). The reduced FA production as a result of deleting *sigD* and thus of a reduced *accE* expression (Taniguchi et al., 2017), which could be restored by transformation with pEKEx2_*accE* suggests a similar function of AccE in *C. glutamicum*.

With a maximum total FA titer of 663 ± 48 mg_{FA} L^{-1} from 20 g glucose L^{-1} obtained by the best-performing strain *C. glutamicum* Δ*fasR* (pEKEx2_*accD1BC*), the constructed strains in this study generally performed inferior to other engineered non-oleaginous bacteria like *E. coli* (Liu et al., 2012; Xu et al., 2013) and oleaginous organisms (Huang et al., 2016). Particularly, the latter are known to accumulate significant amounts of lipids natively (Alvarez et al., 2000), which makes them ideal organisms for food and feed applications where genetically modified organisms (GMOs) may have a legally restricted use. Nevertheless, this work elucidated some mechanisms involved in the FA biosynthesis of *C. glutamicum*. It may, therefore, provide valuable information regarding the production of FA(-derived) products and the pathway's impact on cell permeability and resilience.

5.2 FAL production with FA-producing *C. glutamicum* strains

5.2.1 Heterologous FAL production and modulation of competing reactions

As a chassis with increased flux through the FA biosynthesis pathway, *C. glutamicum* Δ*fasR* was a suitable basis strain to be engineered for subsequent FAL production.

Screening of the two FAR Maqu_2220 and Maqu_2507 of *M. hydrocarbonoclasticus* VT8 with the original codon usage revealed that both enzymes were active in *C. glutamicum*. Maqu_2220 was more suited for FAL production by *C. glutamicum* as 35 % higher titers were reached with this reductase within 24 h. The observed efficient conversion of long-chain acyl-CoAs into their corresponding alcohols fits with enzymatic studies reporting a high affinity to long-chain acyl-CoA thioesters (Hofvander et al., 2011b; Willis et al., 2011). Additionally, the obtained FAL distribution was in agreement with the previously reported FA distribution of *C. glutamicum* (Collins et al., 1982a) and indicated that neither of the reductases had a bias toward one of the three available acyl-CoA substrates.

As reported previously, *C. glutamicum* natively possesses high thioesterase activity (Ikeda et al., 2020; Takeno et al., 2013). While reducing this competing side reaction led to an increased FAL production of up to 750 % in plasmid-free strains, the introduced start codon exchange adversely affected plasmid-harboring strains. It can be speculated whether the extensive pressure on the acyl-CoA node by a reduced flux towards mycolic acids and additionally high FAR expression and, thus, depletion of acyl-CoAs led to some metabolic burden in those strains. Nevertheless, extracellular FAL titers increased by 120 %, and the relative amount of extracellular FAL increased from 12 to 30 % in plasmid-harboring TTG start codon mutants. Portevin et al. (2004) and Takeno et al. (2018) reported an increased permeability of *C. glutamicum* upon deleting or downregulating genes directly involved in the mycolic acid biosynthesis downstream of the acyl-CoA node. Attenuating the thioesterase expression thus had a similar effect and could, in the future, be applied when a more permeable production strain is desired.

5.2.1.1 Nitrogen-rich conditions favor both FAL production and degradation

While nitrogen limitation was essential for FA production, FAL synthesis followed a growth-coupled production kinetic. Thus, changing the growth medium's composition to obtain nitrogen surplus cultivation conditions improved yield, titer, and volumetric productivity. Similarly, Fillet et al. (2015) reported that a high C:N ratio was beneficial for FA production with *Rhodosporidium toruloides*, while a low C:N ratio positively influenced FAL production. However, the underlying molecular mechanisms in *C. glutamicum* still need to be elucidated. When cultivated under solely carbon-limiting conditions, a decrease of FAL during the stationary phase was observed. FAL degradation experiments using the WT revealed that *C. glutamicum* seems to be natively equipped to metabolize long-chain primary alcohols. The respective experiment additionally verified that FAL were primarily metabolized when glucose was depleted, suggesting that no potentially occurring degradation reactions

were masked by FAL-forming reactions during exponential growth. As the organism lacks essential genes required for the β-oxidation of FA (Barzantny et al., 2012), it seems plausible that FAL are oxidized to provide NAD(P)H or used as a direct precursor, e.g., for membrane lipids instead of being fully degraded and used as a carbon source. While the involved enzymes, products, and metabolic pathways remain unknown, the involvement of catabolite repression could be hypothesized due to the effect's appearance towards the end of the exponential growth phase. Similar modes of action for *C. glutamicum* are, for instance, reported for the sequential metabolization of ethanol, where the transcription of the ethanol-oxidizing alcohol dehydrogenase (ADH) AdhA-encoding gene is repressed in the presence of glucose (Arndt et al., 2008; Arndt & Eikmanns, 2007). AdhA belongs to the long-chain, zinc-dependent group I ADHs and was reported to share sequence similarities with the ADH I of *S. cerevisiae* (Arndt & Eikmanns, 2007). Ottone et al. (2018) reported an immobilized S. cerevisiae AHD I affinity towards long-chain primary alcohols. Thus, it is possible that AdhA also accepts those compounds as substrates and is responsible for the observed FAL degradation.

5.2.1.2 Preventing foam formation as a hurdle for establishing a stable bioprocess

The attempt to reduce foam formation by *in situ* product removal of the potentially foam-stabilizing FAL (Egan et al., 1984) indicated that the solvents' observed cytotoxicity seemed to depend on the alkyl group's length with propyl decanoate showing a better FAL production compared to the shorter ethyl or even methyl derivate. The contrast in the good biocompatibility reported by Tharmasothirajan et al. (2021) and the observed adverse effects on FAL production could be explained by the FAL producer's genotype. Due to the engineered reduced thioesterase expression, *C. glutamicum* Δ*fasR* cg2692$_{TTG}$ (pEKEx2_*maqu2220*) most likely has an impaired MA layer. This affects the cell's permeability and susceptibility to compounds such as antibiotics (Gebhardt et al., 2007; Portevin et al., 2004), which could also result in a reduced resilience towards organic solvents. As large, macroscopic cell aggregates were observed upon adding the solvents, their interaction with the exposed cell wall seems plausible. This observation highlights the delicate interplay between engineering a strain with increased product efflux while sacrificing the praised robustness of *C. glutamicum* to some extent.

5.2.1.3 FAL production with the complex substrate wheat straw hydrolysate

Due to its robustness to phenolic compounds and organic acids, all *C. glutamicum* mutants grew excellently in the used lignocellulosic hydrolysate. This was possibly partly attributed

to the ability of *C. glutamicum* to metabolize aromatic molecules (Becker & Wittmann, 2019; Ding et al., 2015; Shen et al., 2012; Siebert et al., 2021) and due to the molecules' ability to increase iron availability by the abiotic reduction of Fe^{3+} to Fe^{2+} (Müller et al., 2020). Respective compounds are commonly found in lignocellulosic hydrolysates as they are degradation products of lignin (Becker & Wittmann, 2019; Ding et al., 2015; Shen et al., 2012; Siebert et al., 2021). While the sampling intervals of 3 h in shaking flask cultivations did not allow for calculating accurate growth rates, it was noticeable that hydrolysate-grown cells grew at least as well as glucose-grown ones. Interestingly, cultivating the FAL-producing strains in a minimal medium pre-culture containing hydrolysate (glucose equivalent of 10 g L^{-1}) was necessary to obtain any growth in the subsequent main cultivation at higher hydrolysate concentrations. The apparent adaption process's underlying mechanism is unknown, but similar cultivation strategies are commonly used for cultivations on acetate (Kiefer et al., 2022; Wendisch et al., 2000). As the pulsed fed-batch cultivations demonstrated, the described adaption step was sufficient to enable growth with up to 10-fold increased hydrolysate concentrations relative to the pre-culture's hydrolysate content. While the discussed adaption procedure appeared to be essential, it could be speculated whether different *C. glutamicum* strain backgrounds would initially display different levels of resilience towards the hydrolysate. This consideration is particularly important because the engineered strain used in the respective cultivations is most likely more susceptible to inhibitory substances present in the hydrolysate due to its reduced MA biosynthesis and, thus, its increased permeability (Portevin et al., 2004). Consequently, *C. glutamicum* strains with an intact (mycomembrane)lipid metabolism might display an even better growth performance with the respective lignocellulosic substrate. This is an important consideration, as many other product classes do not necessarily need alterations in the host's mycomembrane.

Despite the successfully introduced xylose-utilization module, the majority of carbon provided by xylose and acetate seemed to not end up in FAL. When grown on xylose (Buschke et al., 2013a) or acetate (Wendisch et al., 2000), *C. glutamicum* exhibits a strongly increased TCA cycle activity, resulting in increased carbon flux from acetyl-CoA into the TCA cycle. There, a substantial amount of the substrate's carbon is oxidized into CO_2 (Buschke et al., 2013a; Wendisch et al., 2000). For both substrates alike, just a minor fraction of carbon is channeled through gluconeogenesis and can thus enter the PPP via the NADPH-regenerating reactions catalyzed by the G6PDH and the 6PGDH (Buschke et al., 2013a; Wendisch et al., 2000). As a consequence, NADPH might become limiting in the NADPH-expensive FAL production despite having an increased carbon flux through

the NADPH-generating reactions catalyzed by the ICD and MalE (Buschke et al., 2013a; Wendisch et al., 2000). When expressing the NAPDH-regenerating *E. coli* transhydrogenase PntAB, titers, yields, and volumetric productivities were improved in xylose-utilizing strains. Nevertheless, since HPLC data still suggested that product formation was primarily based on carbon provided by glucose, the precursor supply for FAL synthesis might be limiting when growing on xylose. As Buschke et al. (2013a) reported a 60 % increased CS activity in xylose-grown cells, this assumption seemed plausible. Reducing the CS expression as an attempt to increase the acetyl-CoA pool impacted FAL production negatively. Those findings contrast a study by Milke et al. (2019a), who reportedly improved the malonyl-CoA supply for plant polyphenol production by reducing the CS expression in a *C. glutamicum* mutant. The same authors simultaneously overexpressed the native ACC subunit-encoding genes *accD1* and *accBC* (Milke et al., 2019a), which may also be a suitable approach for the FAL producers described in this current study. Even though the transcription of the genes *accD1* and *accBC* was already deregulated by deleting *fasR* in the FAL-producing strains, the increased flux towards malonyl-CoA might have still not been sufficient to fully de-bottleneck the respective pathway. The enzyme complex's crucial role was discussed in detail in section 5.1.2. In addition, *C. glutamicum* ATCC 13032 possesses one CS, GltA (Eikmanns et al., 1994), and two methylcitrate synthases, PrpC1 and PrpC2, with CS activities (Claes et al., 2002). However, both methylcitrate synthase-encoding genes (*prpC1* and *prpC2*) are not expressed when the organism grows on glucose, as the encoded enzymes' activities are primarily required for propionate utilization (Claes et al., 2002; Hüser et al., 2003; Radmacher & Eggeling, 2007). Nevertheless, occurring mutations in the gene encoding the transcriptional regulator PrpR were reported in Δ*gltA* Δ*prpC1* mutants. These mutations enabled the transcription of *prpC2* in the presence of glucose, thereby restoring the essential CS activity in the respective mutants (Radmacher & Eggeling, 2007). Interestingly, a 2.3-fold increased transcription level of *prpC2* was reported for xylose-grown *C. glutamicum* mutants compared to a glucose-grown control (Buschke et al., 2013a). It may, therefore, be plausible that the potential presence of PrpC2 compensated for a reduced *gltA*-expression in the FAL-producing promoter mutants cultivated with hydrolysate, even though preliminary experiments with the respective strains on glucose suggested otherwise (data not shown).

When working with complex substrates such as hydrolysates, it is common practice to calculate KPI such as yields based on the quantifiable carbon sources (sugars) within that mixture (Mao et al., 2018; Shaigani et al., 2021). While those approaches usually just require access to an HPLC, they often neglect the presence of other consumed carbon

sources in the hydrolysate. Thus, analyzing the total present and consumed organic carbon in the complex broth may offer a superior strategy to estimate yields accurately while not being forced to identify and quantify every single compound separately. When applying the described method to analyze the hydrolysate and its metabolization, it became evident that a major fraction of carbon was neither metabolized by *C. glutamicum* during the investigated time frame nor was the carbon's origin identifiable. Based on the certificate of analysis provided by the manufacturer, an identifiable TOC content of about 220 g_C L^{-1} would be expected in the hydrolysate (Table 6). However, analysis revealed a TOC concentration of over 350 g_C L^{-1}, resulting in a 50 % higher carbon content than suggested by the manufacturer's analysis. Similar findings were made by Katharina Hofer of the Institute of Biochemical Engineering at the University of Stuttgart, employing the same method described in this work (data not shown). Some of the carbon could potentially be attributed to the enzymes used in the hydrolysis of the lignocellulosic biomass (Rarbach & Söltl, 2013). At the same time, residual lignin may have also contributed to a major fraction of unknown and non-utilizable carbon (Rarbach & Söltl, 2013; Zavrel et al., 2015). In fact, the observation of fine particulate in the hydrolysate, even after a long centrifugation step (3.3.6.8), suggests the general presence of insoluble compounds in the complex mixture. With a wheat straw dry matter lignin content between 15 and 30 % (w/w) (Rabemanolontsoa & Saka, 2013; Wildschut et al., 2013; Yang et al., 2016; Zavrel et al., 2015), it seems plausible that the chemically and biologically recalcitrant polymer is responsible for a major fraction of the non-utilizable carbon content. However, some of the unknown carbon source's origin remains to be elucidated. While a method-related measuring bias cannot be entirely ruled out, the detection of CO_2 via a nondispersive infrared sensor is known to be a sensitive yet robust approach (Dinh et al., 2016).

5.2.2 Xylose uptake is responsible for the sequential metabolization of glucose and xylose

Despite different rational attempts to increase the xylose utilization efficiency, the metabolization of the pentose always followed a sequential uptake kinetic. Just when glucose was entirely consumed, xylose was taken up. This was particularly evident during the pulsed fed-batch processes, where the sugar accumulated throughout the process until no additional glucose was pulsed into the reactor. The observed sequential metabolization of xylose under aerobic conditions by engineered *C. glutamicum* strains has been well described in literature (Kawaguchi et al., 2006; Radek et al., 2014; Wang et al., 2014). In this regard, the pentose's uptake has been identified as the responsible step in heterologous

xylose co-utilization (Brüsseler et al., 2018; Sasaki et al., 2009). It was demonstrated that in *C. glutamicum* ATCC 13032, a PTS-dependent (Wang et al., 2014) and PTS-independent xylose uptake natively exist (Brüsseler et al., 2018). The latter is mediated via the glucose/*myo*-inositol permease IolT1 (Brüsseler et al., 2018). Since transcription of the IolT1-encoding gene *iolT1* is repressed by the transcriptional regulator IolR (Klaffl et al., 2013), inactivating the respective regulator was shown to generally improve xylose uptake of both Weimberg pathway and isomerase pathway mutants (Brüsseler et al., 2018). The improved IolT1-mediated xylose uptake resulted in increased growth rates in a medium containing either pure xylose or a glucose and xylose mixture. In the latter cultivation condition, a single growth phase was reported in contrast to the otherwise diauxic growth behavior of *iolR*-expressing strains (Brüsseler et al., 2018), which was also observed in this work. Another commonly applied strategy to ensure co-utilization of glucose and xylose is the expression of heterologous transporter-encoding genes, like *araE* of *B. subtilis* encoding for the arabinose transporter AraE (Jin et al., 2020; Mao et al., 2018; Sasaki et al., 2009; Sun et al., 2022), which also functions as a xylose transporter (Krispin & Allmansberger, 1998). Sun et al. (2022) further optimized the heterologous expression of a chromosomally integrated *araE* and, thus, xylose uptake of xylose-utilizing *C. glutamicum* strains by ALE. Combined with other obtained mutations, co-utilization of glucose and xylose was achieved, in addition to an increased specific growth rate of the evolved strains to 0.36 h^{-1}, which represents the highest reported growth rate of *C. glutamicum* on xylose (Sun et al., 2022). The described results highlight the importance of targeting xylose import to improve xylose utilization by applying targeted and non-targeted methods.

5.2.3 Scaled-up FAL production with wheat straw hydrolysate

Even though numerous studies about microbial FAL production have been published using primarily different yeasts (Cordova et al., 2020; d'Espaux et al., 2017; Runguphan & Keasling, 2014; Schultz et al., 2022) or *E. coli* (Cao et al., 2015; Fatma et al., 2018; Liu et al., 2016), *C. glutamicum* has not been engineered yet for the production thereof. Reported titers and volumetric productivities obtained by oleaginous yeasts range from 98 mg_{FAL} L^{-1} and 0.6 mg_{FAL} L^{-1} h^{-1} (Runguphan & Keasling, 2014), over 3.7 g_{FAL} L^{-1} and 22 mg_{FAL} L^{-1} h^{-1} (Schultz et al., 2022), to 5.8 g_{FAL} L^{-1} and 24 mg_{FAL} L^{-1} h^{-1} (Cordova et al., 2020) using *S. cerevisiae*, *Rhodotorula toruloides*, and *Y. lipolytica*, respectively. For FAL production with *E. coli* titers and volumetric productivities of up to 12.5 g_{FAL} L^{-1} and 174 mg_{FAL} L^{-1} h^{-1} are reported (Fatma et al., 2018). However, respective cultivations with *E. coli* were often conducted in minimal salts media, which, besides the main carbon

source, additionally contain significant concentrations of complex substrates such as yeast extract or tryptone (Cao et al., 2015; Fatma et al., 2018; Liu et al., 2016). Thus, data about the actual yields, including metabolization of the complex substrates, were rarely provided or solely calculated based on the main substrate's consumption. Additionally, studies using real second-generation feedstocks like lignocellulosic hydrolysates for FAL production are rare (d'Espaux et al., 2017). To our knowledge, no such attempts have been published with *E. coli* yet. This current work reports a yield, volumetric productivity, and titer of 0.054 ± 0.005 Cmol Cmol^{-1}, 0.109 ± 0.005 g_{FAL} L^{-1} $h^{-1,}$ and 2.45 ± 0.09 g_{FAL} L^{-1}, respectively, which were obtained in a pulsed-fed batch process in a 1 L scale using wheat straw hydrolysate as a carbon source. In particular, achieved volumetric productivities are competitive and, in many cases, even outcompete published productivities with both *E. coli* and (oleaginous) yeasts. As the stability of the developed fed-batch process was one of the major limiting factors, it seems plausible that higher titers than described in this work could be achieved with the engineered production strains by optimizing the process's stability. A brief comparison of the aforementioned microbial FAL production approaches, providing relevant KPI and cultivation conditions, is summarized in Table 22. Yields obtained with wheat straw hydrolysate (initially given in Cmol Cmol^{-1}) were recalculated solely based on the consumed glucose to ensure comparability to other published yields (Table 22).

While strain performance can be further improved through targeted and non-targeted approaches, the constructed final strain *C. glutamicum* Δ*fasR* cg2692$_{TTG}$ CgLP12::(P_{tac}-*pntAB*-T_{rrnB}) gX (pEKEx2-*maqu2220*) still provides a competitive base for future strain engineering. Therefore, this study does not just represent the first report of FAL production with *C. glutamicum* but also provides valuable insights into the production thereof from lignocellulosic hydrolysate and the substrate's metabolization. Furthermore, the organism's apparent resilience towards high hydrolysate concentrations provides a solid base for sustainable FAL production.

Table 22: Comparison of published microbial FAL production data. The $Y_{P/S}$ is given in $g_{FAL}\ g_{Glucose}^{-1}$, as published by the respective authors. $Y_{P/S}$ values presented in this work were recalculated on a glucose basis to ensure comparability. The chain lengths of the produced FAL range from 8 to 18 carbon atoms but are not closer specified here. Data is only represented by means to ensure the readability of this table. SF: shaking flask; n.d.: not determined; n.a.: not applicable.

Organism	Carbon source	Cultivation type	Titer | g L^{-1}	$Y_{P/S}$ | g g^{-1}	Q_P | g L^{-1} h^{-1}	Reference
R. toruloides	Glucose	Fed-batch	3.7	0.024	0.022	(Schultz et al., 2022)
S. cerevisiae	Glucose + galactose	SF	0.1	n.d.	0.0006	(Runguphan & Keasling, 2014)
	Glucose + yeast extract	Fed-batch	6	0.06	0.03	(d'Espaux et al., 2017)
	Sorghum hydrolysate + yeast extract + peptone	SF	0.7	0.06	0.01	(d'Espaux et al., 2017)
Y. lipolytica	Glucose	Fed-batch	5.8	0.036	0.024	(Cordova et al., 2020)
E. coli	Glycerol + yeast extract	Fed-batch	1.95	n.d.	0.071	(Cao et al., 2015)
	Glycerol + yeast extract + tryptone	Fed-batch	6.33	n.d.	0.115	(Liu et al., 2016)
	Glucose + yeast extract	Fed-batch	12.5	n.d.	0.174	(Fatma et al., 2018)
C. glutamicum	Glucose	SF	0.54	0.027	0.036	This work (Werner et al., 2023)
	Wheat straw hydrolysate	SF	0.75	0.045	0.062	This work (Werner et al., 2023)
	Wheat straw hydrolysate	Fed-batch	2.45	0.031	0.109	This work (Werner et al., 2023)

6. Conclusion

Initially, the production of FA and FAL with engineered *C. glutamicum* strains was intended. While the achieved FA production was not competitive with other published microbial lipid producers, novel insights into the native FA biosynthesis were gained. Verifying the ACC's role as a rate-limiting entry point into the respective pathway highlights the importance of alleviating this bottleneck in future strain engineering approaches. In that context, it was shown that the non-catalytic subunit AccE seems to play an important and, so far, neglected role in the ACC's catalytic activity. Additionally, nitrogen limitation and, most likely, iron availability are essential factors to consider when producing FA with this non-oleaginous organism. However, the molecular mechanisms of those effects are yet to be elucidated.

This study resulted in the first published *de novo* FAL production with *C. glutamicum* from first- and second-generation feedstock and provided a rare example of microbial oleochemical biosynthesis with a lignocellulosic hydrolysate. Hence, this study highlights the suitability of *C. glutamicum* as a platform to produce oleochemicals and the organism's compatibility with lignocellulosic feedstocks. Besides the general proof of concept of FAL production with *C. glutamicum*, it was possible to successfully scale up the developed bioprocess. Besides targeting low yields obtained with all tested substrates, hydrolysate utilization requires improvement. In that context, the non-metabolizable carbon fraction in the hydrolysate and intracellular carbon fluxes of strains grown with xylose should be investigated.

7. References

[1] Abe, S., Takayama, K.-I., & Kinoshita, S. (1967). Taxonomical studies on glutamic acid-producing bacteria. *The Journal of General and Applied Microbiology*, *13*(3), 279-301. https://doi.org/10.2323/jgam.13.279

[2] Akhtar, M. K., Turner, N. J., & Jones, P. R. (2013). Carboxylic acid reductase is a versatile enzyme for the conversion of fatty acids into fuels and chemical commodities. *Proceedings of the National Academy of Sciences*, *110*(1), 87-92. https://doi.org/10.1073/pnas.1216516110

[3] Alvarez, H. M., Herrero, O. M., Silva, R. A., Hernández, M. A., Lanfranconi, M. P., & Villalba, M. S. (2019). Insights into the metabolism of oleaginous *Rhodococcus spp. Applied and Environmental Microbiology*, *85*(18), e00498-00419. https://doi.org/10.1128/AEM.00498-19

[4] Alvarez, H. M., Kalscheuer, R., & Steinbüchel, A. (2000). Accumulation and mobilization of storage lipids by *Rhodococcus opacus* PD630 and *Rhodococcus rube*r NCIMB 40126. *Applied Microbiology and Biotechnology*, *54*(2), 218-223. https://doi.org/10.1007/s002530000395

[5] Alvarez, H. M., Mayer, F., Fabritius, D., & Steinbüchel, A. (1996). Formation of intracytoplasmic lipid inclusions by *Rhodococcus opacus* strain PD630. *Archives of Microbiology*, *165*(6), 377-386. https://doi.org/10.1007/s002030050341

[6] Ariga, N., Maruyama, K., & Kawaguchi, A. (1984). Comparative studies of fatty acid synthases of corynebacteria. *The Journal of General and Applied Microbiology*, *30*(2), 87-95. https://doi.org/10.2323/jgam.30.87

[7] Arndt, A., Auchter, M., Ishige, T., Wendisch, V. F., & Eikmanns, B. J. (2008). Ethanol catabolism in *Corynebacterium glutamicum*. *Microbial Physiology*, *15*(4), 222-233. https://doi.org/10.1159/000107370

[8] Arndt, A., & Eikmanns, B. J. (2007). The alcohol dehydrogenase gene *adhA* in *Corynebacterium glutamicum* is subject to carbon catabolite repression. *Journal of Bacteriology*, *189*(20), 7408-7416. https://doi.org/10.1128/jb.00791-07

[9] Asselineau, J., & Lederer, E. (1950). Structure of the mycolic mcids of Mycobacteria. *Nature*, *166*(4227), 782-783. https://doi.org/10.1038/166782a0

[10] Barrett, E., Stanton, C., Zelder, O., Fitzgerald, G., & Ross, R. P. (2004). Heterologous expression of lactose- and galactose-utilizing pathways from lactic acid bacteria in *Corynebacterium glutamicum* for production of lysine in whey. *Applied and Environmental Microbiology*, *70*(5), 2861-2866. https://doi.org/10.1128/AEM.70.5.2861-2866.2004

[11] Barry, C. E., Lee, R. E., Mdluli, K., Sampson, A. E., Schroeder, B. G., Slayden, R. A., & Yuan, Y. (1998). Mycolic acids: structure, biosynthesis and physiological functions. *Progress in Lipid Research*, *37*(2), 143-179. https://doi.org/10.1016/S0163-7827(98)00008-3

[12] Bartek, T., Blombach, B., Lang, S., Eikmanns Bernhard, J., Wiechert, W., Oldiges, M., Nöh, K., & Noack, S. (2011). Comparative ^{13}C metabolic flux analysis of pyruvate dehydrogenase

complex-deficient, L-valine-producing *Corynebacterium glutamicum*. *Applied and Environmental Microbiology*, *77*(18), 6644-6652. https://doi.org/10.1128/AEM.00575-11

[13] Baruah, J., Nath, B. K., Sharma, R., Kumar, S., Deka, R. C., Baruah, D. C., & Kalita, E. (2018). Recent trends in the pretreatment of lignocellulosic biomass for value-added products [Review]. *Frontiers in Energy Research*, *6*. https://doi.org/10.3389/fenrg.2018.00141

[14] Barzantny, H., Brune, I., & Tauch, A. (2012). Molecular basis of human body odour formation: insights deduced from corynebacterial genome sequences. *International Journal of Cosmetic Science*, *34*(1), 2-11. https://doi.org/10.1111/j.1468-2494.2011.00669.x

[15] Bäumchen, C., Krings, E., Bringer, S., Eggeling, L., & Sahm, H. (2009). *Myo*-inositol facilitators IolT1 and IolT2 enhance D-mannitol formation from D-fructose in *Corynebacterium glutamicum*. *FEMS microbiology letters*, *290*(2), 227-235. https://doi.org/10.1111/j.1574-6968.2008.01425.x

[16] Baumgart, M., Unthan, S., Rückert, C., Sivalingam, J., Grünberger, A., Kalinowski, J., Bott, M., Noack, S., & Frunzke, J. (2013). Construction of a prophage-free variant of Corynebacterium glutamicum ATCC 13032 for use as a platform strain for basic research and industrial biotechnology. *Applied and Environmental Microbiology*, *79*(19), 6006-6015. https://doi.org/10.1128/AEM.01634-13

[17] Becker, J., & Wittmann, C. (2012). Bio-based production of chemicals, materials and fuels – *Corynebacterium glutamicum* as versatile cell factory. *Current Opinion in Biotechnology*, *23*(4), 631-640. https://doi.org/10.1016/j.copbio.2011.11.012

[18] Becker, J., & Wittmann, C. (2019). A field of dreams: lignin valorization into chemicals, materials, fuels, and health-care products. *Biotechnology Advances*, *37*(6), 107360. https://doi.org/10.1016/j.biotechadv.2019.02.016

[19] Bergler, H., Fuchsbichler, S., Högenauer, G., & Turnowsky, F. (1996). The enoyl-[acyl-carrier-protein] reductase (FabI) of *Escherichia coli*, which catalyzes a key regulatory step in fatty acid biosynthesis, accepts NADH and NADPH as cofactors and is inhibited by palmitoyl-CoA. *European Journal of Biochemistry*, *242*(3), 689-694. https://doi.org/10.1111/j.1432-1033.1996.0689r.x

[20] Blattner, F. R., Plunkett, G., Bloch, C. A., Perna, N. T., Burland, V., Riley, M., Collado-Vides, J., Glasner, J. D., Rode, C. K., Mayhew, G. F., Gregor, J., Davis, N. W., Kirkpatrick, H. A., Goeden, M. A., Rose, D. J., Mau, B., & Shao, Y. (1997). The complete genome sequence of *Escherichia coli* K-12. *Science*, *277*(5331), 1453-1462. https://doi.org/10.1126/science.277.5331.1453

[21] Bligh, E. G., & Dyer, W. J. (1959). A rapid method of total lipid extraction and purification. *Canadian journal of biochemistry and physiology*, *37 8*, 911-917.

[22] Bloch, K. (1971). *β*-hydroxydecanoyl thioester dehydrase. In P. D. Boyer (Ed.), *The Enzymes* (Vol. 5, pp. 441-464). Academic Press. https://doi.org/10.1016/S1874-6047(08)60098-0

[23] Bloch, K., & Vance, D. (1977). Control mechanisms in the synthesis of saturated fatty acids. *Annual Review of Biochemistry*, *46*(1), 263-298. https://doi.org/10.1146/annurev.bi.46.070177.001403

[24] Blombach, B., Buchholz, J., Busche, T., Kalinowski, J., & Takors, R. (2013). Impact of different CO_2/HCO_3^- levels on metabolism and regulation in *Corynebacterium glutamicum*. *Journal of Biotechnology*, *168*(4), 331-340. https://doi.org/10.1016/j.jbiotec.2013.10.005

[25] Blombach, B., Riester, T., Wieschalka, S., Ziert, C., Youn, J. W., Wendisch, V. F., & Eikmanns, B. J. (2011). *Corynebacterium glutamicum* tailored for efficient isobutanol production. *Applied and Environmental Microbiology*, *77*(10), 3300-3310. https://doi.org/10.1128/aem.02972-10

[26] Blombach, B., Schreiner Mark, E., Holátko, J., Bartek, T., Oldiges, M., & Eikmanns Bernhard, J. (2007). L-valine production with pyruvate dehydrogenase complex-deficient *Corynebacterium glutamicum*. *Applied and Environmental Microbiology*, *73*(7), 2079-2084. https://doi.org/10.1128/AEM.02826-06

[27] Blombach, B., & Seibold, G. M. (2010). Carbohydrate metabolism in *Corynebacterium glutamicum* and applications for the metabolic engineering of L-lysine production strains. *Applied Microbiology and Biotechnology*, *86*(5), 1313-1322. https://doi.org/10.1007/s00253-010-2537-z

[28] Brand, S., Niehaus, K., Pühler, A., & Kalinowski, J. (2003). Identification and functional analysis of six mycolyltransferase genes of *Corynebacterium glutamicum* ATCC 13032: the genes *cop1*, *cmt1*, and *cmt2* can replace each other in the synthesis of trehalose dicorynomycolate, a component of the mycolic acid layer of the cell envelope. *Archives of Microbiology*, *180*(1), 33-44. https://doi.org/10.1007/s00203-003-0556-1

[29] Brüsseler, C., Radek, A., Tenhaef, N., Krumbach, K., Noack, S., & Marienhagen, J. (2018). The *myo*-inositol/proton symporter IolT1 contributes to D-xylose uptake in *Corynebacterium glutamicum*. *Bioresource Technology*, *249*, 953-961. https://doi.org/10.1016/j.biortech.2017.10.098

[30] Buchholz, J., Graf, M., Blombach, B., & Takors, R. (2014). Improving the carbon balance of fermentations by total carbon analyses. *Biochemical Engineering Journal*, *90*, 162-169. https://doi.org/10.1016/j.bej.2014.06.007

[31] Buchholz, J., Schwentner, A., Brunnenkan, B., Gabris, C., Grimm, S., Gerstmeir, R., Takors, R., Eikmanns Bernhard, J., & Blombach, B. (2013). Platform engineering of *Corynebacterium glutamicum* with reduced pyruvate dehydrogenase complex activity for omproved production of L-lysine, L-valine, and 2-ketoisovalerate. *Applied and Environmental Microbiology*, *79*(18), 5566-5575. https://doi.org/10.1128/AEM.01741-13

[32] Burgardt, A., Prell, C., & Wendisch, V. F. (2021). Utilization of a wheat sidestream for 5-aminovalerate production in *Corynebacterium glutamicum* [Original Research]. *Frontiers in Bioengineering and Biotechnology*, *9*. https://doi.org/10.3389/fbioe.2021.732271

[33] Buschke, N., Becker, J., Schäfer, R., Kiefer, P., Biedendieck, R., & Wittmann, C. (2013a). Systems metabolic engineering of xylose-utilizing *Corynebacterium glutamicum* for production of 1,5-diaminopentane. *Biotechnology Journal*, *8*(5), 557-570. https://doi.org/10.1002/biot.201200367

[34] Buschke, N., Schäfer, R., Becker, J., & Wittmann, C. (2013b). Metabolic engineering of industrial platform microorganisms for biorefinery applications – optimization of substrate spectrum and process robustness by rational and evolutive strategies. *Bioresource Technology*, *135*, 544-554. https://doi.org/10.1016/j.biortech.2012.11.047

[35] Cao, Y.-X., Xiao, W.-H., Liu, D., Zhang, J.-L., Ding, M.-Z., & Yuan, Y.-J. (2015). Biosynthesis of odd-chain fatty alcohols in *Escherichia coli*. *Metabolic Engineering*, *29*, 113-123. https://doi.org/10.1016/j.ymben.2015.03.005

[36] Cavelius, P., Engelhart-Straub, S., Mehlmer, N., Lercher, J., Awad, D., & Brück, T. (2023). The potential of biofuels from first to fourth generation. *PLOS Biology*, *21*(3), e3002063. https://doi.org/10.1371/journal.pbio.3002063

[37] Chalut, C., Botella, L., de Sousa-D'Auria, C., Houssin, C., & Guilhot, C. (2006). The nonredundant roles of two 4′-phosphopantetheinyl transferases in vital processes of *Mycobacteria*. *Proceedings of the National Academy of Sciences*, *103*(22), 8511. https://doi.org/10.1073/pnas.0511129103

[38] Chandel, A. K., Garlapati, V. K., Singh, A. K., Antunes, F. A. F., & da Silva, S. S. (2018). The path forward for lignocellulose biorefineries: bottlenecks, solutions, and perspective on commercialization. *Bioresource Technology*, *264*, 370-381. https://doi.org/10.1016/j.biortech.2018.06.004

[39] Chandel, A. K., Singh, O. V., Chandrasekhar, G., Rao, L. V., & Narasu, M. L. (2010). Key drivers influencing the commercialization of ethanol-based biorefineries. *Journal of Commercial Biotechnology*, *16*(3), 239-257. https://doi.org/10.1057/jcb.2010.5

[40] Chang, Z., Dai, W., Mao, Y., Cui, Z., Zhang, Z., Wang, Z., Ma, H., & Chen, T. (2022). Enhanced 3-hydroxypropionic acid production from acetate via the malonyl-CoA pathway in *Corynebacterium glutamicum* [Original Research]. *Frontiers in Bioengineering and Biotechnology*, *9*. https://doi.org/10.3389/fbioe.2021.808258

[41] Chen, Z., Huang, J., Wu, Y., Wu, W., Zhang, Y., & Liu, D. (2017). Metabolic engineering of *Corynebacterium glutamicum* for the production of 3-hydroxypropionic acid from glucose and xylose. *Metabolic Engineering*, *39*, 151-158. https://doi.org/10.1016/j.ymben.2016.11.009

[42] Cheng, Z., Jiang, J., Wu, H., Li, Z., & Ye, Q. (2016). Enhanced production of 3-hydroxypropionic acid from glucose via malonyl-CoA pathway by engineered *Escherichia coli*. *Bioresource Technology*, *200*, 897-904. https://doi.org/10.1016/j.biortech.2015.10.107

[43] Chirani, M. R., Kowsari, E., Teymourian, T., & Ramakrishna, S. (2021). Environmental impact of increased soap consumption during COVID-19 pandemic: biodegradable soap production

and sustainable packaging. *Science of the Total Environment*, *796*, 149013. https://doi.org/10.1016/j.scitotenv.2021.149013

[44] Cho, H., & Cronan, J. E. (1993). *Escherichia coli* thioesterase I, molecular cloning and sequencing of the structural gene and identification as a periplasmic enzyme. *Journal of Biological Chemistry*, *268*(13), 9238-9245. https://doi.org/10.1016/S0021-9258(18)98341-9

[45] Chubukov, V., Sauer, U., & Spormann, A. M. (2014). Environmental Dependence of Stationary-Phase Metabolism in Bacillus subtilis and Escherichia coli. *Applied and Environmental Microbiology*, *80*(9), 2901-2909. https://doi.org/10.1128/AEM.00061-14

[46] Claes, W. A., Pühler, A., & Kalinowski, J. (2002). Identification of two *prpDBC* gene clusters in *Corynebacterium glutamicum* and their involvement in propionate degradation via the 2-methylcitrate cycle. *Journal of Bacteriology*, *184*(10), 2728-2739. https://doi.org/10.1128/jb.184.10.2728-2739.2002

[47] Collins, M. D., Goodfellow, M., & Minnikin, D. E. (1982a). Fatty acid composition of some mycolic acid-containing coryneform bacteria. *Microbiology*, *128*(11), 2503-2509. https://doi.org/10.1099/00221287-128-11-2503

[48] Collins, M. D., Goodfellow, M., & Minnikin, D. E. (1982b). A survey of the structures of mycolic acids in *Corynebacterium* and related taxa. *Microbiology*, *128*(1), 129-149. https://doi.org/10.1099/00221287-128-1-129

[49] Cordova, L. T., Butler, J., & Alper, H. S. (2020). Direct production of fatty alcohols from glucose using engineered strains of *Yarrowia lipolytica*. *Metabolic Engineering Communications*, *10*, e00105. https://doi.org/10.1016/j.mec.2019.e00105

[50] Cronan, J. E., & Thomas, J. (2009). Bacterial fatty acid synthesis and its relationships with polyketide synthetic pathways. In *Methods in Enzymology* (Vol. 459, pp. 395-433). Academic Press. https://doi.org/10.1016/S0076-6879(09)04617-5

[51] Cronan, J. J. E., & Rock Charles, O. (2008). Biosynthesis of membrane lipids. *EcoSal Plus*, *3*(1). https://doi.org/10.1128/ecosalplus.3.6.4

[52] Cumming , G., Fidler , F., & Vaux , D. L. (2007). Error bars in experimental biology. *Journal of Cell Biology*, *177*(1), 7-11. https://doi.org/10.1083/jcb.200611141

[53] d'Espaux, L., Ghosh, A., Runguphan, W., Wehrs, M., Xu, F., Konzock, O., Dev, I., Nhan, M., Gin, J., Reider Apel, A., Petzold, C. J., Singh, S., Simmons, B. A., Mukhopadhyay, A., García Martín, H., & Keasling, J. D. (2017). Engineering high-level production of fatty alcohols by *Saccharomyces cerevisiae* from lignocellulosic feedstocks. *Metabolic Engineering*, *42*, 115-125. https://doi.org/10.1016/j.ymben.2017.06.004

[54] Dabirian, Y., Gonçalves Teixeira, P., Nielsen, J., Siewers, V., & David, F. (2019). FadR-based biosensor-assisted screening for genes enhancing fatty acyl-CoA pools in *Saccharomyces cerevisiae*. *ACS Synthetic Biology*, *8*(8), 1788-1800. https://doi.org/10.1021/acssynbio.9b00118

[55] Daffé, M. (2005). The cell envelope of corynebacteria. In L. Eggeling & M. Bott (Eds.), *Handbook of Corynebacterium glutamicum* (pp. 121-148). CRC Press.

[56] Daverey, A., & Dutta, K. (2021). COVID-19: eco-friendly hand hygiene for human and environmental safety. *Journal of Environmental Chemical Engineering*, *9*(2), 104754. https://doi.org/10.1016/j.jece.2020.104754

[57] Davis, M. S., Solbiati, J., & Cronan, J. E. (2000). Overproduction of acetyl-CoA carboxylase activity increases the rate of fatty acid biosynthesis in *Escherichia coli*. *Journal of Biological Chemistry*, *275*(37), 28593-28598. https://doi.org/https://doi.org/10.1074/jbc.M004756200

[58] De Bhowmick, G., Sarmah, A. K., & Sen, R. (2018). Lignocellulosic biorefinery as a model for sustainable development of biofuels and value added products. *Bioresource Technology*, *247*, 1144-1154. https://doi.org/10.1016/j.biortech.2017.09.163

[59] de Mendoza, D., & Cronan, J. E. (1983). Thermal regulation of membrane lipid fluidity in bacteria. *Trends in Biochemical Sciences*, *8*(2), 49-52. https://doi.org/10.1016/0968-0004(83)90388-2

[60] De Sousa-D'Auria, C., Kacem, R., Puech, V., Tropis, M., Leblon, G., Houssin, C., & Daffé, M. (2003). New insights into the biogenesis of the cell envelope of corynebacteria: identification and functional characterization of five new mycoloyltransferase genes in *Corynebacterium glutamicum*. *FEMS microbiology letters*, *224*(1), 35-44. https://doi.org/10.1016/S0378-1097(03)00396-3

[61] de Wild, P. J., Huijgen, W. J. J., & Heeres, H. J. (2012). Pyrolysis of wheat straw-derived organosolv lignin. *Journal of Analytical and Applied Pyrolysis*, *93*, 95-103. https://doi.org/10.1016/j.jaap.2011.10.002

[62] Dellomonaco, C., Clomburg, J. M., Miller, E. N., & Gonzalez, R. (2011). Engineered reversal of the *β*-oxidation cycle for the synthesis of fuels and chemicals. *Nature*, *476*(7360), 355-359. https://doi.org/10.1038/nature10333

[63] Demling, P., von Campenhausen, M., Grütering, C., Tiso, T., Jupke, A., & Blank, L. M. (2020). Selection of a recyclable *in situ* liquid–liquid extraction solvent for foam-free synthesis of rhamnolipids in a two-phase fermentation [10.1039/D0GC02885A]. *Green Chemistry*, *22*(23), 8495-8510. https://doi.org/10.1039/D0GC02885A

[64] Ding, W., Si, M., Zhang, W., Zhang, Y., Chen, C., Zhang, L., Lu, Z., Chen, S., & Shen, X. (2015). Functional characterization of a vanillin dehydrogenase in *Corynebacterium glutamicum*. *Scientific Reports*, *5*(1), 8044. https://doi.org/10.1038/srep08044

[65] Dinh, T.-V., Choi, I.-Y., Son, Y.-S., & Kim, J.-C. (2016). A review on non-dispersive infrared gas sensors: improvement of sensor detection limit and interference correction. *Sensors and Actuators B: Chemical*, *231*, 529-538. https://doi.org/10.1016/j.snb.2016.03.040

[66] Dodić, S., Popov, S., Dodić, J., Ranković, J., Zavargo, Z., & Jevtić Mučibabić, R. (2009). Bioethanol production from thick juice as intermediate of sugar beet processing. *Biomass and Bioenergy*, *33*(5), 822-827. https://doi.org/10.1016/j.biombioe.2009.01.002

[67] Dominguez, H., Cocaign-Bousquet, M., & Lindley, N. D. (1997). Simultaneous consumption of glucose and fructose from sugar mixtures during batch growth of *Corynebacterium glutamicum*. *Applied Microbiology and Biotechnology*, *47*(5), 600-603. https://doi.org/10.1007/s002530050980

[68] Dominguez, H., Rollin, C., Guyonvarch, A., Guerquin-Kern, J.-L., Cocaign-Bousquet, M., & Lindley, N. D. (1998). Carbon-flux distribution in the central metabolic pathways of *Corynebacterium glutamicum* during growth on fructose. *European Journal of Biochemistry*, *254*(1), 96-102. https://doi.org/10.1046/j.1432-1327.1998.2540096.x

[69] Dover, L. G., Cerdeño-Tárraga, A. M., Pallen, M. J., Parkhill, J., & Besra, G. S. (2004). Comparative cell wall core biosynthesis in the mycolated pathogens, *Mycobacterium tuberculosis* and *Corynebacterium diphtheriae*. *FEMS Microbiology Reviews*, *28*(2), 225-250. https://doi.org/10.1016/j.femsre.2003.10.001

[70] Draper, P. (1998). The outer parts of the mycobacterial envelope as permeability barriers. *Frontiers in bioscience : a journal and virtual library*, *3*, 1253-1261. https://doi.org/10.2741/a360

[71] Edwards, P., Sabo Nelsen, J., Metz, J. G., & Dehesh, K. (1997). Cloning of the *fabF* gene in an expression vector and *in vitro* characterization of recombinant *fabF* and *fabB* encoded enzymes from *Escherichia coli*. *Febs Letters*, *402*(1), 62-66. https://doi.org/10.1016/S0014-5793(96)01437-8

[72] Egan, R. R., Earl, G. W., & Ackerman, J. (1984). Properties and uses of some unsaturated fatty alcohols and their derivatives. *Journal of the American Oil Chemists' Society*, *61*(2), 324-329. https://doi.org/10.1007/BF02678789

[73] Eggeling, L., & Bott, M. (2005). *Handbook of Corynebacterium glutamicum* (L. Eggeling & M. Bott, Eds.). CRC Press. https://doi.org/10.1201/9781420039696

[74] Eikmanns, B. J. (2005). Central metabolism: tricarboxylic acid cycle and anaplerotic reactions. In L. Eggeling & M. Bott (Eds.), *Handbook of Corynebacterium glutamicum* (pp. 241-276). CRC Press.

[75] Eikmanns, B. J., & Blombach, B. (2014). The pyruvate dehydrogenase complex of *Corynebacterium glutamicum*: an attractive target for metabolic engineering. *Journal of Biotechnology*, *192*, 339-345. https://doi.org/10.1016/j.jbiotec.2013.12.019

[76] Eikmanns, B. J., Metzger, M., Reinscheid, D., Kircher, M., & Sahm, H. (1991). Amplification of three threonine biosynthesis genes in *Corynebacterium glutamicum* and its influence on carbon flux in different strains. *Applied Microbiology and Biotechnology*, *34*(5), 617-622. https://doi.org/10.1007/BF00167910

[77] Eikmanns, B. J., Rittmann, D., & Sahm, H. (1995). Cloning, sequence analysis, expression, and inactivation of the *Corynebacterium glutamicum icd* gene encoding isocitrate dehydrogenase and biochemical characterization of the enzyme. *Journal of Bacteriology*, *177*(3), 774-782. https://doi.org/10.1128/jb.177.3.774-782.1995

[78] Eikmanns, B. J., Thum-Schmitz, N., Eggeling, L., Lüdtke, K.-U., & Sahm, H. (1994). Nucleotide sequence, expression and transcriptional analysis of the *Corynebacterium glutamicum gltA* gene encoding citrate synthase. *Microbiology*, *140*(8), 1817-1828. https://doi.org/10.1099/13500872-140-8-1817

[79] Fargione, J., Hill, J., Tilman, D., Polasky, S., & Hawthorne, P. (2008). Land clearing and the biofuel carbon debt. *Science*, *319*(5867), 1235-1238. https://doi.org/10.1126/science.1152747

[80] Fatma, Z., Hartman, H., Poolman, M. G., Fell, D. A., Srivastava, S., Shakeel, T., & Yazdani, S. S. (2018). Model-assisted metabolic engineering of *Escherichia coli* for long chain alkane and alcohol production. *Metabolic Engineering*, *46*, 1-12. https://doi.org/10.1016/j.ymben.2018.01.002

[81] Feria Bourrellier, A. B., Valot, B., Guillot, A., Ambard-Bretteville, F., Vidal, J., & Hodges, M. (2010). Chloroplast acetyl-CoA carboxylase activity is 2-oxoglutarate–regulated by interaction of PII with the biotin carboxyl carrier subunit. *Proceedings of the National Academy of Sciences*, *107*(1), 502-507. https://doi.org/10.1073/pnas.0910097107

[82] Fernandez-Moya, R., Leber, C., Cardenas, J., & Da Silva, N. A. (2015). Functional replacement of the *Saccharomyces cerevisiae* fatty acid synthase with a bacterial type II system allows flexible product profiles. *Biotechnology and Bioengineering*, *112*(12), 2618-2623. https://doi.org/10.1002/bit.25679

[83] Fillet, S., Gibert, J., Suárez, B., Lara, A., Ronchel, C., & Adrio, J. L. (2015). Fatty alcohols production by oleaginous yeast. *Journal of Industrial Microbiology and Biotechnology*, *42*(11), 1463-1472. https://doi.org/10.1007/s10295-015-1674-x

[84] Fitzherbert, E. B., Struebig, M. J., Morel, A., Danielsen, F., Brühl, C. A., Donald, P. F., & Phalan, B. (2008). How will oil palm expansion affect biodiversity? *Trends in Ecology & Evolution*, *23*(10), 538-545. https://doi.org/10.1016/j.tree.2008.06.012

[85] Frohwitter, J., Heider, S. A. E., Peters-Wendisch, P., Beekwilder, J., & Wendisch, V. F. (2014). Production of the sesquiterpene (+)-valencene by metabolically engineered *Corynebacterium glutamicum*. *Journal of Biotechnology*, *191*, 205-213. https://doi.org/10.1016/j.jbiotec.2014.05.032

[86] Gago, G., Kurth, D., Diacovich, L., Tsai, S.-C., & Gramajo, H. (2006). Biochemical and structural characterization of an essential acyl coenzyme A carboxylase from *Mycobacterium tuberculosis*. *Journal of Bacteriology*, *188*(2), 477-486. https://doi.org/10.1128/JB.188.2.477-486.2006

[87] Gande, R., Dover, L. G., Krumbach, K., Besra, G. S., Sahm, H., Oikawa, T., & Eggeling, L. (2007). The two carboxylases of *Corynebacterium glutamicum* essential for fatty acid and

mycolic acid synthesis. *Journal of Bacteriology*, *189*(14), 5257-5264. https://doi.org/10.1128/jb.00254-07

[88] Gande, R., Gibson, K. J. C., Brown, A. K., Krumbach, K., Dover, L. G., Sahm, H., Shioyama, S., Oikawa, T., Besra, G. S., & Eggeling, L. (2004). Acyl-CoA carboxylases (*accD2* and *accD3*), together with a unique polyketide synthase (*Cg-pks*), are key to mycolic acid biosynthesis in *Corynebacterianeae* such as *Corynebacterium glutamicum* and *Mycobacterium tuberculosis*. *Journal of Biological Chemistry*, *279*(43), 44847-44857. https://doi.org/10.1074/jbc.M408648200

[89] Gao, R., Li, Z., Zhou, X., Bao, W., Cheng, S., & Zheng, L. (2020). Enhanced lipid production by *Yarrowia lipolytica* cultured with synthetic and waste-derived high-content volatile fatty acids under alkaline conditions. *Biotechnology for Biofuels*, *13*(1), 3. https://doi.org/10.1186/s13068-019-1645-y

[90] Garwin, J. L., Klages, A. L., & Cronan, J. E. (1980). Structural, enzymatic, and genetic studies of beta-ketoacyl-acyl carrier protein synthases I and II of *Escherichia coli*. *Journal of Biological Chemistry*, *255*(24), 11949-11956. https://doi.org/10.1016/S0021-9258(19)70226-9

[91] Gebhardt, H., Meniche, X., Tropis, M., Krämer, R., Daffé, M., & Morbach, S. (2007). The key role of the mycolic acid content in the functionality of the cell wall permeability barrier in *Corynebacterineae*. *Microbiology*, *153*(5), 1424-1434. https://doi.org/10.1099/mic.0.2006/003541-0

[92] Gerhardt, E. C. M., Rodrigues, T. E., Müller-Santos, M., Pedrosa, F. O., Souza, E. M., Forchhammer, K., & Huergo, L. F. (2015). The Bacterial signal transduction protein GlnB regulates the committed step in fatty acid biosynthesis by acting as a dissociable regulatory subunit of acetyl-CoA carboxylase. *Molecular Microbiology*, *95*(6), 1025-1035. https://doi.org/10.1111/mmi.12912

[93] Gibson, D. G. (2011). Enzymatic assembly of overlapping DNA fragments. In C. Voigt (Ed.), *Methods in Enzymology* (Vol. 498, pp. 349-361). Academic Press. https://doi.org/10.1016/B978-0-12-385120-8.00015-2

[94] Gibson, D. G., Young, L., Chuang, R.-Y., Venter, J. C., Hutchison, C. A., & Smith, H. O. (2009). Enzymatic assembly of DNA molecules up to several hundred kilobases. *Nature Methods*, *6*(5), 343-345. https://doi.org/10.1038/nmeth.1318

[95] Glickman, M. S., Cox, J. S., & Jacobs, W. R., Jr. (2000). A novel mycolic acid cyclopropane synthetase Is required for cording, persistence, and virulence of *Mycobacterium tuberculosis*. *Molecular Cell*, *5*(4), 717-727. https://doi.org/10.1016/S1097-2765(00)80250-6

[96] Gopinath, V., Meiswinkel, T. M., Wendisch, V. F., & Nampoothiri, K. M. (2011). Amino acid production from rice straw and wheat bran hydrolysates by recombinant pentose-utilizing *Corynebacterium glutamicum*. *Applied Microbiology and Biotechnology*, *92*(5), 985-996. https://doi.org/10.1007/s00253-011-3478-x

[97] Gourdon, P., Baucher, M.-F., Lindley, N. D., & Guyonvarch, A. (2000). Cloning of the malic enzyme gene from *Corynebacterium glutamicum* and role of the enzyme in lactate metabolism. *Applied and Environmental Microbiology*, *66*(7), 2981-2987. https://doi.org/10.1128/AEM.66.7.2981-2987.2000

[98] Graf, M., Haas, T., Teleki, A., Feith, A., Cerff, M., Wiechert, W., Nöh, K., Busche, T., Kalinowski, J., & Takors, R. (2020). Revisiting the growth modulon of *Corynebacterium glutamicum* under glucose limited chemostat conditions [Original Research]. *Frontiers in Bioengineering and Biotechnology*, *8*. https://doi.org/10.3389/fbioe.2020.584614

[99] Hanahan, D. (1983). Studies on transformation of *Escherichia coli* with plasmids. *Journal of Molecular Biology*, *166*(4), 557-580. https://doi.org/10.1016/S0022-2836(83)80284-8

[100] Heath, R. J., & Rock, C. O. (1995). Enoyl-acyl carrier protein reductase (*fabI*) plays a determinant role in completing cycles of fatty acid elongation in *Escherichia coli*. *Journal of Biological Chemistry*, *270*(44), 26538-26542. https://doi.org/10.1074/jbc.270.44.26538

[101] Heath, R. J., & Rock, C. O. (1996). Roles of the FabA and FabZ *β*-hydroxyacyl-acyl carrier protein dehydratases in *Escherichia coli* fatty acid biosynthesis. *Journal of Biological Chemistry*, *271*(44), 27795-27801. https://doi.org/10.1074/jbc.271.44.27795

[102] Henke, N. A., Krahn, I., & Wendisch, V. F. (2021a). Improved plasmid-based inducible and constitutive gene expression in *Corynebacterium glutamicum*. *Microorganisms*, *9*(1).

[103] Henke, N. A., Krahn, I., & Wendisch, V. F. (2021b). Improved Plasmid-Based Inducible and Constitutive Gene Expression in Corynebacterium glutamicum. *Microorganisms*, *9*(1), 204. https://doi.org/10.3390/microorganisms9010204

[104] Hernández, M. A., Lara, J., Gago, G., Gramajo, H., & Alvarez, H. M. (2017). The pleiotropic transcriptional regulator NlpR contributes to the modulation of nitrogen metabolism, lipogenesis and triacylglycerol accumulation in oleaginous rhodococci. *Molecular Microbiology*, *103*(2), 366-385. https://doi.org/10.1111/mmi.13564

[105] Hill, E. F., Wilson, G. R., & Steinle, E. C. (1954). Production, properties, and uses of fatty alcohols. *Industrial & Engineering Chemistry*, *46*(9), 1917-1921. https://doi.org/10.1021/ie50537a042

[106] Hiltunen, J. K., Schonauer, M. S., Autio, K. J., Mittelmeier, T. M., Kastaniotis, A. J., & Dieckmann, C. L. (2009). Mitochondrial fatty acid synthesis type II: more than just fatty acids *Journal of Biological Chemistry*, *284*(14), 9011-9015. https://doi.org/10.1074/jbc.R800068200

[107] Hoekman, S. K., Broch, A., Robbins, C., Ceniceros, E., & Natarajan, M. (2012). Review of biodiesel composition, properties, and specifications. *Renewable and Sustainable Energy Reviews*, *16*(1), 143-169. https://doi.org/10.1016/j.rser.2011.07.143

[108] Hofvander, P., Doan, T. T., & H·mberg, M. (2011a). A prokaryotic acyl-CoA reductase performing reduction of fatty acyl-CoA to fatty alcohol. *FEBS Letters*, *585*.

[109] Hofvander, P., Doan, T. T., & Hamberg, M. (2011b). A prokaryotic acyl-CoA reductase performing reduction of fatty acyl-CoA to fatty alcohol. *Febs Letters*, *585*. https://doi.org/10.1016/j.febslet.2011.10.016

[110] Hsu, F.-F., Soehl, K., Turk, J., & Haas, A. (2011). Characterization of mycolic acids from the pathogen *Rhodococcus equi* by tandem mass spectrometry with electrospray ionization. *Analytical Biochemistry*, *409*(1), 112-122. https://doi.org/10.1016/j.ab.2010.10.006

[111] Huang, L., Zhao, L., Zan, X., Song, Y., & Ratledge, C. (2016). Boosting fatty acid synthesis in *Rhodococcus opacus* PD630 by overexpression of autologous thioesterases. *Biotechnology Letters*, *38*(6), 999-1008. https://doi.org/10.1007/s10529-016-2072-9

[112] Hüser, A. T., Becker, A., Brune, I., Dondrup, M., Kalinowski, J., Plassmeier, J., Pühler, A., Wiegräbe, I., & Tauch, A. (2003). Development of a *Corynebacterium glutamicum* DNA microarray and validation by genome-wide expression profiling during growth with propionate as carbon source. *Journal of Biotechnology*, *106*(2), 269-286. https://doi.org/10.1016/j.jbiotec.2003.08.006

[113] Ikeda, M., Nagashima, T., Nakamura, E., Kato, R., Ohshita, M., Hayashi, M., & Takeno, S. (2017). In vivo roles of fatty acid biosynthesis enzymes in biosynthesis of biotin and alpha-lipoic acid in *Corynebacterium glutamicum*. *Applied and Environmental Microbiology*, *83*(19), Article UNSP e01322-17. https://doi.org/10.1128/aem.01322-17

[114] Ikeda, M., & Nakagawa, S. (2003). The *Corynebacterium glutamicum* genome: features and impacts on biotechnological processes. *Applied Microbiology and Biotechnology*, *62*(2), 99-109. https://doi.org/10.1007/s00253-003-1328-1

[115] Ikeda, M., Takahashi, K., Ohtake, T., Imoto, R., Kawakami, H., Hayashi, M., & Takeno, S. (2020). A futile metabolic cycle of fatty acyl-CoA hydrolysis and resynthesis in *Corynebacterium glutamicum* and its disruption leading to fatty acid production. *Applied and Environmental Microbiology*, AEM.02469-02420. https://doi.org/10.1128/aem.02469-20

[116] Irzik, K., van Ooyen, J., Gatgens, J., Krumbach, K., Bott, M., & Eggeling, L. (2014). Acyl-CoA sensing by FasR to adjust fatty acid synthesis in *Corynebacterium glutamicum*. *Journal of Biotechnology*, *192*, 96-101. https://doi.org/10.1016/j.jbiotec.2014.10.031

[117] Jackowski, S., & Rock, C. O. (1987). Acetoacetyl-acyl carrier protein synthase, a potential regulator of fatty acid biosynthesis in bacteria. *Journal of Biological Chemistry*, *262*(16), 7927-7931. https://doi.org/10.1016/S0021-9258(18)47657-0

[118] Jackson, M. (2014). The mycobacterial cell envelope—lipids. *Cold Spring Harbor Perspectives in Medicine*, *4*(10). https://doi.org/10.1101/cshperspect.a021105

[119] Jawed, K., Mattam, A. J., Fatma, Z., Wajid, S., Abdin, M. Z., & Yazdani, S. S. (2016). Engineered production of short chain fatty acid in *Escherichia coli* using fatty acid synthesis pathway. *Plos One*, *11*(7), e0160035. https://doi.org/10.1371/journal.pone.0160035

[120] Jin, C., Huang, Z., & Bao, J. (2020). High-titer glutamic acid production from lignocellulose using an engineered *Corynebacterium glutamicum* with simultaneous co-utilization of xylose and glucose. *ACS Sustainable Chemistry & Engineering*, *8*(16), 6315-6322. https://doi.org/10.1021/acssuschemeng.9b07839

[121] Jönsson, L. J., & Martín, C. (2016). Pretreatment of lignocellulose: formation of inhibitory by-products and strategies for minimizing their effects. *Bioresource Technology*, *199*, 103-112. https://doi.org/10.1016/j.biortech.2015.10.009

[122] Kabus, A., Georgi, T., Wendisch, V. F., & Bott, M. (2007). Expression of the *Escherichia coli pntAB* genes encoding a membrane-bound transhydrogenase in *Corynebacterium glutamicum* improves L-lysine formation. *Applied Microbiology and Biotechnology*, *75*(1), 47-53. https://doi.org/10.1007/s00253-006-0804-9

[123] Kalinowski, J., Bathe, B., Bartels, D., Bischoff, N., Bott, M., Burkovski, A., Dusch, N., Eggeling, L., Eikmanns, B. J., Gaigalat, L., Goesmann, A., Hartmann, M., Huthmacher, K., Krämer, R., Linke, B., McHardy, A. C., Meyer, F., Möckel, B., Pfefferle, W., . . . Tauch, A. (2003). The complete *Corynebacterium glutamicum* ATCC 13032 genome sequence and its impact on the production of L-aspartate-derived amino acids and vitamins. *Journal of Biotechnology*, *104*(1), 5-25. https://doi.org/10.1016/S0168-1656(03)00154-8

[124] Kalscheuer, R., Stolting, T., & Steinbuchel, A. (2006). Microdiesel: Escherichia coli engineered for fuel production [Article]. *Microbiology-Sgm*, *152*, 2529-2536. https://doi.org/10.1099/mic.0.29028-0

[125] Kawaguchi, A., & Okuda, S. (1977). Fatty acid synthetase from *Brevibacterium ammoniagenes*: formation of monounsaturated fatty acids by a multienzyme complex. *Proceedings of the National Academy of Sciences*, *74*(8), 3180-3183. https://doi.org/10.1073/pnas.74.8.3180

[126] Kawaguchi, H., Vertès Alain, A., Okino, S., Inui, M., & Yukawa, H. (2006). Engineering of a xylose metabolic pathway in *Corynebacterium glutamicum*. *Applied and Environmental Microbiology*, *72*(5), 3418-3428. https://doi.org/10.1128/AEM.72.5.3418-3428.2006

[127] Keilhauer, C., Eggeling, L., & Sahm, H. (1993). Isoleucine synthesis in *Corynebacterium glutamicum*: molecular analysis of the *ilvB-ilvN-ilvC* operon. *Journal of Bacteriology*, *175*(17), 5595-5603. https://doi.org/10.1128/jb.175.17.5595-5603.1993

[128] Kiefer, D., Merkel, M., Lilge, L., Hausmann, R., & Henkel, M. (2021). High cell density cultivation of *Corynebacterium glutamicum* on bio-based lignocellulosic acetate using pH-coupled online feeding control. *Bioresource Technology*, *340*, 125666. https://doi.org/10.1016/j.biortech.2021.125666

[129] Kiefer, D., Tadele, L. R., Lilge, L., Henkel, M., & Hausmann, R. (2022). High-level recombinant protein production with *Corynebacterium glutamicum* using acetate as carbon source. *Microbial biotechnology*, *15*(11), 2744-2757. https://doi.org/10.1111/1751-7915.14138

[130] Kinoshita, S., Nakayama, K., & Akita, S. (1958). Taxonomical study of glutamic acid accumulating bacteria, *Micrococcus glutamicus* nov. sp. *Bulletin of the Agricultural Chemical Society of Japan*, *22*(3), 176-185. https://doi.org/10.1080/03758397.1958.10857463

[131] Kinoshita, S., Udaka, S., & Shimono, M. (1957). Studies on the amino acid fermentation part I. Production of L-glutamic acid by various microorganisms *The Journal of General and Applied Microbiology*, *3*(3), 193-205. https://doi.org/10.2323/jgam.3.193

[132] Klaffl, S., Brocker, M., Kalinowski, J., Eikmanns Bernhard, J., & Bott, M. (2013). Complex regulation of the phosphoenolpyruvate carboxykinase gene *pck* and characterization of its GntR-type regulator IolR as a repressor of *myo*-inositol utilization genes in *Corynebacterium glutamicum*. *Journal of Bacteriology*, *195*(18), 4283-4296. https://doi.org/10.1128/JB.00265-13

[133] Knoche, H. W., & Koths, K. E. (1973). Characterization of a fatty acid synthetase from *Corynebacterium diphtheriae*. *Journal of Biological Chemistry*, *248*(10), 3517-3519. https://doi.org/10.1016/S0021-9258(19)43960-4

[134] Kreutzer, U. R. (1984). Manufacture of fatty alcohols based on natural fats and oils. *Journal of the American Oil Chemists' Society*, *61*(2), 343-348. https://doi.org/10.1007/BF02678792

[135] Krishnan, A., McNeil, B. A., & Stuart, D. T. (2020). Biosynthesis of fatty alcohols in engineered microbial cell factories: advances and limitations [Review]. *Frontiers in Bioengineering and Biotechnology*, *8*. https://doi.org/10.3389/fbioe.2020.610936

[136] Krispin, O., & Allmansberger, R. (1998). The *Bacillus subtilis* AraE protein displays a broad substrate specificity for several different sugars. *Journal of Bacteriology*, *180*(12), 3250-3252. https://doi.org/10.1128/JB.180.12.3250-3252.1998

[137] Krüger, A., Wiechert, J., Gätgens, C., Polen, T., Mahr, R., Frunzke, J., & Becker, A. (2019). Impact of CO2/HCO3– Availability on Anaplerotic Flux in Pyruvate Dehydrogenase Complex-Deficient Corynebacterium glutamicum Strains. *Journal of Bacteriology*, *201*(20), e00387-00319. https://doi.org/10.1128/JB.00387-19

[138] Küberl, A., Mengus-Kaya, A., Polen, T., Bott, M., & Parales Rebecca, E. (2020). The Iron Deficiency Response of Corynebacterium glutamicum and a Link to Thiamine Biosynthesis. *Applied and Environmental Microbiology*, *86*(10), e00065-00020. https://doi.org/10.1128/AEM.00065-20

[139] Lai, C.-Y., & Cronan, J. E. (2003). *β*-ketoacyl-acyl aarrier protein synthase III (FabH) Is essential for bacterial fatty acid synthesis *Journal of Biological Chemistry*, *278*(51), 51494-51503. https://doi.org/10.1074/jbc.M308638200

[140] Lai, C.-Y., & Cronan John, E. (2004). Isolation and characterization of *β*-ketoacyl-acyl carrier protein reductase (*fabG*) mutants of *Escherichia coli* and S*almonella enterica* Serovar Typhimurium. *Journal of Bacteriology*, *186*(6), 1869-1878. https://doi.org/10.1128/JB.186.6.1869-1878.2004

[141] Lanéelle, M.-A., Tropis, M., & Daffé, M. (2013). Current knowledge on mycolic acids in *Corynebacterium glutamicum* and their relevance for biotechnological processes. *Applied Microbiology and Biotechnology*, *97*(23), 9923-9930. https://doi.org/10.1007/s00253-013-5265-3

[142] Lange, J., Müller, F., Bernecker, K., Dahmen, N., Takors, R., & Blombach, B. (2017). Valorization of pyrolysis water: a biorefinery side stream, for 1,2-propanediol production with engineered *Corynebacterium glutamicum*. *Biotechnology for Biofuels*, *10*(1), 277. https://doi.org/10.1186/s13068-017-0969-8

[143] Lange, J., Müller, F., Takors, R., & Blombach, B. (2018). Harnessing novel chromosomal integration loci to utilize an organosolv-derived hemicellulose fraction for isobutanol production with engineered *Corynebacterium glutamicum*. *Microbial biotechnology*, *11*(1), 257-263. https://doi.org/10.1111/1751-7915.12879

[144] Lange, L., Connor, K. O., Arason, S., Bundgård-Jørgensen, U., Canalis, A., Carrez, D., Gallagher, J., Gøtke, N., Huyghe, C., Jarry, B., Llorente, P., Marinova, M., Martins, L. O., Mengal, P., Paiano, P., Panoutsou, C., Rodrigues, L., Stengel, D. B., van der Meer, Y., & Vieira, H. (2021). Developing a sustainable and circular bio-based economy in EU: by partnering across sectors, upscaling and using new knowledge faster, and for the benefit of climate, environment & biodiversity, and people & business. *Frontiers in Bioengineering and Biotechnology*, *8*. https://doi.org/10.3389/fbioe.2020.619066

[145] Lea-Smith, D. J., Pyke, J. S., Tull, D., McConville, M. J., Coppel, R. L., & Crellin, P. K. (2007). The reductase that catalyzes mycolic motif synthesis is required for efficient attachment of mycolic acids to arabinogalactan. *Journal of Biological Chemistry*, *282*(15), 11000-11008. https://doi.org/10.1074/jbc.M608686200

[146] Leal, M. R. L. V., Galdos, M. V., Scarpare, F. V., Seabra, J. E. A., Walter, A., & Oliveira, C. O. F. (2013). Sugarcane straw availability, quality, recovery and energy use: a literature review. *Biomass and Bioenergy*, *53*, 11-19. https://doi.org/10.1016/j.biombioe.2013.03.007

[147] Lee, R. A., & Lavoie, J.-M. (2013). From first- to third-generation biofuels: challenges of producing a commodity from a biomass of increasing complexity. *Animal Frontiers*, *3*(2), 6-11. https://doi.org/10.2527/af.2013-0010

[148] Lennen, R. M., Braden, D. J., West, R. M., Dumesic, J. A., & Pfleger, B. F. (2010). A process for microbial hydrocarbon synthesis: overproduction of fatty acids in *Escherichia coli* and catalytic conversion to alkanes [10.1002/bit.22660]. *Biotechnology and Bioengineering*, *106*(2), 193-202. https://doi.org/https://doi.org/10.1002/bit.22660

[149] Liang, M. H., & Jiang, J. G. (2013). Advancing oleaginous microorganisms to produce lipid via metabolic engineering technology [Review]. *Progress in Lipid Research*, *52*(4), 395-408. https://doi.org/10.1016/j.plipres.2013.05.002

[150] Liebl, W. (2005). *Corynebacterium* taxonomy. In L. Eggeling & M. Bott (Eds.), *Handbook of Corynebacterium glutamicum* (pp. 9-34). CRC Press.

[151] Liebl, W., Bayerl, A., Schein, B., Stillner, U., & Schleifer, K. H. (1989). High efficiency electroporation of intact *Corynebacterium glutamicum* cells. *FEMS microbiology letters*, *53*(3), 299-303. https://doi.org/10.1016/0378-1097(89)90234-6

[152] Lin, C. Y., & Smith, S. (1978). Properties of the thioesterase component obtained by limited trypsinization of the fatty acid synthetase multienzyme complex. *Journal of Biological Chemistry*, *253*(6), 1954-1962. https://doi.org/10.1016/S0021-9258(19)62341-0

[153] Lindner, S. N., Seibold, G. M., Henrich, A., Krämer, R., & Wendisch, V. F. (2011). Phosphotransferase system-independent glucose utilization in *Corynebacterium glutamicum* by inositol permeases and glucokinases. *Applied and Environmental Microbiology*, *77*(11), 3571-3581. https://doi.org/10.1128/AEM.02713-10

[154] Liu, A., Tan, X., Yao, L., & Lu, X. (2013). Fatty alcohol production in engineered *E. coli* expressing Marinobacter fatty acyl-CoA reductases. *Applied Microbiology and Biotechnology*, *97*(15), 7061-7071. https://doi.org/10.1007/s00253-013-5027-2

[155] Liu, H., Yu, C., Feng, D., Cheng, T., Meng, X., Liu, W., Zou, H., & Xian, M. (2012). Production of extracellular fatty acid using engineered *Escherichia coli*. *Microbial Cell Factories*, *11*(1), 41. https://doi.org/10.1186/1475-2859-11-41

[156] Liu, Y., Chen, S., Chen, J., Zhou, J., Wang, Y., Yang, M., Qi, X., Xing, J., Wang, Q., & Ma, Y. (2016). High production of fatty alcohols in *Escherichia coli* with fatty acid starvation. *Microbial Cell Factories*, *15*(1), 129. https://doi.org/10.1186/s12934-016-0524-5

[157] Lopes, H. J. S., Bonturi, N., Kerkhoven, E. J., Miranda, E. A., & Lahtvee, P.-J. (2020). C/N ratio and carbon source-dependent lipid production profiling in *Rhodotorula toruloides*. *Applied Microbiology and Biotechnology*, *104*(6), 2639-2649. https://doi.org/10.1007/s00253-020-10386-5

[158] Lu, H., & Tonge, P. J. (2010). Mechanism and inhibition of the FabV enoyl-ACP reductase from *Burkholderia mallei*. *Biochemistry*, *49*(6), 1281-1289. https://doi.org/10.1021/bi902001a

[159] Luo, L., van der Voet, E., & Huppes, G. (2009). Life cycle assessment and life cycle costing of bioethanol from sugarcane in Brazil. *Renewable and Sustainable Energy Reviews*, *13*(6), 1613-1619. https://doi.org/10.1016/j.rser.2008.09.024

[160] Lynd, L. R., Wyman, C. E., & Gerngross, T. U. (1999). Biocommodity engineering. *Biotechnology Progress*, *15*(5), 777-793. https://doi.org/10.1021/bp990109e

[161] Lynen, F., Engeser, H., Foerster, E.-C., Fox, J. L., Hess, S., Kresze, G.-B., Schmitt, T., Schreckenbach, T., Siess, E., Wieland, F., & Winnewisser, W. (1980). On the structure of fatty acid synthetase of yeast. *European Journal of Biochemistry*, *112*(3), 431-442. https://doi.org/10.1111/j.1432-1033.1980.tb06105.x

[162] Ma, W., Wang, J., Li, Y., Hu, X., Shi, F., & Wang, X. (2016). Enhancing pentose phosphate pathway in *Corynebacterium glutamicum* to improve L-isoleucine production. *Biotechnology and Applied Biochemistry*, *63*(6), 877-885. https://doi.org/10.1002/bab.1442

[163] Magnuson, K., Oh, W., Larson, T. J., & Cronan, J. E. (1992). Cloning and nucleotide sequence of the *fabD* gene encoding malonyl coenzyme A-acyl carrier protein transacylase of *Escherichia coli*. *Febs Letters*, *299*(3), 262-266. https://doi.org/10.1016/0014-5793(92)80128-4

[164] Mankar, A. R., Pandey, A., Modak, A., & Pant, K. K. (2021). Pretreatment of lignocellulosic biomass: a review on recent advances. *Bioresource Technology*, *334*, 125235. https://doi.org/10.1016/j.biortech.2021.125235

[165] Mao, Y., Li, G., Chang, Z., Tao, R., Cui, Z., Wang, Z., Tang, Y.-j., Chen, T., & Zhao, X. (2018). Metabolic engineering of *Corynebacterium glutamicum* for efficient production of succinate from lignocellulosic hydrolysate. *Biotechnology for Biofuels*, *11*(1), 95. https://doi.org/10.1186/s13068-018-1094-z

[166] Marchand, C. H., Salmeron, C., Bou Raad, R., Méniche, X., Chami, M., Masi, M., Blanot, D., Daffé, M., Tropis, M., Huc, E., Le Maréchal, P., Decottignies, P., & Bayan, N. (2012). Biochemical disclosure of the mycolate outer membrane of *Corynebacterium glutamicum*. *Journal of Bacteriology*, *194*(3), 587-597. https://doi.org/10.1128/JB.06138-11

[167] Marella, E. R., Holkenbrink, C., Siewers, V., & Borodina, I. (2018). Engineering microbial fatty acid metabolism for biofuels and biochemicals. *Current Opinion in Biotechnology*, *50*, 39-46. https://doi.org/10.1016/j.copbio.2017.10.002

[168] Martin, M. A. (2010). First generation biofuels compete. *New Biotechnology*, *27*(5), 596-608. https://doi.org/10.1016/j.nbt.2010.06.010

[169] Massengo-Tiassé, R. P., & Cronan, J. E. (2008). *Vibrio cholera* FabV defines a new class of enoyl-acyl carrier protein reductase. *Journal of Biological Chemistry*, *283*(3), 1308-1316. https://doi.org/10.1074/jbc.M708171200

[170] Meiswinkel, T. M., Gopinath, V., Lindner, S. N., Nampoothiri, K. M., & Wendisch, V. F. (2013). Accelerated pentose utilization by *Corynebacterium glutamicum* for accelerated production of lysine, glutamate, ornithine and putrescine. *Microbial biotechnology*, *6*(2), 131-140. https://doi.org/10.1111/1751-7915.12001

[171] Menon, V., & Rao, M. (2012). Trends in bioconversion of lignocellulose: biofuels, platform chemicals & biorefinery concept. *Progress in Energy and Combustion Science*, *38*(4), 522-550. https://doi.org/10.1016/j.pecs.2012.02.002

[172] Merkens, H., Beckers, G., Wirtz, A., & Burkovski, A. (2005). Vanillate metabolism in *Corynebacterium glutamicum*. *Current Microbiology*, *51*(1), 59-65. https://doi.org/10.1007/s00284-005-4531-8

[173] Mhatre, A., Shinde, S., Jha, A. K., Rodriguez, A., Wardak, Z., Jansen, A., Gladden, J. M., George, A., Davis, R. W., & Varman, A. M. (2022). *Corynebacterium glutamicum* as an efficient omnivorous microbial host for the bioconversion of lignocellulosic biomass. *Frontiers in Bioengineering and Biotechnology*, *10*. https://doi.org/10.3389/fbioe.2022.827386

[174] Michel, A., Koch-Koerfges, A., Krumbach, K., Brocker, M., & Bott, M. (2015). Anaerobic growth of *Corynebacterium glutamicum* via mixed-acid fermentation. *Applied and Environmental Microbiology*, *81*(21), 7496-7508. https://doi.org/10.1128/AEM.02413-15

[175] Milke, L., Ferreira, P., Kallscheuer, N., Braga, A., Vogt, M., Kappelmann, J., Oliveira, J., Silva, A. R., Rocha, I., Bott, M., Noack, S., Faria, N., & Marienhagen, J. (2019a). Modulation of the central carbon metabolism of Corynebacterium glutamicum improves malonyl-CoA availability and increases plant polyphenol synthesis. *Biotechnology and Bioengineering*, *116*(6), 1380-1391. https://doi.org/10.1002/bit.26939

[176] Milke, L., Kallscheuer, N., Kappelmann, J., & Marienhagen, J. (2019b). Tailoring Corynebacterium glutamicum towards increased malonyl-CoA availability for efficient synthesis of the plant pentaketide noreugenin. *Microbial Cell Factories*, *18*, Article 71. https://doi.org/10.1186/s12934-019-1117-x

[177] Mobley, H. L., Island, M. D., & Hausinger, R. P. (1995). Molecular biology of microbial ureases. *Microbiological Reviews*, *59*(3), 451-480. https://doi.org/10.1128/mr.59.3.451-480.1995

[178] Morão, A., Maia, C. I., Fonseca, M. M. R., Vasconcelos, J. M. T., & Alves, S. S. (1999). Effect of antifoam addition on gas-liquid mass transfer in stirred fermenters. *Bioprocess Engineering*, *20*(2), 165-172. https://doi.org/10.1007/s004490050576

[179] Müller, F., Rapp, J., Hacker, A.-L., Feith, A., Takors, R., Blombach, B., & Lee Sang, Y. (2020). CO_2/HCO_3^- accelerates iron reduction through phenolic compounds. *mBio*, *11*(2), e00085-00020. https://doi.org/10.1128/mBio.00085-20

[180] Müller, T., Strösser, J., Buchinger, S., Nolden, L., Wirtz, A., Krämer, R., & Burkovski, A. (2006). Mutation-induced metabolite pool alterations in *Corynebacterium glutamicum*: Towards the identification of nitrogen control signals. *Journal of Biotechnology*, *126*(4), 440-453. https://doi.org/10.1016/j.jbiotec.2006.05.015

[181] Mullis, K. B., & Faloona, F. A. (1987). Specific synthesis of DNA *in vitro* via a polymerase-catalyzed chain reaction. In *Methods in Enzymology* (Vol. 155, pp. 335-350). Academic Press. https://doi.org/10.1016/0076-6879(87)55023-6

[182] Munkajohnpong, P., Kesornpun, C., Buttranon, S., Jaroensuk, J., Weeranoppanant, N., & Chaiyen, P. (2020). Fatty alcohol production: an opportunity of bioprocess. *Biofuels, Bioproducts and Biorefining*, *14*(5), 986-1009. https://doi.org/10.1002/bbb.2112

[183] Muscat, A., de Olde, E. M., de Boer, I. J. M., & Ripoll-Bosch, R. (2020). The battle for biomass: a systematic review of food-feed-fuel competition. *Global Food Security*, *25*, 100330. https://doi.org/10.1016/j.gfs.2019.100330

[184] Naggert, J., Narasimhan, M. L., DeVeaux, L., Cho, H., Randhawa, Z. I., Cronan, J. E., Jr., Green, B. N., & Smith, S. (1991). Cloning, sequencing, and characterization of *Escherichia coli* thioesterase II. *Journal of Biological Chemistry*, *266*(17), 11044-11050. https://doi.org/10.1016/S0021-9258(18)99125-8

[185] Nickel, J., Irzik, K., van Ooyen, J., & Eggeling, L. (2010). The TetR-type transcriptional regulator FasR of *Corynebacterium glutamicum* controls genes of lipid synthesis during growth on acetate. *Molecular Microbiology*, *78*(1), 253-265. https://doi.org/10.1111/j.1365-2958.2010.07337.x

[186] Nishimura, T., Vertès, A. A., Shinoda, Y., Inui, M., & Yukawa, H. (2007). Anaerobic growth of *Corynebacterium glutamicum* using nitrate as a terminal electron acceptor. *Applied Microbiology and Biotechnology*, *75*(4), 889-897. https://doi.org/10.1007/s00253-007-0879-y

[187] Nishiuchi, Y., Baba, T., Hotta, H. H., & Yano, I. (1999). Mycolic acid analysis in *Nocardia* species: the mycolic acid compositions of *Nocardia asteroides*, *N. farcinica*, and *N. nova*. *Journal of Microbiological Methods*, *37*(2), 111-122. https://doi.org/10.1016/S0167-7012(99)00055-X

[188] Nolden, L., Ngouoto-Nkili, C.-E., Bendt, A. K., Krämer, R., & Burkovski, A. (2001). Sensing nitrogen limitation in *Corynebacterium glutamicum*: the role of *glnK* and *glnD*. *Molecular Microbiology*, *42*(5), 1281-1295. https://doi.org/10.1046/j.1365-2958.2001.02694.x

[189] OECD, & FAO. (2022). *OECD-FAO Agricultural Outlook 2022-2031*. OECD Publishing. https://doi.org/10.1787/f1b0b29c-en

[190] Olukoshi, E. R., & Packter, N. M. (1994). Importance of stored triacylglycerols in *Streptomyces*: possible carbon source for antibiotics. *Microbiology*, *140*(4), 931-943. https://doi.org/10.1099/00221287-140-4-931

[191] Ottone, C., Bernal, C., Serna, N., Illanes, A., & Wilson, L. (2018). Enhanced long-chain fatty alcohol oxidation by immobilization of alcohol dehydrogenase from *S. cerevisiae*. *Applied Microbiology and Biotechnology*, *102*(1), 237-247. https://doi.org/10.1007/s00253-017-8598-5

[192] Pagliaro, M., Ciriminna, R., Kimura, H., Rossi, M., & Della Pina, C. (2007). From glycerol to value-added products. *Angewandte Chemie International Edition*, *46*(24), 4434-4440. https://doi.org/10.1002/anie.200604694

[193] Park, Y. K., Dulermo, T., Ledesma-Amaro, R., & Nicaud, J. M. (2018). Optimization of odd chain fatty acid production by *Yarrowia lipolytica*. *Biotechnology for Biofuels*, *11*, Article 158. https://doi.org/10.1186/s13068-018-1154-4

[194] Patel, A., Karageorgou, D., Rova, E., Katapodis, P., Rova, U., Christakopoulos, P., & Matsakas, L. (2020). An overview of potential oleaginous microorganisms and their role in biodiesel and omega-3 fatty acid-based industries. *Microorganisms*, *8*(3).

[195] Peralta-Yahya, P. P., Zhang, F., del Cardayre, S. B., & Keasling, J. D. (2012). Microbial engineering for the production of advanced biofuels. *Nature*, *488*(7411), 320-328. https://doi.org/10.1038/nature11478

[196] Pfeifer-Sancar, K., Mentz, A., Rückert, C., & Kalinowski, J. (2013). Comprehensive analysis of the *Corynebacterium glutamicum* transcriptome using an improved RNAseq technique. *Bmc Genomics*, *14*(1), 888. https://doi.org/10.1186/1471-2164-14-888

[197] Pfleger, B. F., Gossing, M., & Nielsen, J. (2015). Metabolic engineering strategies for microbial synthesis of oleochemicals. *Metabolic Engineering*, *29*, 1-11. https://doi.org/10.1016/j.ymben.2015.01.009

[198] Plassmeier, J., Li, Y. Y., Rueckert, C., & Sinskey, A. J. (2016). Metabolic engineering *Corynebacterium glutamicum* to produce triacylglycerols. *Metabolic Engineering*, *33*, 86-97. https://doi.org/10.1016/j.ymben.2015.11.002

[199] Portevin, D., de Sousa, D., Auria, C., Houssin, C., Grimaldi, C., Chami, M., Daffé, M., & Guilhot, C. (2004). A polyketide synthase catalyzes the last condensation step of mycolic acid biosynthesis in mycobacteria and related organisms. *Proceedings of the National Academy of Sciences*, *101*(1), 314. https://doi.org/10.1073/pnas.0305439101

[200] Portevin, D., de Sousa-D'Auria, C., Montrozier, H., Houssin, C., Stella, A., Lanéelle, M.-A., Bardou, F., Guilhot, C., & Daffé, M. (2005). The acyl-AMP ligase FadD32 and AccD4-containing acyl-CoA carboxylase are required for the synthesis of mycolic acids and essential for Mycobacterial growth: identification of the carboxylation product and determination of the acyl-CoA carboxylase components. *Journal of Biological Chemistry*, *280*(10), 8862-8874. https://doi.org/10.1074/jbc.M408578200

[201] Prescott, D. J., Elovson, J., & Vagelos, P. R. (1969). Acyl Carrier Protein: The specificity of acyl carrier protein synthase. *Journal of Biological Chemistry*, *244*(16), 4517-4521. https://doi.org/10.1016/S0021-9258(18)94348-6

[202] Rabemanolontsoa, H., & Saka, S. (2013). Comparative study on chemical composition of various biomass species [10.1039/C3RA22958K]. *RSC Advances*, *3*(12), 3946-3956. https://doi.org/10.1039/C3RA22958K

[203] Radek, A., Krumbach, K., Gätgens, J., Wendisch, V. F., Wiechert, W., Bott, M., Noack, S., & Marienhagen, J. (2014). Engineering of *Corynebacterium glutamicum* for minimized carbon loss during utilization of D-xylose containing substrates. *Journal of Biotechnology*, *192*, 156-160. https://doi.org/10.1016/j.jbiotec.2014.09.026

[204] Radek, A., Tenhaef, N., Müller, M. F., Brüsseler, C., Wiechert, W., Marienhagen, J., Polen, T., & Noack, S. (2017). Miniaturized and automated adaptive laboratory evolution: evolving *Corynebacterium glutamicum* towards an improved D-xylose utilization. *Bioresource Technology*, *245*, 1377-1385. https://doi.org/10.1016/j.biortech.2017.05.055

[205] Radmacher, E., Alderwick, L. J., Besra, G. S., Brown, A. K., Gibson, K. J. C., Sahm, H., & Eggeling, L. (2005). Two functional FAS-I type fatty acid synthases in *Corynebacterium glutamicum*. *Microbiology-Sgm*, *151*, 2421-2427. https://doi.org/10.1099/mic.0.28012-0

[206] Radmacher, E., & Eggeling, L. (2007). The three tricarboxylate synthase activities of *Corynebacterium glutamicum* and increase of L-lysine synthesis. *Applied Microbiology and Biotechnology*, *76*(3), 587-595. https://doi.org/10.1007/s00253-007-1105-7

[207] Rand, P. B. (1984). *Stabilized aqueous foam systems, concentrate for producing a stabilized aqueous foam and method of producing said foam* (United States Patent No. US 4442018). U. D. o. Energy. https://www.osti.gov/servlets/purl/5840466

[208] Rarbach, M., & Söltl, Y. (2013). sunliquid®: sustainable and competitive cellulosic ethanol from agricultural residues. *CHIMIA*, *67*(10), 732. https://doi.org/10.2533/chimia.2013.732

[209] Reinscheid, D. J., Schnicke, S., Rittmann, D., Zahnow, U., Sahm, H., & Eikmanns, B. J. (1999). Cloning, sequence analysis, expression and inactivation of the *Corynebacterium glutamicum pta-ack* operon encoding phosphotransacetylase and acetate kinase. *Microbiology*, *145*(2), 503-513. https://doi.org/10.1099/13500872-145-2-503

[210] Rieke, R. D., Thakur, D. S., Roberts, B. D., & White, G. T. (1997). Fatty methyl ester hydrogenation to fatty alcohol part II: Process issues. *Journal of the American Oil Chemists' Society*, *74*(4), 341-345. https://doi.org/10.1007/s11746-997-0089-x

[211] Rock, C. O., & Jackowski, S. (2002). Forty years of bacterial fatty acid synthesis. *Biochemical and Biophysical Research Communications*, *292*(5), 1155-1166. https://doi.org/10.1006/bbrc.2001.2022

[212] Rodrigues, T. E., Gerhardt, E. C. M., Oliveira, M. A., Chubatsu, L. S., Pedrosa, F. O., Souza, E. M., Souza, G. A., Müller-Santos, M., & Huergo, L. F. (2014). Search for novel targets of the PII signal transduction protein in bacteria identifies the BCCP component of acetyl-CoA carboxylase as a PII binding partner. *Molecular Microbiology*, *91*(4), 751-761. https://doi.org/10.1111/mmi.12493

[213] Rodrigues, T. E., Sassaki, G. L., Valdameri, G., Pedrosa, F. O., Souza, E. M., & Huergo, L. F. (2019). Fatty acid biosynthesis is enhanced in *Escherichia coli* strains with deletion in genes encoding the PII signaling proteins. *Archives of Microbiology*, *201*(2), 209-214. https://doi.org/10.1007/s00203-018-1603-2

[214] Rulli, M. C., Bellomi, D., Cazzoli, A., De Carolis, G., & D'Odorico, P. (2016). The water-land-food nexus of first-generation biofuels. *Scientific Reports*, *6*(1), 22521. https://doi.org/10.1038/srep22521

[215] Runguphan, W., & Keasling, J. D. (2014). Metabolic engineering of *Saccharomyces cerevisiae* for production of fatty acid-derived biofuels and chemicals. *Metabolic Engineering*, *21*, 103-113. https://doi.org/10.1016/j.ymben.2013.07.003

[216] Saiki, R. K., Scharf, S., Faloona, F., Mullis, K. B., Horn, G. T., Erlich, H. A., & Arnheim, N. (1985). Enzymatic amplification of β-globin genomic sequences and restriction site analysis for diagnosis of sickle cell anemia. *Science*, *230*(4732), 1350-1354. https://doi.org/10.1126/science.2999980

[217] Sajjadi, B., Raman, A. A. A., & Arandiyan, H. (2016). A comprehensive review on properties of edible and non-edible vegetable oil-based biodiesel: composition, specifications and prediction models. *Renewable and Sustainable Energy Reviews*, *63*, 62-92. https://doi.org/10.1016/j.rser.2016.05.035

[218] Sambrook, J., Russel, D. W., Irwin, N., & Janssen, U. A. (2001). *Molecular Cloning: A Laboratory Manual*. Cold Spring Harbor Laboratory Press.

[219] Santamaría, R., Gil, J. A., Mesas, J. M., & Martín, J. F. (1984). Characterization of an Endogenous Plasmid and Development of Cloning Vectors and a Transformation System in Brevibacterium lactofermentum. *Microbiology*, *130*(9), 2237-2246. https://doi.org/10.1099/00221287-130-9-2237

[220] Sasaki, M., Jojima, T., Inui, M., & Yukawa, H. (2008). Simultaneous utilization of D-cellobiose, D-glucose, and D-xylose by recombinant *Corynebacterium glutamicum* under oxygen-deprived conditions. *Applied Microbiology and Biotechnology*, *81*(4), 691-699. https://doi.org/10.1007/s00253-008-1703-z

[221] Sasaki, M., Jojima, T., Kawaguchi, H., Inui, M., & Yukawa, H. (2009). Engineering of pentose transport in *Corynebacterium glutamicum* to improve simultaneous utilization of mixed sugars. *Applied Microbiology and Biotechnology*, *85*(1), 105-115. https://doi.org/10.1007/s00253-009-2065-x

[222] Sasikumar, K., Hannibal, S., Wendisch, V. F., & Nampoothiri, K. M. (2021). Production of biopolyamide precursors 5-amino valeric acid and putrescine from rice straw hydrolysate by engineered *Corynebacterium glutamicum*. *Frontiers in Bioengineering and Biotechnology*, *9*. https://doi.org/10.3389/fbioe.2021.635509

[223] Schäfer, A., Tauch, A., Jäger, W., Kalinowski, J., Thierbach, G., & Pühler, A. (1994). Small mobilizable multi-purpose cloning vectors derived from the Escherichia coli plasmids pK18 and pK19: selection of defined deletions in the chromosome of Corynebacterium glutamicum. *Gene*, *145*(1), 69-73. https://doi.org/10.1016/0378-1119(94)90324-7

[224] Schirmer, A., Rude, M. A., Li, X., Popova, E., & del Cardayre, S. B. (2010). Microbial biosynthesis of alkanes. *Science*, *329*(5991), 559-562. https://doi.org/10.1126/science.1187936

[225] Schmollack, M., Werner, F., Huber, J., Kiefer, D., Merkel, M., Hausmann, R., Siebert, D., & Blombach, B. (2022). Metabolic engineering of *Corynebacterium glutamicum* for acetate-based itaconic acid production. *Biotechnology for Biofuels and Bioproducts*, *15*(1), 139. https://doi.org/10.1186/s13068-022-02238-3

[226] Schultz, J. C., Mishra, S., Gaither, E., Mejia, A., Dinh, H., Maranas, C., & Zhao, H. (2022). Metabolic engineering of *Rhodotorula toruloides* IFO0880 improves C16 and C18 fatty alcohol production from synthetic media. *Microbial Cell Factories*, *21*(1), 26. https://doi.org/10.1186/s12934-022-01750-3

[227] Schweizer, E., & Hofmann, J. (2004a). Microbial type I fatty acid synthases (FAS): Major players in a network of cellular FAS systems. *Microbiology and Molecular Biology Reviews*, *68*(3), 501-+. https://doi.org/10.1128/mmbr.68.3.501-517.2004

[228] Schweizer, E., & Hofmann, J. (2004b). Microbial type I fatty acid synthases (FAS): Major players in a network of cellular FAS systems. *Microbiology and Molecular Biology Reviews*, *68*(3), 501-517. https://doi.org/10.1128/mmbr.68.3.501-517.2004

[229] Seyama, Y., & Kawaguchi, A. (1987). Fatty acid synthesis and the role of pyridine nucleotides. *Pyridine nucleotide coenzymes: chemical, biochemical, and medical aspects*, *2*, 381-431.

[230] Shaigani, P., Awad, D., Redai, V., Fuchs, M., Haack, M., Mehlmer, N., & Brueck, T. (2021). Oleaginous yeasts- substrate preference and lipid productivity: a view on the performance of microbial lipid producers. *Microbial Cell Factories*, *20*(1), 220. https://doi.org/10.1186/s12934-021-01710-3

[231] Sharma, H. K., Xu, C., & Qin, W. (2019). Biological pretreatment of lignocellulosic biomass for biofuels and bioproducts: an overview. *Waste and Biomass Valorization*, *10*(2), 235-251. https://doi.org/10.1007/s12649-017-0059-y

[232] Shen, X.-H., Zhou, N.-Y., & Liu, S.-J. (2012). Degradation and assimilation of aromatic compounds by *Corynebacterium glutamicum*: another potential for applications for this bacterium? *Applied Microbiology and Biotechnology*, *95*(1), 77-89. https://doi.org/10.1007/s00253-012-4139-4

[233] Sherry, A. E., Chapman, B. E., Creedon, M. T., Jordan, J. M., & Moese, R. L. (1995). Nonbleach process for the purification of palm C16–18 methyl ester sulfonates. *Journal of the American Oil Chemists' Society*, *72*(7), 835-841. https://doi.org/10.1007/BF02541034

[234] Shi, F., Luan, M., & Li, Y. (2018). Ribosomal binding site sequences and promoters for expressing glutamate decarboxylase and producing γ-aminobutyrate in *Corynebacterium glutamicum*. *AMB Express*, *8*(1), 61. https://doi.org/10.1186/s13568-018-0595-2

[235] Shokravi, H., Shokravi, Z., Heidarrezaei, M., Ong, H. C., Rahimian Koloor, S. S., Petrů, M., Lau, W. J., & Ismail, A. F. (2021). Fourth generation biofuel from genetically modified algal biomass: Challenges and future directions. *Chemosphere*, *285*, 131535. https://doi.org/10.1016/j.chemosphere.2021.131535

[236] Siebert, D., Altenbuchner, J., & Blombach, B. (2021). A timed off-switch for dynamic control of gene expression in *Corynebacterium glutamicum*. *Frontiers in Bioengineering and Biotechnology*, *9*. https://doi.org/10.3389/fbioe.2021.704681

[237] Siebert, D., & Wendisch, V. F. (2015). Metabolic pathway engineering for production of 1,2-propanediol and 1-propanol by *Corynebacterium glutamicum*. *Biotechnology for Biofuels*, *8*(1), 91. https://doi.org/10.1186/s13068-015-0269-0

[238] Siedler, S., Lindner, S. N., Bringer, S., Wendisch, V. F., & Bott, M. (2013). Reductive whole-cell biotransformation with *Corynebacterium glutamicum*: improvement of NADPH generation from glucose by a cyclized pentose phosphate pathway using *pfkA* and *gapA* deletion mutants. *Applied Microbiology and Biotechnology*, *97*(1), 143-152. https://doi.org/10.1007/s00253-012-4314-7

[239] Silberbach, M., Schäfer, M., Hüser Andrea, T., Kalinowski, J., Pühler, A., Krämer, R., & Burkovski, A. (2005). Adaptation of *Corynebacterium glutamicum* to ammonium limitation: a global analysis using transcriptome and proteome techniques. *Applied and Environmental Microbiology*, *71*(5), 2391-2402. https://doi.org/10.1128/AEM.71.5.2391-2402.2005

[240] Silver, W. L., & Miya, R. K. (2001). Global patterns in root decomposition: comparisons of climate and litter quality effects. *Oecologia*, *129*(3), 407-419. https://doi.org/10.1007/s004420100740

[241] Singh, J., Suhag, M., & Dhaka, A. (2015). Augmented digestion of lignocellulose by steam explosion, acid and alkaline pretreatment methods: a review. *Carbohydrate Polymers*, *117*, 624-631. https://doi.org/10.1016/j.carbpol.2014.10.012

[242] Soetaert, W., & Vandamme, E. (2006). The impact of industrial biotechnology. *Biotechnology Journal*, *1*(7-8), 756-769. https://doi.org/10.1002/biot.200600066

[243] Srinivasan, S. (2009). The food v. fuel debate: a nuanced view of incentive structures. *Renewable Energy*, *34*(4), 950-954. https://doi.org/10.1016/j.renene.2008.08.015

[244] Stackebrandt, E., Rainey, F. A., & Ward-Rainey, N. L. (1997). Proposal for a new hierarchic classification system, *Actinobacteria* classis nov. *International Journal of Systematic and Evolutionary Microbiology*, *47*(2), 479-491. https://doi.org/10.1099/00207713-47-2-479

[245] Strösser, J., Lüdke, A., Schaffer, S., Krämer, R., & Burkovski, A. (2004). Regulation of GlnK activity: modification, membrane sequestration and proteolysis as regulatory principles in the network of nitrogen control in *Corynebacterium glutamicum*. *Molecular Microbiology*, *54*(1), 132-147. https://doi.org/10.1111/j.1365-2958.2004.04247.x

[246] Sul, H. S., & Smith, S. (2008). Chapter 6 - Fatty acid synthesis in eukaryotes. In D. E. Vance & J. E. Vance (Eds.), *Biochemistry of Lipids, Lipoproteins and Membranes (Fifth Edition)* (pp. 155-190). Elsevier. https://doi.org/10.1016/B978-044453219-0.50008-8

[247] Sun, X., Mao, Y., Luo, J., Liu, P., Jiang, M., He, G., Zhang, Z., Cao, Q., Shen, J., Ma, H., Chen, T., & Wang, Z. (2022). Global cellular metabolic rewiring adapts *Corynebacterium glutamicum* to efficient nonnatural xylose utilization. *Applied and Environmental Microbiology*, *0*(0), e01518-01522. https://doi.org/10.1128/aem.01518-22

[248] Takeno, S., Hirata, Y., Kitamura, K., Ohtake, T., Aoki, K., Murata, N., Hayashi, M., & Ikeda, M. (2023). Metabolic engineering to produce palmitic acid or palmitoleic acid in an oleic acid-producing *Corynebacterium glutamicum* strain. *Metabolic Engineering*, *78*, 148-158. https://doi.org/10.1016/j.ymben.2023.06.002

[249] Takeno, S., Murata, N., Kura, M., Takasaki, M., Hayashi, M., & Ikeda, M. (2018). The *accD3* gene for mycolic acid biosynthesis as a target for improving fatty acid production by fatty acid-producing *Corynebacterium glutamicum* strains. *Applied Microbiology and Biotechnology*, *102*(24), 10603-10612. https://doi.org/10.1007/s00253-018-9395-5

[250] Takeno, S., Murata, R., Kobayashi, R., Mitsuhashi, S., & Ikeda, M. (2010). Engineering of *Corynebacterium glutamicum* with an NADPH-generating glycolytic pathway for L-lysine production. *Applied and Environmental Microbiology*, *76*(21), 7154-7160. https://doi.org/10.1128/AEM.01464-10

[251] Takeno, S., Ohnishi, J., Komatsu, T., Masaki, T., Sen, K., & Ikeda, M. (2007). Anaerobic growth and potential for amino acid production by nitrate respiration in *Corynebacterium glutamicum*. *Applied Microbiology and Biotechnology*, *75*(5), 1173-1182. https://doi.org/10.1007/s00253-007-0926-8

[252] Takeno, S., Takasaki, M., Urabayashi, A., Mimura, A., Muramatsu, T., Mitsuhashi, S., & Ikeda, M. (2013). Development of fatty acid-producing *Corynebacterium glutamicum* strains. *Applied and Environmental Microbiology*, *79*(21), 6776-6783. https://doi.org/10.1128/aem.02003-13

[253] Takors, R., Bathe, B., Rieping, M., Hans, S., Kelle, R., & Huthmacher, K. (2007). Systems biology for industrial strains and fermentation processes - Example: Amino acids. *Journal of Biotechnology*, *129*(2), 181-190. https://doi.org/10.1016/j.jbiotec.2007.01.031

[254] Taniguchi, H., Busche, T., Patschkowski, T., Niehaus, K., Pátek, M., Kalinowski, J., & Wendisch, V. F. (2017). Physiological roles of sigma factor SigD in Corynebacterium glutamicum. *BMC Microbiology*, *17*(1), 158. https://doi.org/10.1186/s12866-017-1067-6

[255] Tauch, A., Kirchner, O., Löffler, B., Götker, S., Pühler, A., & Kalinowski, J. (2002). Efficient electrotransformation of *Corynebacterium diphtheriae* with a mini-replicon derived from the *Corynebacterium glutamicum* plasmid pGA1. *Current Microbiology*, *45*(5), 362-367. https://doi.org/10.1007/s00284-002-3728-3

[256] Tesch, M., de Graaf, A. A., & Sahm, H. (1999). *In vivo* fluxes in the ammonium-assimilatory pathways in *Corynebacterium glutamicum* studied by ^{15}N nuclear magnetic resonance. *Applied and Environmental Microbiology*, *65*(3), 1099-1109. https://doi.org/10.1128/AEM.65.3.1099-1109.1999

[257] Thakur, D. S., & Kundu, A. (2016). Catalysts for fatty alcohol production from renewable resources. *Journal of the American Oil Chemists' Society*, *93*(12), 1575-1593. https://doi.org/10.1007/s11746-016-2902-x

[258] Tharmasothirajan, A., Wellfonder, M., & Marienhagen, J. (2021). Microbial polyphenol production in a biphasic process. *ACS Sustainable Chemistry & Engineering*, *9*(51), 17266-17275. https://doi.org/10.1021/acssuschemeng.1c05865

[259] Thompson, P. B. (2012). The agricultural ethics of biofuels: the food vs. fuel debate. *Agriculture*, *2*(4), 339-358.

[260] Tropis, M., Meniche, X., Wolf, A., Gebhardt, H., Strelkov, S., Chami, M., Schomburg, D., Krämer, R., Morbach, S., & Daffé, M. (2005). The crucial role of trehalose and structurally related oligosaccharides in the biosynthesis and transfer of mycolic acids in Corynebacterineae. *Journal of Biological Chemistry*, *280*(28), 26573-26585. https://doi.org/10.1074/jbc.M502104200

[261] UN General Assembly. (2015). Transforming our world : the 2030 Agenda for Sustainable Development. *A/RES/70/1*. Retrieved 2 May, 2023, from https://www.refworld.org/docid/57b6e3e44.html

[262] USDA-FAS. (2021). *Biofuels annual*. U. F. A. Service. https://www.fas.usda.gov/data/argentina-biofuels-annual-6

[263] Valentine, J., Clifton-Brown, J., Hastings, A., Robson, P., Allison, G., & Smith, P. (2012). Food vs. fuel: the use of land for lignocellulosic 'next generation' energy crops that minimize competition with primary food production. *GCB Bioenergy*, *4*(1), 1-19. https://doi.org/10.1111/j.1757-1707.2011.01111.x

[264] van der Rest, M. E., Lange, C., & Molenaar, D. (1999). A heat shock following electroporation induces highly efficient transformation of *Corynebacterium glutamicum* with xenogeneic plasmid DNA. *Applied Microbiology and Biotechnology*, *52*(4), 541-545. https://doi.org/10.1007/s002530051557

[265] van Ooyen, J., Noack, S., Bott, M., Reth, A., & Eggeling, L. (2012). Improved L-lysine production with *Corynebacterium glutamicum* and systemic insight into citrate synthase flux and activity. *Biotechnology and Bioengineering*, *109*(8), 2070-2081. https://doi.org/10.1002/bit.24486

[266] Vardar-Sukan, F. (1998). Foaming: consequences, prevention and destruction. *Biotechnology Advances*, *16*(5), 913-948. https://doi.org/10.1016/S0734-9750(98)00010-X

[267] Verwoert, I. I., Verbree, E. C., van der Linden, K. H., Nijkamp, H. J., & Stuitje, A. R. (1992). Cloning, nucleotide sequence, and expression of the *Escherichia coli fabD* gene, encoding malonyl coenzyme A-acyl carrier protein transacylase. *Journal of Bacteriology*, *174*(9), 2851-2857. https://doi.org/10.1128/jb.174.9.2851-2857.1992

[268] Vijay, V., Pimm, S. L., Jenkins, C. N., & Smith, S. J. (2016). The impacts of oil palm on recent deforestation and biodiversity loss. *Plos One*, *11*(7), e0159668. https://doi.org/10.1371/journal.pone.0159668

[269] Visek, K. (2003). Amines, Fatty. In *Kirk-Othmer Encyclopedia of Chemical Technology*. https://doi.org/10.1002/0471238961.0601202022091905.a01.pub2

[270] Voelker, T. A., & Davies, H. M. (1994). Alteration of the specificity and regulation of fatty acid synthesis of *Escherichia coli* by expression of a plant medium-chain acyl-acyl carrier protein thioesterase. *Journal of Bacteriology*, *176*(23), 7320-7327. https://doi.org/10.1128/jb.176.23.7320-7327.1994

[271] Wang, C., Cai, H., Zhou, Z., Zhang, K., Chen, Z., Chen, Y., Wan, H., & Ouyang, P. (2014). Investigation of ptsG gene in response to xylose utilization in *Corynebacterium glutamicum*. *Journal of Industrial Microbiology and Biotechnology*, *41*(8), 1249-1258. https://doi.org/10.1007/s10295-014-1455-y

[272] Wang, S., Jin, X., Jiang, W., Wang, Q., Qi, Q., & Liang, Q. (2022). The expression modulation of the key enzyme Acc for highly efficient 3-hydroxypropionic acid production [Original Research]. *Frontiers in Microbiology*, *13*. https://doi.org/10.3389/fmicb.2022.902848

[273] Wang, W., Wei, H., Knoshaug, E., Van Wychen, S., Xu, Q., Himmel, M. E., & Zhang, M. (2016). Fatty alcohol production in Lipomyces starkeyi and Yarrowia lipolytica. *Biotechnology for Biofuels*, *9*, 227-227. https://doi.org/10.1186/s13068-016-0647-2

[274] Wendisch, V. F. (2020). Metabolic engineering advances and prospects for amino acid production. *Metabolic Engineering*, *58*, 17-34. https://doi.org/10.1016/j.ymben.2019.03.008

[275] Wendisch, V. F., de Graaf, A. A., Sahm, H., & Eikmanns, B. J. (2000). Quantitative determination of metabolic fluxes during coutilization of two carbon sources: Comparative analyses with *Corynebacterium glutamicum* during growth on acetate and/or glucose. *Journal of Bacteriology*, *182*(11), 3088-3096. https://doi.org/10.1128/JB.182.11.3088-3096.2000

[276] Werner, F., Schwardmann, L. S., Siebert, D., Rückert-Reed, C., Kalinowski, J., Wirth, M.-T., Hofer, K., Takors, R., Wendisch, V. F., & Blombach, B. (2023). Metabolic engineering of *Corynebacterium glutamicum* for fatty alcohol production from glucose and wheat straw hydrolysate. *Biotechnology for Biofuels and Bioproducts*, *16*(1), 116. https://doi.org/10.1186/s13068-023-02367-3

[277] White, S. W., Zheng, J., Zhang, Y.-M., & Rock, C. O. (2005). The structural biology of type II fatty acid biosynthesis. *Annual Review of Biochemistry*, *74*(1), 791-831. https://doi.org/10.1146/annurev.biochem.74.082803.133524

[278] Wildschut, J., Smit, A. T., Reith, J. H., & Huijgen, W. J. J. (2013). Ethanol-based organosolv fractionation of wheat straw for the production of lignin and enzymatically digestible cellulose. *Bioresource Technology*, *135*, 58-66. https://doi.org/10.1016/j.biortech.2012.10.050

[279] Willis, R. M., Wahlen, B. D., Seefeldt, L. C., & Barney, B. M. (2011). Characterization of a Fatty Acyl-CoA Reductase from Marinobacter aquaeolei VT8: A Bacterial Enzyme Catalyzing the Reduction of Fatty Acyl-CoA to Fatty Alcohol. *Biochemistry*, *50*(48), 10550-10558. https://doi.org/10.1021/bi2008646

[280] Wittmann, C., Kiefer, P., & Zelder, O. (2004). Metabolic fluxes in *Corynebacterium glutamicum* during lysine production with sucrose as carbon source. *Applied and Environmental Microbiology*, *70*(12), 7277-7287. https://doi.org/10.1128/AEM.70.12.7277-7287.2004

[281] Wolf, S., Becker, J., Tsuge, Y., Kawaguchi, H., Kondo, A., Marienhagen, J., Bott, M., Wendisch, Volker F., & Wittmann, C. (2021). Advances in metabolic engineering of *Corynebacterium glutamicum* to produce high-value active ingredients for food, feed, human health, and well-being. *Essays in Biochemistry*, *65*(2), 197-212. https://doi.org/10.1042/ebc20200134

[282] Woo, H. M., & Park, J.-B. (2014). Recent progress in development of synthetic biology platforms and metabolic engineering of *Corynebacterium glutamicum*. *Journal of Biotechnology*, *180*, 43-51. https://doi.org/10.1016/j.jbiotec.2014.03.003

[283] Wu, H., Karanjikar, M., & San, K.-Y. (2014). Metabolic engineering of *Escherichia coli* for efficient free fatty acid production from glycerol. *Metabolic Engineering*, *25*, 82-91. https://doi.org/10.1016/j.ymben.2014.06.009

[284] Xu, P., Gu, Q., Wang, W., Wong, L., Bower, A. G. W., Collins, C. H., & Koffas, M. A. G. (2013). Modular optimization of multi-gene pathways for fatty acids production in *E. coli*. *Nature Communications*, *4*(1), 1409. https://doi.org/10.1038/ncomms2425

[285] Yan, Q., & Pfleger, B. F. (2020). Revisiting metabolic engineering strategies for microbial synthesis of oleochemicals [Review]. *Metabolic Engineering*, *58*, 35-46. https://doi.org/10.1016/j.ymben.2019.04.009

[286] Yang, H., Xie, Y., Zheng, X., Pu, Y., Huang, F., Meng, X., Wu, W., Ragauskas, A., & Yao, L. (2016). Comparative study of lignin characteristics from wheat straw obtained by soda-AQ and kraft pretreatment and effect on the following enzymatic hydrolysis process. *Bioresource Technology*, *207*, 361-369. https://doi.org/10.1016/j.biortech.2016.01.123

[287] Yang, Y., Shi, F., Tao, G., & Wang, X. (2012). Purification and structure analysis of mycolic acids in *Corynebacterium glutamicum*. *The Journal of Microbiology*, *50*(2), 235-240. https://doi.org/10.1007/s12275-012-1459-0

[288] Yeong, S. K., Idris, Z., & Hassan, H. A. (2012). Palm oleochemicals in non-food applications. In O.-M. Lai, C.-P. Tan, & C. C. Akoh (Eds.), *Palm Oil* (pp. 587-624). AOCS Press. https://doi.org/10.1016/B978-0-9818936-9-3.50023-X

[289] Yim, S. S., Choi, J. W., Lee, S. H., Jeon, E. J., Chung, W.-J., & Jeong, K. J. (2017). Engineering of *Corynebacterium glutamicum* for consolidated conversion of hemicellulosic biomass into xylonic acid. *Biotechnology Journal*, *12*(11), 1700040. https://doi.org/10.1002/biot.201700040

[290] Yim, S. S., Choi, J. W., Lee, S. H., & Jeong, K. J. (2016). Modular optimization of a hemicellulose-utilizing pathway in *Corynebacterium glutamicum* for consolidated bioprocessing of hemicellulosic biomass. *ACS Synthetic Biology*, *5*(4), 334-343. https://doi.org/10.1021/acssynbio.5b00228

[291] Yokota, A., & Lindley, N. D. (2005). Central metabolism: sugar uptake and conversion. In L. Eggeling & M. Bott (Eds.), *Handbook of Corynebacterium glutamicum* (Vol. 2005, pp. 215-242). CRC Press.

[292] Yoshimura, M., Oshima, T., & Ogasawara, N. (2007). Involvement of the YneS/YgiH and PlsX proteins in phospholipid biosynthesis in both *Bacillus subtilis* and *Escherichia coli*. *BMC Microbiology*, *7*(1), 69. https://doi.org/10.1186/1471-2180-7-69

[293] Zavrel, M., Dennewald, D., Bartuch, J., & Marckmann, H. (2015). *Process for the hydrolysis of lignocellulosic material, wherein the hydrolysate is used for microbial hydrolase production* EP2947152A1). E. P. Office.

[294] Zhan, M. L., Kan, B. J., Dong, J. J., Xu, G. C., Han, R. Z., & Ni, Y. (2019). Metabolic engineering of *Corynebacterium glutamicum* for improved l-arginine synthesis by enhancing NADPH supply. *Journal of Industrial Microbiology & Biotechnology*, *46*(1), 45-54. https://doi.org/10.1007/s10295-018-2103-8

[295] Zhang, Y., Shinoda, M., Shiki, Y., & Tsubaki, N. (2007). The function of added noble metal to Co/active carbon catalysts for oxygenate fuels synthesis via hydroformylation at low pressure. In B. H. Davis & M. L. Occelli (Eds.), *Studies in Surface Science and Catalysis* (Vol. 163, pp. 87-99). Elsevier. https://doi.org/10.1016/S0167-2991(07)80474-5

[296] Zhang, Y., Su, M., Qin, N., Nielsen, J., & Liu, Z. (2020). Expressing a cytosolic pyruvate dehydrogenase complex to increase free fatty acid production in *Saccharomyces cerevisiae*. *Microbial Cell Factories*, *19*(1), 226. https://doi.org/10.1186/s12934-020-01493-z

[297] Zhao, N., Qian, L., Luo, G., & Zheng, S. (2018). Synthetic biology approaches to access renewable carbon source utilization in *Corynebacterium glutamicum*. *Applied Microbiology and Biotechnology*, *102*(22), 9517-9529. https://doi.org/10.1007/s00253-018-9358-x

[298] Zhao, X., Li, S., Wu, R., & Liu, D. (2017). Organosolv fractionating pre-treatment of lignocellulosic biomass for efficient enzymatic saccharification: chemistry, kinetics, and substrate structures. *Biofuels, Bioproducts and Biorefining*, *11*(3), 567-590. https://doi.org/10.1002/bbb.1768

[299] Zheng, Y.-N., Li, L.-L., Liu, Q., Yang, J.-M., Wang, X.-W., Liu, W., Xu, X., Liu, H., Zhao, G., & Xian, M. (2012). Optimization of fatty alcohol biosynthesis pathway for selectively enhanced production of C12/14 and C16/18 fatty alcohols in engineered *Escherichia coli*. *Microbial Cell Factories*, *11*(1), 65. https://doi.org/10.1186/1475-2859-11-65

[300] Zheng, Z., Gong, Q., Liu, T., Deng, Y., Chen, J.-C., & Chen, G.-Q. (2004). Thioesterase II of *Escherichia coli* plays an important role in 3-hydroxydecanoic acid production. *Applied and Environmental Microbiology*, *70*(7), 3807-3813. https://doi.org/10.1128/AEM.70.7.3807-3813.2004

[301] Zhou, C.-H., Beltramini, J. N., Fan, Y.-X., & Lu, G. Q. (2008). Chemoselective catalytic conversion of glycerol as a biorenewable source to valuable commodity chemicals [10.1039/B707343G]. *Chemical Society Reviews*, *37*(3), 527-549. https://doi.org/10.1039/B707343G

[302] Zhou, Y. J., Buijs, N. A., Zhu, Z., Qin, J., Siewers, V., & Nielsen, J. (2016). Production of fatty acid-derived oleochemicals and biofuels by synthetic yeast cell factories. *Nature Communications*, *7*(1), 11709. https://doi.org/10.1038/ncomms11709

[303] Zimhony, O., Schwarz, A., Raitses-Gurevich, M., Peleg, Y., Dym, O., Albeck, S., Burstein, Y., & Shakked, Z. (2015). AcpM, the meromycolate extension acyl carrier protein of *Mycobacterium tuberculosis*, is activated by the 4′-phosphopantetheinyl transferase PptT, a potential target of the multistep mycolic mcid biosynthesis. *Biochemistry*, *54*(14), 2360-2371. https://doi.org/10.1021/bi501444e

[304] Zoghlami, A., & Paës, G. (2019). Lignocellulosic biomass: understanding recalcitrance and predicting hydrolysis [Mini Review]. *Frontiers in Chemistry*, *7*. https://doi.org/10.3389/fchem.2019.00874

Appendix

A.1. Supplementary methods

A.1.1. Chemicals

Table S. 1: Chemicals

Chemical	Manufacturer	Cat. No.
Acetic acid	Carl Roth GmbH & Co. KG, Karlsruhe, Germany	3738.1
Agar-Agar, Kobe I	Carl Roth GmbH & Co. KG, Karlsruhe, Germany	5210.4
Agarose SERVA Wide Range	SERVA Electrophoresis GmbH, Heidelberg, Germany	11406.02
Ammonium sulfate	Carl Roth GmbH & Co. KG, Karlsruhe, Germany	3746.1
Difco™ Tryptone	Life Technologies Corporation, Detroit, United States	211921
Difco™ Yeast Extract	Life Technologies Corporation, Detroit, United States	211929
BBL™ Brain Heart Infusion	Becton, Dickinson and Company, Sparks, United States	211059
Calcium chloride dihydrate	VWR International GmbH, Darmstadt, Germany	22317260
Chloroform	VWR International GmbH, Darmstadt, Germany	22711.324
CONTRASPUM® A 4050	Zschimmer & Schwarz GmbH & Co KG, Lahnstein, Germany	170000399
Copper sulfate pentahydrate	Merck KGaA, Darmstadt, Germany	1027900250
Dimethyl sulfoxide	Carl Roth GmbH & Co. KG, Karlsruhe, Germany	4720.2
Dipotassium hydrogen phosphate	Carl Roth GmbH & Co. KG, Karlsruhe, Germany	P749.1
D-biotin	Merck KGaA, Darmstadt, Germany	8512090005
D(+)-glucose monohydrate	Carl Roth GmbH & Co. KG, Karlsruhe, Germany	6887.2
D-sorbitol	Carl Roth GmbH & Co. KG, Karlsruhe, Germany	6213.1

D(+)-sucrose	VWR International GmbH, Darmstadt, Germany	27483294
D-xylose	Carl Roth GmbH & Co. KG, Karlsruhe, Germany	5537.1
Ethylenediaminetetraacetic acid	Carl Roth GmbH & Co. KG, Karlsruhe, Germany	8040.3
Ethyl acetate	VWR International GmbH, Darmstadt, Germany	23.882.310
Ethyl decanoate	Thermo Fisher Scientific, Ward Hill, United States	165001000
GelGreen® Nucleic Acid Gel Stain	Biotium Inc., Fremont, United States	41005
Gel Loading Dye, Purple (6X)	New England Biolabs GmbH, Frankfurt am Main, Germany	B7024A
Glycerol	Carl Roth GmbH & Co. KG, Karlsruhe, Germany	7533.1
Heptadecanoic acid	Alfa Aesar, Haverhill, United States	L05928
1-heptadecanol	SIGMA-ALDRICH Chemie GmbH, Steinheim, Germany	241695-5G
1-hexadecanol	Alfa Aesar, Haverhill, United States	A11180
Hexane	SIGMA-ALDRICH Chemie GmbH, Steinheim, Germany	32293-1L-M
Iron sulfate heptahydrate	Carl Roth GmbH & Co. KG, Karlsruhe, Germany	P015.1
Isopropyl β-D-1-thiogalactopyranoside	Carl Roth GmbH & Co. KG, Karlsruhe, Germany	CN08.2
Kanamycin sulfate	Carl Roth GmbH & Co. KG, Karlsruhe, Germany	T832.2
Magnesium sulfate heptahydrate	VWR International GmbH, Darmstadt, Germany	25167298
Manganese sulfate monohydrate	Merck KGaA, Darmstadt, Germany	25167298
Methanol	SIGMA-ALDRICH Chemie GmbH, Steinheim, Germany	34860-2.5L-R
Methyl decanoate	Thermo Fisher Scientific, Ward Hill, United States	A15658
Nickel chloride hexahydrate	Carl Roth GmbH & Co. KG, Karlsruhe, Germany	4489.1
1-octadecanol	Alfa Aesar, Haverhill, United States	A12020

Oleic acid	Carl Roth GmbH & Co. KG, Karlsruhe, Germany	7213.1
Oleyl alcohol	Alfa Aesar, Haverhill, United States	A18018
o-phosphoric acid	Carl Roth GmbH & Co. KG, Karlsruhe, Germany	4334.1
Palmitic acid	Carl Roth GmbH & Co. KG, Karlsruhe, Germany	5907.1
Potassium dihydrogen phosphate	Carl Roth GmbH & Co. KG, Karlsruhe, Germany	P018.2
Potassium hydroxide	VWR International GmbH, Darmstadt, Germany	26669290
n-propyl decanoate	Thermo Fisher Scientific, Ward Hill, United States	B25159.18
Protocatechuic acid	Alfa Aesar, Haverhill, United States	B24016.14
Ready-to-Use 1 kb DNA Ladder	Biotium Inc., Fremont, United States	31022
Sodium acetate	SIGMA-ALDRICH Chemie GmbH, Steinheim, Germany	S8750-500G
Sodium bicarbonate	Carl Roth GmbH & Co. KG, Karlsruhe, Germany	HN01.1
Sodium chloride	Carl Roth GmbH & Co. KG, Karlsruhe, Germany	3957.1
Sodium L-lactate	SIGMA-ALDRICH Chemie GmbH, Steinheim, Germany	71718-10G
Sodium pyruvate	Carl Roth GmbH & Co. KG, Karlsruhe, Germany	8793.2
Sodium sulfate	Merck KGaA, Darmstadt, Germany	1.06649.0500
Spectinomycin dichloride pentahydrate	Alfa Aesar, Haverhill, United States	J61820.06
Struktol® J 647	Schill+Seilacher GmbH, Hamburg, Germany	18412
Struktol® J 673 A	Schill+Seilacher GmbH, Hamburg, Germany	02158
Struktol® SB 2121	Schill+Seilacher GmbH, Hamburg, Germany	18413
Sulfuric acid	Carl Roth GmbH & Co. KG, Karlsruhe, Germany	4623.1
Tributyrin	Thermo Fisher Scientific, Ward Hill, United States	150882500

Tris(hydroxymethyl)aminomethane	Carl Roth GmbH & Co. KG, Karlsruhe, Germany	AE15.2
Water for HPLC HiPerSolv CHROMANORM	VWR International GmbH, Darmstadt, Germany	23595.328
Zinc sulfate heptahydrate	Carl Roth GmbH & Co. KG, Karlsruhe, Germany	K301.1
2-propanol for HPLC HiPerSolv CHROMANORM	VWR International GmbH, Darmstadt, Germany	20880.320
3-(N-morpholino)propanesulfonic acid	SIGMA-ALDRICH Chemie GmbH, Steinheim, Germany	M1254-1KG

A.1.2. Abbreviations of chemicals

Table S. 2: Abbreviations of chemcials

Abbreviation	Chemical
C16:0	1-hexadecanoic acid (palmitic acid)
C18:0	1-octadecanoic acid (stearic acid)
C18:1	*cis*-9-Octadecenoic acid (oleic acid)
C16:0-OH	1-hexadecanol (cetyl alcohol)
C18:0-OH	1-octadecanol (stearyl alcohol)
C18:1-OH	*cis*-9-Octadecenol (oleyl alcohol)
$CaCl_2$ x 2 H_2O	Calcium chloride dihydrate
CO_2	Carbon dioxide
CO_3^{2-}	Carbonate
$CuSO_4$ x 5 H_2O	Copper sulfate pentahydrate
DI-H_2O	Deionized water
DMSO	Dimethyl sulfoxide
EDTA	Ethylenediaminetetraacetic acid
Fe^{2+}	Ferrous iron
Fe^{3+}	Ferric iron
$FeSO_4$ x 7 H_2O	Iron sulfate heptahydrate
HCl	Hydrochloric acid
HCO_3^-	Bicarbonate
H_2SO_4	Sulfuric acid
IPTG	Isopropyl β-D-1-thiogalactopyranoside
K_2HPO	Dipotassium hydrogen phosphate
KH_2PO_4	Potassium dihydrogen phosphate
KOH	Potassium hydroxide
$MgCl_2$	Magnesium chloride
$MgCl_2$ x 7 H_2O	Magnesium chloride heptahydrate
$MnSO_4$ x H_2O	Manganese sulfate monohydrate
MOPS	3-(N-morpholino)propanesulfonic acid
NaCl	Sodium chloride

$NaHCO_3$	Sodium bicarbonate
$(NH_4)_2SO_4$	Ammonium sulfate
$NiCl_2$ x 6 H_2O	Nickel chloride hexahydrate
PCA	3,4-Dihydroxybenzoic acid (protocatechuic acid)
TAE	TRIS-acetate-EDTA
Tris	Tris(hydroxymethyl)aminomethane
$ZnSO_4$ x 7 H_2O	Zinc sulfate heptahydrate

A.1.3. Kits

Table S. 3: Kits

Kit	Manufacturer	Cat. No.
NucleoSpin® Gel and PCR Clean-up, Mini kit for gel extraction and PCR clean up	MACHEREY-NAGEL GmbH & Ko. KG, Düren, Germany	740609.250
NucleoSpin® Microbial DNA mini kit for DNA from microorganisms	MACHEREY-NAGEL GmbH & Ko. KG, Düren, Germany	740235.250
NucleoSpin® Plasmid, Mini kit for plasmid DNA	MACHEREY-NAGEL GmbH & Ko. KG, Düren, Germany	740588.250

A.1.4. Software

Table S. 4: Software

Name	Purpose	Manufacturer
BioRender	Visualization of seedtrains	BioRender.com
ChemDraw® Professional	Visualization of metabolic pathways	PerkinElmer, Inc., Waltham, United States
Clone Manager	*In silico* design of oligonucleotides and plasmids; analysis of sequencing data	Sci Ed Software LLC, Westminster, United States
Grammarly	Spelling and grammar assistance	Grammarly Inc., San Francisco, United States
multiWin®	Acquisition and analysis of total carbon data	Analytik Jena GmbH, Jena, Germany
MATLAB®	Data analysis and visualization	The MathWorks, Inc., Natick, United States
Microsoft® Excel	Data analysis	Microsoft Corporation, Redmond, United States
Microsoft® Word	Writing	Microsoft Corporation, Redmond, United States
New Brunswick™ BioCommand® Track and Trend/Batch Control	Control of BioFlo® 120 processes	Eppendorf SE, Hamburg, Germany
OpenLab CDS – Chemstation Edition	Acquisition and analysis of HPLC and GC data	Agilent Technologies, Waldbronn, Germany

A.1.5. Devices and equipment

Table S. 5: Devices and relevant equipment

Name	Device	Manufacturer
1260 Infinity II system	HPLC equipped with RID	Agilent Technologies, Waldbronn, Germany
7693A Automatic Liquid Sampler	Autoinjector and tray for GC	Agilent Technologies, Waldbronn, Germany
8890 GC system	GC equipped with FID	Agilent Technologies, Waldbronn, Germany
BioFlo® 120	Bioreactor	Eppendorf SE, Hamburg, Germany
Biometra Casting System Compact	Agarose gel casting system	Analytik Jena GmbH, Jena, Germany
Biometra Compact M	Agarose gel electrophoresis system (medium)	Analytik Jena GmbH, Jena, Germany
Biometra Compact XS/S	Agarose gel electrophoresis system (small)	Analytik Jena GmbH, Jena, Germany
Biometra Standard Power Pack P25 T	Power supply for gel electro-phoresis	Analytik Jena GmbH, Jena, Germany
Biometra TAdvanced Twin 48 G	Thermocycler	Analytik Jena GmbH, Jena, Germany
Biometra TOne 96	Thermocycler	Analytik Jena GmbH, Jena, Germany
Biometra TProfessional Basic Grad 96w	Thermocycler	Analytik Jena GmbH, Jena, Germany
Centrifuge 5425	Benchtop centrifuge	Eppendorf SE, Hamburg, Germany
Centrifuge 5910R	Refrigerated high-capacity cen-trifuge	Eppendorf SE, Hamburg, Germany
Concentrator plus	Vacuum evaporator	Eppendorf SE, Hamburg, Germany
Cooling trap, 250 mL	Cooling trap	Gebr. Rettberg GmbH, Göttingen, Germany
Corning® Cap, PTFE Liner	Cap with PTFE liner	Corning, Inc., Corning, United States
DB-FATWAX-UI	GC column for fatty acid and fatty alcohol analysis; 30 m x 0.25 mm x 0.25 µm	Agilent Technologies, Waldbronn, Germany

DO Sensor InPro6830	DO electrode for BioFlo® 120	Mettler-Toledo GmbH, Urdorf, Switzerland
E-BOX CX5 TS	Gel documentation system	Vilber Lourmat Deutschland GmbH, Eberhardzell, Germany
Entris® 124i-1S	Balance	Sartorius AG, Göttingen, Germany
Entris® 420i-1S	Analytical balance	Sartorius AG, Göttingen, Germany
E-BOX CX5 TS	Gel imaging system	Vilber Lourmat Deutschland GmbH, Eberhardzell, Germany
FiveEasy pH meter F20	pH meter	Mettler Toledo GmbH, Gießen, Germany
Gene Pulser Xcell™	Electroporation system	Bio-Rad Laboratories Inc., Hercules, United States
Heraeus Multifuge 4KR	Refrigerated high-capacity centrifuge	Thermo Electron LED GmbH, Osterode am Harz, Germany
Hi-Plex H column	HPLC column for carbohydrate analysis; 7.7 x 300 mm, 8 µm	Agilent Technologies, Waldbronn, Germany
Hi-Plex H guard cartridge	Guard cartridge for HPLC column; 3.0 x 5.0 mm, 8 µm	Agilent Technologies, Waldbronn, Germany
Medi-Test Glucose	Test strips for glucose analysis	MACHEREY-NAGEL GmbH & Ko. KG, Düren, Germany
Modell BD 115	Incubator	BINDER GmbH, Tuttlingen, Germany
Multi N/C 2100s analyzer	Total carbon analyzer	Analytik Jena GmbH, Jena, Germany
Multitron Standard SU252	Orbital shaker (25 mm eccentricity)	Infors AG, Bottmingen, Switzerland
NanoPhotometer® NP80	Small volume spectrophotometer	Implen GmbH, Munich, Germany
pH Electrode LE407	pH electrode for pH meter	Mettler-Toledo GmbH, Urdorf, Switzerland
pH Sensor 405-DPAS-SC-K8S/200	pH electrode for BioFLo® 120	Mettler-Toledo GmbH, Urdorf, Switzerland
PYREX® Disposable Glass Conical Centrifuge Tubes	Glass tubes for fatty acid extraction; 10 mL	Corning, Inc., Corning, United States
QuickSpin	Microcentrifuge	EDWARDS Instruments Co., Narellan, Australia

Syringe pump LA-30	Syringe pump	Landgraf Laborsysteme Hill GmbH, Langenhagen, Germany
ThermoMixer® C	Benchtop mixing and temperature-control device	Eppendorf SE, Hamburg, Germany
Ultrospec® 10 Cell Density Meter	Hand-held spectrophotometer	Biochrom Ltd, Cambridge, United Kingdom
Vortex-Genie 2	Vortex mixer	Scientific Industries, Inc., Bohemia, United States

A.1.6. Enzymes and enzyme buffers

Table S. 6: Enzymes and enzyme buffers. All enzymes and corresponding buffers were purchased from New England Biolabs GmbH (Frankfurt am Main, Germany). n.a.: not applicable.

Polymerases	**Concentration | U mL^{-1}**	**Buffer**
Quick-Load® *Taq* 2x Master Mix	n.a.	(ready to use)
Phusion® High-Fidelity DNA Polymerase	2,000	5x Phusion HF Buffer
Endonucleases	**Concentration | U mL^{-1}**	**Buffer**
BamHI-HF®	20,000	rCutSmart™ Buffer
BbvCI	2,000	rCutSmart™ Buffer
EcoRI-HF®	20,000	rCutSmart™ Buffer
NcoI-HF®	20,000	rCutSmart™ Buffer
NheI-HF®	20,000	rCutSmart™ Buffer
NotI-HF®	20,000	rCutSmart™ Buffer
SmaI	20,000	rCutSmart™ Buffer
XhoI	20,000	rCutSmart™ Buffer
Others	**Concentration | U mL^{-1}**	**Buffer**
Quick CIP	5,000	rCutSmart™ Buffer
T5 exonuclease	10,000	-
T4 DNA ligase	400,000	-

A.1.7. Strains and plasmids

Table S. 7: Strains and plasmids

Strain or plasmid	Relevant characteristics	Reference
Strains		
E. coli DH5α	F-Φ80*lacZ*ΔM15 Δ(*lacZYA-argF*) U169 *endA1 recA1 hsdR17* (rK^-, mK^+) *supE44 thi-1 gyrA96 relA1 phoA*	(Hanahan, 1983)
E. coli K-12 MG1655	*E. coli* wild type (WT)	(Blattner et al., 1997)
C. glutamicum ATCC 13032	*C. glutamicum* wild type (WT)	(Abe et al., 1967; Kinoshita et al., 1958)
C. glutamicum Δ*fasR*	*C. glutamicum* ATCC 13032 derivate with deletion of the transcriptional regulator FasR-encoding gene *fasR*	This work (Werner et al., 2023)
C. glutamicum Δ*fasR* $cg2692_{GTG}$	*C. glutamicum* Δ*fasR* derivate with start codon GTG of the thioesterase-encoding gene cg2692	This work (Werner et al., 2023)
C. glutamicum Δ*fasR* $cg2692_{TTG}$	*C. glutamicum* Δ*fasR* derivate with start codon TTG of the thioesterase-encoding gene cg2692	This work (Werner et al., 2023)
C. glutamicum Δ*fasR* CgLP11::(P_{tac}-*maqu2220*-T_{rrnB})	*C. glutamicum* Δ*fasR* derivate with *maqu_2220* of *M. hydrocarbonoclasticus* VT8 under control of P_{tac} and terminated by T_{rrnB} integrated into landing pad CgLP11	This work (Werner et al., 2023)
C. glutamicum Δ*fasR* $cg2692_{GTG}$ CgLP11::(P_{tac}-*maqu2220*-T_{rrnB})	*C. glutamicum* Δ*fasR* CgLP11::(P_{tac}-*maqu_2220*-T_{rrnB}) derivate with start codon GTG of the thioesterase-encoding gene cg2692	This work (Werner et al., 2023)
C. glutamicum Δ*fasR* $cg2692_{TTG}$ CgLP11::(P_{tac}-*maqu2220*-T_{rrnB})	*C. glutamicum* Δ*fasR* CgLP11::(P_{tac}-*maqu_2220*-T_{rrnB}) derivate with start codon TTG of the thioesterase-encoding gene cg2692	This work (Werner et al., 2023)
C. glutamicum Δ*fasR* $cg2692_{TTG}$ CgLP12::(P_{tac}-*pntAB*-T_{rrnB})	*C. glutamicum* Δ*fasR* $cg2692_{TTG}$ derivate with *pntAB* of *E. coli* under control of P_{tac} and terminated by T_{rrnB} integrated into landing pad CgLP12	This work (Werner et al., 2023)

C. glutamicum Δ*fasR* cg2692$_{TTG}$ gX	*C. glutamicum* Δ*fasR* cg2692$_{TTG}$ derivate with insertion of the synthetic operon consisting of *xylA* (*X. campestris*) and *xylB* (*C. glutamicum*) with evolved sequence upstream of *xylA* (gX) into the gene locus *actA*	This work (Werner et al., 2023)
C. glutamicum Δ*fasR* cg2692$_{TTG}$ CgLP12::(P$_{tac}$-*pntAB*-T$_{rrnB}$) gX	*C. glutamicum* Δ*fasR* cg2692$_{TTG}$ gX derivate with *pntAB* of *E. coli* under control of P$_{tac}$ and terminated by T$_{rrnB}$ integrated into landing pad CgLP12	This work (Werner et al., 2023)
C. glutamicum Δ*fasR* cg2692$_{TTG}$ CgLP12::(P$_{tac}$-*pntAB*-T$_{rrnB}$) ΔP*gltA*::P*dapA*-A25 gX	*C. glutamicum* Δ*fasR* cg2692$_{TTG}$ CgLP12::(P$_{tac}$-*pntAB*-T$_{rrnB}$) gX derivate with exchanged *gltA* promoter for the *dapA* promoter variant A25	This work (Werner et al., 2023)
C. glutamicum Δ*fasR* cg2692$_{TTG}$ CgLP12::(P$_{tac}$-*pntAB*-T$_{rrnB}$) ΔP*gltA*::P*dapA*-C7 gX	*C. glutamicum* Δ*fasR* cg2692$_{TTG}$ CgLP12::(P$_{tac}$-*pntAB*-T$_{rrnB}$) gX derivate with exchanged *gltA* promoter for the *dapA* promoter variant C7	This work (Werner et al., 2023)
C. glutamicum Δ*fasR* cg2692$_{TTG}$ CgLP12::(P$_{tac}$-*pntAB*-T$_{rrnB}$) ΔP*gltA*::P*dapA*-L1 gX	*C. glutamicum* Δ*fasR* cg2692$_{TTG}$ CgLP12::(P$_{tac}$-*pntAB*-T$_{rrnB}$) gX derivate with exchanged *gltA* promoter for the *dapA* promoter variant L1	This work (Werner et al., 2023)
C. glutamicum ΔP$_{fasA}$::P$_{tuf}$	*C. glutamicum* derivate with exchanged *fasA* promoter for the strong *tuf* promoter	This work
C. glutamicum ΔP$_{fasA}$::P$_{tuf}$ ΔP$_{fasB}$::P$_{tuf}$	*C. glutamicum* ΔP$_{fasA}$::P$_{tuf}$ derivate with exchanged *fasB* promoter for the strong *tuf* promoter	This work
C. glutamicum Δ*fasR* Δ*gdh*	*C. glutamicum* Δ*fasR* derivate with deletion of *gdh*	This work (Schmollack et al., 2022)
C. glutamicum Δ*fasR* Δ*sigD*	*C. glutamicum* Δ*fasR* derivate with deletion of the sigma factor D-encoding gene *sigD*	This work
Plasmids		
pK19*mobsacB*	Km^r; Mobilizable cloning vector to construct insertion or deletion mutants of *C. glutamicum* (pK18 *ori*V$_{E.c.}$, *sacB*, *lacZα*)	(Schäfer et al., 1994)
pK19*mobsacBlacI*^{q}	Km^r; pK19*mobsacB* derivate with *lacI*^{q} downstream of MCS	This work (Werner et al., 2023)
pK19*mobsacB*_cg2692$_{GTG}$	Km^r; pK19*mobsacB* derivate for exchanging the native start codon of cg2692 to GTG	This work (Werner et al., 2023)

pK19*mobsacB*_cg2692$_{TTG}$	Km^r; pK19*mobsacB* derivate for exchanging the native start codon of cg2692 to TTG	This work (Werner et al., 2023)
pK19*mobsacB*_ Δ*fasR*	Km^r; pK19*mobsacB* derivate for the deletion of *fasR*	This work (Werner et al., 2023)
pK19*mobsacB*_ Δ*gdh*	Km^r; pK19*mobsacB* derivate for the deletion of *gdh*	This work (Schmollack et al., 2022)
pK19*mobsacB*_ ΔP_{fasA}::P_{tuf}	Km^r; pK19*mobsacB* derivate for exchanging the native promoter of *fasA* for the constitutive *tuf* promoter	This work
pK19*mobsacB*_ ΔP_{fasB}::P_{tuf}	Km^r; pK19*mobsacB* derivate for exchanging the native promoter of *fasB* for the constitutive *tuf* promoter	This work
pK19*mobsacB*_ ΔP_{gltA}::P_{dapA}-A25	Km^r; pK19*mobsacB* derivate for exchanging the native promoter of *gltA* for the *dapA* promoter variant A25	(van Ooyen et al., 2012)
pK19*mobsacB*_ ΔP_{gltA}::P_{dapA}-C7	Km^r; pK19*mobsacB* derivate for exchanging the native promoter of *gltA* for the *dapA* promoter variant C7	(van Ooyen et al., 2012)
pK19*mobsacB*_ ΔP_{gltA}::P_{dapA}-L1	Km^r; pK19*mobsacB* derivate for exchanging the native promoter of *gltA* for the *dapA* promoter variant L1	(van Ooyen et al., 2012)
pK19*mobsacB*_ Δ*sigD*	Km^r; pK19*mobsacB* derivate for the deletion of *sigD*	This work
pK19*mobsacBlacI^q*_ *maqu2220*$_{CgLP11}$	Km^r; pK19*mobsacBlacI^q* derivate for the integration of *maqu_2220* under the control of the *tac* promoter and terminated by the *rrnB* terminator into the integration locus CgLP11	This work (Werner et al., 2023)
pK19*mobsacBlacI^q*_ *pntAB*$_{CgLP12}$	Km^r; pK19*mobsacBlacI^q* derivate for the integration of *pntAB* under the control of the *tac* promoter and terminated by the *rrnB* terminator into the integration locus CgLP12	This work (Werner et al., 2023)
pECXT_P_{syn}	Tet^r; *E. coli-C. glutamicum* expression shuttle vector for constitutive expression from the strong synthetic promoter P_{syn} (P_{syn}, *lacI^q*, pGA1 *oriV$_{C.g.}$*)	(Henke et al., 2021a)

pECXT_P_{syn}_*maqu220*	Tet^r; pECXT_P_{syn} derivate with coding sequence of *maqu_2220* of *M. hydrocarbonoclasticus* VT8 in MCS	This work (Werner et al., 2023)
pEKEx2	Km^r; *E. coli-C. glutamicum* expression shuttle vector (P_{tac}, *lacI*^{q}, pBL1 *ori*$V_{C.g.}$, pUC18 *ori*$V_{E.c.}$)	(Eikmanns et al., 1994)
pEKEx2_*accD1BC*	Km^r; pEKEx2 derivate with coding sequence of *accD1* and *accBC* of *C. glutamicum* in MCS. Mutated *accD1* sequence in FasR binding region as described by Milke et al. (2019b)	This work
pEKEx2_*accE*	Km^r; pEKEx2 derivate with coding sequence of *accE* of *C. glutamicum* in MCS	This work
pEKEx2_*maqu2220*	Km^r; pEKEx2 derivate with coding sequence of *maqu_2220* of *M. hydrocarbonoclasticus* VT8 in MCS	This work (Werner et al., 2023)
pEKEx2_*maqu2507*	Km^r; pEKEx2 derivate with coding sequence of *maqu_2507* of *M. hydrocarbonoclasticus* VT8 in MCS	This work (Werner et al., 2023)
pEKEx2_*pntAB*	Km^r; pEKEx2 derivate with coding sequence of *pntAB* of *E. coli* K-12 MG1655	This work (Werner et al., 2023)

A.1.8. Oligonucleotides

Table S. 8: Oligonucleotides and respective applications. All oligonucleotides were purchased from SIGMA-ALDRICH Chemie GmbH (Steinheim, Germany). Complementary overlaps are italicized and synthetic RBS + spacer sequences as described by Shi et al. (2018) are displayed bold. Mutated nucleotides are highlighted in red.

No.	Primer	Purpose	Sequence (5' → 3')
1	pK19lacI_fw	Amplification of MCS of pK19*mobsacB*-derived plasmids & sequencing	TCAGTGAGCGAGGAAGCG
2	pK19lacZ_rv	Amplification of MCS of pK19*mobsacB*-derived plasmids & sequencing	TTAGCAGCCCTTGCGCC
3	FW_pEKEx2	Amplification of MCS of pEKEx2-derived plasmids & sequencing	GCACTCCCGTTCTGGATAATGTT
4	RW_pEKEx2	Amplification of MCS of pEKEx2-derived plasmids & sequencing	GCGTTCTGATTTAATCTGTATCAGGCTG
5	FW_F1_FasR	Amplification of Flank1 of *fasR*; template: DNA of S3	*GTCGACTCTAGAGGATCCCC*TGCCTAATGATTCGGGTTCGAC
6	RV_F1_fasR	Amplification of Flank1 of *fasR*; template: DNA of S3	*CGTGCGTGTTGACTATCCAGTAG*TAAAATTTCAGTGCCTGCCGCT
7	FW_F2_fasR	Amplification of Flank2 of *fasR*; template: DNA of S3	*AGCGGCAGGCACTGAAATTTTA*CTACTGGATAGTCAACACGCACG
8	RV_F2_FasR	Amplification of Flank2 of *fasR*; template: DNA of S3	*TGAATTCGAGCTCGGTACCC*GCCGACGGCGCCAACTCTGC
9	FW_ΔfasR_validation	Validation of *fasR* deletion	CCATATGCAAGGTATCTACATCGAAGAG
10	RV_ΔfasR_validation	Validation of *fasR* deletion	AACACCCTCCAACAGCTCG
11	FW_F1_fasA	Amplification of Flank1 of *fasA*; template: DNA of S3	*GTCGACTCTAGAGGATCCCC*CAGGCCCGTCATGCGTG
12	RV_F1_fasA	Amplification of Flank1 of *fasA*; template: DNA of S3	*CCACGAAGTCCAGGAGGACATACATATG*GTGACCGAATTGAGCAGGAACTT
13	FW_Ptuf_fasA	Amplification of P_{tuf}; template: DNA of S3; sequencing	*GCAGGTTTCCCTCACTTGTTGGCCCGGG*CCACAGGGTAGCTGGTAGTTTGA

14	RV_Ptuf_fasA	Amplification of P_{tuf}; template: DNA of S3; sequencing	*AAGTTCCTGCTCAATTCGGTCACCATATG*-TATGTCCTCCTGGACTTCGTGG
15	FW_F2_fasA	Amplification of Flank2 of *fasA*; template: DNA of S3	*TCAAACTACCAGCTACCCTGTGGCCCGGG*-CCAACAAGTGAGGGAAACCTGC
16	RV_F2_fasA	Amplification of Flank2 of *fasA*; template: DNA of S3	*TGAATTCGAGCTCGGTACCC*AATATTCC-TGCTGCTGCGCG
17	FW_Ptuf-fasA_validation	Validation of *fasA* promoter exchange; sequencing	ATCTCCGCAGGGACTTCGG
18	RV_Ptuf-fasA_validation	Validation of *fasA* promoter exchange; sequencing	GACGGAGATTCTTGCGCAGAA
19	FW_F1_fasB	Amplification of Flank1 of *fasB*; template: DNA of S3	*GTCGACTCTAGAGGATCCCC*CCACGTG-AAGCGCAATTGC
20	RV_F1_fasB	Amplification of Flank1 of *fasB*; template: DNA of S3	*TCAAACTACCAGCTACCCTGTGGCCCGGG*-GATAACGGTGTCGTTAAAGGTCG-AA
21	FW_Ptuf_fasB	Amplification of P_{tuf}; template: DNA of S3; sequencing	*TTCGACCTTTAACGACACCGTTATCCCCG-GG*CCACAGGGTAGCTGGTAGTTT-GA
22	RV_Ptuf_fasB	Amplification of P_{tuf}; template: DNA of S3; sequencing	*GCGGTGTCAGTGAAGAAATACTCACTCTA-GA*TATGTCCTCCTGGACTTCGTGG
23	FW_F2_fasB	Amplification of Flank1 of *fasB*; template: DNA of S3	*CCACGAAGTCCAGGAGGACATATCTAGA*G-TGAGTATTTCTTCACTGACACCGC
24	RV_F2_fasB	Amplification of Flank1 of *fasB*; template: DNA of S3	*TGAATTCGAGCTCGGTACCC*GACAGGC-CGCGAACAGAG
25	FW_Ptuf-fasB_validation	Validation of *fasB* promoter exchange; sequencing	AATGCCTGGAGGTAGGGGC
26	RV_Ptuf-fasB_validation	Validation of *fasB* promoter exchange; sequencing	TGCCTCTGGCTTACCAGAGAC
27	FW_accE	Amplification of *accE*; template: DNA of S3	*ATCCCCGGGTACCGAGCTCG***GAAAGGAG-AGGATTG**ATGTCTGAAGAAACCACT-CAGGAC
28	RV_accE	Amplification of *accE*; template: DNA of S3	*CTGTAAAACGACGGCCAGTG*CTAGAAG-AAATTCACATTCTGAAACGCG
29	FW_accBC_pEKEx2	Amplification of *accBC*; template: DNA of S3	*CTGTAAAACGACGGCCAGTG*TTACTTG-ATCTCGAGGAGAACAACGC
30	RV_accBC	Amplification of *accBC*; template: DNA of S3; sequencing	**GAAAGGAGAGGATTG**GTGTCAGTCG-AGACTAGGAAGATCA
31	FW_accD1	Amplification of *accD1*; template: DNA of S3	*CAATCCTCTCCTTTC*TTACAGTGGCAT-GTTGCCGTG

32	RV_accD1_pEKEx2	Amplification of *accD1* with mutated *fasO* motif; template: DNA of S3	*ATCCCCGGGTACCGAGCTCG***GAAAGGAG-AGGATTG**ATGACCATTAGTAGCCCT-TTGATTGACGTCGC
33	FW_seq_accBC	Sequencing	CGTGAAGCAACCGCAGC
34	FW_seq2_ac-cBC	Sequencing	GCAAAGCTGATCGTTTGGGG
35	FW_seq_accD1	Sequencing	GCCCAGCTCTGACCGACT
36	FW_seq2_accD1	Sequencing	GCGCAGGCCAGGAGTAC
37	FW_F1_ ΔsigD	Amplification of Flank1 of *sigD*; template: DNA of S3	*GTCGACTCTAGAGGATCCCCC*AACTGC-CAGTCCCAGAAGTC
38	RV_F1_ ΔsigD	Amplification of Flank1 of *sigD*; template: DNA of S3	*ACCATGTAGACGTCGAGTCA*GTTCTCG-CACCTTCCTGCATC
39	FW_F2_ ΔsigD	Amplification of Flank2 of *sigD*; template: DNA of S3	*GATGCAGGAAGGTGCGAGAAC*TGACTC-GACGTCTACATGGTGG
40	RV_F2_ ΔsigD	Amplification of Flank2 of *sigD*; template: DNA of S3	*TGAATTCGAGCTCGGTACCCCACCC*ACC-AAACCGCTAAGG
41	FW_validation_ ΔsigD	Validation of *sigD* deletion	TGCACAGATGGCCTTTGCG
42	RV_validation_ ΔsigD	Validation of *sigD* deletion	TTGCCAAACAGCTGCTGATTC
43	FW_F1_Δgdh	Amplification of Flank1 of *gdh*; template: DNA of S3	*GTCGACTCTAGAGGATCCCC*CAACTAC-GGTCTGGAACCATCAC
44	RV_F1_Δgdh	Amplification of Flank1 of *gdh*; template: DNA of S3	*GAGATGGGAACGAGGAAATC*GACCCCT-GCGCTTTACTTAAACC
45	FW_F2_Δgdh	Amplification of Flank2 of *gdh*; template: DNA of S3	GATTTCCTCGTTCCCATCTCGG
46	RV_F2_Δgdh	Amplification of Flank2 of *gdh*; template: DNA of S3	*TGAATTCGAGCTCGGTACCC*TCGTACC-AATTCCATTTGAGGGC
47	FW_validation_ Δgdh	Validation of *gdh* deletion	TTCCAGTCAGCGCAAAGGG
48	RV_validation_ Δgdh	Validation of *gdh* deletion	CGGTCGCCCAATTGAGGAG
49	FW_maqu_2220	Amplification of *maqu2220*; sequencing	*ATCCCCGGGTACCGAGCTCG***GAAAGGAG-AGGATTG**ATGGCAATACAGCAGG-TACATCAC
50	RV_maqu_2220	Amplification of *maqu2220*; sequencing	*CTGTAAAACGACGGCCAGTG*TCAGGCA-GCTTTTTTGCGC

51	FW_maqu_2507	Amplification of *maqu2507*; sequencing	*ATCCCCGGGTACCGAGCTCG***GAAAGGAG-AGGATTG**ATGAATTATTTCCTGACA-GGCGGC
52	RV_aqu_2507	Amplification of *maqu2507*; sequencing	*CTGTAAAACGACGGCCAGTG*TTACCAG-TATATCCCCCGCATAATCG
53	FW_maqu_2220 _pECXT	Amplification of *maqu2220*; sequencing	*GTGTTATAATGGTTCCATGG***GAAAGGAGA-GGATTG**ATGGCAATACAG
54	RV_maqu_2220 _pECXT	Amplification of *maqu2220*; sequencing	*CCTGCAGGTCGACTCTAGAG*TCAGGCA-GCTTTTTTGCGC
55	FW_trrnB	Sequencing	CTGTTTTGGCGGATGAGAGAAGA-TT
56	RV_trrnB	Sequencing	AGGAGAGCGTTCACCGACAA
57	FW_F1_CgLP11	Amplification of Flank1 of CgLP11; template: DNA of S3; sequencing	*GTCGACTCTAGAGGATCCCC*GAATCGG-CCTCCGTGGAATTC
58	RV_F1_CgLP11 _universal	Amplification of Flank1 of CgLP11; template: DNA of S3	AAATGGGAAAGGCGTGATTCCG
59	FW_F2_CgLP11 _universal	Amplification of Flank2 of CgLP11; template: DNA of S3; sequencing	CCGCGTTAAAATACCAGGTCAAC-AC
60	RV_F2_CgLP11	Amplification of Flank2 of CgLP11; template: DNA of S3; sequencing	*TGAATTCGAGCTCGGTACCCC*TGCGAT-GACATCGATGAGCAATTC
61	FW_CgLP11_val idation	Validation of insertion into CgLP11; sequencing	CGGCTAACGCCGTCTTAAAGG
62	RV_CgLP11_va-lidation	Validation of insertion into CgLP11; sequencing	CGCCGGTGGAGGTGTC
63	FW_Ptac_pEKE x_CgLP11	Amplification of (P_{tac}-*maqu2220*-T_{rrnB}); template: P20; sequencing	*CGGAATCACGCCTTTCCCATTT*GAGCTG-TTGACAATTAATCATCGGC
64	RV_Ptac_pEKEx _CgLP11	Amplification of (P_{tac}-*maqu2220*-T_{rrnB}); template: P20	*GTGTTGACCTGGTATTTTAACGCGG*CAA-AAGAGTTTGTAGAAACGCAAAAA-GG
65	FW_lacIq_2	Amplification of $lacI^q$; template: P17	*ATGGCGAATGGCGCGATAAG*TCAAGCC-TTCGTCACTGGTC
66	RV_laqIq	Amplification of $lacI^q$; template: P17	*GTGCTTGCGGCAGCGTGAAG*GCGGCA-TGCATTTACGTTGAC
67	FW_F1_cg2692	Amplification of Flank1 of cg2692; template: DNA of S3	*GTCGACTCTAGAGGATCCCC*CCGCACC-TGAGGTGATAGAAAGAG

68	RV_F1_cg2692 GTG	Amplification of Flank1 of cg2692 for GTG start codon mutation; template: DNA of S3	TAGGCGAACCCCGTGGCAG
69	FW_F2_cg2692 GTG	Amplification of Flank2 of cg2692 with GTG start codon mutation; template: DNA of S3	CTGCCACGGGGTTCGCCTA
70	RV_F2_cg2692	Amplification of Flank2 of cg2692; template: DNA of S3	*TGAATTCGAGCTCGGTACCC*GATCGCT-ACAGCTGCGCTCC
71	RV_F1_cg2692TTG	Amplification of Flank1 of cg2692 for TTG start codon mutation; template: DNA of S3	TAGGCGAACCCCTTGGCAGC
72	FW_F2_cg2692 TTG	Amplification of Flank2 of cg2692 with TTG start codon mutation; template: DNA of S3	CTGCCAAGGGGTTCGCCTA
73	FW_cg2692_validation	Validation of start codon mutation of cg2692; sequencing	CGACGCCGTCACGTTGAA
74	RV_cg2692_validation	Validation of start codon mutation of cg2692; sequencing	GCGGATCCCCATGGTTTAGG
75	FW_F1_CgLP12	Amplification of Flank1 of CgLP12; template: DNA of S3	*GTCGACTCTAGAGGATCCCC*TGCAGAC-CGAAGGTGAAATCG
76	RV_F1_CgLP12 _universal	Amplification of Flank1 of CgLP12; template: DNA of S3	AATATGCCGATTGCAAGAAACGA-GAAG
77	FW_F2_CgLP12 _universal	Amplification of Flank2 of CgLP12; template: DNA of S3	CAGTCAAAAAATGTTGAAATCAGC-ACTTTCA
78	RV_Flank2_CgLP12	Amplification of Flank2 of CgLP12; template: DNA of S3	*TGAATTCGAGCTCGGTACCCC*AATAATT-GGTGCCCCAACTTTTGGA
79	FW_Ptac_pEKEx2_CgLP12	Amplification of (P_{tac}-*pntAB*-T_{rrnB}); template: P22	*CTTCTCGTTTCTTGCAATCGGCATATT*GA-GCTGTTGACAATTAATCATCGGC
80	RV_trrnB_pEKEx2_CgLP12	Amplification of (P_{tac}-*pntAB*-T_{rrnB}); template: P22	*TGAAAGTGCTGATTTCAACATTTTTTGACT-G*CAAAAGAGTTTGTAG-AAACGCAAAAAGG
81	FW_pntAB_Ec_pEKEx2	Amplification of *pntAB*; template: S2	*ATCCCCGGGTACCGAGCTCG***GAAAGGAG-AGGATTG**ATGCGAATTGGCATACCA-AGAGAAC
82	RV_pntAB_Ec_pEKEx2	Amplification of *pntAB*; template: S2	*CTGTAAAACGACGGCCAGTG*TTACAGA-GCTTTCAGGATTGCATCCA
83	FW_pntAB_Ec	Sequencing	GAAACCTACGAAAGGATTTTTTAC-CCATGCGAATTGGCATACCAAGA-GAAC

84	RV_pntAB_Ec	Sequencing	AATCTTCTCTCATCCGCCAAAACA-GTTACAGAGCTTTCAGGATTGCA-TCCA
85	FW_pntAB_Ec_seq1	Sequencing	CGCGGAATTCCTCGAGCTG
86	FW_pntAB_Ec_seq2	Sequencing	GCTTCCTTAGTTTTATCGCGGTGC
87	FW_pntAB_Ec_seq3	Sequencing	GCGGGCTTTATGCTCAGCAA
88	FW_seq1_F1_CgLP12	Sequencing	CGCACCAGTCCCATTCCAC
89	FW_seq1_F2_CgLP12	Sequencing	TTGGATTTGTGCTTTTACTT-GTCTCG
90	FW_gltA_validation	Validation of *gltA* promoter exchange; sequencing	AGCCAAGGAGCAAGCTTAGAAG
91	RV_gltA_validation	Validation of *gltA* promoter exchange; sequencing	CATGAGGCGAACGGTTGC

A.1.9. Gibson Assembly master mixes

Table S. 9: 5x Iso reaction buffer

Component	Amount
PEG-8000	1.5 g
Tris-HCl, pH 7.5 (1 M)	3 mL
$MgCl_2$ (2 M)	150 µL
DTT (1 M)	300 µL
dNTPs (100 mM)	60 µL (of each nucleotide)
NAD (100 mM)	300 µL

Table S. 10: Iso enzyme-reagent mix

Component	Amount
5x ISO reaction buffer	320 µL
T5 exonuclease (10 U mL^{-1})	0.64 µL
T4 DNA ligase (40 U mL^{-1})	160 µL
Phusion® High-Fidelity DNA Polymerase	20 µL
H_2O	*Ad* 1.2 mL

A.2. Supplementary results

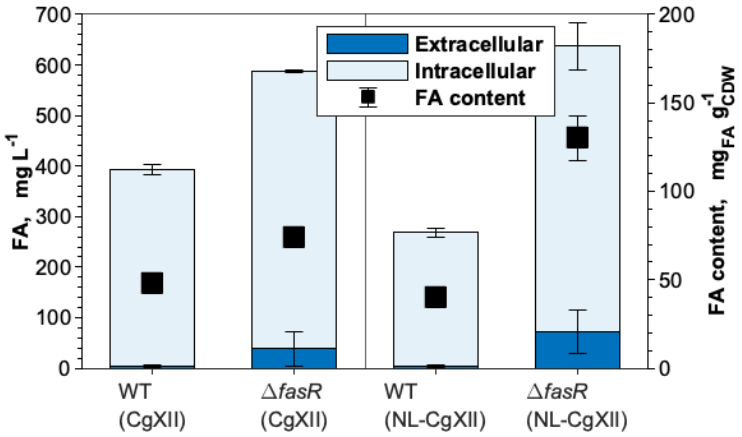

Figure S. 1: FA production in CgXII and NL-CgXII media at 120 rpm. Cultivations of the WT and the Δ*fasR* mutant were conducted in standard CgXII medium and in the nitrogen-limiting NL-CgXII medium. Both media contained per liter 20 g glucose as a carbon source. Samples for analysis were taken after 24 h. Data represents means of ≥ 3 biological replicates with standard deviations. (Werner et al., 2023)

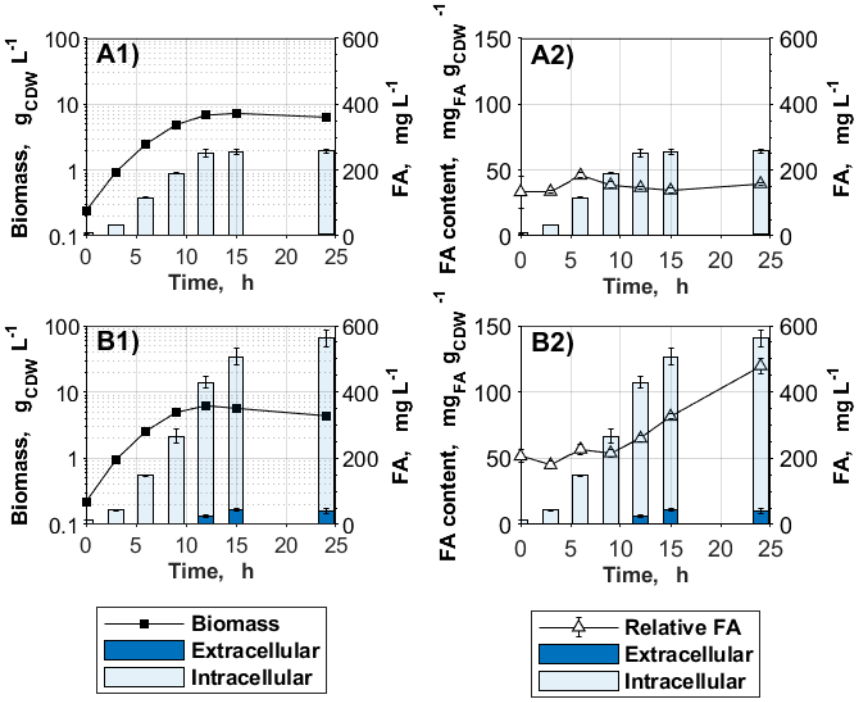

Figure S. 2: Influence of *fasR* deletion on FA production under nitrogen-limiting conditions at 120 rpm. Cultivations were conducted in the nitrogen-limiting NL-CgXII medium containing per liter 20 g glucose as the carbon source. A) *C. glutamicum* ATCC 13032 (WT); B) *C. glutamicum* Δ*fasR*. Data represents means of ≥ 3 biological replicates with standard deviations. (Werner et al., 2023)

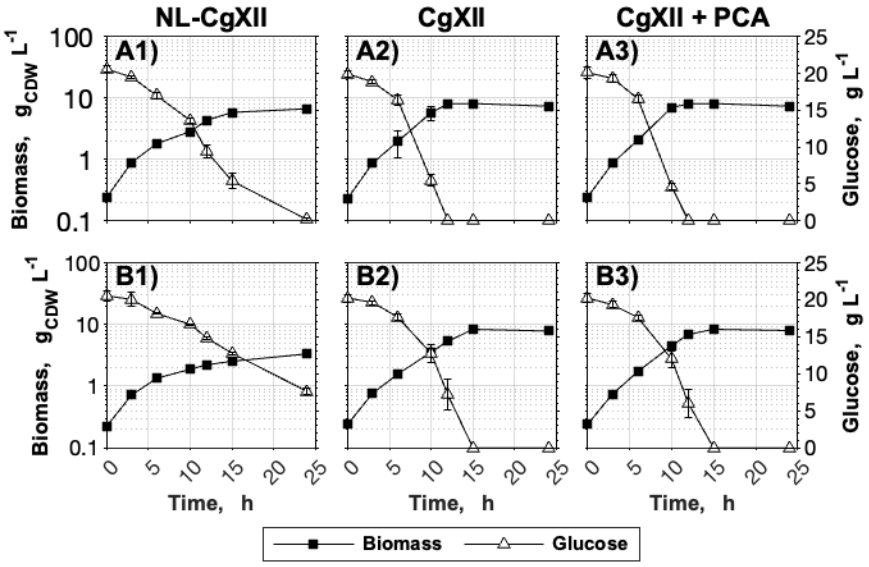

Figure S. 3: Optimization of the medium composition for the efficient production of FAL; glucose consumption. The two best-performing strains (A) *C. glutamicum* Δ*fasR* (pEKEx2-*maqu2220*) and (B) *C. glutamicum* Δ*fasR* cg2692$_{TTG}$ (pEKEx2-*maqu2220*) were cultivated in media: (1) NL-CgXII, (2) CgXII or (3) CgXII with 195 µM PCA. All media contained per liter 20 g glucose as a carbon source. Data represents means of 3 biological replicates with standard deviations.

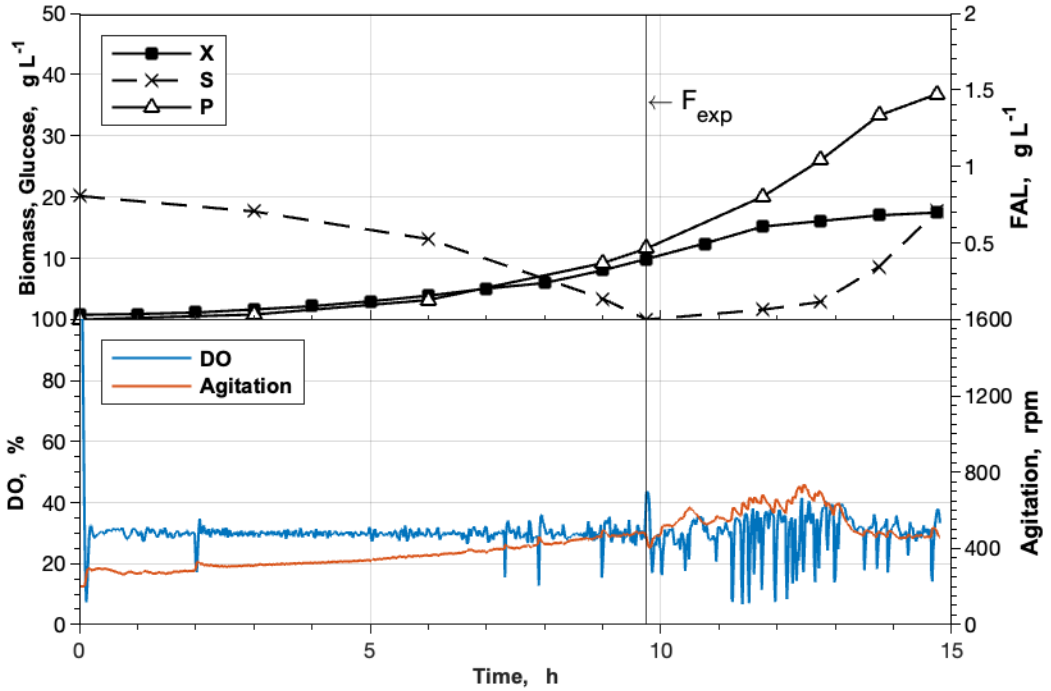

Figure S. 4: Fed-batch cultivation with glucose. Fed-batch cultivations were conducted in a 1 L BioFlo120® bioreactor system with an initial batch volume of 0.5 L. The cultivations of *C. glutamicum* Δ*fasR* cg2692$_{TTG}$ (pEKEx2-*maqu2220*) were performed at 30 °C in CgXII$_{mod}$ medium. The medium was supplemented with 195 µM PCA and had an initial glucose concentration of 20 g L^{-1}. The exponential feed rate was set to obtain a growth rate of 0.15 h^{-1}. F$_{exp}$ indicates the start of the feed upon depletion of the carbon source. Data was obtained from a single experiment. X: biomass; S: glucose; P: FAL; DO: dissolved oxygen.

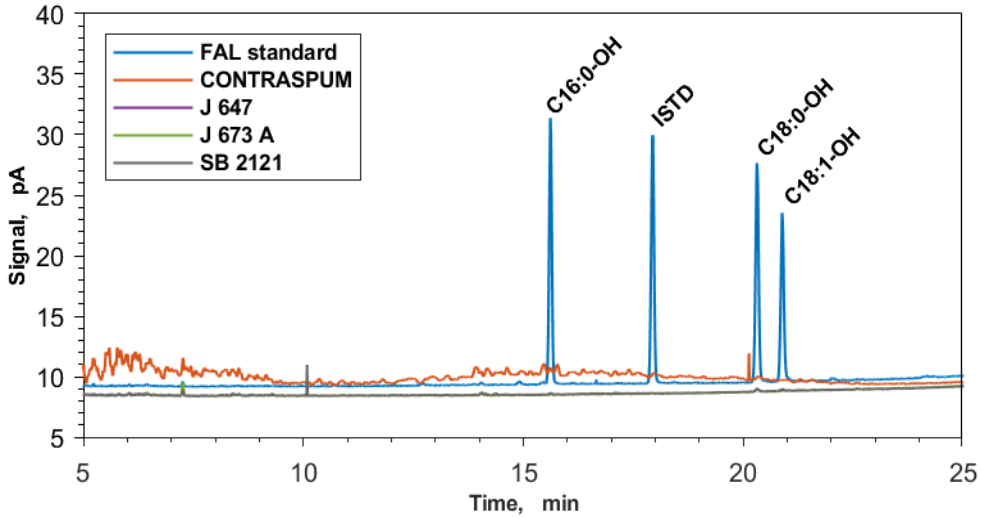

Figure S. 5: Influence of different antifoaming agents on the FAL GC analysis. Aqueous samples containing 0.2 % (v/v) of the antifoaming agents CONTRASPUM® A 4050 (Zschimmer & Schwarz GmbH & Co KG, Lahnstein, Germany), Struktol® J 647, Struktol® J 673 A, or Struktol® SB 2121 (Schill+Seilacher GmbH,Hamburg, Germany) were extracted with ethyl acetate and analyzed via the standard FAL GC method. Respective chromatograms are overlaid with a FAL standard containing 1-hexadecanol (C16:0-OH), heptadecanol (ISTD), octadecanol (C18:0-OH), and oleyl alcohol (C18:1-OH) (50 mg L^{-1} each).

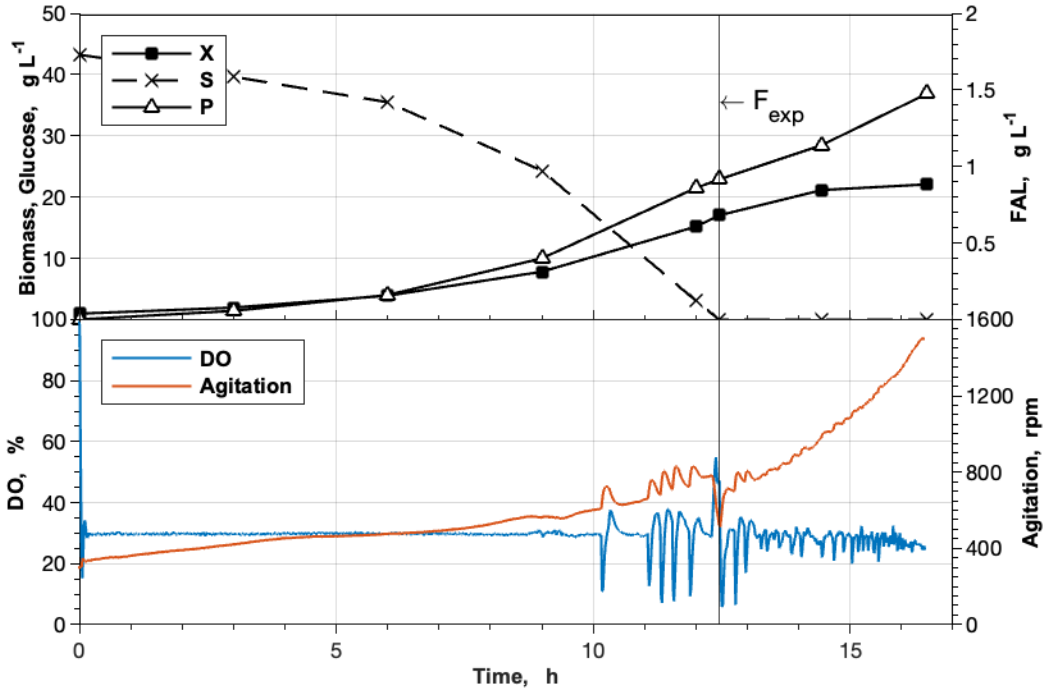

Figure S. 6: Usage of Struktol® SB 2121 as an antifoaming agent in a fed-batch cultivation. Fed-batch cultivations were conducted in a 1 L BioFlo120® bioreactor system with an initial batch volume of 0.5 L. The cultivations of *C. glutamicum* Δ*fasR* cg2692$_{TTG}$ (pEKEx2-*maqu2220*) were performed at 30 °C in CgXII$_{mod,2}$ medium. The medium was supplemented with 195 µM PCA, 0.5 mL Struktol® SB 2121, and had an initial glucose concentration of 40 g L^{-1}. The exponential feed rate was set to obtain a growth rate of 0.15 h^{-1}. F_{exp} indicates the start of the feed upon depletion of the carbon source. Data was obtained from a single experiment. X: biomass; S: glucose; P: FAL; DO: dissolved oxygen.

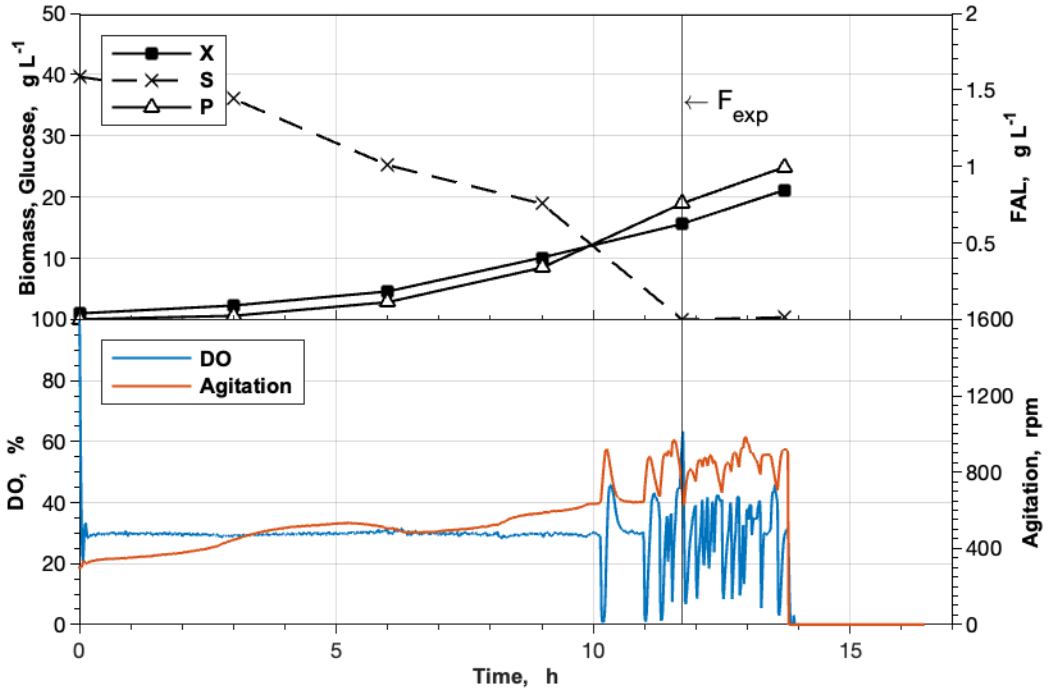

Figure S. 7: Usage of Struktol® J 673 A as an antifoaming agent in a fed-batch cultivation. Fed-batch cultivations were conducted in a 1 L BioFlo120® bioreactor system with an initial batch volume of 0.5 L. The cultivations of *C. glutamicum* Δ*fasR* cg2692$_{TTG}$ (pEKEx2-*maqu2220*) were performed at 30 °C in CgXII$_{mod,2}$ medium. The medium was supplemented with 195 µM PCA, 0.5 mL Struktol® J 673 A, and had an initial glucose concentration of 40 g L^{-1}. The exponential feed rate was set to obtain a growth rate of 0.15 h^{-1}. F_{exp} indicates the start of the feed upon depletion of the carbon source. Data was obtained from a single experiment. X: biomass; S: glucose; P: FAL; DO: dissolved oxygen.

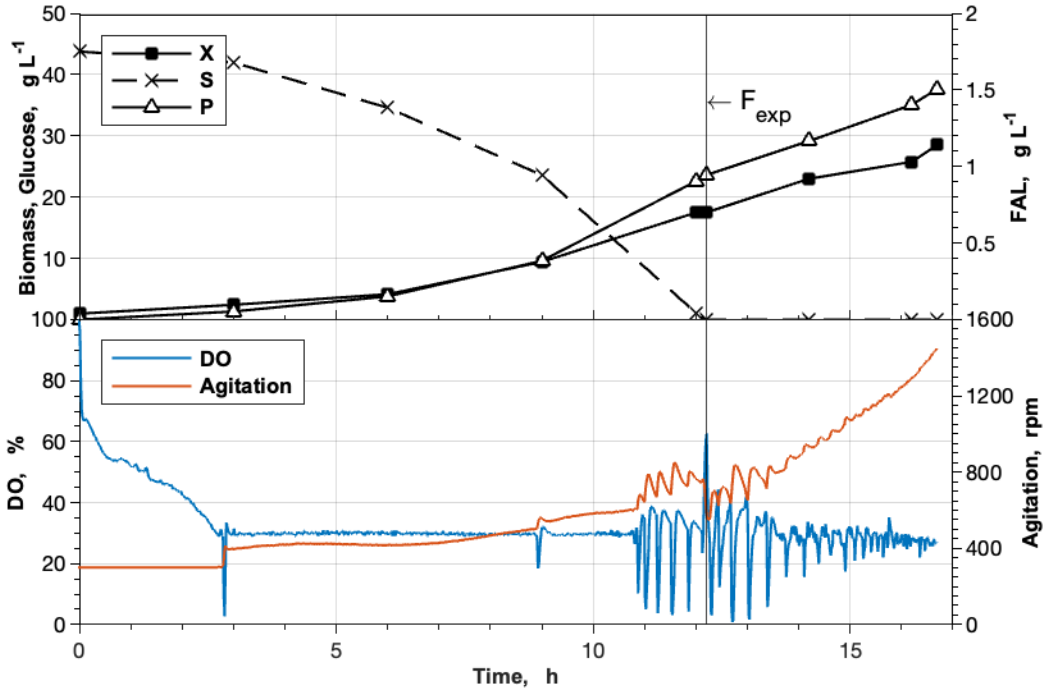

Figure S. 8: Usage of Struktol® J 647 as an antifoaming agent in a fed-batch cultivation. Fed-batch cultivations were conducted in a 1 L BioFlo120® bioreactor system with an initial batch volume of 0.5 L. The cultivations of *C. glutamicum* Δ*fasR* cg2692$_{TTG}$ (pEKEx2-*maqu2220*) were performed at 30 °C in CgXII$_{mod,2}$ medium. The medium was supplemented with 195 µM PCA, 0.5 mL Struktol® J 647, and had an initial glucose concentration of 40 g L^{-1}. The exponential feed rate was set to obtain a growth rate of 0.15 h^{-1}. F_{exp} indicates the start of the feed upon depletion of the carbon source. Data was obtained from a single experiment. X: biomass; S: glucose; P: FAL; DO: dissolved oxygen.

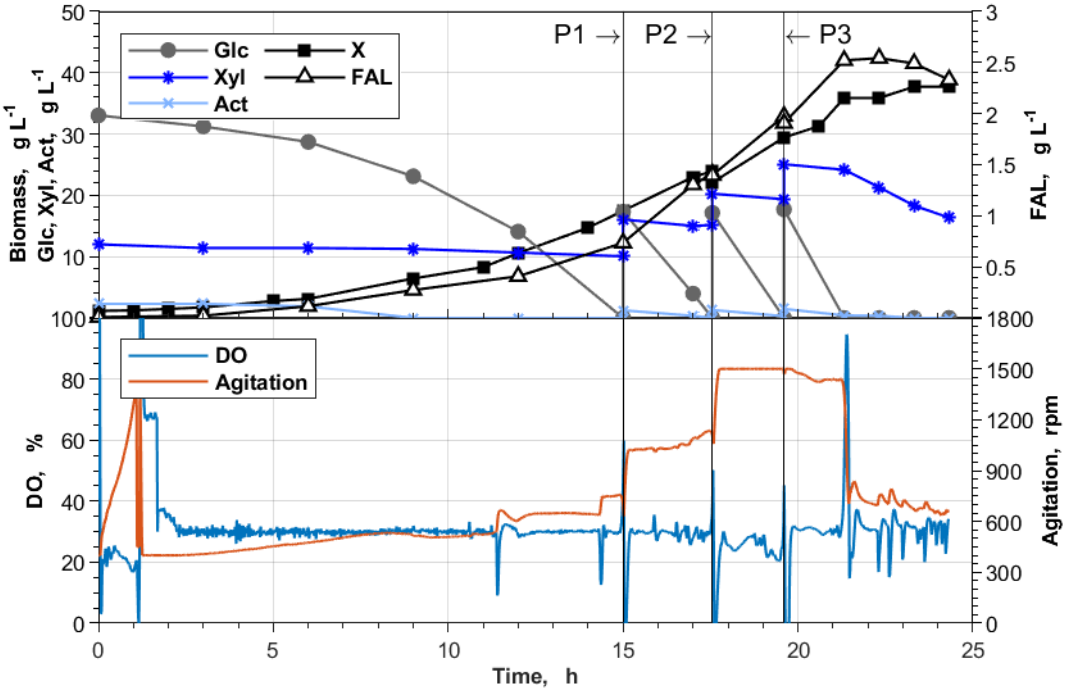

Figure S. 9: Pulsed fed-batch cultivation with wheat straw hydrolysate (2). Fed-batch cultivations of *C. glutamicum* Δ*fasR* cg2692$_{TTG}$ CgLP12::(P_{tac}-*pntAB*-T_{rrnB}) gX (pEKEx2-*maqu2220*) were conducted in a 1 L BioFlo120® bioreactor system with an initial batch volume of 0.5 L in $CgXII_{mod,3}$ medium supplemented with 195 µM PCA. The carbon source during the batch phase was provided by hydrolysate, normalized to a concentration of 40 g glucose L^{-1}. 30 mL Pulses (P) of a 350 g glucose L^{-1} hydrolysate stock solution were added three times upon a sharp increase of the DO signal. The shown process data is representative of three conducted bioreactor cultivations using the same process conditions. Act: acetate; DO: dissolved oxygen; Glc: glucose; X: biomass; Xyl: xylose.

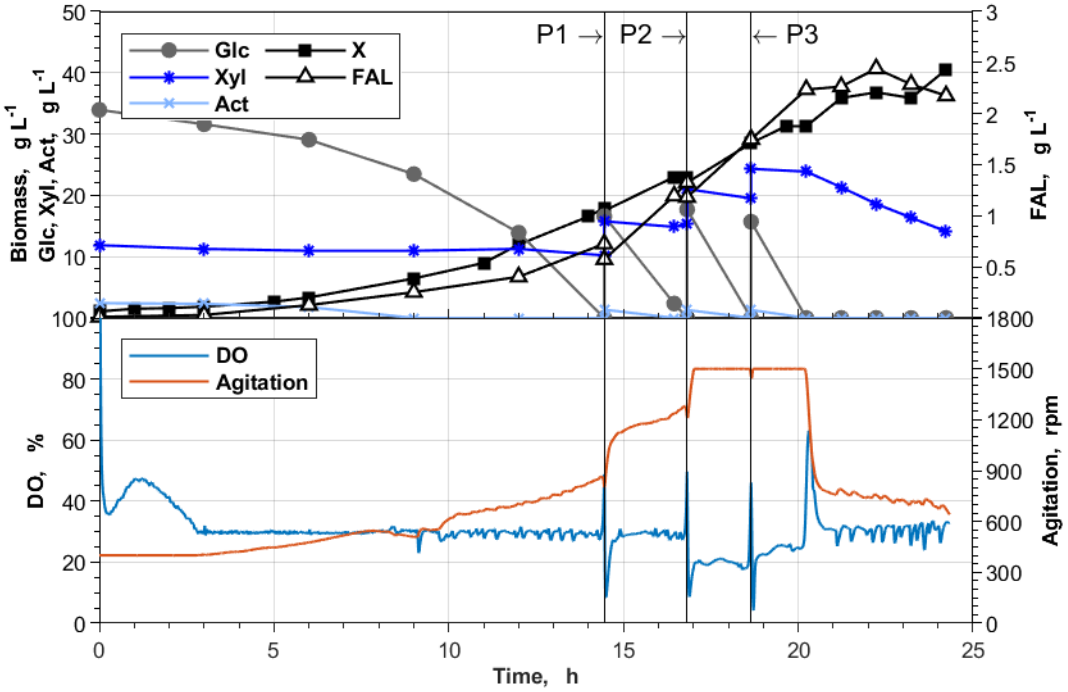

Figure S. 10: Pulsed fed-batch cultivation with wheat straw hydrolysate (3). Fed-batch cultivations of *C. glutamicum* Δ*fasR* cg2692$_{TTG}$ CgLP12::(P_{tac}-*pntAB*-T_{rrnB}) gX (pEKEx2-*maqu2220*) were conducted in a 1 L BioFlo120® bioreactor system with an initial batch volume of 0.5 L in $CgXII_{mod,3}$ medium supplemented with 195 µM PCA. The carbon source during the batch phase was provided by hydrolysate, normalized to a concentration of 40 g glucose L^{-1}. 30 mL Pulses (P) of a 350 g glucose L^{-1} hydrolysate stock solution were added three times upon a sharp increase of the DO signal. The shown process data is representative of three conducted bioreactor cultivations using the same process conditions. Act: acetate; DO: dissolved oxygen; Glc: glucose; X: biomass; Xyl: xylose.